CREST
CLIMATE RESILIENT COAST

FINAL SCIENTIFIC REPORT
TAKE HOME MESSAGES
& PROJECT RESULTS

2020

GHENT UNIVERSITY
FACULTY OF ENGINEERING AND ARCHITECTURE
AGENTSCHAP INNOVEREN & ONDERNEMEN
Vlaanderen is ondernemen

IN COOPERATION WITH

WITH SUPPORT OF

Cite as:

CREST, 2020. Final Scientific Report. Take home messages and project results. VLIZ Special Publication 85.
Jaak Monbaliu, Tina Mertens, Annelies Bolle, Toon Verwaest, Pieter Rauwoens, Erik Toorman, Peter Troch and Vincent Gruwez (*Editors)* - Corrado Altomare, Annelies Bolle, Evelien Brand, Margaret Chen, Sebastian Dan, Lars De Sloover, Alain Dewulf, Juan Sebastian Escobar Ramos, Vincent Gruwez, Rik Houthuys, Dogan Kisacik, Britt Lonneville, Tina Mertens, Jaak Monbaliu, Anne-Lise Montreuil, Mohamed Ouda, Stéphanie Ponsar, Pieter Rauwoens, Bart Roest, Erik Toorman, Glenn Strypsteen, Tomohiro Suzuki, Peter Troch, Koen Trouw, Samuel Van Ackere, Ine Vandebeek, Dries Van den Eynde, Toon Verwaest, Samor Wongsoredjo, & Qinghui Zhang (*Contributors)*.

TABLE OF CONTENTS

INTRODUCTION 1

1. FACTS AND FIGURES 1
2. RESEARCH OBJECTIVES 2
3. VALORISATION OBJECTIVES 3
4. CREST OUTPUT 4

THEME 1 CLIMATE CHANGE INCLUDING MORPHOLOGICAL EVOLUTION ON LONG TIME SCALE FOR THE BELGIAN COAST AS A WHOLE 5

THM 1.1 CLIMATE CHANGE SCENARIOS 6
THM 1.2 EXTREME WAVES AND STORM SURGES 8
THM 1.3 MEAN SEA LEVEL AND TEMPERATURE 11
THM 1.4 TIDAL AMPLITUDE 13
THM 1.5 HISTORICAL COASTLINE EVOLUTION 17
THM 1.6 NATURAL FEEDING 19
THM 1.7 NATURAL RESILIENCE TO SEA LEVEL RISE 20
THM 1.8 EFFECT OF STORMS IN DECADAL MORPHOLOGICAL EVOLUTION 21
THM 1.9 EFFECT OF NOURISHMENTS IN DECADAL MORPHOLOGICAL EVOLUTION 22
THM 1.10 DIGITISATION OF OLD MORPHOLOGICAL DATA 23
THM 1.11 DOCUMENTING DATA 24
THM 1.12 INCREASING THE ACCURACY OF BATHYMETRIC MONITORING 25
THM 1.13 DOCUMENTING SAND WORKS 26
THM 1.14 EXTENDING THE BATHYMETRIC MONITORING? 27

THEME 2 MORPHODYNAMICS ON TIME SCALE OF DAYS (STORMS) TO YEARS (LIFETIME OF NOURISHMENTS) FOR THE TWO PILOT AREAS MARIAKERKE AND KOKSIJDE 30

THM 2.1 STATIC TERRESTRIAL LASER SCAN 31
THM 2.2 MOBILE LIDAR 34
THM 2.3 TOPOGRAPHIC DATA SETS 37

THM 2.4 WAVES, CURRENTS AND SEDIMENT SUPPLY SHAPE THE INTERTIDAL ZONE 40
THM 2.5 DATA COLLECTION OF AEOLIAN SAND TRANSPORT RATES 44
THM 2.6 PREDICTED AND OBSERVED AEOLIAN TRANSPORT RATES 45
THM 2.7 SPATIAL-TEMPORAL VARIABILITY IN DUNE VOLUME CHANGES 49
THM 2.8 POTENTIAL AEOLIAN SEDIMENT TRANSPORT 51
THM 2.9 AEOLIAN TRANSPORT PREDICTION AT DECADAL TIMESCALE 55
THM 2.10 WIND FLOW AND FETCH EFFECT ACROSS AN ARTIFICIALLY CONSTRUCTED COASTAL FLAT BERM 57
THM 2.11 MINIMIZING AEOLIAN SAND TRANSPORT 59
THM 2.12 RECOMMENDATIONS FOR FUTURE AEOLIAN MONITORING TECHNIQUES 60
THM 2.13 BEACH MORPHOLOGY IMPACTS BEACH RECOVERY 62
THM 2.14 BEACH RECOVERY ALSO OCCURS ON DEVELOPED BEACHES IN URBAN AREA 63

THEME 3 PYSHICAL PROCESSES AND INNOVATION IN MODELLING 65

THM 3.1 CORRECTION FACTOR FOR INFRA-GRAVITY WAVE RUN-UP 66
THM 3.2 EFFECT OF SHEET FLOW ON THE BOTTOM ROUGHNESS 67
THM 3.3 ALTERNATIVE BOUNDARY TREATMENT FOR TURBULENCE MODELLING.. 69
THM 3.4 A PHYSICS-BASED TURBULENCE CLOSURE 70
THM 3.5 VALIDATION OF A 2D SAND-MUD MODEL FOR THE BELGIAN CONTINENTAL SHELF 71
THM 3.6 COUPLING OF DIFFERENT NUMERICAL MODELS FOR WAVE OVERTOPPING CALCULATIONS 73
THM 3.7 A WEB-BASED TOOL FOR FLOOD VISUALISATION TO INCREASE PUBLIC AWARENESS 74
THM 3.8 INTERNET OF FLOODS AS A DECISION TOOL DURING FLOOD EVENTS 75
THM 3.9 FLIAT: A NEW RISK ASSESSMENT TOOL 77
THM 3.10 VERTICAL EVACUATION TO MINIMISE CASUALTIES DURING STORMS 80

THEME 4 PREDICTION OF WAVE IMPACT (OVERTOPPING AND LOADS) ON THE DIKE DURING STORMS 82

THM 4.1 INVISIBLE BUT STRONG: LONG WAVES 83

THM 4.2 WIDE BEACHES TO PROTECT AGAINST VIOLENT STORMS 83

THM 4.3 OUR COMPLEX COASTAL DEFENCE SYSTEM REQUIRES STATE OF THE ART NUMERICAL MODELLING 83

THM 4.4 IMPROVEMENT OF SAFETY ASSESSMENT METHODOLOGY 83

THM 4.5 IMPACT FORCE ESTIMATE BASED ON A HYDROSTATIC PRESSURE 86

THM 4.6 WAVE FLUME SCALE MODEL EXPERIMENTS 88

THM 4.7 WAVE BASIN SCALE MODEL EXPERIMENTS 91

THM 4.8 SPECTRAL WAVE PERIOD $T_{M-1,0,T}$ 94

THM 4.9 EFFECT FORESHORE SLOPE AND DIKE GEOMETRY ON OVERTOPPING AND IMPACT 96

THM 4.10 IMPORTANCE OF LONG WAVES FOR OVERTOPPING/IMPACT 98

THM 4.11 LONG WAVE REFLECTION 101

THM 4.12 IMPORTANCE OF ACTIVE WAVE ABSORPTION OF LONG WAVES 103

THM 4.13 REPEATABILITY MEASURED IMPACT FORCES 106

THM 4.14 DYNAMIC IMPACT FORCE SAFETY FACTOR 109

THM 4.15: DIRECTIONAL SPREADING 109

THM 4.16 IMPORTANCE OF 2ND ORDER WAVE GENERATION 110

THM 4.17 ACCURACY OF SWASH FOR WAVE IMPACT 113

THM 4.18 NECESSITY OF FULL NAVIER-STOKES MODELS 115

THM 4.19 IMPORTANCE OF SEED NUMBER ON LOW OCCURRENCE OVERTOPPING/IMPACTS 116

THM 4.20 EFFECT BEACH MORPHODYNAMICS ON OVERTOPPING 119

SUMMARY AND CONCLUSIONS 120

VALORISATION AND FURTHER APPLICATION 124

RECOMMENDATIONS 127

FUTURE FIELD AND LAB MEASUREMENTS 127

SHARING RESULTS AND DATA 128

IMPACT ON COASTAL ZONE MANAGEMENT 129
FUTURE RESEARCH AND STUDIES 130
MULTI-DISCIPLINARY APPROACH 132
EXPERT GROUP COASTAL PROTECTION 133

REFERENCES 134

INTRODUCTION

Coastlines worldwide attract people to live there, to work there and to recreate there. But that attraction implies pressure from various stakeholders resulting in a fragile environment. Climate change reinforces the vulnerability. Sea level rise and severe storms require policymakers to assess flood risks on a regular basis in the coastal areas most exposed to catastrophes. The Belgian coast is one of the most vulnerable coastlines in Europe, while it challenges at the same time new spatial developments. To ensure coastal safety, the Flemish government invests millions of euros for the implementation of the Master Plan Coastal Safety. The main protective measure consists in the repeated supply of sand on beaches and the foreshore. Despite the fact that this is in principle an old and widely used protection technique, the design and the implementation of an efficient and sustainable nourishment scheme is still a big challenge.

Local accretion and erosion of our beaches are indeed complex processes and the result of a combination of different and even interacting forcing mechanisms including waves, tidal currents and wind resulting in various forms of sediment transport. Moreover, climate change scenarios reveal large uncertainties related to the rate of change. Possible consequences and mitigation strategies are therefore difficult to assess. Experts in the domain of coastal protection and coastal risks agreed on the need of further research related to coastal processes and established the Climate REsilient coaST (CREST) project.

1. FACTS AND FIGURES

This project with primarily a social finality is part of the Strategic Basic Research (SBO) programme of the Flanders Innovation & Entrepreneurship, VLAIO (previously known as IWT). CREST ran from 1 November 2015 until 31 October 2019 with a budget of 1.9 M€. Added to the budget financed by VLAIO, several partners co-financed the project:

- Maritime Access Division: 267 K€ to finance the design of the Artificial Dike and an in kind contribution of more than 3 person months. Additional funds are foreseen to finance the construction and maintenance of the artificial dike.
- Coastal Division: 3 person months
- IMDC: 40 K€ (an equal budget is financed by VLAIO)
- Fides Engineering: 20 K€ (an equal budget is financed by VLAIO)
- Flanders Hydraulics Research: in kind contribution of 44 person-months and investments in measuring equipment
- The other partners (KU Leuven, UGent, VUB, R-BINS and VLIZ) connected some of the research question in CREST to other research projects and invested in that way an extra effort of more than 100 person months on top of the more than 350 person months charged to the CREST budget.

The consortium existed of experts from the Universities of Leuven, Ghent and Brussels, Flanders Hydraulics Research, Coastal Division and Maritime Access Division of the Flemish Government, RBINS-OD Nature and Flanders Marine Institute complemented with valorisation partners IMDC

and Fides Engineering. All partners have a research background in physical aspects of coastal processes (waves, currents, sediment dynamics). In addition, interim feedback was organised with a Guidance Committee and technical experts from Belgium and abroad.

Project coordinator was Jaak Monbaliu, professor at KU Leuven. Tina Mertens, vice-director of VLIZ, took an at least equal share of the coordination work load.

Photo: Left: CREST Guidance Committee - Right: CREST Technical Experts

2. RESEARCH OBJECTIVES

The main objective of CREST was to gain a better understanding of the nearshore and onshore physical processes and of the flood risks, and to determine the resilience of the coastal system, in order to deal in the most appropriate way with the possible impacts of climate change. Five main scientific objectives were identified at the start of the project:

1. better understanding of nearshore and onshore physical processes including improved models and the validation of 'grey' data about coastal dynamics;
2. better understanding of the flood risks along the coast and the impact of wave overtopping on structures, buildings and people;
3. determine the resilience of the natural coastal system (coastal protection) in relation to storms and wind;
4. validate calculations with today's state of the art models on the basis of laboratory and field measurements in selected pilot areas;
5. define improved climate change scenarios for the Belgian coast.

Separate attention was paid to the dissemination of the results of the project which can then be used by other researchers and professionals, such as: biologists, socio-economists, spatial planners.

These objectives were worked out in three research activities and three supporting activities. As can be seen in Figure 1 below, each activity focussed on a specific topic, while the supporting activities clearly had links with all of them.

Figure 1: Research and supporting activities

3. VALORISATION OBJECTIVES

The five scientific objectives are translated into valorisation objectives:

1. provide information and practical advice (including guidelines) about new models for the calculation and simulation of physical coastal processes, wind impact on dunes and beaches and wave impact on structures, buildings and people;
2. provide advice to stakeholders in the context of coastal zone management, particularly coastal safety, contingency planning and land use planning along the coast;
3. provide information to better assess the environmental impact of coastal protection measures, navigation, etc.;
4. provide practical information (e.g. policy indicators, maps and test sites on the beach) to communicate the impact of climate change, storms and wind on our coastline to a broad audience.

The valorisation approach of the project included:

1. continuous dissemination of information (project website, newsletters, brochures, etc.);
2. regular meetings with the Guidance Committee;

3. technical workshops on the development of new computational models including quality assurance by an international scientific advisory board;
4. feedback with end users and the general public through conferences;
5. innovative models and practical guidelines for policy makers, scientists, engineering consultants, dredging companies;
6. products for educators and policy makers (indicators, reports and maps);
7. scientific outreach through scientific publications, presentations at scientific conferences, posters and scientific reports;
8. dissemination of project information via (social) media.

4. CREST OUTPUT

The output of the CREST project has been summarized into nine general take home messages that are further refined in an extensive list of detailed take home messages.

The **general take home messages** are:

1. Coping with long-term climate change involves many uncertainties. Several climate scenarios have been updated to support policies.
2. Over the past thirty years, it appears that a net natural supply of sediment from the sea to the Belgian west and east coasts has taken place, which has contributed to the soft coastal defence.
3. The technology to follow evolutions in beach morphology is available.
4. Providing sufficient sand on the beaches not only strengthens the beach itself, but also contributes to strengthening the dunes.
5. After a storm, our beaches recover at least partially, and this within a period of barely a few months.
6. Taking fundamental processes better into account is a good basis for understanding and simulating the patterns of coastal sediment transport.
7. The FLIAT model developed under CREST provides a solid basis for hinterland flood risk calculations.
8. Wider beaches reduce the impact of waves on the dikes.
9. Physical tests in the test facilities of Ghent University, Flanders Hydraulics Research and Deltares have largely contributed to estimating the impact of waves on hard structures.

The project results formulated as more **detailed and extended take home messages** are clustered into the four following themes:

- THEME 1: Climate change including morphological evolution on long time scale (decades) for the Belgian coast as a whole
- THEME 2: Morphodynamics on time scale of days (storms) to years (lifetime of nourishments) for the two pilot areas Mariakerke and Koksijde
- THEME 3: Physical processes and innovation in modelling
- THEME 4: Prediction of wave impact (overtopping and loads) on the dike during storms

The report finishes with a summary and conclusions, valorisation and further application, and recommendations towards policy makers.

THEME 1
CLIMATE CHANGE INCLUDING MORPHOLOGICAL EVOLUTION ON LONG TIME SCALE FOR THE BELGIAN COAST AS A WHOLE

THM 1.1 CLIMATE CHANGE SCENARIOS

In concertation with Complex Project Coastal Vision, climate change scenarios for Belgium were agreed upon.

As stated by the Intergovernmental Panel on Climate Change (IPCC - https://www.ipcc.ch/) to deal with the uncertainty in climate change, related to the uncertain worldwide climate policy development, it is necessary to make use of different climate change scenarios, where one is not more probable than the other. In the 5th assessment report of IPCC (AR5) (2014) the "business as usual" Representative Concentration Pathways (RCP) 8.5 scenario (dealing with a radiative forcing in 2100 of 8.5 W/m²), the global mean sea level rise anno 2100 is projected to be 0.45 to 0.82 m (likely range); in the most ambitious scenario regarding reduction of greenhouse gasses (RCP 2.6), a global mean sea level rise is projected to be 0.26 to 0.55 m. Remark that notwithstanding the United Nations Paris agreement (2015), the emissions of CO2 in recent years still follow the business as usual scenario (see **Error! Reference source not found.**).

In December 2018 a workshop was held with contributions from KU Leuven, Flanders Hydraulics Research, VLIZ, RBINS, Royal Meteorological Institute (RMI), VMM, Complex Project Coastal Vision and the CREST project, explaining the latest scientific results by Belgian research teams for different aspects. These presentations and the discussions of the results formed the basis of the definition of four scenarios for 2100 for the Belgian coast.

These four scenarios were defined for different primary parameters. Three scenarios are based on the IPCC scenarios RCP 2.6, RCP 4.5 and RCP 8.5 from AR5, while one extreme scenario (ES) is a collection of some worst-case assumptions. The scenarios are presented in Table 1.

Primary parameter	RCP 2.6	RCP 4.5	RCP 8.5	ES
Global air temperature	+1.0°C (0.3 – 1.7)	+1.8°C (1.1 – 2.6)	+3.7°C (2.6 – 4.8)	+4.8°C
Global mean sea level rise	+50 cm (38 – 73)	+60 cm (39 – 86)	+85 cm (56 – 112)	+295 cm
Change in wind direction	No	No	No	No
Average wind speed	+0%	+0%	+0%	+0%
Average winter precipitation	+9%	+11%	+22%	-
Average summer precipitation	-6%	-12%	-30%	-
Extreme winter precipitation	+5%	+8%	+18%	-
Extreme summer precipitation	+6%	+4%	+2%	-

Table 1: Four climate projections for the Belgian coast by 2100 w.r.t. base-year 1990 (5th - 95th percentiles).

An evaluation by European experts was carried out. The Belgian scenarios are in line with climate change scenarios of neighboring countries.

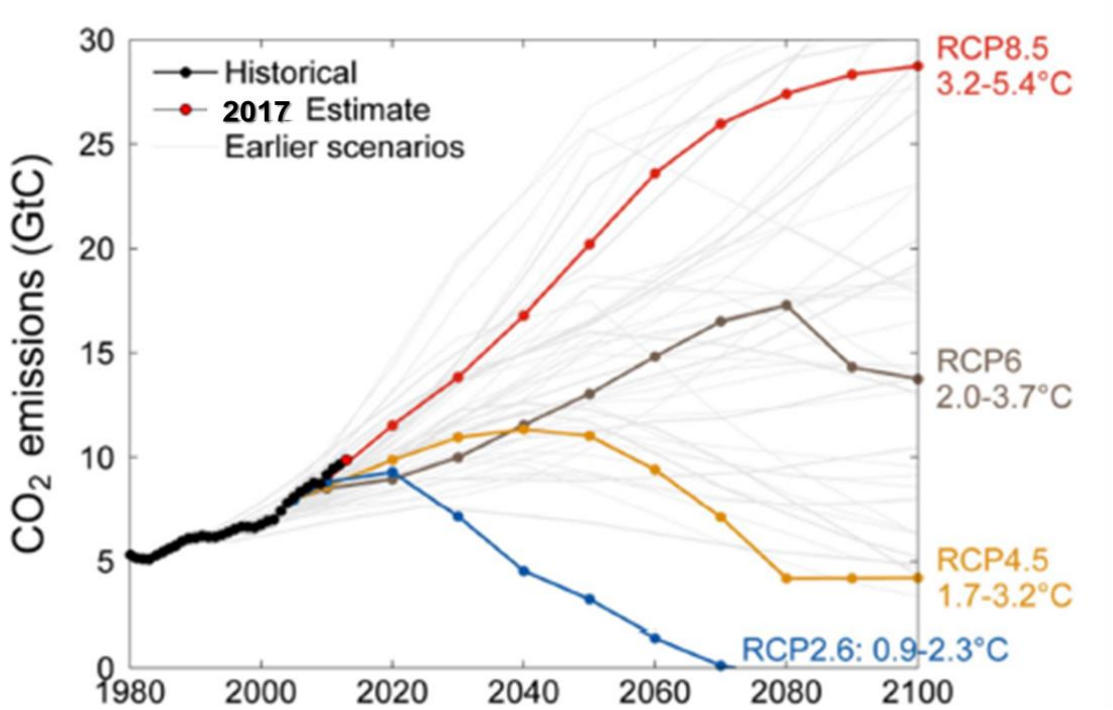

Figure 2: The CO2 emissions in recent years compared with the Representative Concentration Pathways (RCP's) defined in the 5th assessment report of IPCC (2014).

Remark that climate change is expected to continue after 2100. IPCC provides guidance based on available literature. The projections diverge further after 2100. This is confirmed by the findings in the latest IPCC Special Report on the Ocean and Cryosphere in a Changing Climate (IPCC SROCC, 2019), see for example Figure 3 below.

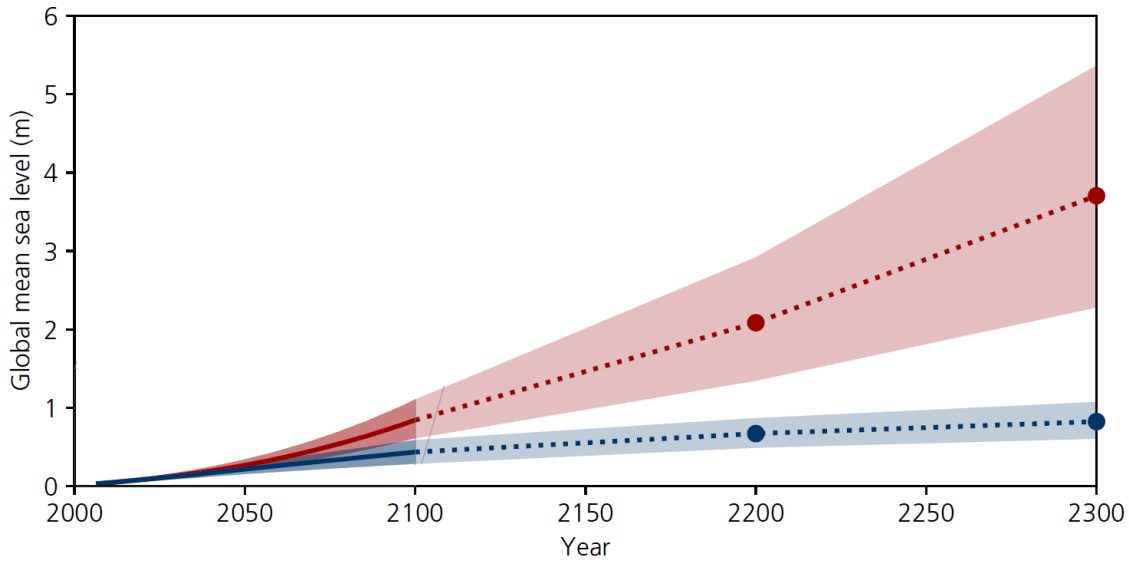

Figure 3: Projections for global mean sea level rise until 2300 for climate change scenarios RCP8.5 (in red) and RCP2.6 (in blue) (IPCC, SROCC 25/9/2019).

In a "business as usual" scenario (RCP8.5), IPCC SROCC (2019) projects the global mean sea level rise anno 2300 to be 2.3 to 5.4m (likely range); in the most ambitious scenario regarding reduction of greenhouse gasses (RCP2.6) global mean sea level rise anno 2300 is projected to be 0.6 à 1.1m (likely range). The largest uncertainty anno 2300 is related to the uncertain worldwide climate policy development.

For more details the reader is referred to the report Complex Project Coastal Vision and CREST (2019).

THM 1.2 EXTREME WAVES AND STORM SURGES

Although according to projected changes in the climate extreme waves conditions and storm surges are not expected to change much, sea level rise will increase the impact at the Belgian coast unless the level of coastal protection can grow at equal pace.

Different regional climate model results were used to force a hydrodynamic model and a wave model for the current climate and for the last 30 years of the 21th century for the RCP 8.5 scenario.

The effect of possible changes in meteorological conditions on the extreme wind speed, significant wave height and storm surges at the Belgian coast were studied. Seven results of regional atmospheric models were obtained in the framework of the CORDEX.be project (financed by Belgian Science Policy Office; Termonia *et al.* (2018)) or were downloaded from the CORDEX website[1]. All models cover the North-west European Continental Shelf with a resolution of about 12.5 km and a time resolution of 6 h or better. A 30-year period covering the current climate (historical run) and a 30-year period, covering the last 30 years of the 21th century, assuming the IPCC RCP8.5 scenario, were studied. Apart from the climate and historical model runs, also some results of 'evaluation runs' were included in the study, which are the results of some regional climate models to simulate the actual weather during the period 1976-2005 and which could be compared to measurements to evaluate the behavior of the regional climate models.

A two-dimensional hydrodynamic model COHERENS (Luyten *et al.*, 2016), was used to calculate the storm surges, while a third-generation WAM model (WAMDI Group, 1988; Günther *et al.*, 1992), was used to calculate the waves.

A comparison of the mean wind speeds, produced by the different regional climate models, showed some differences between the historical runs and the evaluation runs, demonstrating the uncertainties in the model predictions of the regional climate models.

The study focused on the extreme events and used a Weibull distribution to parametrize the probability distribution functions and to calculate the return periods for a certain level (of wave height, wind speed or storm surge). A bias-correction method, based on quantile mapping (Fang *et al.*, 2015), was used to correct the model results for the bias between the model results for the current climate and the measurements that were available.

[1] http://www.euro-cordex.be/

The research showed that for the extreme wind speeds, some increase could be expected due to climate change, see Figure 4. In this figure, the maximum wind speed for a certain return period is shown for the measurements, and for the (bias-corrected) maximum wind speeds in the climate model results. Although a large variability exists in the model results, most models indicate an increase in high wind speeds.

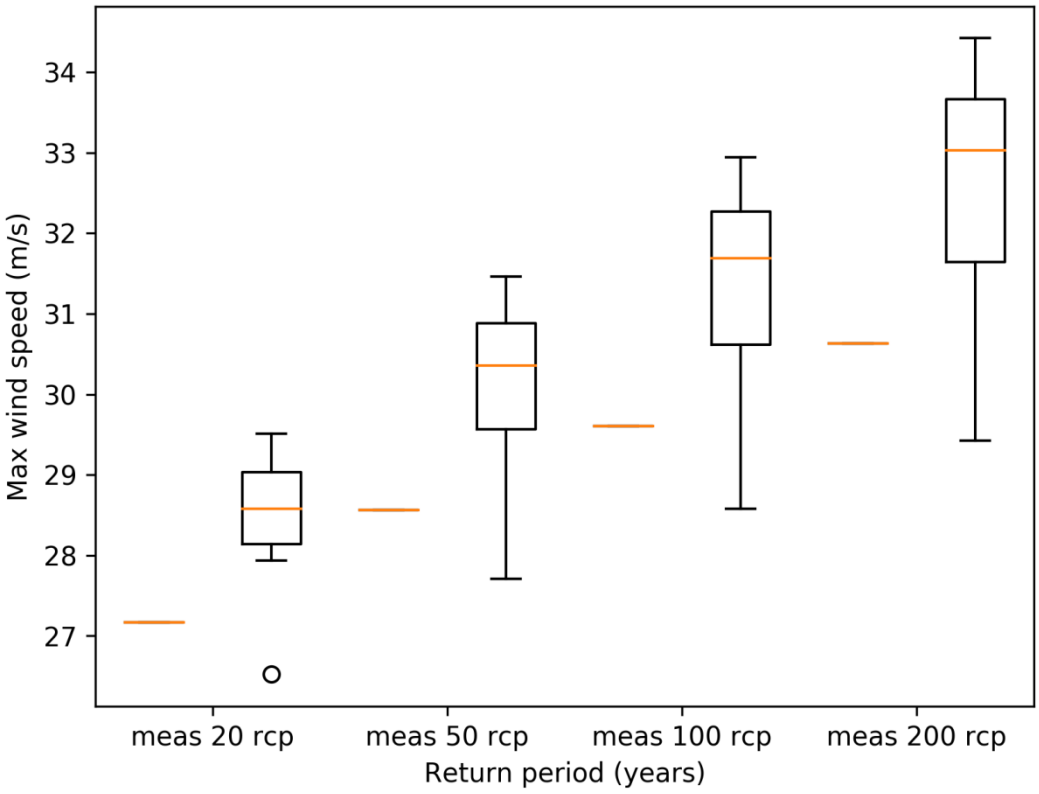

Figure 4: Box plot of the maximum wind speed with a certain return period (20, 50, 100 and 200 years). Left: results of measurements (and historical simulations) - Right: results of the climate RCP 8.5 simulations (bias corrected).

This is however not the case for the extreme wave heights. Here no significant changes are to be expected, see Figure 5**Error! Reference source not found.**. One must again take into account the large variability in the model results. Inclusion of more results of regional climate models could decrease the uncertainties in these results. This will be done, when more results are available.

Also for the extreme storm surges, no significant changes are obtained in the model results, but the variation in the model results is even larger, indicating more uncertainty in these results.

Remark that also the number of extreme events in the historical results and the climate results are not changing significantly.

A first attempt has been made to explain why the wind speeds are expected to increase, while this is not the case for the waves and the storm surges. One of the main reasons that could be found is the fact that for the higher wind speeds a slight change in wind direction reduces the chance of high waves and high storm surges.

Although the results indicated that the extreme significant wave heights at the Belgian coast would not increase due to changes in meteorological conditions, changes are expected due to sea level rise. Assuming that the coastal bathymetry does not change, wave breaking is expected to move landwards resulting in higher waves at the coast. In Figure 6, the effect of a sea level rise of 0.85 cm (scenario RCP 8.5, see THM 1) on a wave of 3.5 m, propagating to the coast, is evaluated. It can be seen that near the coast, an increase in significant wave height up to more than 0.30 m can be expected.

For more details, the reader is referred to Van den Eynde *et al.* (2019a) and Van den Eynde (2020).

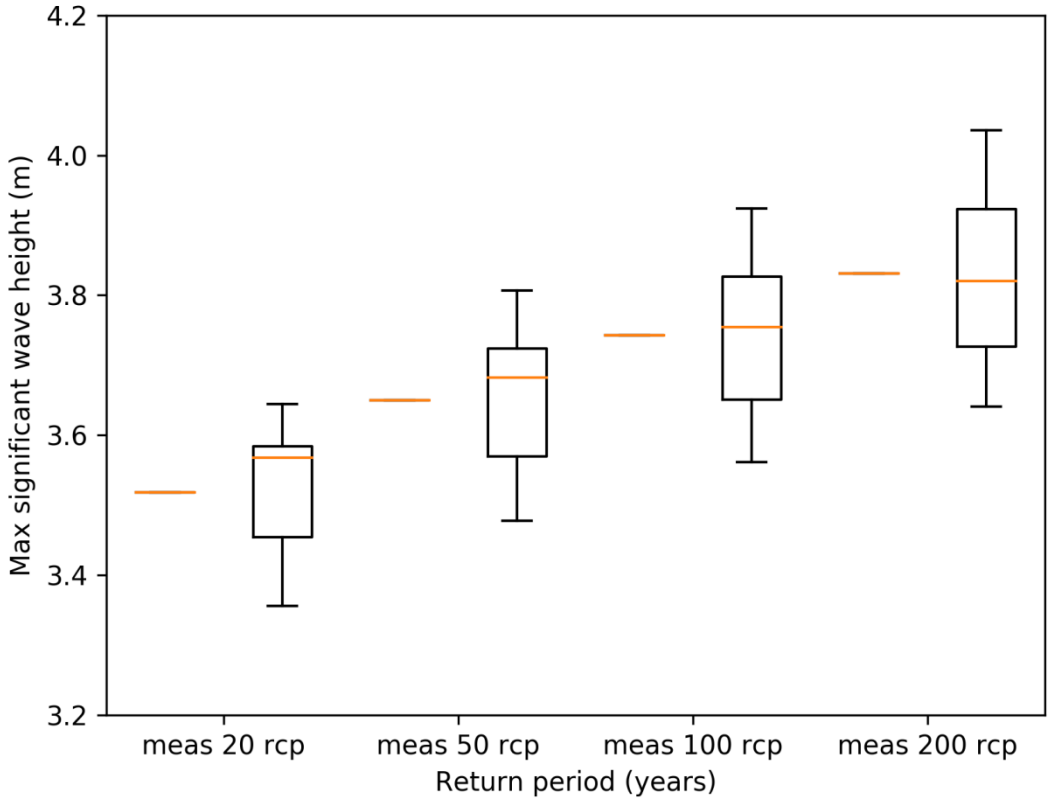

Figure 5: Box plot of the maximum significant wave height with a certain return period (20, 50, 100 and 200 years). Left: results of measurements (and historical simulations) - Right: results of the climate RCP8.5 simulations (bias corrected).

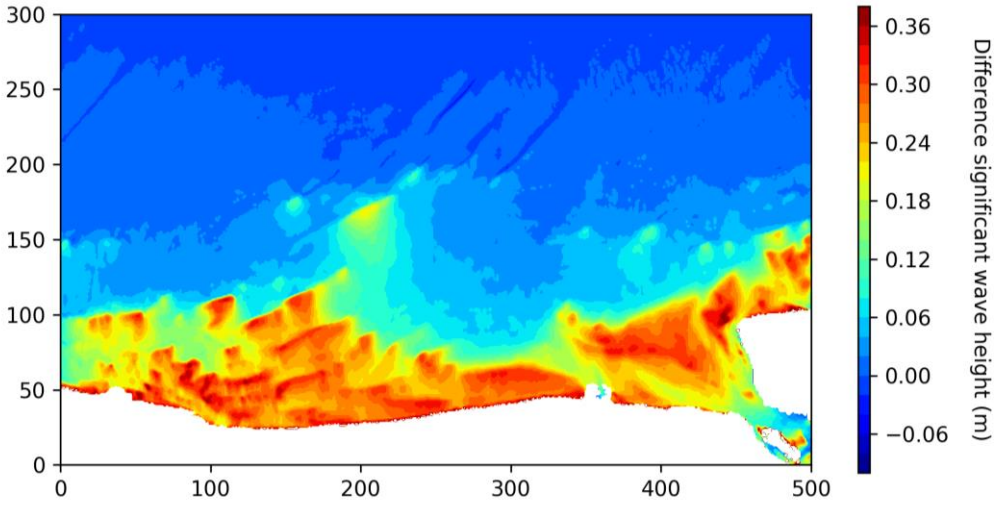

Figure 6: Difference in significant wave height. Waves at boundaries: Hs=3.5 m, Dir=NNW; Tp=13.14 s; wind speed=18.1 m/s; water level=0 m MSL; sea level rise = 0.85 m.

THM 1.3 MEAN SEA LEVEL AND TEMPERATURE

A sea level rise of 2.4 mm per year for the last decades has been confirmed. A temperature increase in the order of 0.1 degree Celsius per decade in Belgian waters has been observed.

The yearly mean sea level values were analysed for the period 1936-2016. The sea level rise of the entire period is estimated at 1.8 mm/year. During the period 1972-2016, an increase of about 2.4 mm/year is found, indicating that an increase in the rate of sea level rise could be happening.

The sea level rise has been assessed in the past e.g., by Van Cauwenberghe (1993, 1995, 1999), Ozer *et al.* (2008) and Willems (2015). An estimation of the increase in seawater temperature was done in the framework of the CLIMAR project (Van den Eynde *et al.*, 2011). An update of these results was attempted in the framework of the CREST project.

To ensure homogeneity of the dataset for the evaluation of the sea level rise, yearly mean sea levels obtained from the Permanent Service of Mean Sea Level were used. Data for the period 1937-2016 could be used. Some data gaps are however present before 1951. Five mathematical models were used to fit the dataset, including a constant trend and a piecewise linear or inflexion model, where the trend is changing at a certain moment in time. A least-squares fit is used to minimise the sum of the squared errors.

When using the linear model for the full period, a sea level rise of 1.8 mm/year is found. These values are slightly higher than the values reported in previous studies.

If the inflexion model is used, a change in trend is found in 1972 with a value of 0.6 mm/year before 1972 and 2.4 mm/year after 1972 (Figure 7**Error! Reference source not found.**). This seems to indicate an increase in the rate of sea level rise over the last decades, which agrees with other recent studies. Remark however that the nodal cycle of about 18 years is not included in the analysis, which could influence the results. Therefore, the results should be treated with caution.

Change in seawater temperature in the Belgian coastal water is analysed. Monthly mean data in the Belgian coastal water were gathered from three different datasets. Data in the box 51°N to 52°N and 2°E to 3.6°E were selected. The three datasets are 1) the 4Demon dataset, obtained in a historical data recovery project, financed by Science Policy Office, 2) the ODAS dataset, the automatic temperature measurements on board of the Research Vessel Belgica, and 3) data from the World Ocean Data Base 2013 (WODB). A long time series with data from 1903 are available in the last dataset. However, only from 1949 onwards, less data gaps were present.

The long-term trends and the seasonal cycles were separated and the method of Visser *et al.* (1996) is used to fill in data gaps.

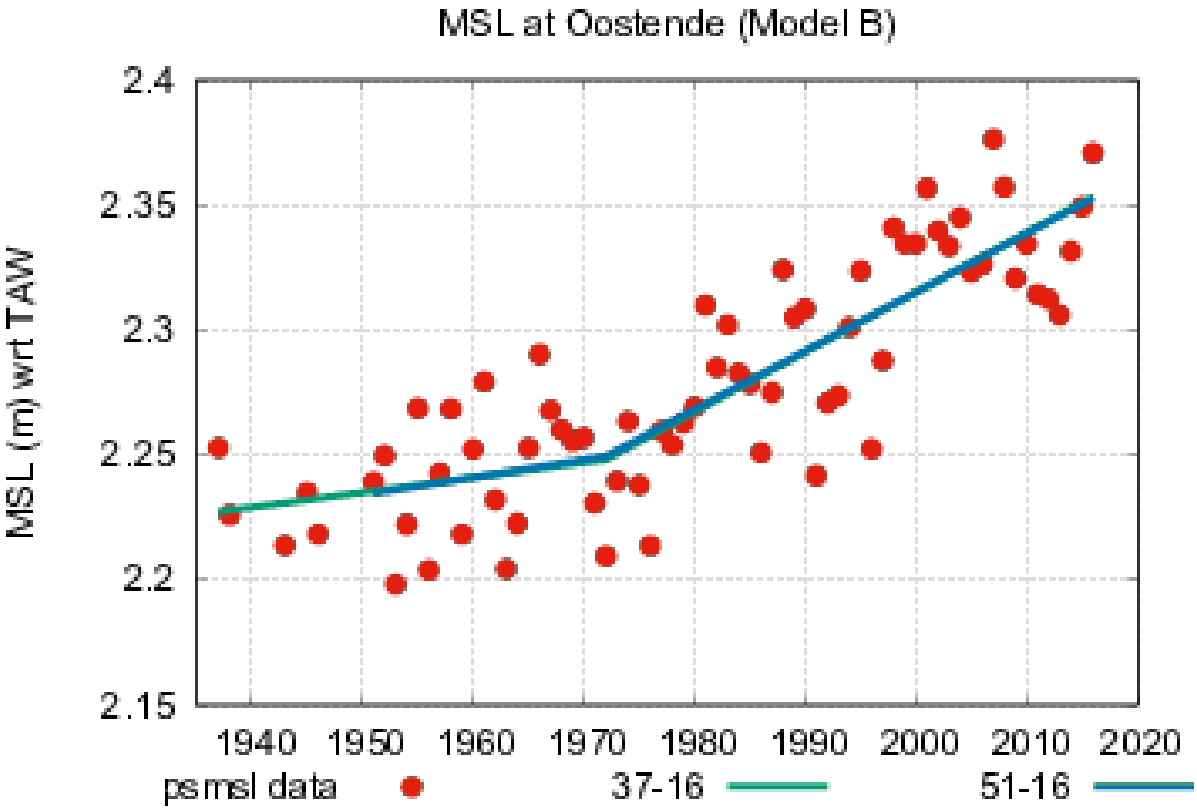

Figure 7: Fitting the yearly mean sea level data points at Ostend with a broken line.

The seawater temperature shows a natural variability with a period of 7 to 8 years, possibly related to the variability in the North Atlantic Oscillation Index (NAO), which was already noted by Sündermann *et al.* (1996). The clear increase in seawater temperature around 1990 to 1995 is visible in the three datasets.

The linear regression of the long-term trend for the dataset from WODB for the period 1949-2015 is 0.010°C/year, while the 4Demon dataset gives a significantly higher increase of temperature of 0.045°C/year (Figure 7). The ODAS data on the other hand gives a much lower value, but uses a much smaller period and has much higher values than the other data sets in the period 1990-2000.

The trend value of the WODB is lower than found in other literature, that expects an increase of 2°C to 4°C by 2100 (Ponsar *et al.*, 2007; Hulme *et al.*, 2002) or found in Van den Eynde *et al.*, 2008, where for the Southern Bight of the North Sea, a value of 0.034°C / year was found. The analysis

stresses the importance of longer datasets to get reliable data and indicate the natural variability of the seawater temperature.

For more details the reader is referred to Ozer *et al.* (2019) and Van den Eynde *et al.* (2019).

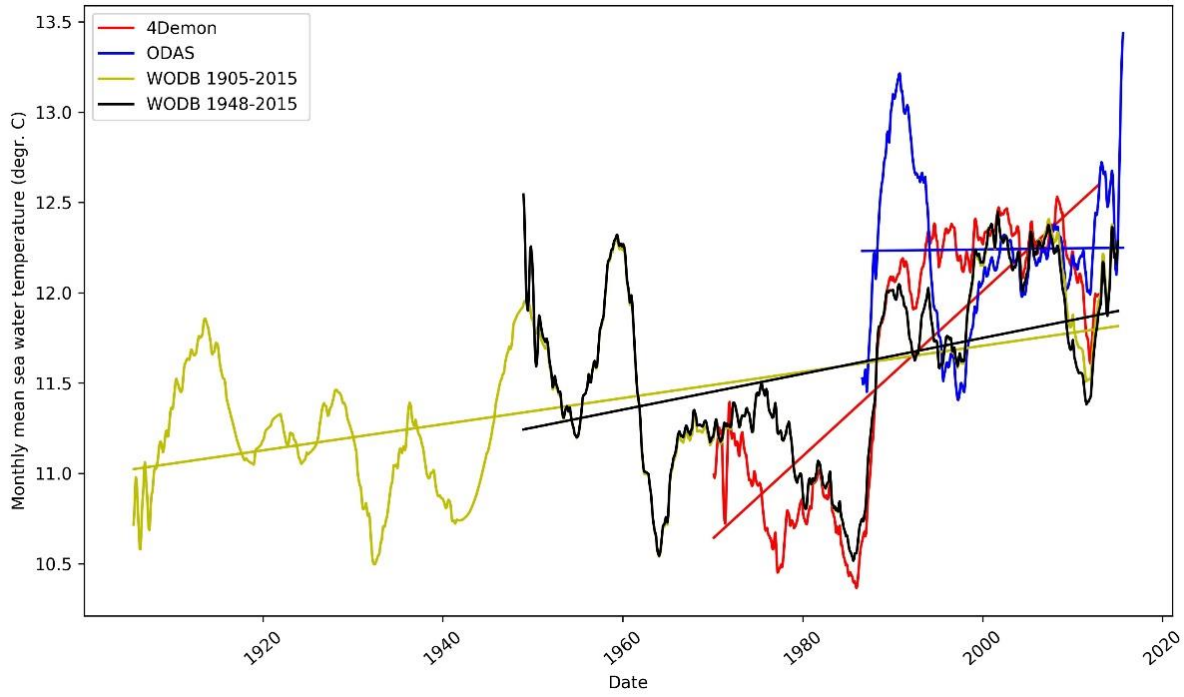

Figure 8: Linear regressions for the long term trends of the four datasets.

THM 1.4 TIDAL AMPLITUDE

Sea level rise will cause higher high tides and lower low tides.

The water elevations on the Belgian Continental Shelf are computed using two values of sea level rise: 85 cm and 295 cm. Because of sea level rise, at Ostend, the water elevations at high tide are expected to increase by up to 6.6 cm (resp. 22.5 cm) for a sea level rise of 85 cm (resp. 295 cm) and to decrease by 6.1 cm (resp. 20.9 cm) for a sea level rise of 85 cm (resp. 295 cm) at low tide.

Pickering et al. (2012) have studied the impact of future sea level rise on tides on the European Shelf. These tides are dominated by semi-diurnal components. Their results indicate that, under a 2 m sea level rise scenario, the changes in the M2 amplitude and in the amphidromic positions lead to a coherent spatial pattern of amplitude change along the shelf. They report in particular a slight north-eastern migration of the southern North Sea amphidrome and a M2 amplitude change of 0.05 m along the Belgian Continental Shelf for 2 m of sea level rise.

The results reported here focus on the impact of sea level rise on water elevations on the Belgian Continental Shelf. The water elevations are computed using the hydrodynamic component of the COHERENS model (Luyten, 2016) and sea level rise is represented by a bathymetric change of the corresponding value. The model is run for a 4 months period (January-April 1979 was chosen as

reference period) with a time resolution of 5 minutes. The spatial resolution is of about 825 m in longitude and 772 m in latitude. In the vertical, the model is run using 20 σ-levels.

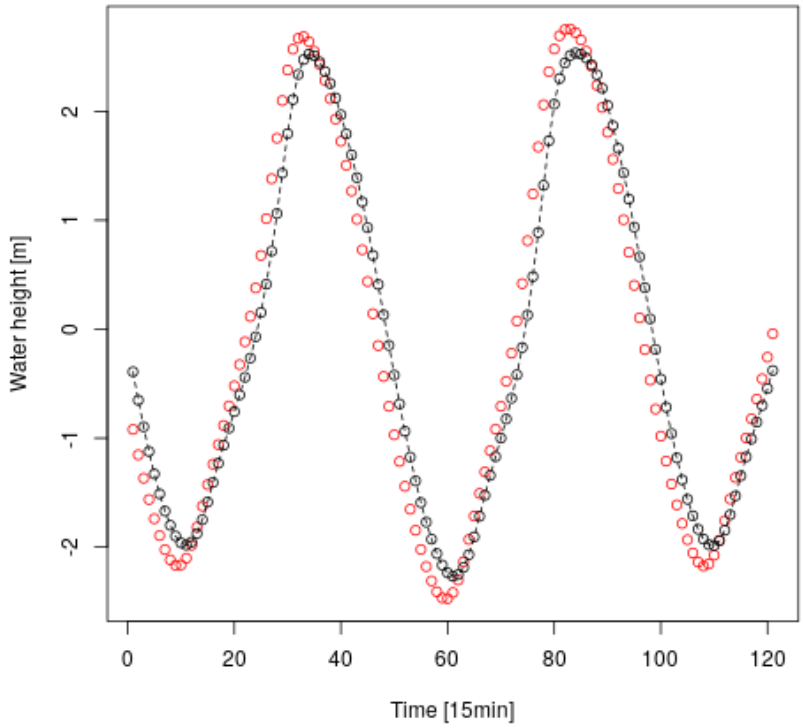

Figure 9: Water elevations at Ostend from the 27th of February 1979 at 9 p.m. till the 1st of March 1979 at 3 a.m., without sea level rise (black) and with a sea level rise of 295 cm (red).

Figure 9 focuses on water elevations around 28 February 1979 without sea level rise and with a sea level rise of 295 cm. Results are plotted with a 15 minutes resolution. The slight temporal shift between the red and the black curve is caused by the change in the position of the amphidrome due to sea level rise.

Sea level rise causes higher high tides and lower low tides in proportion to its value. The differences in water elevations without sea level rise and with a sea level rise of 85 cm are shown on Figure 10 for high tides and on Figure 11 for low tides. The differences in water elevations without sea level rise and with a sea level rise of 295 cm are shown in Figure 12 for high tides and in Figure 13 for low tides.

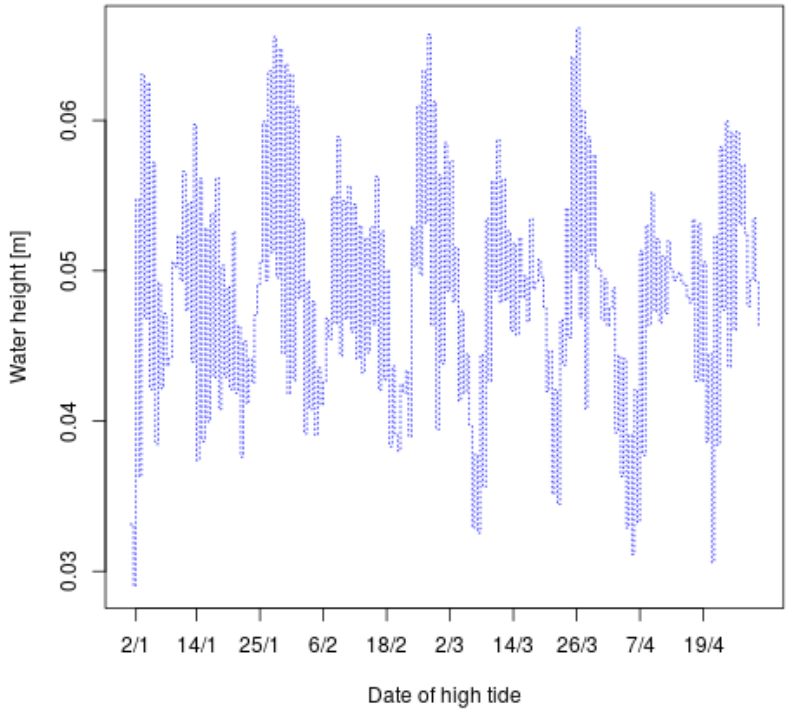

Figure 10: Differences at high tide in water elevation without sea level rise and with a sea level rise of 85 cm.

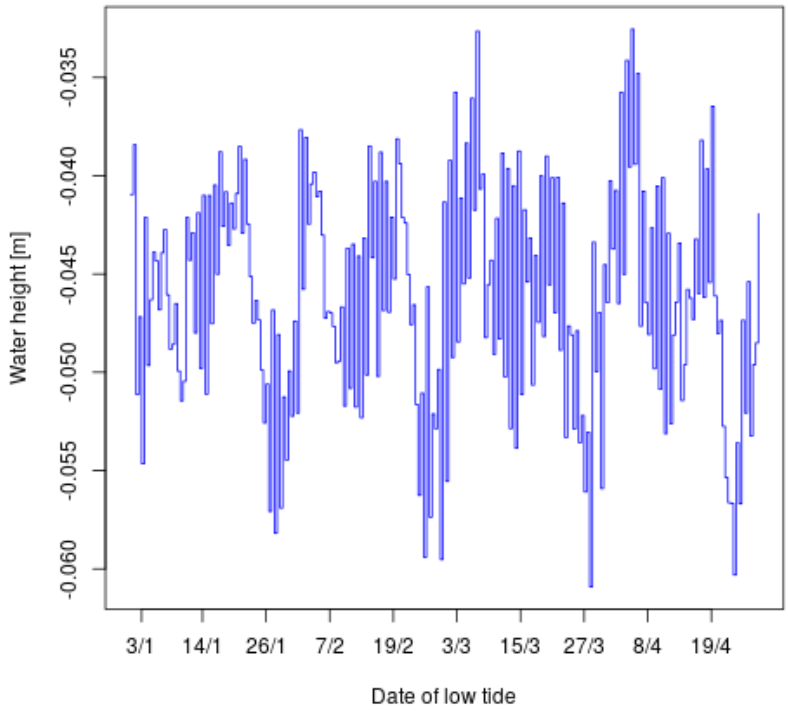

Figure 11: Differences at low tide in water elevation without sea level rise and with a sea level rise of 85 cm.

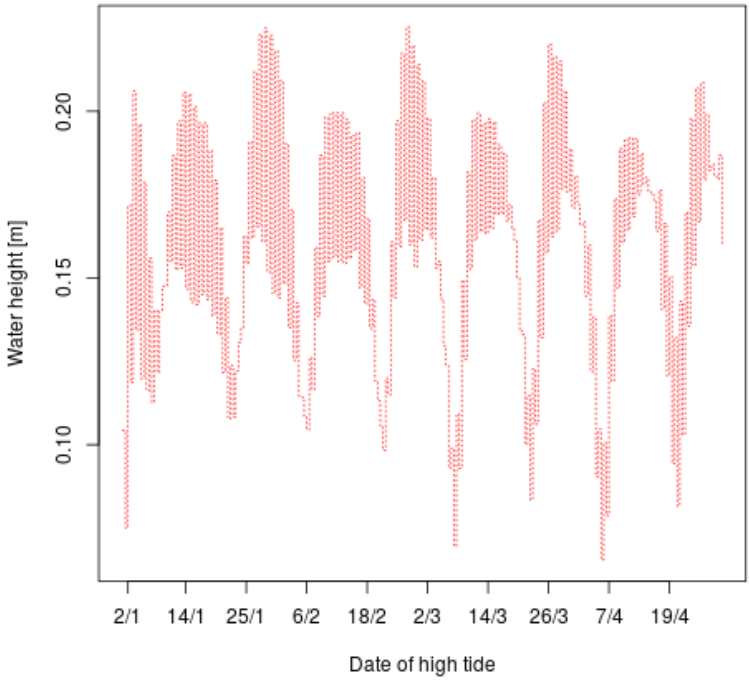

Figure 12: Differences at high tide in water elevation without sea level rise and with a sea level rise of 295 cm.

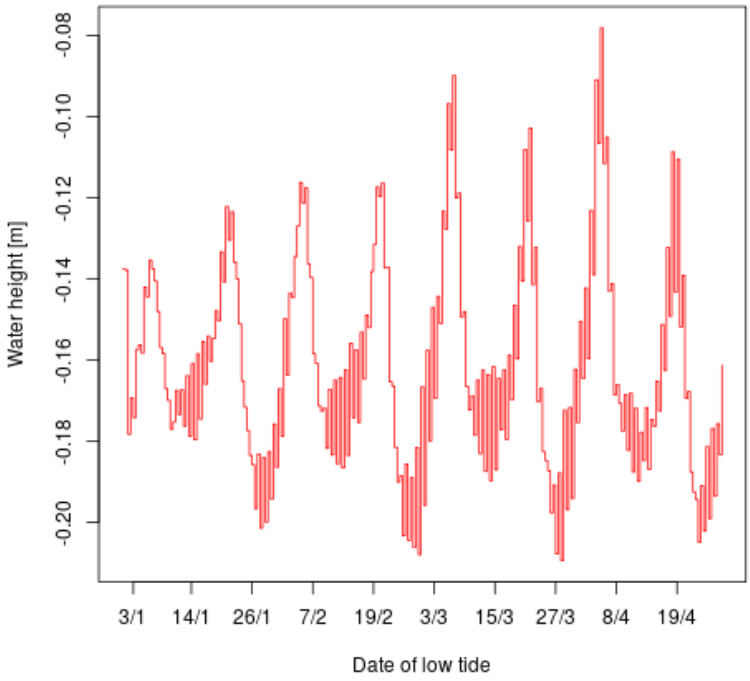

Figure 13: Differences at low tide in water elevation without sea level rise and with a sea level rise of 295 cm.

The maximal change in water elevations at high tide is of 6.6 cm for a sea level rise of 85 cm and of 22.5 cm for a sea level rise of 295 cm. While for low tides, the largest decrease in water elevations is of 6.1 cm for a sea level rise of 85 cm and of 20.9 cm for a sea level rise of 295 cm. This corresponds to a maximal change of the tidal amplitude of about 14 % of the sea level rise value.

THM 1.5 HISTORICAL COASTLINE EVOLUTION

During the last four centuries, the Flemish coast straightened under the combined influence of human activity and natural evolution, advancing in the southwest area, retreating in the central area and both advancing and retreating in the northeast area.

Predicting the coastal evolution was always an objective for the coastal scientist. Usually, complex monitoring programs, tools and methods are employed to predict this evolution. However, the observation of the past evolution of the coast could provide valuable insight on its future behavior at century time scale. The Flemish coast is a good example since many historical maps exist for this area, where also human influence on coastal morphology can be traced back to the 11th century.

Approximately 40 maps were considered for the investigation and amongst them, 20 maps provide relatively reliable information regarding the shoreline position variation in the last four centuries. The oldest map used in the study is the Mercator map (1540, Figure 14) while the most recent set of maps used was realized in 2010.

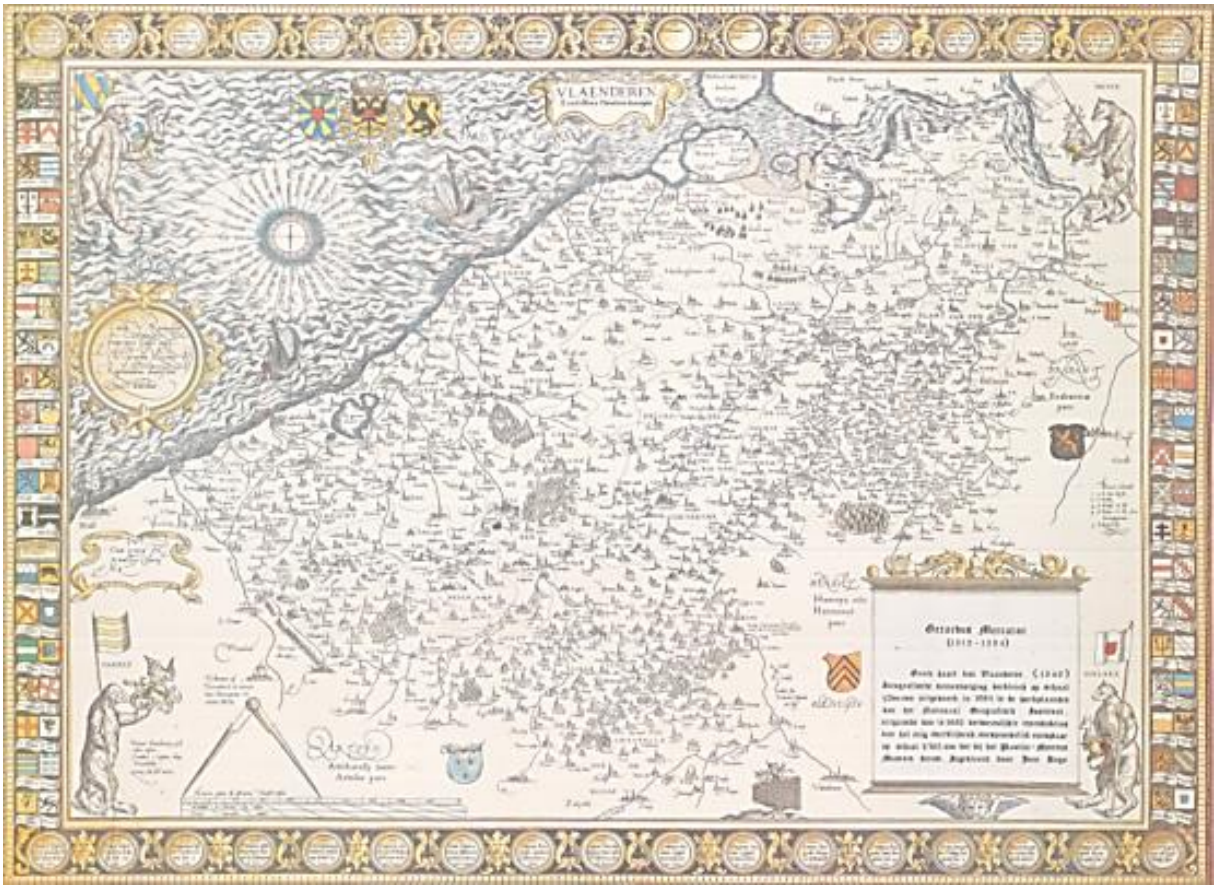

Figure 14: The Mercator map of Flanders in 1540.

In Figure 15 the position of the coastline for seven moments is presented:

- At the year 1540 the shoreline position in respect of the present day was more advanced in the area of Ostend, more inland in the area of Nieuwpoort to De Panne, a similar position in the area De Haan – Zeebrugge and more inland in the area of Zwin inlet (due to the larger extent of this inlet). In fact these tidal inlets were more numerous in the past and they were closed and drained by a combination of human activities and natural processes.
- In 1640, a hundred years later, the situation is different, and the trends of the coastal evolution start to be similar to the present day situation.
- In 1743 the shoreline continues to straighten, but it can be noticed that a considerable advancement in the northeastern part took place, probably due to the presence of a sand bank which had emerged at low tide when the measurements were carried out.
- The first modern map of the coast was made in 1842. This is the moment when the Flemish coast took the position and the orientation which we see in the present day.
- The shoreline positions for the years 1911, 1981-1994 and 2010 are very similar, except for the extension of the harbour of Zeebrugge which increased in surface and offshore extension especially during the 20th century.

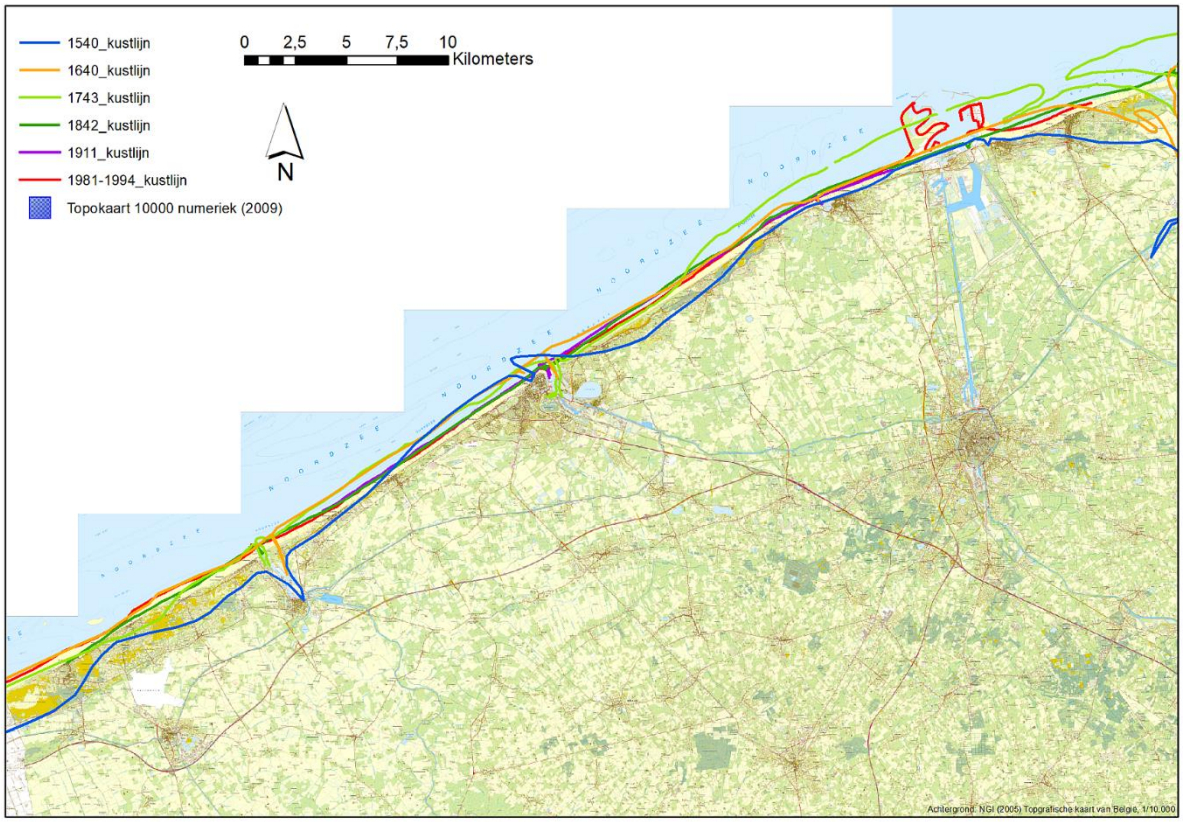

Figure 15: The coastline evolution between 1540 and 2010.

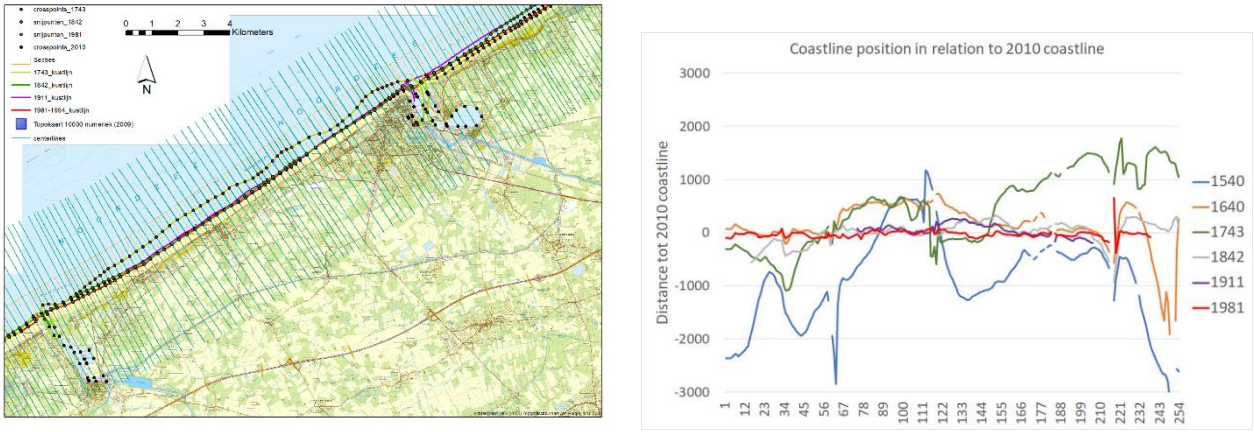

Figure 16: Quantitative evolution of the shoreline.

The shoreline position was quantified using profiles for each of the 255 beach sections (Figure 16). The variation in position are up to 2 and even 3 km respect to present day position for the areas of Oostende, De Panne and Zwin. As expected, the older maps (before 1842) have less precision than the more recent ones (after 1842), so an absolute number of metres for the shoreline position variation is difficult to indicate. Written historic sources indicate that changes near De Panne and in the area just east of Oostende was much smaller than seemingly indicated by the maps. The reason of the large displacement is locally poor rubbersheeting due to a lack of sufficient control points. However, the patterns for the general evolution of the coast are clear.

In can be concluded that in the last four centuries, the Flemish coast became relatively straight with significant advancement in the southwestern area (De Panne – Nieuwpoort), retreat in the central area (Oostende and the vicinities), initial retreat and relative stability for the area De Haan - Zeebrugge and advancement northeast of Zeebrugge due to the sedimentation of the Zwin tidal inlet.

THM 1.6 NATURAL FEEDING

In the past 30 years, the natural sediment supply in the active zone of the Belgian coast was of the same order of magnitude (0.5 million cubic metre per year) as the artificial supply by means of nourishments. The natural supply is the result of cross-shore transport from the offshore towards the coastline. Detailed understanding in the driving mechanisms is still lacking.

The trend of the bulk sediment volume of the entire Belgian coast was determined, taking into account artificial inputs and outputs. The trend is calculated from a time series of volumes, obtained from topographical and bathymetrical surveys.

Annual surveys of the beach and nearshore zone of the Belgian coast are available for at least the last three decades. These surveys describe the topography and bathymetry of the coastal zone, which runs from the dune front or sea dike to 1500 m offshore, covering the entire 65 km long coastline. Taking subsequent surveys, bulk sediment volume differences can be derived. Further,

a database of placed and removed sediment volumes is available, containing the figures for nourishments and dredging operations.

Both measured and artificial volume changes are summed over the entire coast, determining the linear trend. It is assumed that the observed trend is the linear sum of both natural and artificial sediment input, thus these contributions are independent.

It was concluded (Figure 17) that the trend of observed volumes (1.0 Mm^3 per year) is twice the trend of net artificial input of sediments (0.5 Mm^3 per year). Additional information can be found in Montreuil *et al.*, 2019.

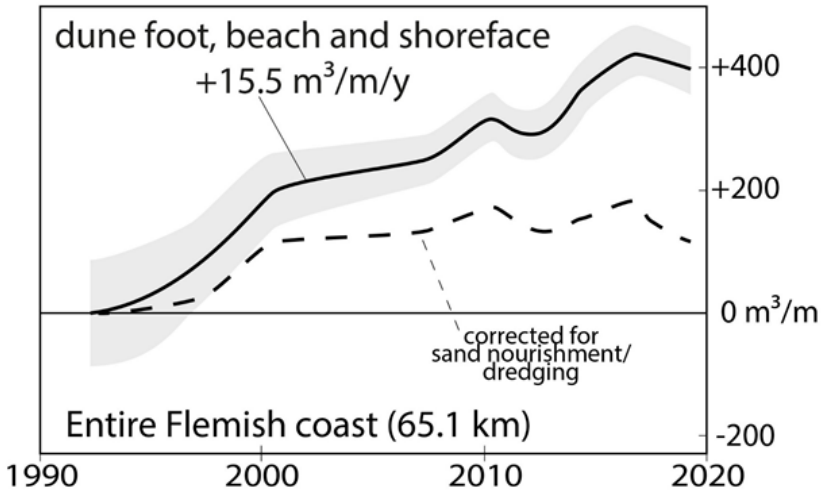

Figure 17: Volume change of the morphologically active zone, relative to the first survey.

THM 1.7 NATURAL RESILIENCE TO SEA LEVEL RISE

In the past 30 years, the natural sea defences at the western and eastern parts of the Belgian coast have heightened more (10 to 30 mm per year) than sea level rise (2 to 3 mm per year), while the central part naturally loses sand (loss of 2 to 8 mm per year). The western and eastern parts thus show a certain natural resilience to sea level rise contributing to the soft coastal defence. Climate change induced coastline retreat can be partly compensated by natural feeding.

The Belgian coast is divided into five zones for which the volumetric trend is determined, taking into account artificial sediment supply. These zones roughly follow the large-scale morphology.

For each zone the observed and natural volumes are calculated. These volumetric trends are compared to the current rate of sea level rise. If the natural sediment supply exceeds sea level rise, that coastal zone is considered resilient (Figure 18).

Only the morphologically active area is taken into account, namely all areas above -4.11 m TAW. Furthermore, the analysis is restricted to the monitoring area (blue outline in Figure 18).

To compare the volumetric trend to the rate of sea level rise, volumes were scaled to the morphologically active area. Thus obtaining the average rate bed-level change per zone.

The central part of the Belgian coast, from Nieuwpoort to Wenduine, shows a natural loss of sediments. Nourishments are required here to maintain coastal safety and compensate for sea level rise. The western zone from France to Nieuwpoort shows a natural input of sediments.

The areas close to Zeebrugge show very strong accretion, induced by the large breakwaters. Combined effects of wave shadowing, tidal current deviations and blockage of longshore drift cause enormous accretion rates up to several kilometres from the breakwaters. It must be noted that the presented figures are an average per zone; local conditions may deviate significantly from the average. The sediment increase contributes to the natural sea defences. Natural dunes actually gain sediment everywhere along the coast, regardless of their location, making them resilient to sea level rise. Sea dikes do not have this ability, nor have dunes with a dune foot revetment.

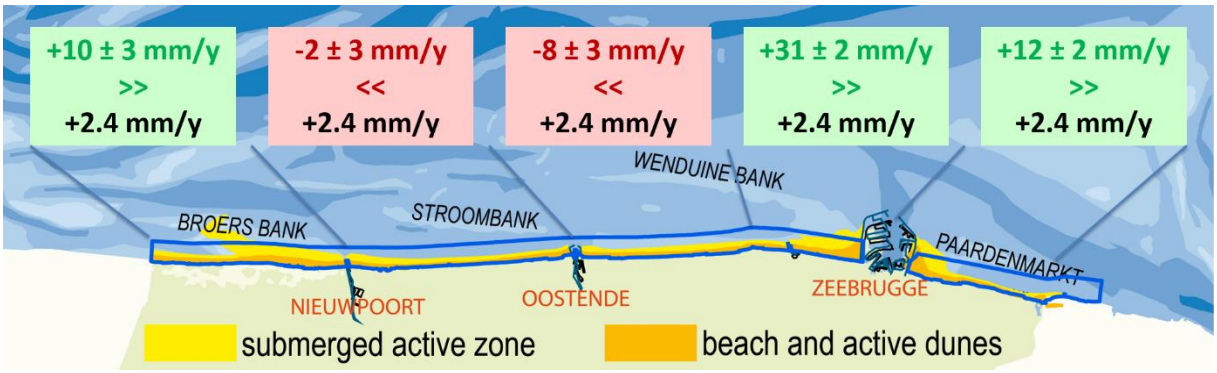

Figure 18: Trend of natural sediment supply for different zones along the Belgian coast.

Uncertainty on the linear trend was estimated through the 95% confidence interval of the estimated trend. Additional information can be found in Montreuil *et al.*, 2019.

THM 1.8 EFFECT OF STORMS IN DECADAL MORPHOLOGICAL EVOLUTION

One-off events, like a storm, show little or no impact in the decadal beach volume morphological time series. Although not seen over the last decades, this does not exclude that extreme events could have a devastating impact.

Storms are known to have an impact on beach morphology. Storms can erode the upper beach and dune front, transporting the sediments further offshore. This is mostly a cross-shore orientated process, however obliquely incident waves also transport sediment alongshore.

On the other hand, calm weather conditions give rise to onshore sediment transport, rebuilding the upper beach with offshore sediments. Several months of average to calm conditions can restore the pre-storm coastal profile.

In time series of volume changes, based on bi-annual surveys, effects of individual storms are not notably present. On the one hand, surveys within weeks after a storm are rare. On the other hand, the effect of a storm on the total sediment volume is rather limited as sand is only displaced. Both aspects make that storm effects are damped out and therefore not visible in the time series. Actual beach profiles are needed to quantify the impact of storms on coastal morphology.

Assessment of storm impact on coastal morphology has been an open question for the Belgian coast. Morphological impact on the time-scale of years may be derived from (bi-)annual surveys. Time series of coastal volume changes are available for at least the last three decades along the whole coast, making it the longest available dataset of coastal morphology in Belgium. Additional information can be found in Montreuil *et al.*, 2019.

THM 1.9 EFFECT OF NOURISHMENTS IN DECADAL MORPHOLOGICAL EVOLUTION

The increased replenishment efforts of the past years have realised permanently wider beaches on nourishment locations. Like with all beach nourishments, erosion rates increase initially, yet after a few years return to the long-term average. The wider beaches enhance the coastal safety level, the touristic use and resilience with respect to sea level rise.

Nourishments put additional sediments into the coastal system to enhance coastal safety or recreation. However, these nourishments also bring the coastal profile out of equilibrium. Natural forcing by waves, currents and wind will eventually create a new equilibrium. The further from equilibrium, the faster the coastal profile will adapt, hence erosion rates are temporarily higher.

Nourishments are also used to realise a permanent seaward extension of the coastline, for instance in Oostende (2004), De Haan (1995) and Knokke (1979). Initial losses are high, yet these beaches are still wider than before these projects were performed, enhancing coastal safety and facilitating touristic use. Figure 19 shows the example of temporarily stronger erosion at De Haan after the nourishment executed in 1995. Additional information can be found in Montreuil *et al.*, 2019.

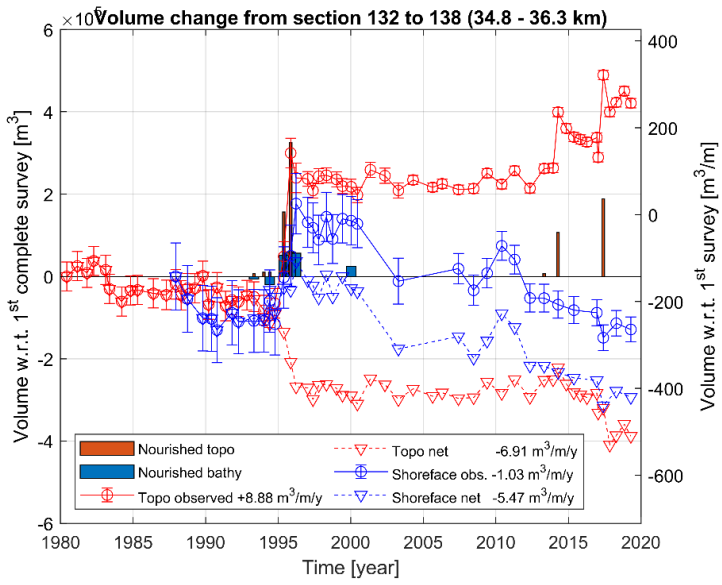

Figure 19: Effects of large-scale nourishments on the volumetric trend. After each nourishment, erosion is temporarily stronger.

THM 1.10 DIGITISATION OF OLD MORPHOLOGICAL DATA

Over 50 historical elevation maps and over 500 beach profiles of Belgian coast were digitized and made available within CREST project. These have already proven valuable to study the difference in response of different types of beaches to sea level rise and storminess over more than 30 years.

As part of the data archaeology effort within the CREST project, four historical beach elevation datasets were digitized and made available in different formats.

Type	Height maps	Beach profiles	Beach profiles	Beach profiles
Source	Coastal Division	Coastal Division	Prof. De Moor	Coastal Division (derived from height maps)
Time period	1983-1996	1971-1983	1979-1996	1983-1996
Location	Study areas: Mariakerke West-Groenendijk Nature reserve Westhoek	Kilometre markers along the Belgian coast	Kilometre markers and points in between (every 500 m) along the Belgian coast	Study areas: Mariakerke West-Groenendijk Nature reserve Westhoek, at kilometre markers
Availability	Geoviewer CREST website Web services VLIZ	RShiny app CREST website (MDA)	RShiny app CREST website (MDA)	RShiny app CREST website (MDA)

Table 2: Overview digitized historical beach elevation datasets.

Accurate elevation data of the coastal area is indispensable in order to assess storm-related impacts and identify long-term trends of coastal morphology. The CREST project intends to open up historical datasets as these provide crucial baseline information for comparison with current and future assessments of the coastal environment. Two types of historical datasets were selected to that effect: (1) height maps created by aerial photogrammetry in four selected areas (period 1983-1996) and (2) a series of beach profiles that cover the entirety of the Belgian coast (period 1971-1996).

- The height maps were digitized by Flanders Marine Institute. The contour lines were vectorised from these height maps as line features using QuantumGIS. Breakwaters, buildings and other features were disregarded during this process. Each line feature was given the following attributes: the height value in metres and centimetres, the data acquisition date as provided on the original maps and remarks concerning the vectorization process. A thorough quality control was performed afterwards. Furthermore, the data was interpolated in order to create Digital Elevation Models (DEMs) and calculate height difference maps to indicate differences over the years. The datasets and derived products

can be consulted in the geoviewer on the CREST website, or visualised and downloaded using the VLIZ webservices (WMS, WFS, WCS) from the VLIZ Geoserver (http://geo.vliz.be).

- The beach profiles were digitized by the Flanders Marine Institute (VLIZ) and Ghent University. VLIZ digitized the beach profiles provided by Coastal Division, Ghent University digitized the beach profiles provided by professor De Moor. As a lot of the metadata describing these datasets is missing, the quality control of these datasets is still ongoing. These datasets are being made available through an RShiny application on the CREST website, where users can visualise them in different ways (e.g. data availability, envelopes…).

The digitizing effort for the height maps has been finished within the project. The beach profiles are still subject to a thorough quality control, both by its originators as by VLIZ. More information on the metadata can be found in De Hauwere *et al.* (2017).

THM 1.11 DOCUMENTING DATA

Your data and research methodology might be invaluable for future researchers, document them well.

Data management in science is gaining more and more attention. This is among others exemplified by the grant application process for Research Foundation Flanders (FWO), where having a solid data management plan is a key requirement for the applicant since 2018, or the set-up of a Research Data Management team with data stewards at Ghent University in 2019.

Nowadays, opening up data (e.g. by creating a DOI for the dataset), setting up a data management plan or adhering to the FAIR principles (i.e. making data findable, accessible, interoperable and reusable) is becoming increasingly important in data management practices and the scientific publication process. To that effect, researchers within the CREST project are encouraged to disclose their (meta)data using IMIS (Integrated Marine Information System, managed by VLIZ) and MDA (Marine Data Archive, managed by VLIZ) or similar (meta)data repositories. The metadata is also provided on the CREST website, along with metadata for other datasets relevant to the project. In this way, over 40 relevant datasets are being documented in IMIS and over 6.5 GB of data is stored in MDA.

Moreover, when scientific data adheres to the FAIR standards, datasets that have been gathered once can be reused several times and other researchers, as well as the general public, can benefit from them. These FAIR Data Principles were introduced in 2016 in a publication by a consortium of scientists and organisations (Wilkinson et al., 2016) and have since gained in importance. The European Commission estimates the minimum cost for the EU of not having FAIR research data is about € 10.2 billion per year (European Commission, 2018).

Historical datasets can be equally relevant, as they are indispensable to understand current and future trends. They are however often stored on paper, encrypted in now obsolete media or formats and/or do not meet the FAIR standards. In order to make them available to a broader audience, two types of historical datasets, that were relevant for the CREST project and otherwise at risk of being lost, were selected to be digitized within the project: (1) height maps created by aerial photogrammetry in four selected areas (period 1983-1996) and (2) a series of beach profiles

that cover the entirety of the Belgian coast (period 1971-1996). As metadata for these datasets was hard to find and people involved in the creation of these datasets did not remember specific details concerning the acquisition process or location of metadata, the importance of meeting the FAIR standards was once more stressed. The digitized data have already proven useful within the CREST project for the comparison of the reaction of a man-made and natural beach to storm impacts.

More information on the metadata can be found in De Hauwere *et al.* (2017).

THM 1.12 INCREASING THE ACCURACY OF BATHYMETRIC MONITORING

The uncertainty on the bathymetric surveys has a large impact on the accuracy of the observations. It can be reduced by performing independent terrestrial control measurements of the low-tide area immediately following echo sounding.

The submerged part of the shore is the base of the coastal barrier and plays a very important role as a sand supply path, a temporal storage place of sand eroded from the beach and a diffuser of wave and flow energy. Though the introduction of new and more accurate positioning systems resulted in better quality surveys, bathymetric echosounding surveys still come with an error on the absolute depth that exceeds the error on absolute elevation obtained by airborne LIDAR by a factor of 3 to 4. Given the large area of the submerged part of the morphological monitoring surveys, often 4 to 5 times the emerged part, the uncertainty effect on volumes and sediment budgets is even multiplied. The result is that in many stretches and zones of the Flemish coast, all of the observed variation trough time of the nearshore volume is often of the same order of magnitude as the uncertainty of the volumes.

As most of the uncertainty arises from converting actual measured depths to absolute datum, it is recommended to perform immediately after each survey mission an independent terrestrial survey in a small area around the low-water mark on the same day, during the first low tide after the bathymetric survey, in the area of overlap. In order to make this work in practice, a reporting obligation of actually performing a bathymetric survey should be imposed in the specifications of the survey mission. The hydrographic authority can then send out an independent surveyor. His small survey can be used for vertically checking the bathymetry results of that day and fitting them to the height datum.

A further specification to bathymetric survey should be that two or three survey lines at the edge of the previously surveyed area should be carried out again. This small overlap would allow corrections between adjoining survey areas.

The execution of a complete survey of the Flemish coast nearshore bathymetry takes 8 days. There may be several weeks between the survey days, as conditions for survey should be optimal.

It is observed that bathymetric surveys done during a particular survey day display a good internal morphological coherence. However, surveys done on different survey days show as clear, artificial breaks in many difference maps (Figure 20). It is also observed that some surveys result in a sea bottom model that is substantially deeper or shallower than that of several previous and

succeeding surveys (i.e., the model is an outlier in the time series of models). In depth difference maps between successive surveys, this effect emerges by this outlier survey showing a relatively important bathymetric change that is annihilated in the next difference map.

The proposed small overlap between areas covered at successive survey days will help to better adjust the models at their side borders.

The proposed terrestrial surveys are a low-cost way for independent control on the absolute elevation of a small area near the low-water mark that was also covered in the bathymetric survey of the preceding high tide. They will allow to perform simple vertical corrections to the bathymetric results. They may even lead to a better insight in the process of depth reduction to datum and may result in improved procedures to carry out the reduction.

More information can be found in Houthuys *et al.* (2019).

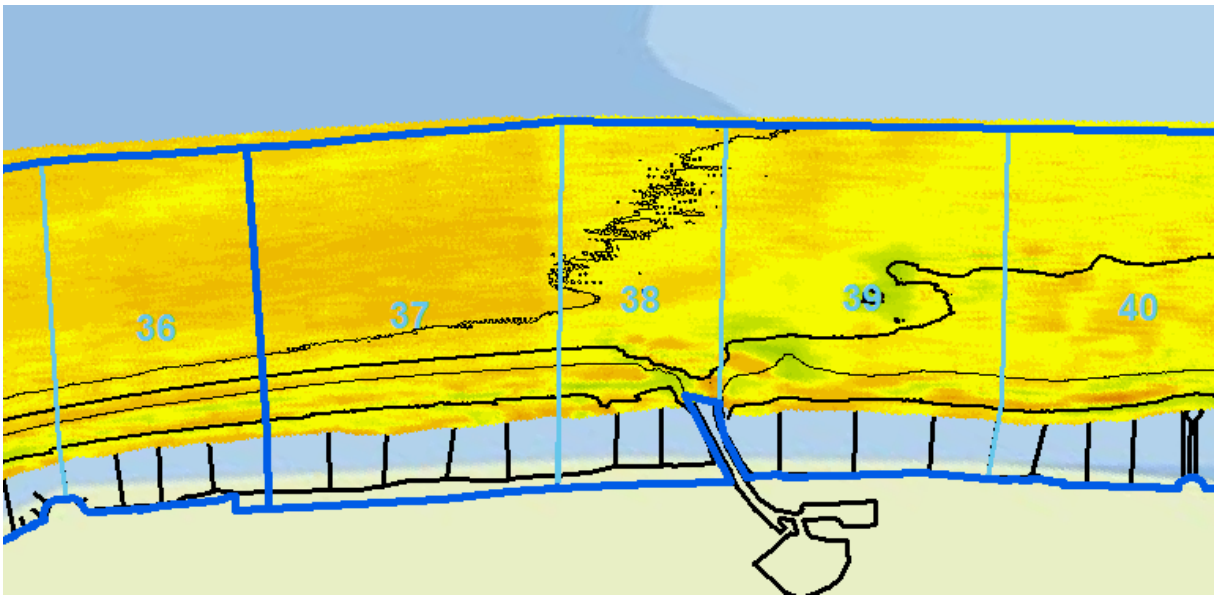

Figure 20: Depth difference map between bathymetric nearshore survey Spring/Summer 2018 and Spring/Summer 2019. Orange = erosion, green = sedimentation; legend in metres. Note coast parallel edge in elevation difference model near the boundary of stretches 37 and 38 between Wenduine and Blankenberge; this edge represents an average elevation step of 15 cm.

THM 1.13 DOCUMENTING SAND WORKS

The human interventions (dredging in navigation channels, beach nourishments and local interventions by municipalities) should be kept in a well-structured database in relation to the morphological monitoring.

Morphological survey volumes are determined inside closed areas, named sections, with fixed boundaries. Neighbouring sections with a comparable morphological evolution are grouped in "stretches". Volumes are determined for each LIDAR survey flight, which covers the emerged part of the beach and the neighbouring dunes, and for each echosounding survey of the submerged part of the beach (the nearshore). While both types of survey are intended to be performed on

about the same date, they are in reality often separated by several weeks. Most often, the start and end date of human interventions, such as beach nourishment, differs from the survey dates; often a survey is done while the replenishment works are still going on. On the other hand, fresh erosion may occur after the completion of a nourishment but before the first survey after the works. The areas where activities are going on, don't often coincide with section or stretch boundaries. Therefore, even if the amount of supplied or removed sand has well been reported, assumptions have to be made both in time and space to distribute reported nourished or removed volumes over the volume time series. These assumptions can be avoided if reporting of human interventions keep well track of work dates and precise areas, and document well the way in which volumes are determined.

For most nourishment operations, before and after nourishment profiles or surveys are available as well as the timeframe of the proceedings. These surveys should be well stored in relation to the morphological survey database.

For dredging operations, use can be made of either volumes determined from before and after operations-echosounding surveys, or the records of the dredging operations stored in the dredging information system. Some research should first be conducted in order to study the availability and relation between both types of reporting. Extracting volume data from the dredging information database relevant for morphological evolution studies would require investing in developing an interface that would allow such queries.

When interpreting morphological trends and making sediment budget analyses, the volumes per coastal stretch are "corrected" for known volumes of sand added or borrowed from the area. If this is done for all available surveys of the past decades, this approach allows to make estimates of the "natural" or "autonomous" morphological behaviour of the coast, i.e. what would have happened if no sand nourishments or sand removals would have taken place?

Records have been kept of various replenishment and dredging works through time. The format, geographical delimitation of the reporting areas and time slicing of reporting periods show much variation. Also, the detail and accuracy of reported volumes is highly variable.

Nevertheless, accurate reporting is needed in order to study the influence of works on the local and regional morphological changes. The study of the morphological impact of nourishments and dredging is not only necessary for understanding the dynamic behaviour of the morphology, but can also contribute to carry out such operations in an economically more efficient and ecologically less disruptive manner.

THM 1.14 EXTENDING THE BATHYMETRIC MONITORING?

In order to study the morphological relationship between the off-shore and the active coastal zone, the surveyed area should be extended seaward.

Extensions of the yearly nearshore surveys are proposed in order to better understand and predict the evolution of the area, as well as the role of interactions to the active coastal zone.

It is proposed to enlarge the extent of the yearly singlebeam echosounding surveys of the nearshore area. For a few areas where the active zone extends beyond the seaward boundary of the current survey area, a box-like extension is proposed. Another evolution of concern is the tidal gully Grote Rede near Wenduine, where consistent erosion is observed over the last decades. Surveying these areas in the same way as the existing nearshore survey programme, will allow to calculate volumes in a manner analogous to the processing of the nearshore but incorporating active areas that are in relation to the coastal system.

In addition, knowledge of elementary morphological change of the offshore area beyond the regular survey area is needed in order to document long-term trends and exchanges from and to the nearshore. Here, a profile method would yield reliable results without impacting too heavily on the operational facilities of the existing monitoring program. It is recommended to perform at each proposed location two parallel survey lines with a separation of 100 m. Surveys don't follow exactly the planned lines. By performing two parallel lines, it would be possible to interpolate the depth on a fixed line situated between the two lines using triangular irregular network interpolation. In that way, surveys can reliably be compared from year to year on that interpolated line.

The proposed areas and long lines are considered additional to the existing survey area, in which monitoring should be continued.

The proposed areal extensions are (Figure 21):

1. Broers Bank, extension situated off sections 22 to 34, about 1 km cross-shore and 2.9 km alongshore. Area 2.9 km².
2. Wenduine, the erosional channel at the bend in the coastline, extension situated off sections 161 to 176, about 1.65 km cross-shore and 3.6 km alongshore. Area 5.94 km².
3. Blankenberge-Zeebrugge, accretion area west of Zeebrugge, extension situated off sections 190 to 216, about 1.5 km cross-shore and 4 km alongshore. Area 6 km².
4. Heist-Knokke, accretion area west of Zeebrugge, extension situated off sections 219 to 232, about 1 km cross-shore and 3.5 km alongshore. Area 3.5 km².

The proposed long survey lines are (outside the existing and extended survey areas):

1. In section 8 (line 5): 4 km across Trapegeer – Westdiep.
2. In section 24, Sint-Idesbald (line 6): 3 km, across Trapegeer – Westdiep.
3. In section 91, Middelkerke-Oost (line 7): 4 km across Kleine Rede – Stroombank – Grote Rede.
4. In section 172, rotonde Wenduine (line 8): 4.5 km, across Grote Rede – Wenduine Bank – de Poortjes.
5. In section 238, Knokke (line 9): 5 km across Paardenmarkt unto Scheur.

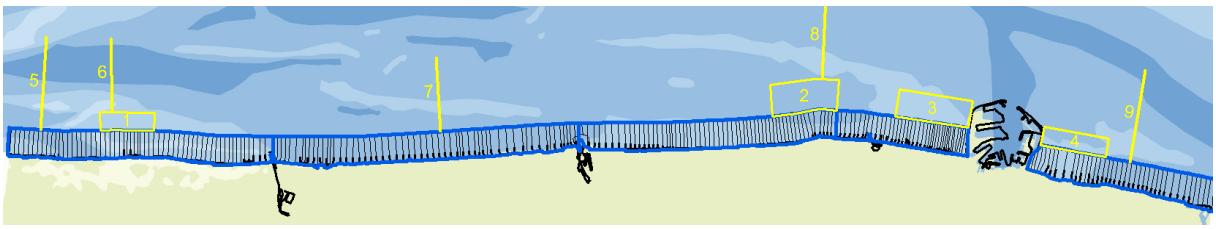

Figure 21: Present survey area (blue outline) and proposal of extended survey area and long profiles (yellow), allowing the study of morphological exchanges between the offshore and shoreface.

At Koksijde (Broers Bank), the active zone is wider than the actual 1.5 km survey area. Some parts of Broers Bank emerge at MLLW. The most seaward part is situated outside the regular survey area. Previous, less frequent surveys have shown the area is highly dynamic. Near Zeebrugge, at both sides of the breakwaters built in 1980-1986, the active zone has accreted so that it now extends beyond the seaward boundaries of the survey area. At Wenduine, the constant deepening of the Grote Rede will pose an extra threat to the future stability of the coastal barrier.

At other locations, long bathymetric profiles would allow to study elementary morphological change of the sandbanks and channels near the coast. This survey type will start to show morphological trends after well persisting the monitoring effort, as morphological change is expected to be small. The locations have been selected at highly dynamic sites, at sites that may be essential in understanding the relation between offshore and nearshore dynamics, and at a site where the present evolution raises some concern about the future stability of the coastal barrier.

Additionally, the following remarks on the morphological monitoring program have been raised. Multibeam (MB) surveys provide excellent images of the detailed morphology. However, performing a MB survey in the shallow nearshore requires sailing at closely spaced tracks. In order to cover the entire coast, a MB survey would require an estimated 10-fold increase of survey time (and thus cost) when compared with the present-day practice of using singlebeam (SB) echosounding. The profit in obtaining accurate sand balances at the level of sections, stretches and zones would probably be marginal. It is therefore recommended to continue using SB survey methods, as the benefit of having regular and complete surveys prevails in this case on having surface detail. Only in focus areas such as at the site of submerged nourishments or dynamic areas like Broers Bank with a varied surface morphology, occasional additional MB surveys are useful.

Furthermore, in order to capture the seasonal variation of nearshore morphology, the survey capacity would have to be increased substantially. The latest spring nearshore surveys had a lower priority than some navigation-related surveys. They caused the routine surveys to be carried out later, so that the spring survey was actually only complete in mid-summer.

Seasonal effects could be interesting in relation to beach and shoreface nourishments. While surveys twice a year in areas affected by nourishments would certainly provide relevant information, having the once-a-year spring survey is nothing less than a basic necessity. Having an autumn survey would certainly be beneficial to our knowledge of the coastal system, but it is secondary to having at least a good spring coverage.

THEME 2
MORPHODYNAMICS ON TIME SCALE OF DAYS (STORMS) TO YEARS (LIFETIME OF NOURISHMENTS) FOR THE TWO PILOT AREAS MARIAKERKE AND KOKSIJDE

THM 2.1 STATIC TERRESTRIAL LASER SCAN

Permanent static terrestrial laser scanning of the dry and intertidal beach yields vertical accuracies < 2 cm and permits very time intensive scanning.

Earlier research states the potential of permanent long-range terrestrial laser scanning for continuous monitoring of coastal dynamics (Vos *et al.*,2017). A similar methodology as Vos *et al.* (2017) was implemented at the North Sea beach in Mariakerke (Ostend, Belgium). A Riegl VZ-2000 Permanent Static Terrestrial Laser Scanner (PLS), mounted on a 42 m high building, scanned the intertidal and dry beach in a test zone of ca. 200 m wide on an hourly basis over a time period of one year. It appeared that the laser scanner cannot be assumed to have a fixed zenith for each hourly scan. The scanner compensator measured a variable deviation of the Z-axis of more than 3.00 mrad. This results in a deviation of ca. 900 mm near the low water line.

The deviation of the vertical axis of the scanner required the development of a robust and automated calibration procedure to correct both the hourly and fixed deviations of the scanner's Z-axis. The variables of the problem are the inclination of the Z-axis in two different preferably independent directions.

The actual calibration procedure is done by making a 2.5D terrain model of each static scan and registering it to a 'truth' set of reference points. The robustness of the alignment implies that the calibration procedure must approximate the following ideal situation:

- independent of the model used and the parameters applied to build the model;
- independent of the truth set of reference points;
- independent of the outlier elimination strategy.

MODEL SELECTION

For the scan-based model, two main approaches were used:

- Triangulated Irregular Network (TIN) or mesh modelling: Delaunay 2.5D triangulation within the convex hull. If an unlimited maximum length for the triangle edges is given, then all triangles output by the triangulation will be kept. Specifying a maximum edge length as parameter allows to remove the biggest triangles that are not necessarily meaningful.
- Grid modelling: the height of each grid cell is computed by averaging the elevation of all points included in this cell. If a given cell contains no points, this cell will be considered as 'empty'. The cell size is the variable applied parameter.

REFERENCE DATA SELECTION

For the choice of truth, three sets of reference points were available:

- ALS: an airborne LiDAR scan (ALS) – acquired on the same day and time as the static scan – of around one million points with an average point density of around 2 points / m^2.
- RTK-GNSS: a set of 800 RTK-GNSS reference points on the seawall and the groin.

- SfM-MVS: image-based modelling (Structure from Motion-Multi-View Stereo), acquired via an unmanned aerial system (UAS) on the same day and time as the static scan and the LiDAR flight with an average point density of around 350 points / m².

Figure 22 shows the workflow applied. Either a TIN model or a gridded model of the static scan was made. In case of the TIN-approach, the difference between the scan model and the truth set is the height difference between individual points of the reference set and the corresponding triangle of the TIN-model of the scan. In the grid-approach, grids of both the scan and the reference set were made. However, the static scan yields different point densities at the end of the groin compared to the end of the seawall. For this reason, the interval distance for the rasterizing was chosen differently in the seawall zone compared to the groin zone to obtain a balanced calibration set in the x- and y-direction. Next, using a Monte Carlo simulation with multiple rotational values, the difference between the scan model and the reference set is minimized. From an angle of -5 mrad till + 5 mrad, 1001 x-axis rotational values are combined with 1001 y-axis rotational values in steps of 0.01 mrad.

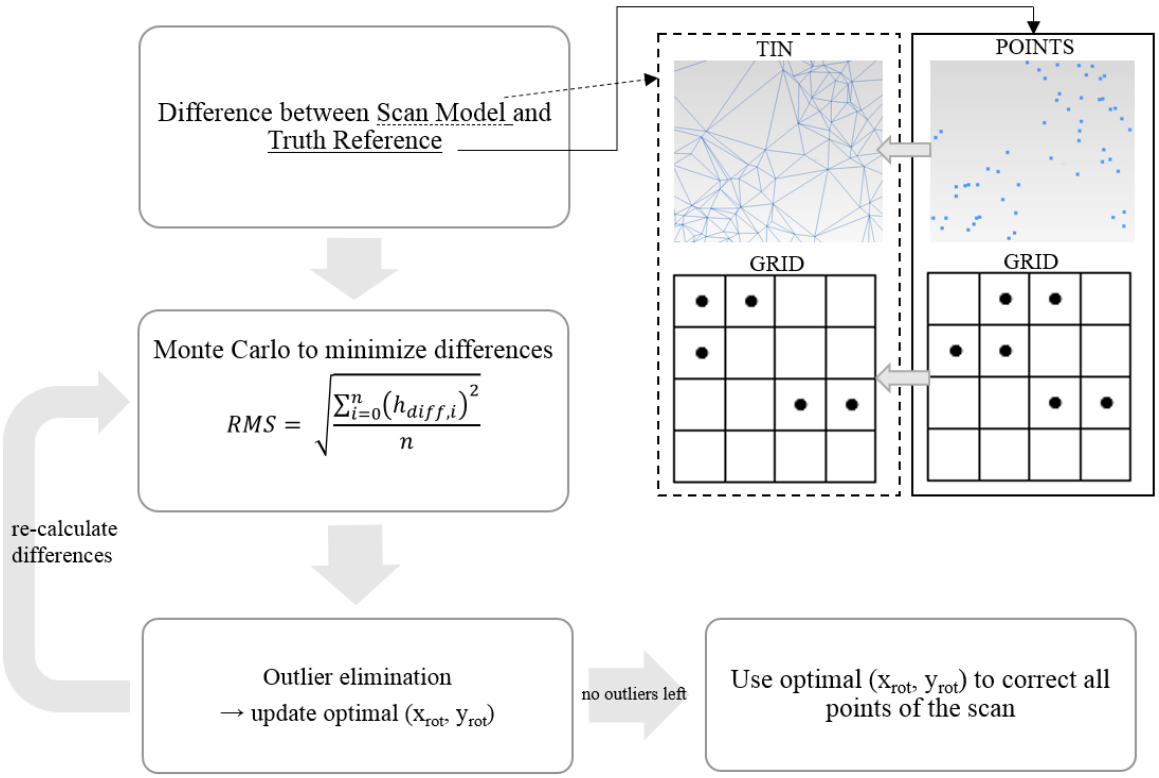

Figure 22: Workflow of the calibration algorithm.

OUTLIER ELIMINATION STRATEGY

Each static scan is expected to contain outliers. The outliers originate mainly from ghosting (e.g. people and obstacles on the seawall and groin that are scanned). These outliers yield elevation values that are significantly higher than the true surface. A severe outlier test is needed but eliminating too many values gives a too optimistic value in terms of calibration quality.

A point *i* of the reference set is an outlier if

$$h_{i,\,diff} \geq \mu_{diff} + (\ldots * \sigma_{diff})$$

with $h_{i,\,diff}$ the difference in elevation between point *i* and the static scan model

μ_{diff}, σ_{diff} the mean and standard deviation of all differenced *h*-values.

Finally, a sigma rule of thumb is applied, considering a width of 2, 2.5 and 3 standard deviations around the mean. After each elimination of outliers, an optimal x- and y-rotation are computed, yielding slightly different values as the reference set was modified in the previous step and subsequently a new outlier test is performed. This iterative process continues till no more outliers are detected. If no more outliers can be detected, all the points of the static scan are corrected with the optimal x- and y-rotation.

The higher the resolution of the grid model, the more accurate the computation of the difference in heights between the static scan model and the reference points. The smaller the cell / edge limit value, the more holes in the model, the less reference points can be interpolated in the model, reducing the quantity and therefore the validity of the difference point set. Overall, the TIN model yields the most means of algebraic differences close to zero, this is thus a good measure of accuracy. The TIN-model (10 m, 5 m, 2 m and unlimited edge size) has the smallest mean of algebraic differences and the smallest RMS and are therefore the most precise (repeatable) models with the smallest random error.

Hence, for further processing, only the TIN-model with 10 m, 5 m, 2 m and unlimited edge size were considered. On the one hand, it can be easily concluded that the ALS truth yields the best overall RMS for all TIN models together (Figure 23A). On the other hand, it shows that the GNSS reference set with 2σ elimination returns a similar RMS. Figure 23B however shows that the outlier removal percentage for 2σ is way higher than 2.5σ with both GNSS and ALS. Moreover, less points available in the reference set reduces the quantity and therefore validity of the calibration.

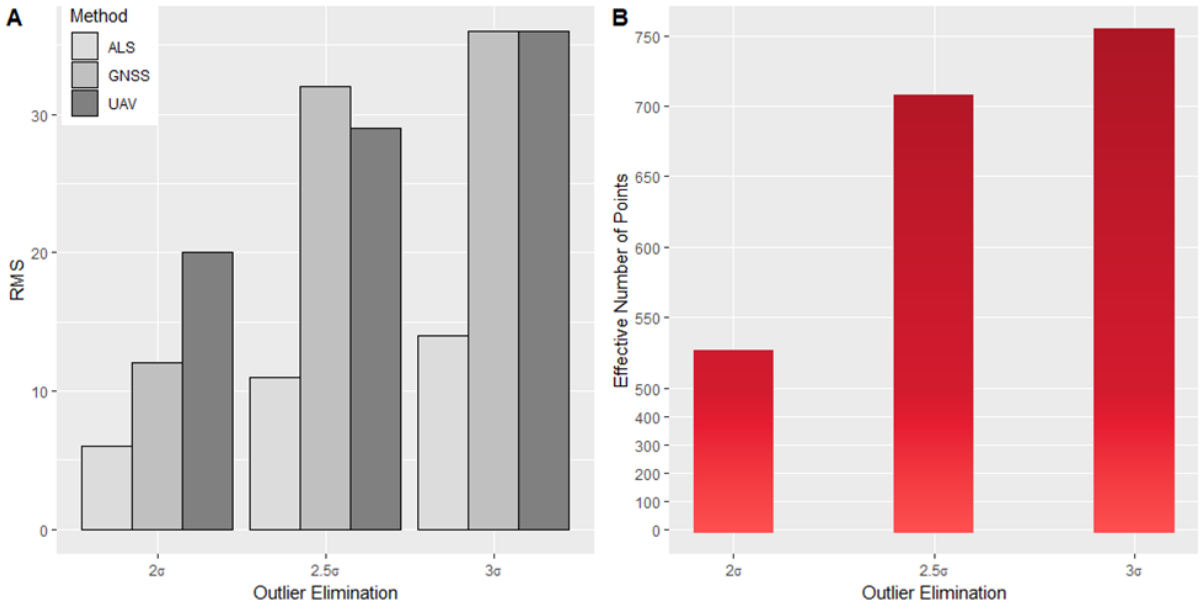

Figure 23: Visualization of RMS as a function of n·sigma per reference set (A) and number of effective points used as a function of n·sigma for the ALS reference set (B).

When looking closer at the results (Table 3) for different edge limit values of the TIN with 2.5σ outlier elimination and ALS truth, several remarks can be made. The applied rotation (in both directions) is more or less the same for all edge limit values. The TINs with smaller edge limit values produce a lower RMS and mean of absolute deviations (MAD) but yield a smaller reference set available for the model interpolation. At the same time, the TINs with bigger edge limit values have less points eliminated, but come with a higher RMS and mean of absolute differences. A TIN with 5 m edge limit value seems to be the middle ground with an RMS of 19 mm, and an accuracy of 15 mm (De Sloover *et al.*, 2019).

Edge Limit Value	Points Used	Mean (mm)	MAD (mm)	RMS (mm)
unlimited	1730	-2	16	21
10 m	1568	-1	15	20
5 m	1493	-1	15	19
2 m	1458	-1	12	16

Table 3: Statistics of the calibration procedure for different TIN sizes.

THM 2.2 MOBILE LIDAR

A special purpose mobile LiDAR vehicle with RTK-GNSS and IMU was developed and gave an absolute accuracy and precision as good as 2 cm, making it a highly accurate and precise technique for topographic monitoring of the intertidal zone at a hyperspatial resolution.

Mobile terrestrial LiDAR technique is a complex real-time, multi-tasking and multi-sensor system, which integrates different devices. A laser scanner, an inertial measurement unit (IMU), an RTK-GNSS receiver and a rugged PC with hydrographic data acquisition software (QINSy), mounted on a special purpose vehicle (SPV) are the main components of the system (Stal *et al.*, 2014). A hybrid accuracy, formed by the root mean squared (RMS) accuracies of the involved individual devices of the system is given below.

The LiDAR (Leica Z&F HDS6100) has a single measurement accuracy of 5 mm over a range between 1 m and 25 m. The RMS of the IMU (Seabed IMU-S2) using RTK-GNSS (Seabed SGR6) amount are 0.035° in true heading, 0.015° in roll and pitch, leading to 0.02 m in planimetric accuracy and 0.03 m in Z direction. The network RTK delivers an accuracy of 2.3 cm in horizontal and 3.4 cm in vertical direction. By cumulating the values above, expected accuracies are 25 mm in planimetry and 35 mm in altimetry within the given range.

Traditionally, the error inherent to mobile laser scanning is divided in multiple components. Systematic errors arise from flaws in the boresight calibration process (Figure 24).

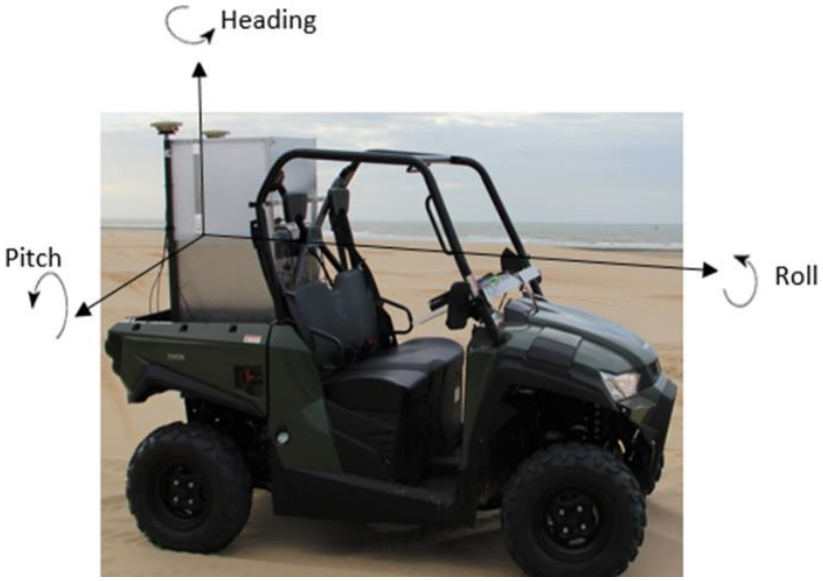

Figure 24: Mounting angle errors of the mobile LiDAR system.

Besides, the quality of the measured point cloud data heavily depends on the incidence angle, range and speed of the multi-sensor platform. Latency (resulting from time errors) is a source for inaccuracies as well. Finally, it should be noted that the network RTK system providing the absolute positioning of the system has a random vertical error of cm-order. Multiple studies have investigated these different components individually. Relative precisions of just 3 mm were achieved for beach surveying with a mobile LiDAR system (Bitenc *et al.*, 2011), while the use of black-and-white targets on a tripod measured with RTK-GNSS precision resulted in a mean vertical bias of -0.104 m (Lim *et al.*, 2013). To the best of the authors' knowledge, only three studies have investigated the absolute vertical accuracy and precision when measuring the actual beach surface with MLS. They are summoned in Table 4.

Author	Validation Points			μ (m)	σ (m)	RMSE (m)	R^2
	Survey Style	Spatial Resolution	Sample Points				
Elsner *et al.* (2018)	Mobile	(5 × 5) m	881	-0.011	0.013	0.113	/
(Donker, Maarseveen, & Ruessink, 2018)	Static	(25 × 5) m	914	0.010	/	0.030	0.99
Spore & Brodie (2017)	Static	?	20	/	0.050	0.099	/

Table 4: Literature review of reported vertical errors in different MLS studies on non-vegetated sandy beaches.

The accuracy assessments mentioned in Table 4 are actually just the measured GNSS elevation of a single observation being compared to the elevation of its closest neighbour in the laser scan point cloud. RMSEs vary from 3 cm to ca. 10 cm while reported vertical biases are in the order of 1 cm (in both directions). Spore & Brodie (2017) use static GNSS points, resulting in an acceptable amount of noise (σ = 5 cm). However, they only use a set of 20 independent check points and they do not mention the spatial distribution of this control set. In contrary, Elsner *et al.* (2018) and

(Donker *et al.*, 2018) use an extremely elaborate set of control points, with a cross-shore spatial resolution of just 5 metres. The difference between them lies in the fact that the former used along-shore mobile mapped GNSS transects (with just 5 metres in between different survey lines), while the latter performed measurements in the cross-shore direction (with 25 m in between transects). It is clear that Donker *et al.* (2018) scores the best in terms of RMSE with a low average systematic error as well. Contrarily to what the title of Donker *et al.* (2018) says, the focus lies not only on the foredune zone, but on the dry beach and intertidal zone as well. Elsner *et al.* (2018), on the other hand, investigate a vast study zone of (150 × 400) m.

In this study, a point-to-model (cloud-to-mesh) approach was applied for the accuracy assessment. The most dense data set (i.e. the monitoring technique) is meshed using a triangulated irregular network (TIN) model and the distance between each point of an airborne LiDAR reference data set and the meshed surface is computed along the local normal of the mesh (Figure 25); Lague *et al.*, 2013).

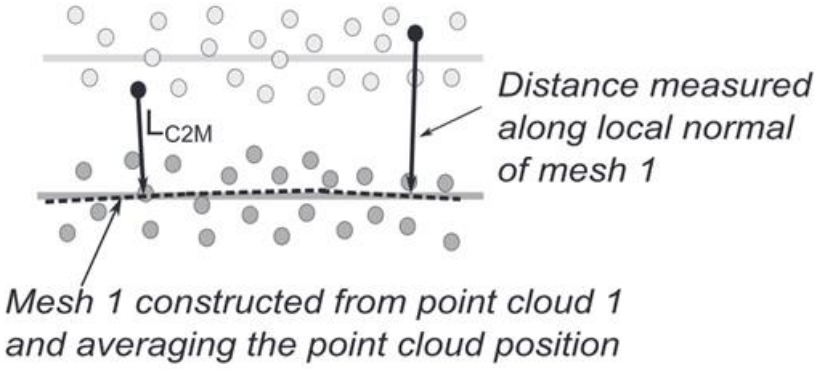

Figure 25: Cloud-to-mesh distance LC2M (Lague et al., 2013)

Different statistical measures were determined to assess the cloud-to-mesh comparisons between the monitoring point cloud and the reference data set. The arithmetic mean μ and standard deviation σ of a cloud-to-mesh distance L_{C2M} between a survey point cloud and the reference set are defined as:

$$algebraic\ mean\ \mu = \frac{1}{n}\sum_{i=1}^{n} L_{C2M}$$

$$standard\ deviation\ \sigma = \sqrt{\frac{\sum_{i=1}^{n}(L_{C2M} - \overline{L_{C2M}})^2}{n-1}}$$

The mean of absolute deviations and root mean squared error are written as:

$$MAD = \frac{1}{n}\sum_{i=1}^{n}|L_{C2M} - \overline{L_{C2M}}|$$

$$RMSE = \frac{1}{n}\sum_{i=1}^{n}(L_{C2M} - \overline{L_{C2M}})^2$$

By using the cloud-to-mesh distance, the correlation between the reference data sets and the mobile terrestrial LiDAR is represented. A simple linear regression is used to assess these correlations. The predicted value in the regression analysis is the reference data set. Since there is no real 'corresponding' point in the model of the investigated technique, the cloud-to-mesh distance is subtracted from the reference value, yielding a forecast value for the regression analysis.

Figure 26 (left panel) depicts the simple linear regression fits of the forecast monitoring elevations as a function of the predicted airborne LiDAR reference. Systematic error μ, precision σ, RMSE, mean of absolute deviations are given between the model and the truth as well as the (Adjusted) R^2 of the regression and the statistical p-value of the regression. Figure 26 (right panel) shows the histogram distribution of the cloud-to-mesh distances between the monitoring techniques and the airborne LiDAR model. Mobile LiDAR measurements appear to have a mean absolute systematic error of just 1.7 cm compared to the airborne LiDAR surface with a precision of 2.2 cm in the intertidal zone. The RMSE (2.1 cm) and R^2 (0,9885) of the linear regression scores slightly less, compared to the other techniques, but considering the mobile LiDAR was only used on the wet intertidal part of the beach (with high surface moisture), this is still a very good result (De Sloover *et al.*, 2020a).

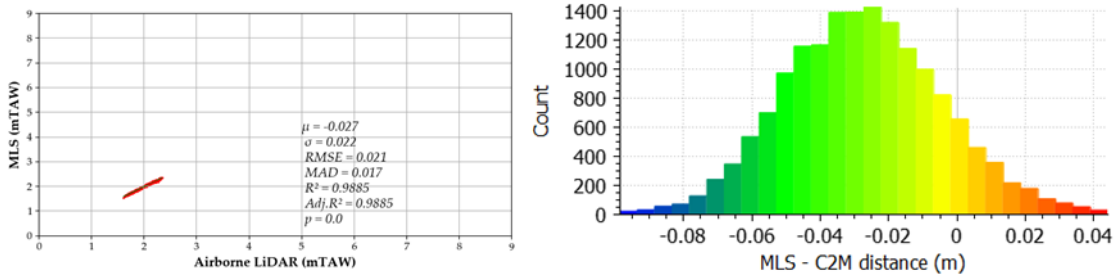

Figure 26: Simple linear regression fits of predicted ALS elevations and the forecast mobile LiDAR (systematic error μ, precision σ, RMSE and mean of absolute deviations) (left panel) and histogram plots of the Cloud-to-Mesh distance distribution of mobile LiDAR (right panel)

THM 2.3 TOPOGRAPHIC DATA SETS

A one-year series of time intensive PLS measurements were acquired at Mariakerke-Beach and during a longer time span of 3 years, incidental mobile LiDAR scans and UAV photogrammetric measurements at both Mariakerke and Koksijde were acquired, in addition to numerous ground-based survey techniques.

Data and metadata products were established based on intensive hyper-temporal permanent terrestrial LiDAR or laser 'scanning' (TLS) measurements of the beach topography at low-tide near Mariakerke-Bad, Belgium (Figure 27).

Figure 27: Riegl® VZ-2000 overlooking the Mariakerke Beach.

A Triangulated Irregular Network model based on Delaunay triangulation was generated from the TLS point clouds. Equidistant points were interpolated every 25 cm in the TIN model to create a digital elevation model (DEM).

The TLS 3D point cloud data (x, y and z coordinate) sets are presented in an open standard format (.las) (American Society for Photogrammetry and Remote Sensing, 2013) with filenames YYMMDD_HHMMSS_RR.las. Figure 28 plots the root mean square error of the scan registration ({_RR} in the filename) and the point density of the point cloud within the window of interest as a function of the survey date. A number of 51 point clouds are available (approximately one every week) acquired from 28th November 2017 to 20th November 2018.

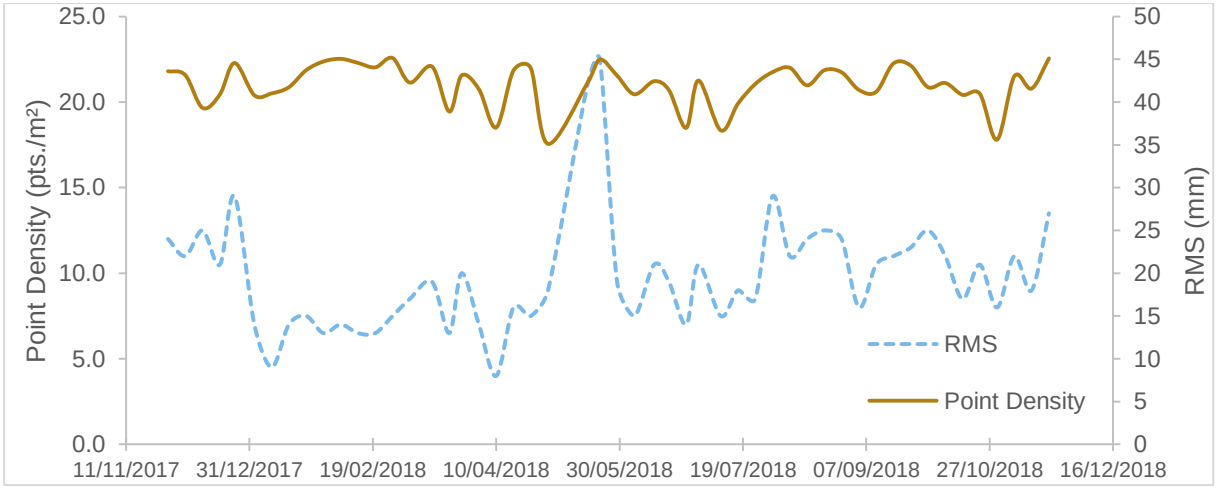

Figure 28: Overview of the TLS surveys (registration RMS and scan density per survey.

The 3D point clouds were measured in a local reference system and then transformed to the Lambert72 (EPSG: 31 370) Belgian national grid with elevation taken towards the 'Tweede Algemene Waterpassing' (TAW) orthometric height system. The point cloud data are clipped within a (cross- × along-shore) area of interest of (220 × 180) metre. This study area is delimited by Lambert72-coordinates (45 459.096, 212 552.351) in the lower-left corner and (45 473.557, 212 836.381) in the upper-right corner. A detailed (0.25 m resolution) DEM with TIN interpolation of the empty zones is made available as a derivative product of every TLS point cloud within the area of interest. The elevation models are presented as geographic image data in an open binary standard GeoTIFF (.tiff) format (OGC, 2019). Figure 29 depicts a 0.25 m cell size DEM within the aforementioned area of interest.

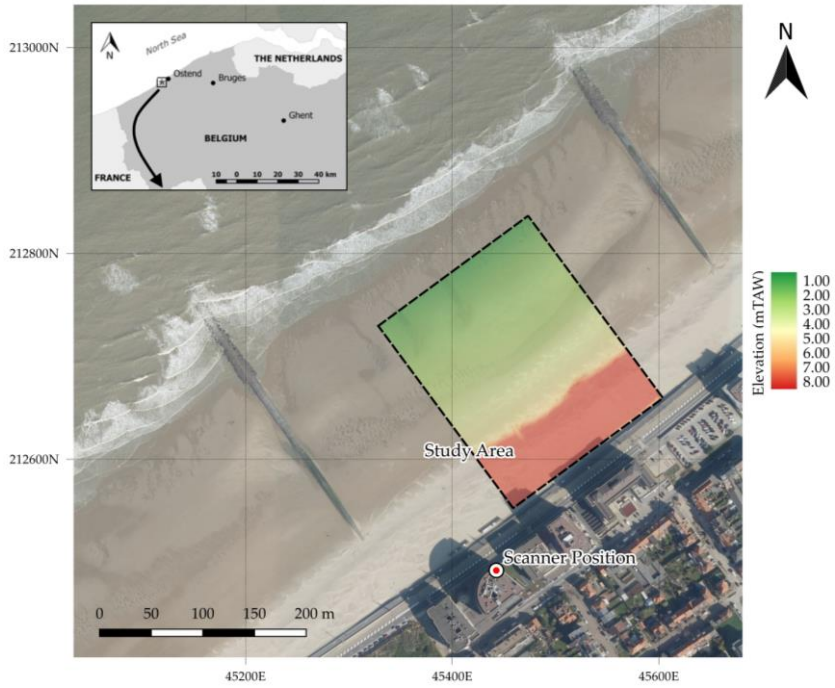

Figure 29: DEM (0.25 m grid size) of the beach topography and location of the study site (coordinates in Belgian Lambert '72, EPSG: 31 370).

Coastal measurements, as reported in this data descriptor (De Sloover *et al.*, 2020b), are deemed necessary components for the calibration of morphological models and the confidence in the results of subsequent modelling efforts. Due to surface moisture and atmospheric conditions (e.g. rain, fog, snow) amongst others, not all of the low tide scans contain a sufficient amount of backscattered data. Besides, daytime TLS measurements (especially during favourable weather conditions), come with a lot of 'ghosting' (i.e. people walking on the beach). A semi-automated procedure that results in a sufficiently dense data set with the least amount of noise is needed.

In addition, different multi-sensor technique measurements (mobile terrestrial LiDAR and UAS photogrammetry through Structure-from-Motion) were performed on the developed beach of Mariakerke and the natural beach of Groenendijk (De Sloover *et al.*, 2020a) on a bi-annual time scale over a time span of 3 years.

Ultimately, the goal is to implement the data set in an online Geographic Information System (GIS) environment, capable of performing spatio-temporal queries regarding coastal morphodynamics.

THM 2.4 WAVES, CURRENTS AND SEDIMENT SUPPLY SHAPE THE INTERTIDAL ZONE

The intertidal zone in Belgium is not only shaped by waves, but equally by tidal currents and, to a lesser extent, by natural variations in sediment supply.

The intertidal zone plays an important role in the protection of the coast. It is a very dynamic area subject to waves, tide, and wind and topographic changes can be large over a short period of time. For macro-tidal coasts (tidal range > 4 m) like the Belgian one, tide is an important factor in the intertidal beach morphodynamics but it remains unclear which specific hydrodynamic conditions lead to topographic changes. This is mainly due to a scarcity of reliable field data of sediment transport and beach topography. The main focus of the PhD research of Brand (2019) was to improve our understanding of the relationship between hydrodynamic forcing and topographic response for tide-dominated, sandy beaches.

Extensive field measurements were carried out in the nearshore, the intertidal zone, and on the dry beach of two study sites, Groenendijk and Mariakerke, along the Belgian coast. The Belgian coast is tide-dominated, with a tidal range of 3.5 m during neap and 5 m during spring tide and medium wave energy. Numerous sand banks, the Flemish Banks, are present in front of the coast. Groenendijk, located near Nieuwpoort (Figure 30), is a natural beach where no protective measures have been taken. It is characterized by four intertidal bars (ridges and runnels) and is connected to a dune area. The intertidal beach is 290 m wide, gently sloping (1%), and consists of medium fine sand (D_{50} of 200 µm). Mariakerke, situated near Oostende (Figure 30), is a developed site with a seawall, groins, nourishments, and regular beach scrapings. The intertidal beach is featureless, but the transition to the dry beach is characterized by a steep slope (37%) of approximately 2 m high. The intertidal beach is 160 m wide, gently sloping (2%), and consists of medium sand (D_{50} of 325 µm).

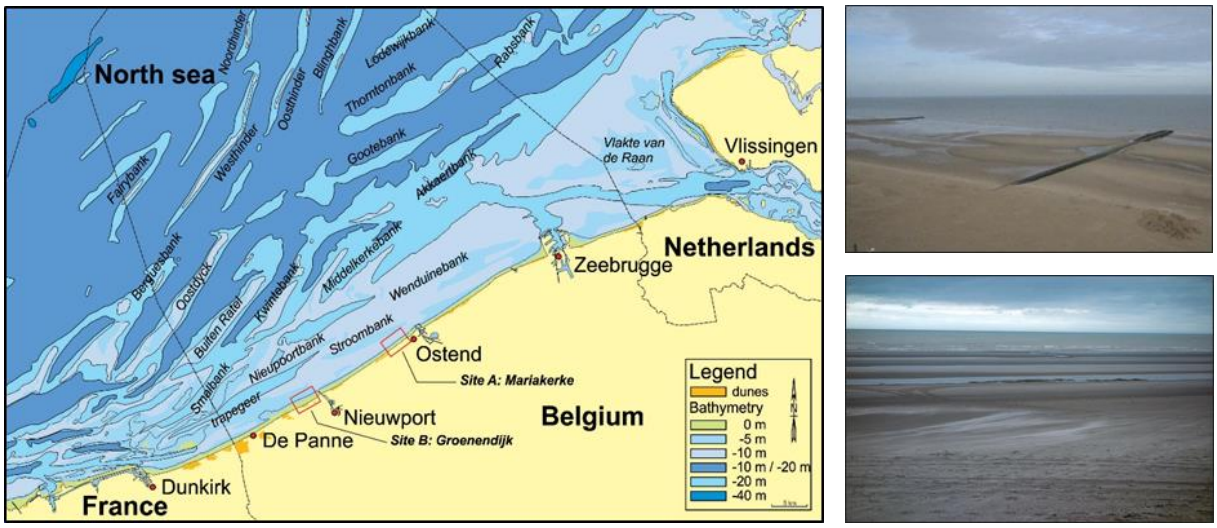

Figure 30: Overview map of the Belgian coast and ground pictures of the study sites: Mariakerke (top) and Groenendijk (bottom).

Monthly cross-shore beach profiles were analyzed to investigate the medium scale (seasonal to monthly) beach dynamics and to quantify the spatial variability in topographic changes. For Mariakerke 3.5 years and for Groenendijk more than 2 years of beach profiles were available. These monthly profiles were compared to the nearshore hydrodynamics and sediment dynamics from continuous wave buoy and tide gauge measurements and three nearshore measuring campaigns of two months each at Mariakerke. Furthermore, three two-week measuring campaigns were carried out in the intertidal zone of each study site to get a more detailed understanding of the intertidal beach morphodynamics. The beach topography of five cross-shore profiles was measured daily during these campaigns. The hydrodynamics and sediment transport were measured continuously at the low water line. Acoustic backscatter was used to survey suspended sediment concentrations over the full water column (Brand et al., 2019a). Additionally, the beach topography was measured half-hourly during two campaigns at Mariakerke. The design of the intertidal measuring campaigns was based on an extensive literature review (Brand et al., 2019c).

No clear seasonal trend in intertidal beach volume is observed from the monthly topographic surveys. Instead, monthly topographic changes seem event-driven, with erosion during events with an offshore wave height exceeding 3.75 m and accretion in between. However, not all months with energetic events are accompanied by erosion. This can be attributed to differences in specific event conditions, the pre-event beach profile, or a fast recovery of the beach. This recovery is often within one or two months, but it will likely take longer when major storm events occur. Monthly beach volume changes can be large, at least up to ±15 m^3/m at Mariakerke and ±25 m^3/m at Groenendijk. Although absolute volume changes are larger at Groenendijk than at Mariakerke, they are of similar magnitude relative to the total intertidal beach volume of each site. Typical monthly variations in beach elevation are 5 cm at Mariakerke and 25 cm at Groenendijk. Intertidal beach volume changes on a daily scale can be up to at least ±5 m^3/m for both Mariakerke and Groenendijk under non-storm conditions and daily variations in beach elevation are typically in the order of a few centimetre. The topographic response to the incoming hydrodynamics is highly variable between the profiles due to the complex beach morphology at both study sites with the groins at Mariakerke and the ridges and runnels at Groenendijk. The ridges and runnels at Groenendijk move onshore and become more pronounced under energetic conditions because of long wave

activity while the beach morphology is smoothened during calm conditions. The bar position differs approximately 20 m and the bar height differs 15 cm between summer and winter. The intertidal zone at Mariakerke is usually featureless but a ridge and runnel morphology arises during energetic (non-storm) conditions. They never fully develop at Mariakerke because of the groins. They are smoothened during calm conditions (Brand et al., 2017a; Brand, 2019).

Wave steepness is found to be the main driver for topographic changes in the intertidal zone. The intertidal beach grows when wave steepness is small (< 0.010), while it erodes when wave steepness is large (> 0.018). This trend is opposite when wave steepness is medium (0.013-0.015), with erosion by small and accretion by large waves. Traditional factors such as wave energy, wave direction, beach slope, and wind cannot explain this. Suspended sediment concentration (SSC) in the nearshore, on the other hand, increases remarkably fast when wave steepness is in this medium range. The suspended sediment is transported shoreward from the nearshore to the intertidal zone by flood dominant currents, which results in (partial) compensation of wave erosion. This suspended sediment is supplied from sources that are likely tens of kilometres away from the beach, such as the tidal banks in front of the coast, since a time lag of 1.3 tidal cycles exists between peaks in wave steepness and peaks in SSC. Besides this supply of sediment from other sources, it was found that part of the sediment that is eroded during energetic conditions is deposited just below the low water line and is transported back to the intertidal zone when wave steepness is small. In conclusion, the effect of waves is twofold: larger waves are primarily erosive, but they also play a role in beach growth through reinforced sediment supply. The effect of variations in sediment supply on the intertidal beach topography is subordinate to the erosive effect of wave steepness though (Brand et al., 2017b, Brand et al., 2018).

Besides wave impact and the influence of variations in sediment supply, it was found that the tidal currents strongly influence the intertidal beach morphodynamics. Currents are cross-shore and wave-dominated during neap tide, while strong tide-induced alongshore currents are observed during spring tide. These spring tidal currents are accompanied by erosion of the intertidal beach. It is hypothesized that spring tidal currents transport sediment that is locally eroded by waves away from the beach, thus enhancing erosion of the intertidal zone. The effect of the tidal currents on the beach topography is of the same magnitude as the effect of waves. The relationship between hydrodynamic forcing and topographic response is summarized in a conceptual model of the intertidal beach morphodynamics (Figure 31). Both study sites respond fairly similar to hydrodynamic forcing, in spite of their differences in beach morphology. The groins at Mariakerke slightly enhance the erosive effect of tidal currents. At Groenendijk the natural sediment supply is larger and the beach is more susceptible to variations in this supply. Furthermore, the beach at Groenendijk is slight more stable and less susceptible to erosion by energetic events thanks to the wider intertidal zone (Brand et al., 2019d).

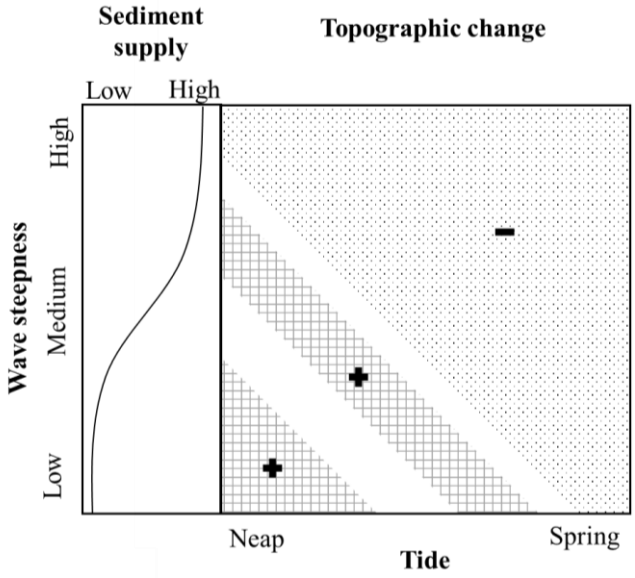

Figure 31: Conceptual model of the combined effects of waves through wave steepness, tide, and sediment supply on the intertidal beach volume.

The suspended sediment is mainly transported by mean currents: tidal currents transport sediment onshore during calm conditions, while undertow (and most likely alongshore tidal currents) transports sediment offshore during energetic conditions. Oscillatory transport is of smaller magnitude and is always onshore because of the flood dominance of the waves. The suspended sediment is generally well-mixed, but during energetic conditions the SSC is highest near the bed. Flow velocity is highest at approximately 1.5 m above the bed. As a result, the suspended sediment transport is rather uniform over the water column with a peak in transport at approximately 1/3 of the (maximum) water column. This peak is most pronounced during energetic conditions due to strong currents and high SSC close to the bottom (Brand et al., 2019b).

Although stated in an affirmative manner, it is clear from the above that the mechanisms are complex and not fully confirmed and understood. To increase the understanding, additional study is necessary and the following recommendations can be taken along to extend this study:

- Survey the beach with a high spatial resolution, especially when the alongshore variability in beach morphology is large, such as at Groenendijk where ridges and runnels are present, and at Mariakerke where the groins affect the beach morphology.
- Investigate the sediment transport near the sandbanks. It is hypothesized that they are an important source of sediment for the Belgian beaches and therefore they might play an important role in the resilience of the beach and in the protection against beach erosion and coastal flooding.
- Carry on with the monthly topographic surveys and add beach surveys prior to and immediately after an energetic event. The monthly cross-shore beach profiles already provided valuable insight in the beach morphodynamics. However, the dataset for Groenendijk is still too small to draw any definite conclusion on a seasonal cycle in beach topography or the response to energetic events. Pre- and post-storm (offshore waves > 3.75 m) beach surveys are necessary because beach recovery can take place rapidly (within a few months).

THM 2.5 DATA COLLECTION OF AEOLIAN SAND TRANSPORT RATES

A unique data set, consisting of wind conditions and aeolian sand transport rates, has been obtained through field experiments in Belgium on the natural beach of Koksijde and developed beach of Mariakerke. Between 2016 and 2018, 40 data sets on aeolian sand transport (20 in Koksijde and 20 in Mariakerke) were obtained during moderate to strong wind conditions. Although sand transport by wind is easily observable, reliable and accurate data sets of sand transport rates are still scarcely available due to measuring difficulties. This accurate field data set has an added value in understanding how coastal environments (managed or natural) respond to wind forces over short to long-term timescales.

The measurement campaigns, conducted between 2016 and 2018, were designed to measure simultaneous aeolian sand transport rates and shear velocities. This allows us to have a unique data set to evaluate the performance of most common and recently used transport models.

Wind speed and direction were mainly measured using four cup anemometers (Vector Instruments A100R) and a wind vane (Vector Instruments W200P) on one or two locations on the dry beach in the study area (Figure 32a). Cup anemometers were positioned at 0.15, 0.30, 0.51 and 1.95 m respectively in mast 1 and in mast 2. The wind vane was installed at 2 m above the surface. Wind speed was recorded at 1 Hz and averaged over 1 minute. Air temperature was recorded at 10-minute intervals. Occasionally, one mast was positioned on the dry beach where all eight anemometers were used with positions at 0.04, 0.22, 0.49, 0.91, 1.29, 1.67, 2.02 and 2.40 m above the surface. Time series of rainfall and tides were obtained from nearby measuring stations.

Modified Wilson And Cook (MWAC) sand traps were exposed to the wind for minutes to sometimes hours to determine the rate of aeolian sand transport (Figure 32b). These sand traps have been extensively used in numerous studies in which efficiencies of between 42% and 120% were reported (e.g. Van Pelt *et al.*, 2009; Sterk & Raats, 1996; Goossens & Offer, 2000; Poortinga *et al.*, 2013; Youssef et al., 2008). The trap collected sediment in seven plastic bottles from 6.5 to 100 cm above the surface. Aeolian sand transport is dominated by saltation, which involves sand grains following ballistic trajectories as they hop intermittently across the sediment surface. When aeolian sand transport occurs, the saltating layer seldom reaches heights above 25 cm (Van Dijk et al., 1996). Therefore, four bottles were placed in the MWAC sand trap array in the near-bed layer at a of height 6.5, 13.5, 21.0 and 28.5 cm above the surface. The total horizontal sediment flux per metre beach width is determined by fitting an exponential decay curve through the flux results of the four measuring points and extrapolating this curve to the bed (Poortinga et al., 2014; Bauer & Davidson-Arnott, 2014). The trap values were not corrected by an efficiency factor. As the traps were only used in dry weather conditions (dry sand), clogging of the intake nozzles did not occur.

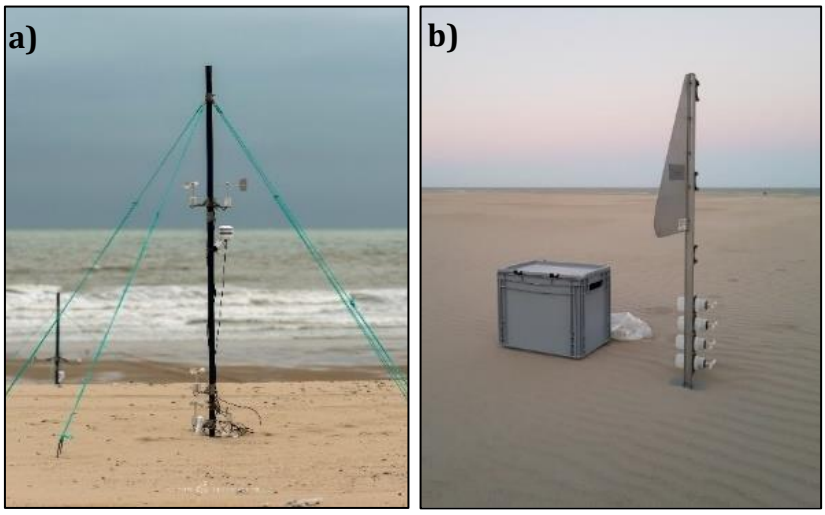

Figure 32: a) Meteorological station with four anemometers, a wind vane and a temperature sensor b) MWAC sand trap deployed at the beach surface.

THM 2.6 PREDICTED AND OBSERVED AEOLIAN TRANSPORT RATES

On short-time scales (hours to days), saturated aeolian sediment transport rate is cubic related with wind speed by a new modified Bagnold model. This model is validated by our own field data set and other international field data sets. The modified Bagnold model performs reasonably well in predicting sand transport.

Three field data sets are used, (1) measurements performed within CREST (THM 2.5) at two Belgian beach sites (Koksijde and Mariakerke), (2) measurements by Campos (2018) at a Belgian beach (Koksijde) and (3) measurements reported in Sherman et al. (1998) to evaluate the predicting ability of six different aeolian transport models.

In order to compare observed with predicted transport rates from the different models, linear regression analysis is used: $Q_{predicted} = m.Q_{observed}$. Correlation coefficients (R^2), root mean square errors (RMSE), and best fit line slope values are computed. Table 5 shows the results of all models for the measurements of the two Belgian sites. Table 6 shows the results for all transport rate measurements. Figure 33 shows the comparison between observed and predicted transport rates for the six aeolian models including all data sets.

Model	Slope (m)	R^2	RMSE (kg/m/min)
Original Bagnold (1937)	1.21	0.35	0.52
Kawamura (1951)	1.68	0.61	1.17
Threshold Bagnold (1954)	0.14	0.53	0.92
Hsu (1971)	0.69	0.44	0.42
Kok et al. (2012)	1.13	0.57	0.45
Modified Bagnold (Van /Rijn, 2018)	1.01	0.60	0.40

Table 5: Summary of results comparing observed transport rates with predicted transport rates for different aeolian models, only data of the two Belgian sites (Mariakerke and Koksijde).

Model	Slope (m)	R^2	RMSE (kg/m/min)
Original Bagnold (1937)	1.26	0.19	0.56
Kawamura (1951)	1.96	0.31	1.28
Threshold Bagnold (1954)	0.15	0.36	0.80
Hsu (1971)	0.72	0.08	0.41
Kok et al. (2012)	1.19	0.26	0.55
Modified Bagnold (Van Rijn, 2018)	1.06	0.42	0.45

Table 6: Summary of all results comparing observed transport rates with predicted transport rates for different aolian models, all data sets.

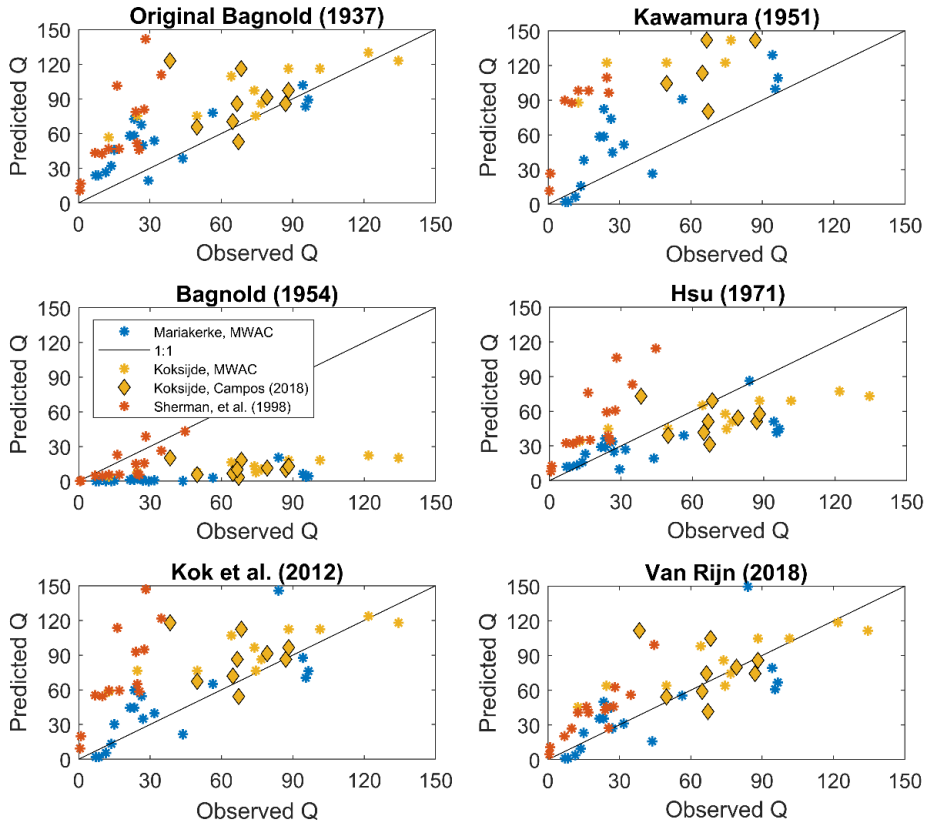

Figure 33: Comparison between observed and predicted sand transport rates Q for six aeolian models; all data sets. Diagonal lines represent the one-to-one correspondence. All transport rates are in kg/m/hr. Blue dots correspond to the measurements in Mariakerke. Yellow dots correspond to the measurements in Koksijde.

Analysis of the results shows that the modified Bagnold model based on Equation 2.6.1 (Van Rijn, 2018) yields the best performance when observed transport rates are compared to predicted transport rates.

$$Q_{s,\,mass} \cong \alpha_B \cdot \sqrt{\frac{d_{50}}{D}} \cdot \left(\frac{\rho_{air}}{g}\right) \cdot \left(u_*^{\,3} - u_{*,th}^{\,3}\right) \qquad (2.6.1)$$

In this equation, u_* is the bed shear velocity (in air), $u_{*,th}$ is a threshold bed-shear velocity, D is a reference grain diameter (set to 250 µm) and α_B (≈2) is a calibration coefficient, for more details the reader is referred to Strypsteen (2019). The modified Bagnold model has the closest fit to the 1 to 1 line slope, a high R^2, and the lowest RMSE. The model of Kok *et al.* (2012) also performs very well but shows a slightly weaker statistical relationship between observed and predicted rates of transport. In contrast, the model of Kawamura (1951) does not produce a good one-to-one prediction and has the largest RMSE. Our results suggest that the Kawamura model overestimates transport substantially. The Kawamura model also displayed a poor performance in the evaluation of Sherman *et al.* (1998) and Sherman & Li (2012). The model of Bagnold (1954) also displays a poor result. The best fit line slope is close to zero, indicating a large underestimation of the transport rate. It also has a relatively large RMSE. However, this model is frequently used in long-term sediment budget calculations. E.g. Hoonhout & Vries (2016) used it as the benchmark model to calculate saturated transport conditions in the numerical model 'Aeolis'. The other models perform intermediately and display similar predictive results.

When considering only the data sets of the two Belgian sites, the models perform slightly better. This could be attributed to the use of different sand traps with different trap efficiencies. Trap efficiency is defined as the relative ratio of trapped sand to the actual quantity of blown sand (Chepil & Milne, 1941). Sherman *et al.* (1998) used cylindrical sand traps with efficiencies ranging from 30% to 70%, which are different from the trap efficiencies of the MWAC sand traps ranging from 35% to 120%. Furthermore, they are not self-oriented compared to the MWAC sand traps. It is possible that the cylindrical traps capture less sand than the MWAC sand traps due to its mechanical structure. The transport rates measured with the vertical nylon mesh traps, used in the study of Campos (2018), show similar results as the transport rates measured with the MWAC sand traps during the same wind conditions on the subaerial beach of Koksijde.

The general variability between observed and predicted transport rates could thus be partly attributed to the use of different mechanical sand traps. Variation between observed and predicted transport rates could also be attributed to the effect of moisture. As sand was trapped during dry conditions, little to no moisture was present in the samples during the measurements at the two Belgian sites. The data of Sherman *et al.* (1998) also refer to dry sand conditions, but moisture values were not measured. Beach slope may have an effect on cross-shore sand transport as measured by Sherman *et al.* (1998). As they did not adjust their data, the effect of beach slope is most likely negligibly small. Beach slope was almost flat during the measurements at the Belgian sites, where sand transport was in the longshore direction.

A large influence on the variability between observed and predicted transport rates could be attributed to the spatial distribution of the different sand traps. It is well known that aeolian sand transport has a spatiotemporal character. During a transport event, one trap could capture more sand than another trap if, for example, wind forces and sand transport are in the form of streamers or streaks. Thus, shear velocity can vary spatiotemporally due to varying wind conditions or even the threshold velocity can vary locally and in time due to a varying grain size or different surface characteristics. In practice, shear velocity can only be determined at one or two locations. Eventually, this has an impact on the calculation of sand transport rates. Figure 34**Error! Reference**

source not found. shows the relation between the variability of the observed transport rates and shear velocity. The variability is determined by the standard deviation. Higher shear velocities cause larger variability of the observed transport rates. It seems that this variation also follows a relationship of the type (u_*^3 - $u_{*,th3}$) with an R^2 equal to 0.54. Most of our transport rates were measured during longshore wind conditions. Poortinga *et al.* (2015) found that on a wide beach on the island of Ameland, The Netherlands, the largest variability of sand transport rates was found for alongshore events. Variability can be reduced by increasing the sampling time provided that the wind conditions are constant (de Vries *et al.*, 2012 and Keijsers *et al.*, 2014).

In this study, we assumed that the estimates of shear velocity are close to the true values. However, it is possible that the actual shear velocities related to the saltating particles vary substantially from the shear velocities, derived from vertical wind profiles due to roughness effects and measurement scatter (Bauer *et al.*, 1992). Therefore, we suggest that in future research the shear velocity would be better estimated based on the effective grain roughness ($k_{s,grain}$). The influence of moisture content and beach armoring and other bed surface properties (e.g. shells) appear to be a critical factor in degrading the performance of aeolian models. Future work should be based on designing a workable and predictive model that can account for these influences.

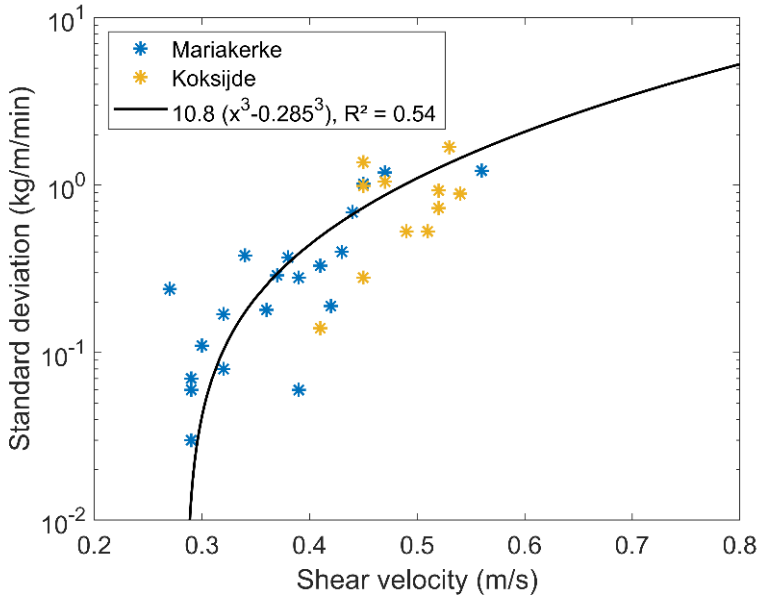

Figure 34: Relation between standard deviation of observed transport rates and shear velocity.

THM 2.7 SPATIAL-TEMPORAL VARIABILITY IN DUNE VOLUME CHANGES

On decadal timescales, the Belgian coastal dunes grow linear in time with a constant rate. Dune growth varies between 0 and 12.3 cubic metre per metre per year with an average dune growth of 6.2 cubic metre per metre per year, featuring large variations in longshore direction. Dune growth is primarily caused by aeolian sediment input from the beach during west to southwest wind conditions.

As an illustrative example of an analysis at a natural dune system, Figure 35 shows the dune volume at section 50 of the Belgian coast. It is found that dune volume increases to a good approximation at a constant rate in time (8.14 m³/m/year with a correlation of 0.99).

To assess if this is valid for all coastal dunes, the decadal trend in the calculation of dune volume changes is based on linear analysis. Fitting linear trendlines for all the coastal sections can test to which extent this linearity in time is valid for the entire Belgian coastline. Linear trends are calculated for the entire period between 1979-2018 and/or for the most recent trend. The correlation coefficient was calculated for all dune sections experiencing dune growth or dune erosion. Figure 36 shows that higher correlation coefficients occur more for dune growth than for dune erosion. It is found that 80% of all coastal dunes with dune growth (total of 93%) have correlation coefficients higher than or equal to 0.9, which yields an overall average dune growth of 6.20 m³/m/year. This percentage is decreasing for smaller correlation coefficients. Similar observations are found by de Vries *et al.* (2012). For the negative rates of dune volume change (7% of all coastal dunes), the occurrence of a lower correlation coefficient increases.

These calculations show that a substantial part of the Belgian coastal dunes is excellently represented using a linear dune growth model in time. Figure 37 indicates that the locations of the coastal dunes, with correlation coefficients larger than 0.9, are distributed over the entire stretch of the Belgian coast. Figure 37 also shows the annual dune development per dune section for the entire Belgian coastline. It is observed that in most areas, dunes are growing. The annual dune growth ranges between 0 and 12.3 m³/m/year, based on the observations between 1979-2018. Dune growth rates at the Holland coast have been calculated in the order 0-40 m³/m/year, which is of the same order of magnitude (de Vries *et al.*, 2012).

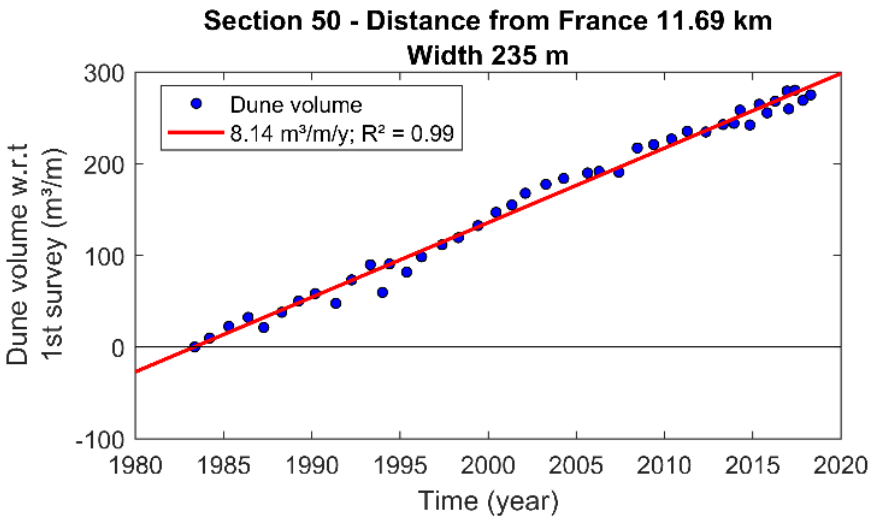

Figure 35: Example of dune volume in time combined with a linear fit (correlation of determination $R^2 = 0.99$) for coastal section 50 (natural dunes).

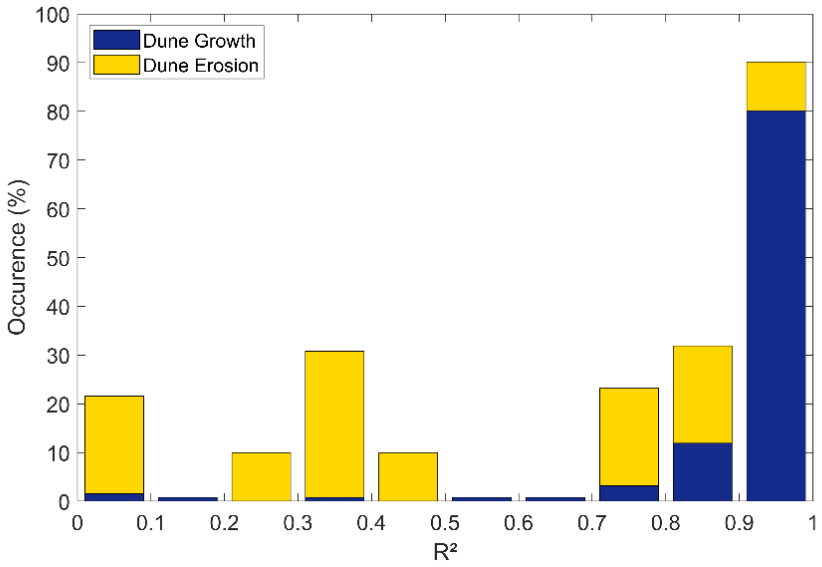

Figure 36: Density of occurrence of linear dune behavior. Of the dune sections with dune growth, 80% show correlation coefficients larger than or equal to 0.9.

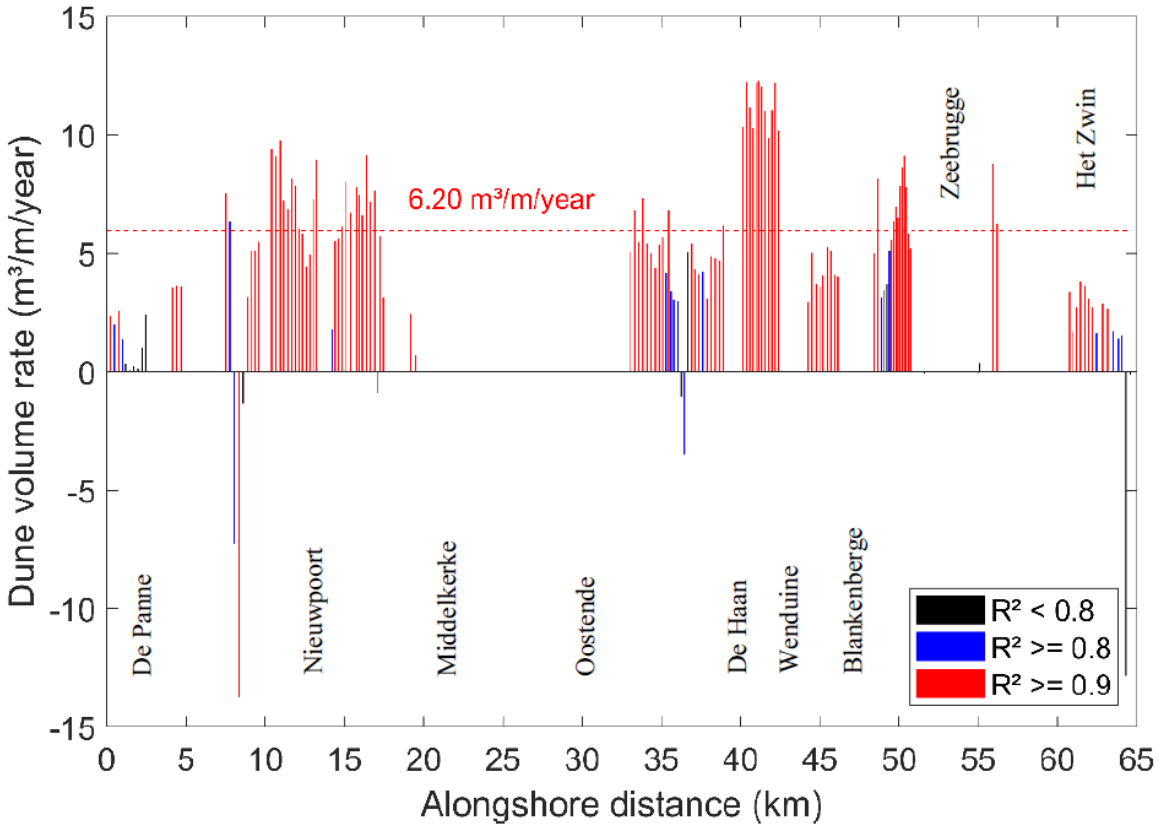

Figure 37: Dune behavior along the Belgian coast. Red bars indicate the places where the correlation coefficient of the linear trend analysis is higher than or equal to 0.9. The red dashed line represents the average annual dune growth for correlations higher than or equal to 0.9

THM 2.8 POTENTIAL AEOLIAN SEDIMENT TRANSPORT

Based on the modified Bagnold model, onshore potential aeolian sediment transport ranges to maximum 9 m³/m/year, while longshore potential aeolian sediment transport could reach up to 20 m³/m/ year towards the Netherlands.

It is well known that dune growth is primarily governed by aeolian sediment processes. Therefore, expectations are that dune volume variability does correlate with variability in wind conditions. Potential aeolian sediment transport is calculated per coastal dune section between the dates where a LiDAR flight is conducted using the representative median grain size and the coastal orientation.

Hourly wind data is available since the year 2000 at Ostend Airport (middle of the coastline and approximately 1 km inland) and is used to calculate the time series of potential transport. The wind sensor is located 4 m above the surface. Figure 38 shows the measured wind data at the weather station of Ostend Airport for the period 2000–2017 in the form of a wind rose. The red line represents the mean direction of the Belgian coastline. Measured over that period, a large west to southwest component of the wind is found. West to southwesterly winds are oblique onshore to longshore with respect to the Belgian coastline.

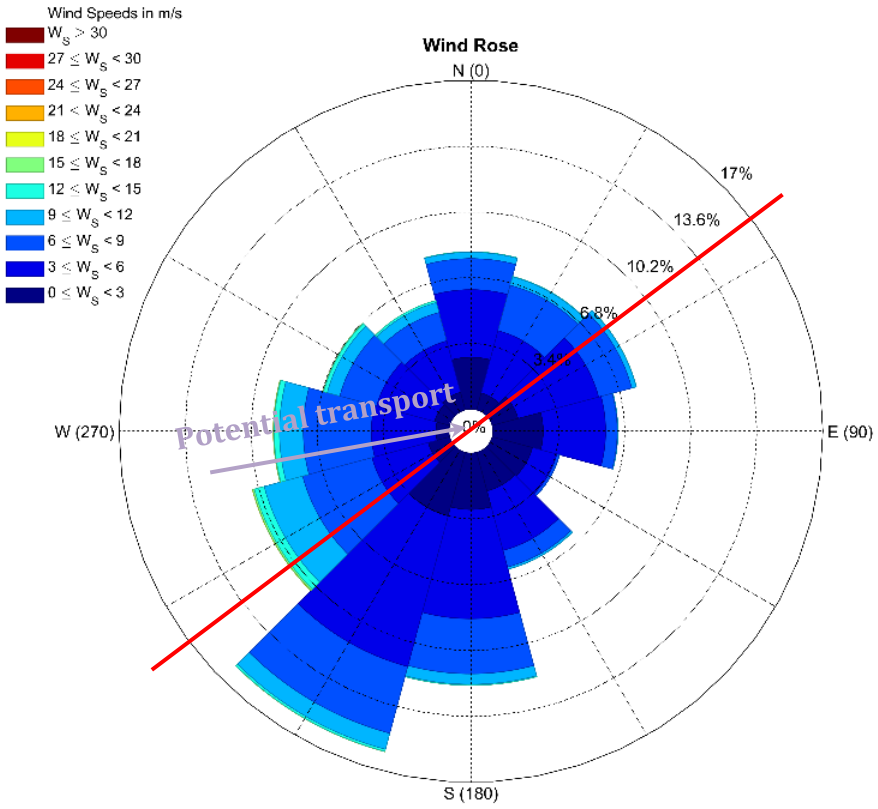

Figure 38: Measured wind speed (Ws) and wind direction at Ostend Airport weather station for the period 2000–2017. The red line represents the mean Belgian coastline direction. The potential transport drift is also given.

Figure 39 shows the annual potential transport and transport direction for the period 2000–2017 derived from measurements at Ostend Airport weather station based on a grain size of 310 µm and coastal orientation of 57° (section 103). Figure 39 indicates considerable temporal variability, caused by annual variations in wind climate. Annual variations are approximately between 0.5 times and 1.6 times the mean transport rate meaning that potential transport is occasionally three times larger for some years than other years. The average direction of potential transport over the period of 17 years is 260° with a standard deviation of 14° implying that the direction is constant. Potential transport has an oblique onshore character with respect to the coastline Figure 38). The larger parallel component (longshore) of the potential transport drift is directed towards the northeast (the Netherlands), while the normal component (onshore) is directed towards the southeast.

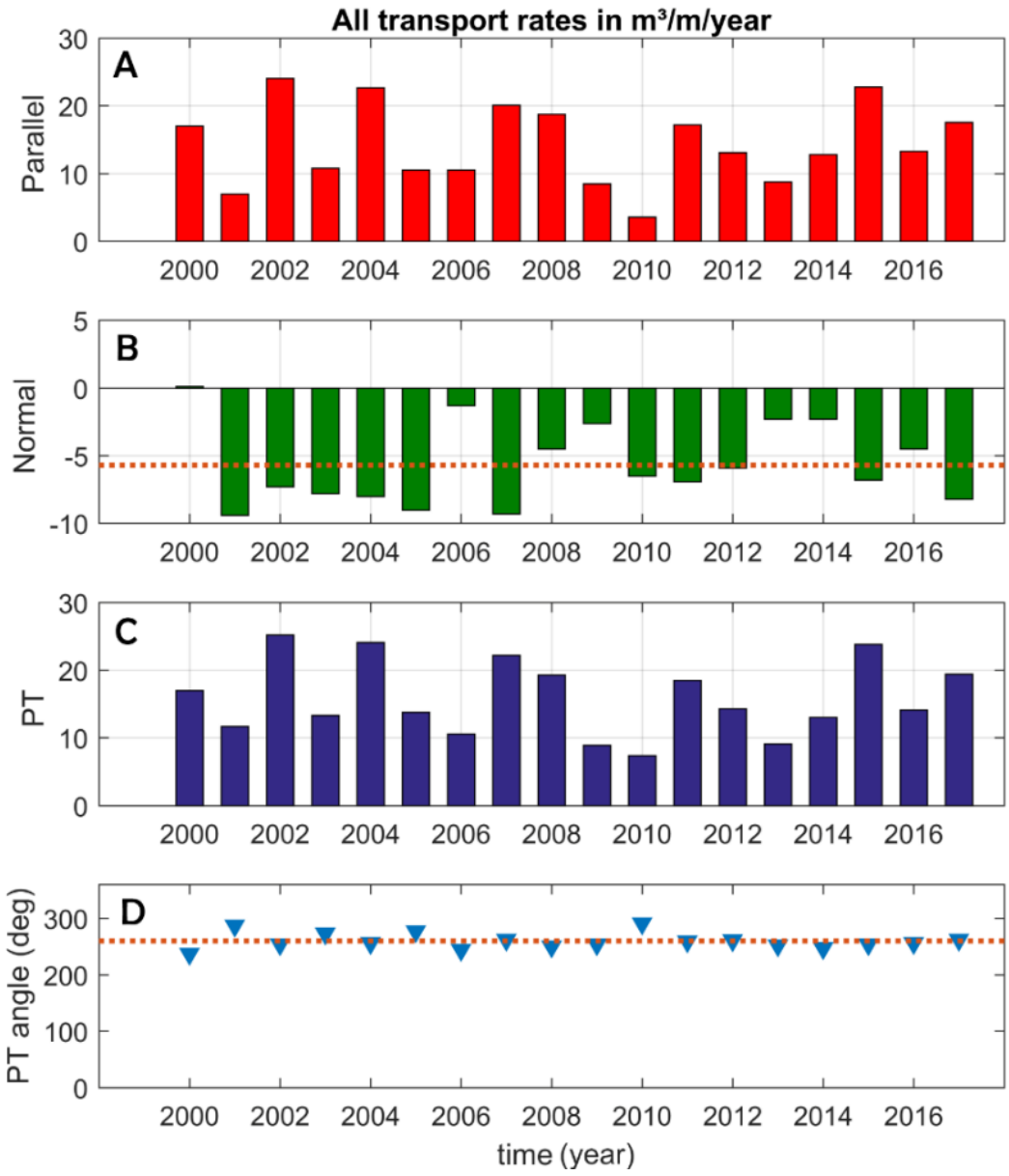

Figure 39: A) Annual potential longshore transport for the period 2000-2017. B) Annual potential cross-shore (or normal) transport for the period 2000-2017. Positive is offshore transport, negative is onshore transport. C) Annual potential transport (PT) for the period 2000–2017. All transport rates are given for section 103 in m³/m/year (based on a grain size of 310 µm and coastal orientation of 57°). D) The angle of potential transport is fairly constant with an average value of 260 degrees to the north.

Interpreting the results on a decadal timescale, all potential transport rates are cumulatively summed. Potential dune volume changes because of aeolian sediment transport appears to vary linearly in time with a constant rate which in return explains the decadal linear dune growth (Figure 40). Considering all coastal dune sections within the period of 2000-2017, Figure 41 indicates that the maximum onshore potential transport can reach up to 9 m³/m/year (average = 5.2 m³/m/year), while the maximum longshore potential transport could reach up to 20 m³/m/year (average = 18.7 m³/m/year) assuming dry beach sand. In return this gives a mean total potential transport of approximately 20 m³/m/year.

Longshore transport is relatively constant along the coastline (4.9% deviation of the mean). Onshore transport has some longshore variations due to a varying coastline orientation, especially behind the protruding point of Wenduine (43 km) where transport is lower due to a more north–northeast coastal orientation. It also implies that longshore transport is almost three to four times higher than onshore transport. This would explain why brushwood fences are so effective for enhancing dune growth locally.

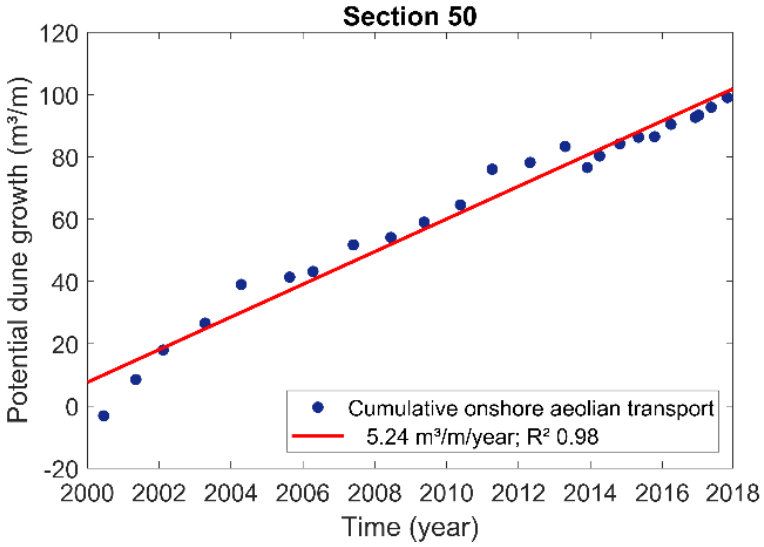

Figure 40: Decadal evolution of potential dune growth at Section 50 of the Belgian coast.

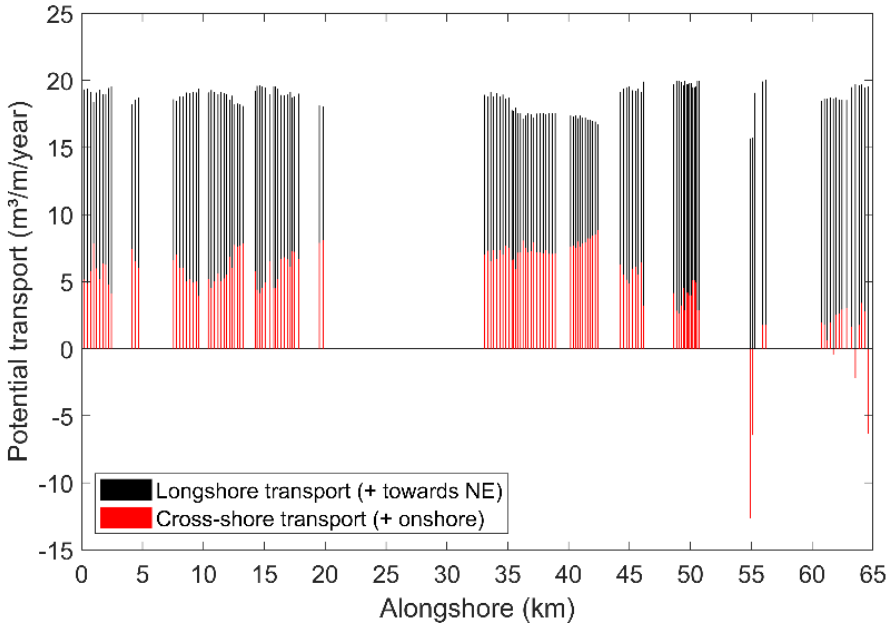

Figure 41: Annual potential longshore and onshore aeolian sediment transport, based on the period between 2000-2017.

THM 2.9 AEOLIAN TRANSPORT PREDICTION AT DECADAL TIMESCALE

There is strong correlation between observed and predicted dune growth on decadal timescales (long-term). Most of the predicted data are within a factor 2 of the measured value. It suggests that annual differences in forcing and transport limiting conditions (wind and moisture) only have a slight effect on the overall variability of dune volume trends.

Decadal timescales are of interest because it is the most appropriate timescale for engineering purposes and coastline development. On decadal timescales, potential dune volume appears to grow linearly with time, with a similar magnitude to the observed dune volume (see THM 2.7). It is of particular interest if both are correlated at this spatial–temporal scale. For all coastal dune sections, the decadal trend of potential dune volume changes is based on linear analysis. Linearity is calculated for the entire period between 2000–2017. It is found that in 93% of all coastal dune sections, the potential dune volume trend has a correlation higher than 0.90.

Figure 42 shows the comparison between observed and predicted dune development on decadal timescales. The yellow dots show the places were regular management activities are carried out. About 75% of all predicted data are within a factor of two of the measured values. Interpreting the results show that the modified Bagnold model (Van Rijn, 2018; Equation 2.6.1) yields a good performance when observed values are compared to predicted dune development rates.

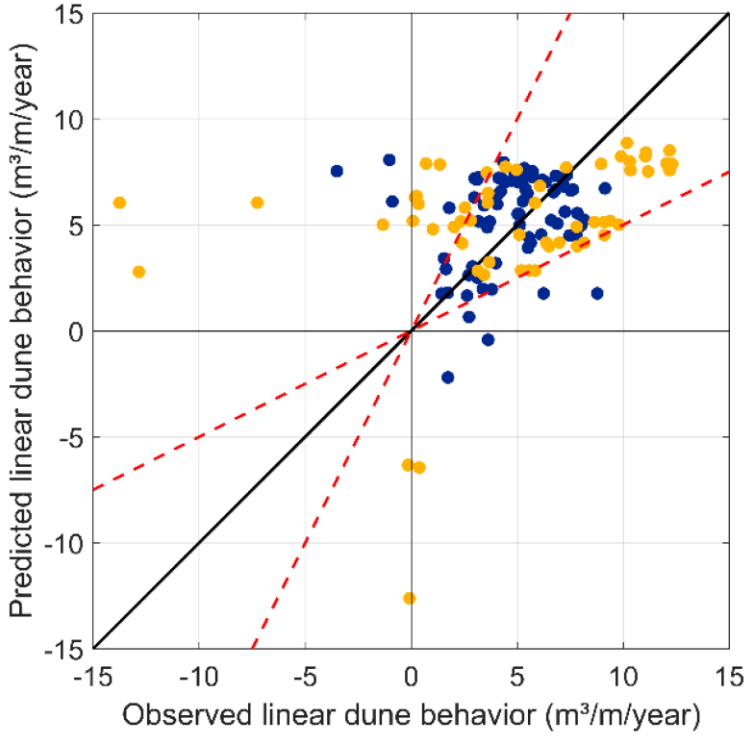

Figure 42: Comparison between observed and predicted linear dune development. Diagonal lines represent the one-to-one correspondence. Red dashed lines show the factor of two variance. Yellow dots represent the locations where managing activities are carried out.

Figure 43 shows the alongshore extent of the observed and predicted dune development rates along the Belgian coastline. The variability in potential transport is well correlated to the variability in dune volume changes at the considered spatiotemporal scale. The general variability, on a decadal timescale, between observed and predicted rates could be partly attributed to the management activities at certain sections along the coast. It is uncertain how many of the dune regions are managed. An attempt has been made to know which dune regions are managed. Based on historical images from Google Earth, approximately 50% of the coastal dunes are managed. Most of these activities include regular plantation of brushwood fences, especially where observed linear dune behaviour is higher than the predicted values (under the line of perfect agreement). The locations including dune foot protection measures, dune foot reinforcements, and dune blowouts, are mostly the locations where predicted values are higher than the observed values. When the managed zones are excluded from the data set, the best fit line slope is approximately one, and the RMSE (Root Mean Square Error) value is 2.9 m^3/m/year. Most (90%) of the predicted data are within a factor of two of the measured values. This is a high score, given all variabilities and non-uniformities involved in aeolian processes (wind field, sand composition, bed topography, surface roughness). The finding of potentially stronger correlations compared to the literature (e.g. Keijsers , 2014) at the Belgian coast are most likely caused by the generally wider beaches (between 150 m and 400 m). This indicates that natural dune behaviour can be predicted with a reasonable accuracy on decadal timescales, and it suggests that annual differences in forcing and transport limiting conditions (wind speed and surface conditions) only have a slight effect on the overall variability of dune volume trends.

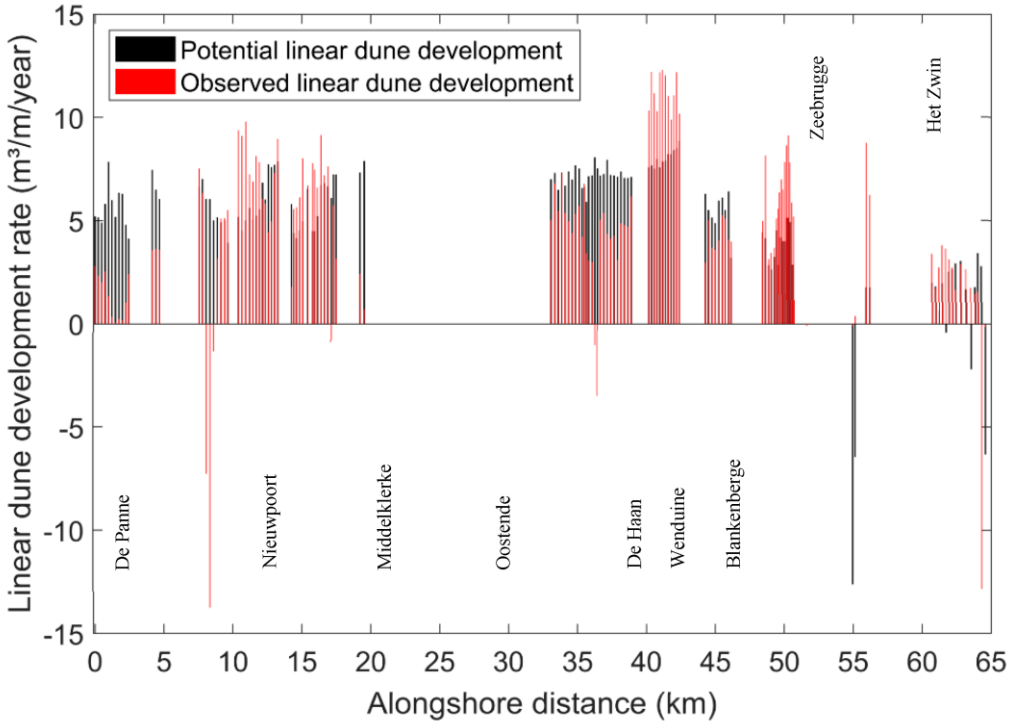

Figure 43: Annual predicted and observed dune volume change along the Belgian coast on a decadal timescale. Red and black bars indicate the observed and predicted values of dune development, respectively.

THM 2.10 WIND FLOW AND FETCH EFFECT ACROSS AN ARTIFICIALLY CONSTRUCTED COASTAL FLAT BERM

Aeolian sand from the foreshore is deposited at the foot of the steep cliff due to a decrease in shear velocity. Large shear velocities are measured at the berm lip due to compression and acceleration of the flow field. Onshore aeolian sand transport starts at the berm lip and increases rapidly towards a maximum downwind until it decreases to a lower equilibrium. The deposition at the foot of the cliff and erosion at the berm lip causes the cliff to change to an equilibrium profile.

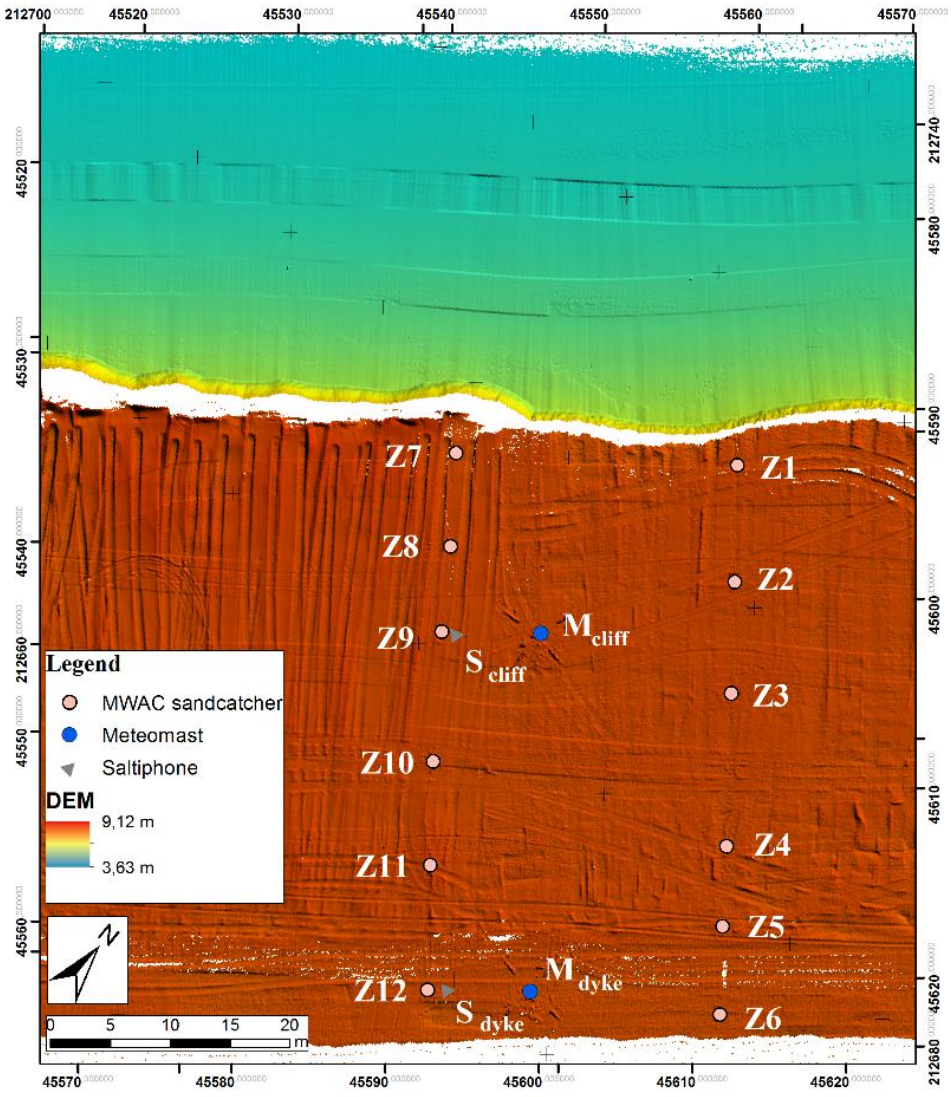

Figure 44: Plan view of the study site with the location of the equipment. 12 Modified Wilson And Cook (MWAC) sand traps were placed at the upper beach together with two meteorological stations and two saltiphones. Coordinates refer to the Lambert 72 coordinate system. The topography is from field surveys conducted on November 7, 2017.

On November 12, during Event 1, aeolian transport was measured from 13:20 until 15:41 (≈ 2 hours sample duration) with an average wind direction of 11° from dyke normal and an average wind speed of 12.75 m/s (measured at Mcliff). The onshore wind direction remained relatively steady during Event 1. On November 18, during Event 2, aeolian transport was measured from 07:00 until 07:48 of the next day (≈ 24 hours sample duration) with an average wind direction of 60° from dyke normal and an average wind speed of 6.64 m/s (measured at Mcliff). The wind direction during Event 2 was obliquely onshore to alongshore with moderate breezes. The wind data refers to the meteorological station positioned at the cliff (Mcliff in Figure 44).

Temporal fluctuations in wind speed at the two locations were similar. However, the flow velocity varies spatially across the berm. Shear velocities were consistently greater at the berm lip than at the back of the berm during strong onshore winds (Event 1). During weaker oblique onshore winds (Event 2), shear velocities were in the same order of magnitude at the back of the berm and at the berm lip. The wind vane measurements show no difference between the two locations, indicating that the flow field was fairly constant in its approach.

Normalized flux is calculated based on the deviation of the mass flux at each MWAC trap in the transect Z1 to Z6 and Z7 to Z12 and maximum mass flux in the transect Z1 to Z6 and Z7 to Z12 accordingly. During Event 1, aeolian sand transport was in the form of streamers. The two-hour transport event revealed a rapid change in topography during onshore moderate wind conditions. The effective fetch distance is approximately equal to the cross-shore distance of the berm, as winds were perpendicular onshore (11° to dyke normal). During Event 1, Figure 45 indicates increasing sand transport over the first half of the upper flat beach with increasing fetch distance (Z1 to Z4 and Z7 to Z11), followed by a decrease in sand transport towards of the dyke (Z4 to Z6 and Z11 to Z12).

The observed growth in sand transport in the downwind direction may be attributed to the downwind fetch effect described by authors such as Anderson & Haff (1991), Cahill et al. (1996), Lynch et al. (2016), Law & Davidson-Arnott (1990) and Delgado-Fernandez (2010). The fetch effect is described as an increase in sediment transport rate with distance downwind until maximum transport rate is reached at the critical fetch distance. The critical fetch distance during Event 1 is approximately 35 m, until it decreases again towards the dyke. The rapid decrease in sand flux in front of the dyke is likely caused by any pressure effects localized to the trench in front of the dyke and the dyke itself. The range of deposition of sand in front of the dyke is similar to the deposition of sand in front of the steep cliff as pressure effects are also present there (Figure 45**Error! Reference source not found.**). Figure 45 shows also the normalized transport in the downwind direction for Event 2. For Event 2, the wind was highly oblique (and rather weak) which means that each of the trap positions had a much longer fetch distance upwind. The effective fetch distance is approximately equal to two times the cross-shore distance of the berm, as winds were 60° to dyke normal. An increase in sand transport was measured between the first two upwind traps (Z1 - Z2 and Z7 - Z8), followed by a decrease to a lower equilibrium value in the downwind direction. The critical fetch distance where maximum transport is achieved is approximately 20 m and is lower than that achieved in Event 1 (35 m). There is supporting field evidence of Davidson-Arnott & Law (1990) showing a strong linear correlation between wind speed and critical fetch length. Stronger wind events need more distance to develop an equilibrium flux profile and vice versa (cf. Event 1). However, the measurements of Event 2 clearly indicate the overshoot effect described by Shao &

Raupauch (1992). The overshoot effect is typically described by a rapid increase in sand flux towards a maximum until it decreases again to a lower equilibrium sand flux. This is due to relaxation and deepening of the boundary layer which distributes the total shear more evenly in the vertical (i.e. it is not as concentrated in the near-surface layer).

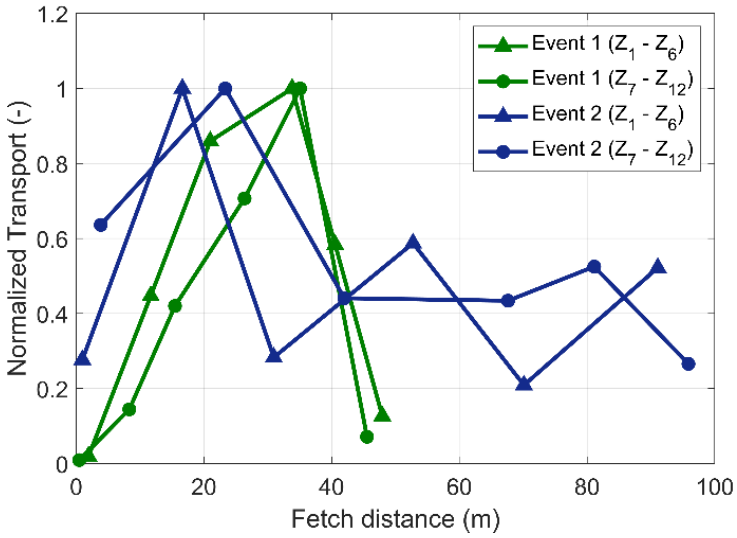

Figure 45 Evolution of sand transport downwind from the lip of the berm for Event 1 and Event 2.

THM 2.11 MINIMIZING AEOLIAN SAND TRANSPORT

The steep cliff in front of the human-constructed coastal berm of Mariakerke is very sensitive to erosion. Sand being eroded from the berm lip is deposited in front of the dyke and in the trench. This specific beach topography is a general good solution to minimize sand transport to the hinterland, but only serves temporally.

The wind flow across a steep cliff accelerates and is maximum at the crest, especially during strong onshore winds. The critical threshold for sand transport ($u_{*,th}$ = 0.29 m/s based on the Bagnold equation) was always exceeded at the two meteorological stations (see THM 2.10), even though sand was not being transported continuously. Sand fluxes close to the berm lip were small and increased in the downwind direction. High shear velocities do not coincide with high transport rates, because the upwind sand traps were at the beginning of the fetch and sand coming from upwind seem to be deposited locally in front of the berm lip. The increase and decrease of transport rates are excellently related to erosion and deposition respectively (Figure 46). The observed growth in sand transport in the downwind direction may be attributed to the downwind fetch effect described by authors such as Anderson & Haff (1991), Cahill et al. (1996), Lynch et al. (2016), Law & Davidson-Arnott (1990) and Delgado-Fernandez (2010). The fetch effect is described as an increase in sediment transport rate with distance downwind until maximum transport rate is reached at the critical fetch distance. The critical fetch distance during Event 1 is approximately 35 m. The rapid decrease in sand flux in front of the dyke is likely caused by pressure effects localized to the trench in front of the dyke and the dyke itself. The range of deposition depths of

sand in front of the dyke is similar to the deposition depths of sand in front of the steep cliff as pressure effects are also present there (Figure 46).

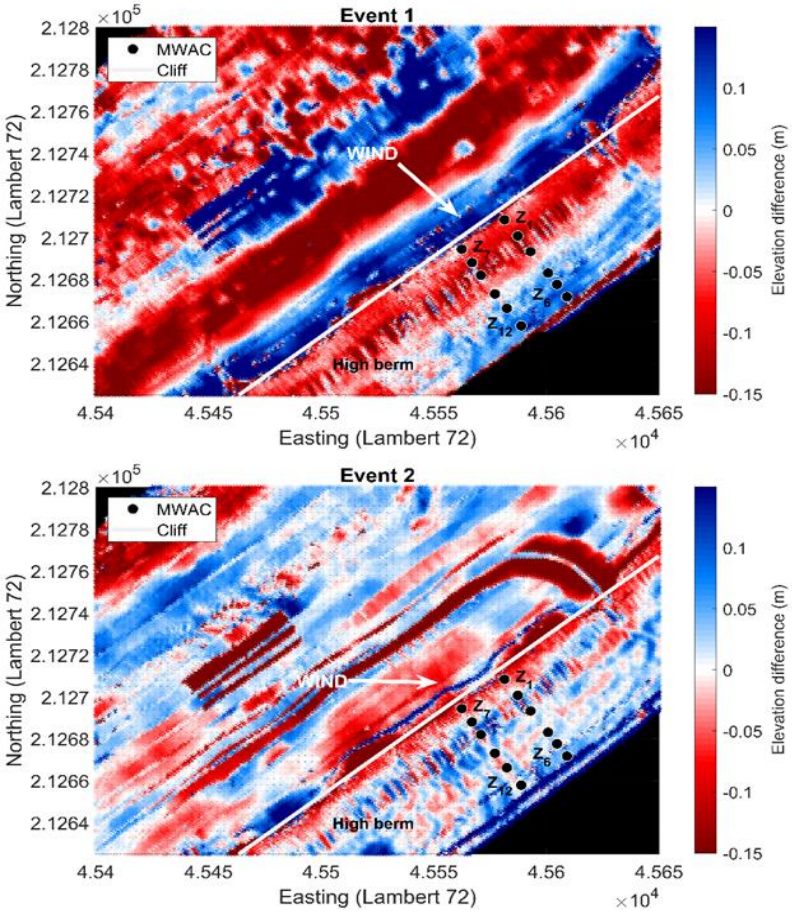

Figure 46: Topographic elevation changes caused by transport Event 1 and Event 2. Red color indicates erosion, while blue color indicates deposition.

THM 2.12 RECOMMENDATIONS FOR FUTURE AEOLIAN MONITORING TECHNIQUES

Further research should focus on better quantifying aeolian sediment transport processes by more innovative monitoring techniques, especially when long-term monitoring is required. A camera-system to monitor the overall weather and wave conditions, bar welding, beach morphology, and the frequency and magnitude of erosional events could be useful. The images could be used to extract moisture maps, beach dimensions, fetch distances and vegetation cover. It would be also of interest to introduce a self-rotating vertical sand trap that measures the whole transport column from surface to a certain distance above the surface to get information of the entire flux profile. A change in decadal dune behaviour due to climate change is also very relevant to study. A changing wind field could cause the dunes to erode instead of the current growth.

Major uncertainties about dune initiation, dune growth, and dune migration on short-term timescales (weeks to months) and long-term timescales (years) are still present today. In future research, measuring the variability in transport limiting factors is equally and/or even more of interest than measuring the varying wind velocities. Especially when long-term sediment transport predictions are considered.

Delgado-Fernandez & Davidson-Arnott (2009) presented some techniques to monitor long-term aeolian sediment transport in coastal environments. They used a camera-system to monitor the overall weather and wave conditions, bar welding, beach morphology, and the frequency and magnitude of erosional events. Moreover, rectified images were used to extract moisture maps, beach dimensions, fetch distances and vegetation cover. Smit et al. (2017) also presented a new method to measure spatial-temporal variation in surface moisture with an infrared terrestrial laser scanner. Williams et al. (2018) and Montreuil et al. (2018) presented some new methods to detect aeolian streamers from images. However, given enough resources (i.e. financially), a static terrestrial laser scanner (e.g. time-of-flight-pulse-based Riegl® VZ-2000 LiDAR) with improved methods for measuring morphological and volumetric changes as a result of individual transport events would be a very good technique to measure process dynamics at the meso-scale for the purpose of knowing how coastal dunes grow. It could be installed on a stable weather-proof frame on a high point above the beach. These high spatial-temporal data would help our understanding of coastal processes on land (intertidal and upper beach).

Very few detailed field studies on aeolian sediment transport are available, especially on different locations on the beach and/or dunes. These detailed studies should mainly focus on measuring wind velocities, wind directions, surface shear velocities, bed roughness, and rates of sediment transport. Bed irregularities should be measured over a distance of at least 100 m upstream of the sand traps/wind mast. When measuring the much needed short-term aeolian sediment transport, attention should be paid to instrumentation use. There are various instruments on the market to measure aeolian sediment transport. Most of them are sand traps, impact detectors, and optical sensors. However, there is no consensus of which one is optimal for a typical aeolian study. The use of passive vertical sand traps, like MWAC sand traps, can sometimes be limited because of issues such as scouring around the base, unsteady rotation due to turbulence, blocked inlets, and relatively poor temporal and spatial resolution (Ellis et al., 2009). Furthermore, MWAC sand traps only measure sediment transport from approximately 5 cm above the beach surface. Most of the total transport occurs in the first few centimetres above the surface (Bagnold, 1954). It would be of interest to introduce a self-rotating vertical sand trap that measures the whole transport column from surface to a certain distance above the surface.

It should be acknowledged that alongshore winds have chances of inputting a reasonable amount of sand to the dunes because of wind deflection close to the dune toe (Bauer *et al.*, 2012). This process is not correctly quantified as yet, and it would be interesting to see how many moving bedforms (e.g. mobile sand strips) formed at the upper beach during alongshore winds actually end up welding to the dune toe area.

Instead of using one or two meteorological stations in the study area, vertical wind profiles should be monitored adjacent to a sand trap to measure to spatial-temporal behavior of the wind field. Furthermore, Spies *et al.* (1995) argued the significance of shear velocity in a blowing sand cloud. The shear velocity is difficult to determine from measured wind profiles when wind-blown sand

occurs, especially at high wind velocities (Dong *et al.*, 2003). When wind-blown sand occurs, the wind profile is altered. Usually, it is assumed that estimates of shear velocity are close to the true values. However, it is possible that the actual shear velocities related to the saltating particles vary substantially from the shear velocities, derived from vertical wind profiles due to roughness effects, damping of turbulence, and measurement scatter (Bauer et al., 1992; Li et al., 2010). Furthermore, it is not yet fully clear what is the effective bed roughness for aeolian sand transport (dynamic grain roughness, form-related roughness or both). The influence of moisture content and beach armoring and other bed surface properties (e.g. shells or shell fragments) also appear to be a critical factor in degrading the performance of aeolian models. Future work should be based on designing a workable and predictive model that can account for these influences.

THM 2.13 BEACH MORPHOLOGY IMPACTS BEACH RECOVERY

Morphological features of the intertidal bars, embryonic dunes and backshore berm play an important role in beach recovery.

Further improving our knowledge on beach recovery is crucial for coastal protection and management. Beach recovery has been shown to depend from a wide range of parameters in addition to wave climate. These include antecedent beach morphology, geological setting, local availability of sediment, beach type and the propensity for sand transfer from the beach to foredunes by aeolian transport. There is a consensus, generally, that beaches commonly recover more or less from storm-induced erosion (if there is enough sand available). However, in contrast to beach erosion response, literature about beach recovery is scarce, sometimes even neglected in studies evaluating the cumulative impact of consecutive storms on beach erosion. The initial recovery can be extremely fast and commence immediately after the storm, but there are also reported cases where an eroded beach can last for over a year, and foredune erosion even persists over several years.

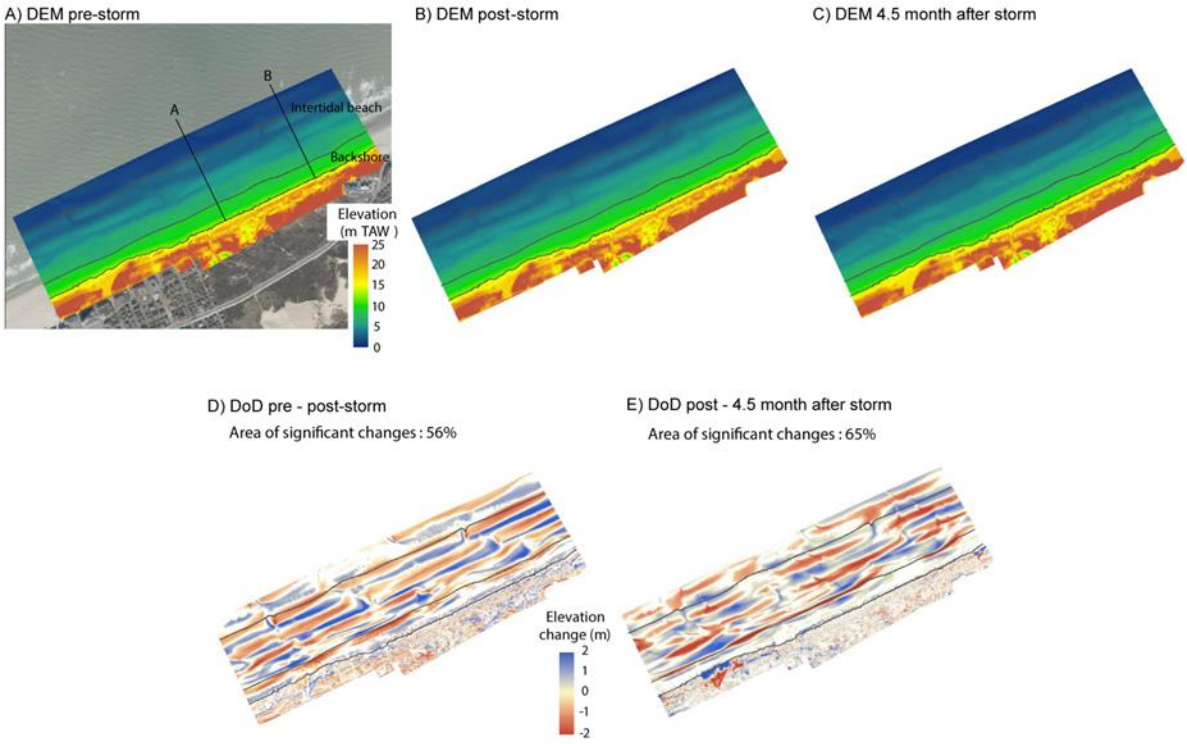

Figure 47: Beach elevation models for A) pre-storm, B) post-storm and C) 4.5 month after storm, and differences of elevation between D) pre- and post-storm and E) post- and 4.5 month after storm at Groenendijk, natural beach.

Storm Dieter hit the Belgian coast on 14-15th January 2017 causing widespread and severe damage to the coastal environment and infrastructures. The beach elevation models before, immediately after and 5 months after the passage of the storm at the Groenendijk site, an area with a natural beach, are shown in Figure 47. In the 5 month following the storm, a number of distinct morphological features such as the intertidal bars, embryo dunes and a backshore berm appeared in the course of net accretion, participating in rapid beach recovery through efficient sediment redistribution with relatively low magnitude elevation changes occurring within, and across the backshore and the intertidal zone.

THM 2.14 BEACH RECOVERY ALSO OCCURS ON DEVELOPED BEACHES IN URBAN AREA

Developed beaches in urban areas can retain some natural ability to rebuild after the storm. In the test sections 98-104 (Mariakerke) up to one third of the eroded volume due to Storm Dieter was recovered within 5 months.

Research on processes and parameters controlling beach recovery is even more limited on developed beaches in urban areas.

At Mariakerke, net accretion within 5 months after the storm was nearly twice greater at the backshore than in the intertidal beach area. It suggests that sediment was removed from the upper

shoreface and transported to the intertidal beach. Although the net storm induced erosion was three times greater than the net accretion in the considered 5 month recovery period after the storm, the recovery is apparent at the urbanized developed beach. This is shown in Figure 48.

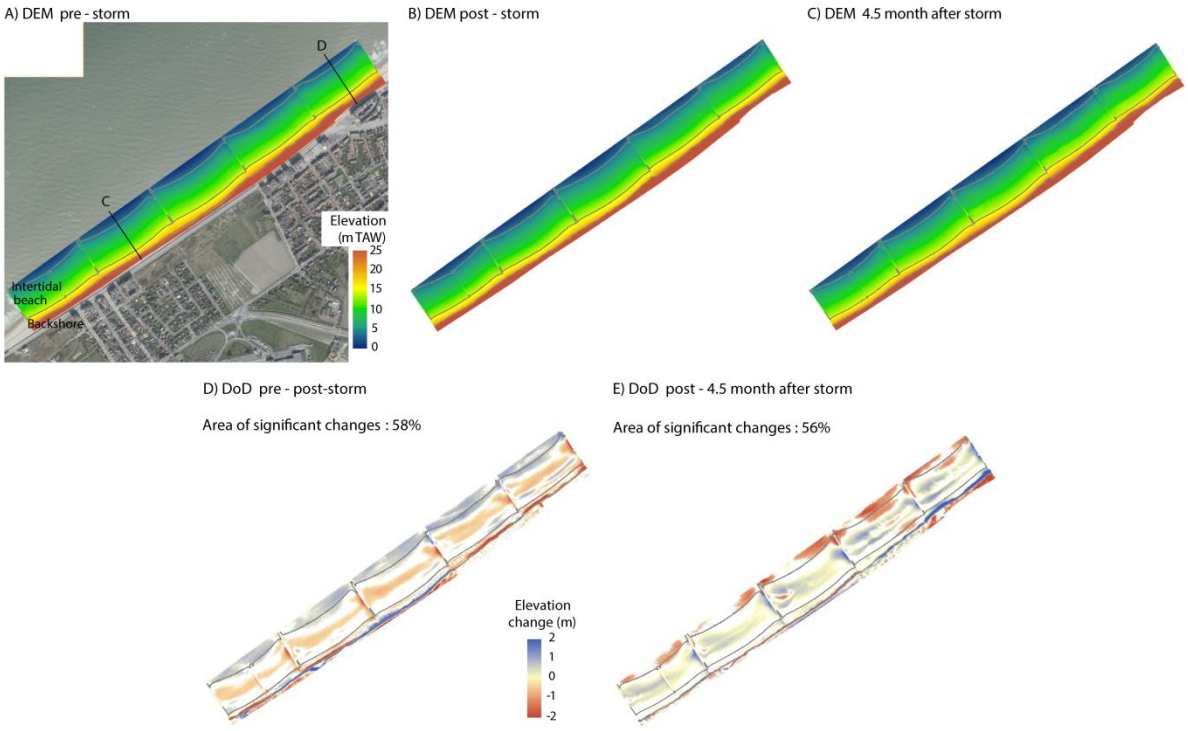

Figure 48: Beach elevation models for A) pre-storm, B) post-storm and C) 4.5 month after storm, and differences of elevation between D) pre- and post-storm and E) post- and 4.5 month after storm at Mariakerke, urbanized developed beach.

THEME 3
PYSHICAL PROCESSES AND INNOVATION IN MODELLING

Computer models for the motion of water and sediments are used **to fill in the data gaps**, both in space and in time, allowing us to better understand how nature functions. And they are used **to predict the future**. **Confidence** in the models is generated by validation through **hindcasting** – reproducing documented past evolutions - making use of **known** boundary conditions (meteo data and boundary fluxes) and known initial and final conditions (topographic data, converted into difference maps showing net erosion-depositions patterns). However, **predicting the future** is not any better than our long term weather predictions. Moreover, our computer models only **approximate** reality:

- still too many physical processes cannot adequately be put into mathematical equations;
- they cannot capture all scales - this would be too expensive in terms of computational cost and time - hence, compromising simplifications need to be made;
- and even if we could, it would be impossible to gather all the necessary (field) data.
- But step by step we find solutions to overcome some of the problems or to reduce the uncertainty;
- by parameterization and upscaling of subgrid scale physical processes that have been neglected;
- and by improving and optimizing numerical techniques.

The THM's have been subdivided into two groups. The first group of THM's (3.1-3.6) concern the lessons learnt from the model development in the CREST project. They illustrate that "**Taking better account of more fundamental processes is a good basis for understanding and simulating the patterns of coastal sediment transport.**" The second group of THM's (3.7-3.10) relate to the risk assessment for coastal flooding, for which the modelling tools are necessary to provide the input data. An important project result is that "**The FLIAT model developed under CREST provides a solid basis for hinterland flood risk calculations.**"

THM 3.1 CORRECTION FACTOR FOR INFRA-GRAVITY WAVE RUN-UP

The widely used Longuet-Higgins & Stewart (1960) method for wave run-up calculations overestimates the long wave energy for a sloping bottom. Therefore, a correction factor has been designed based on parametrizations from semi-analytical solutions that significantly improves the prediction for large normalized bed slopes.

Zhang et al. (2020) investigated the cross-shore propagation and shoaling of infragravity (IG) waves with the aim of proposing a new method to evaluate the IG energy for sloping bottoms since the widely used Longuet-Higgins & Stewart (1960), further annotated as (LHS60), method overestimates the long wave energy for sloping bottoms. By establishing a conceptual 1D model utilizing a constant slope in the shoaling zone, an analytical solution for IG waves could be obtained. Through the use of this semi-analytical solution, a collection of bichromatic conditions have been simulated confirming the dependence of the long wave shoaling rate on a normalized bed slope. This normalized slope was found to be the dominant factor controlling the shoaling of long waves, yet when the bichromatic wave steepness becomes more significant (in this study

around 0.10), the mean primary wave frequencies come into play. A detailed analysis confirmed an overestimation of the equilibrium solution by LHS60, which was derived based on a flat bottom in the first place. This overestimation was found to be the most significant for primary short waves with a small wave steepness in the offshore region. A correction to the equilibrium solution of LHS60 has been derived, and its validity has been verified through a comparison to a high-resolution laboratory experiment under bichromatic wave conditions (see Figure 49). Furthermore, the phase shift between the short wave groups and the IG waves has been discussed. At the innermost of the shoaling zone, the bound IG waves phases are still found to be strongly governed by the local forcing of short wave groups. For the near-resonant case, the bound IG waves are anti-phase to the short wave groups, and a larger phase shift in the shoaling zone might be the result of superposition of incoming free IG waves.

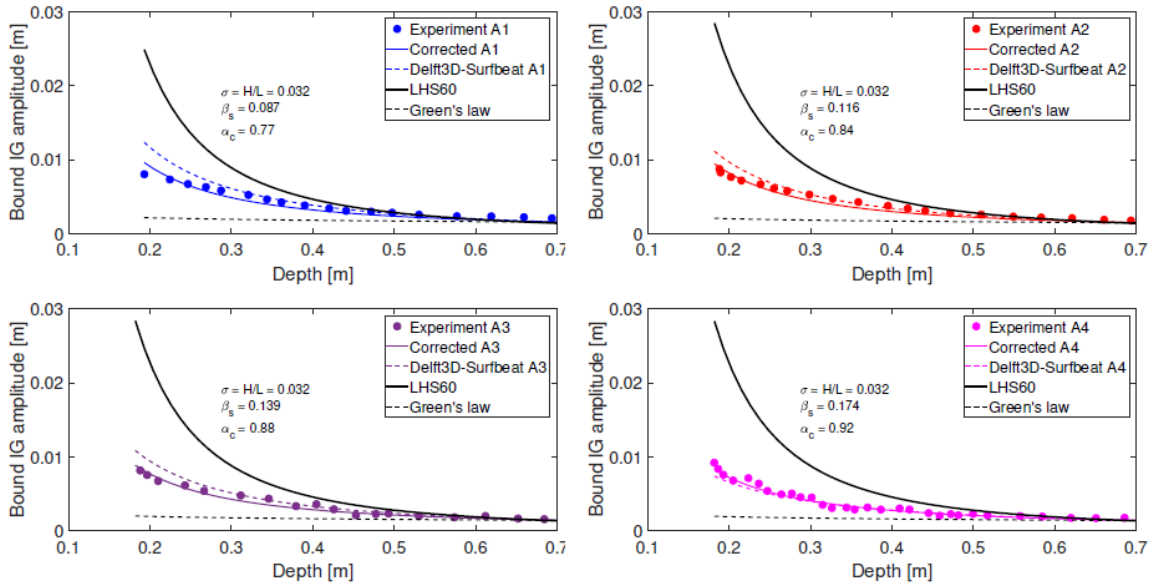

Figure 49: Validation of newly proposed formula to the series A laboratory experiment results of Noorloos (2003).

THM 3.2 EFFECT OF SHEET FLOW ON THE BOTTOM ROUGHNESS

Sheet flow modifies the hydrodynamics under waves because it leads to more significant wave dissipation than skin friction.

When surface gravity waves propagate from offshore deep water to nearshore shallow water, strong interaction takes place between the waves and the sea bottom. On one hand, the waves dissipate energy via bottom friction, and on the other hand, sediments are stirred up and resettle under the oscillatory motion of waves. Accurate prediction of this process requires precise estimation of the wave friction factor, which in turn involves prediction of the roughness height. For less energetic wave conditions, the sand bottom remains flat, which is referred to as the immobile bed regime, under which the roughness is scaled to the physical grain roughness

($\mathcal{O}(d_{50})$). However, if the shear stress exceeds its critical value, sediment movements start and a symmetric regular patterns of ripples are formed at the bottom. In the ripple regime, the bottom roughness is related to ripple dimension and it has been widely investigated, both in the context of sediment transport (Sato, 1987; Clubb, 2001; Davies, 2005) and wave dissipation (Carstens et al., 1969; Grant & Madsen, 1982). High energetic waves lead to washing out of the ripples, and the sheet-flow regime builds up, where the forward and backward oscillatory intense sediment movements form an apparent roughness. In the sheet-flow regime, it is often assumed that the roughness height is of the same order of the sheet-flow layer thickness (Grant & Madsen, 1982; Wilson, 1989). In this study, we employ the newly developed multi-phase model (MixtSedFoam) for sediment transport in free-surface flows (Ouda & Toorman, 2019) as a numerical laboratory, which fills the gap in traditional measurements and offers large detailed information of the wave propagation as well as the sediment movements in sheet flow. Thanks to this detailed information, we evaluate the capacity of the five existing formulas given in **Error! Reference source not found.** from various aspects: the wave energy tracing, sediment flux computation and the sheet flow layer thickness. Three different friction factors formulations (Grant and Madsen (1982), Jonsson (1966) and Nielsen (1992)) are chosen to compute the bed shear stress based on the roughness of five existing methods given in Table 7 for evaluating sheet flow roughness. For each of these combinations, the sediment fluxes are calculated with the widely used Meyer-Peter Müller formula using the maximum orbital velocity of a monochromatic wave. The resulting sediment fluxes are shown in Figure 50 together with the maximum sediment flux within one monochromatic wave cycle obtained with MixtSedFoam. Figure 50 shows that the results obtained with the sheet flow roughness formulation of Wilson (1989) and of Madsen et al. (1993) give the closest match to the MixtSedFoam calculations. Using the sheet flow roughness formulation of Grant & Madsen (1982) overestimates the sand flux by an order of magnitude.

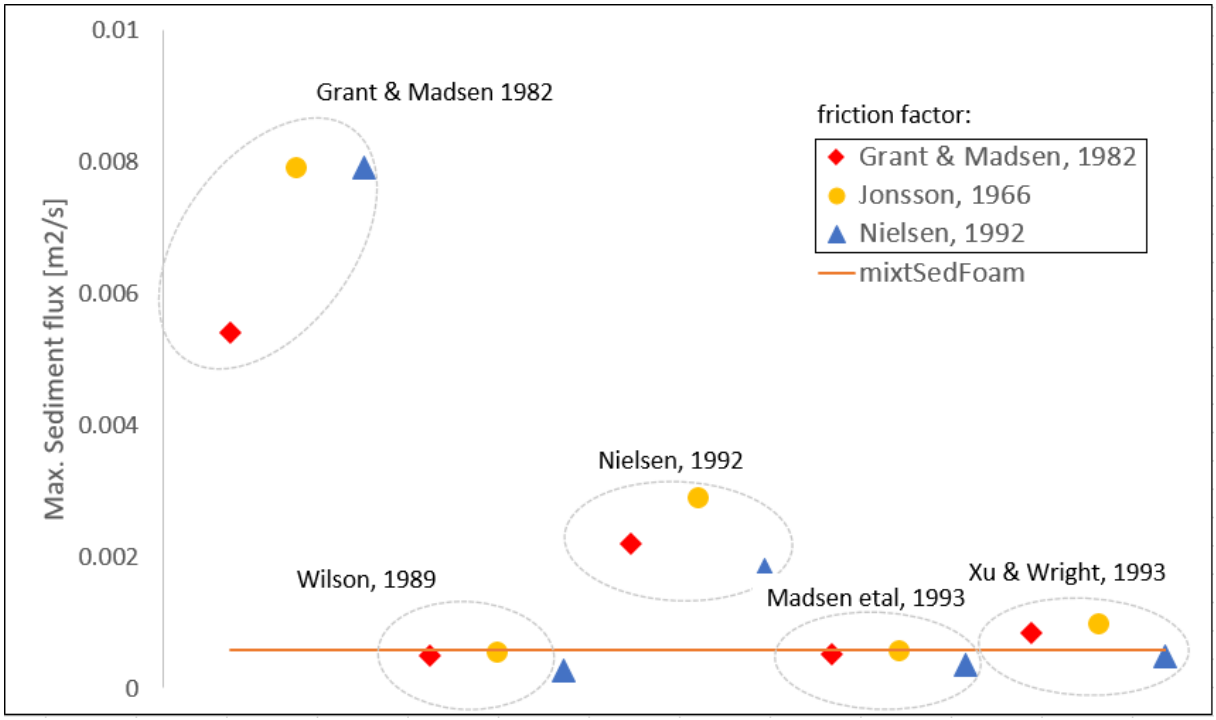

Figure 50: The maximum sediment flux computed by MixtSedFoam is compared to five existing methods for evaluating sheet flow roughness for three data sets.

Author&Year	Formula
Grant & Madsen 1982	$\frac{K_s}{d_{50}} = 160(s + 0.5)\theta_{cr}\left(\sqrt{\frac{\theta'}{\theta_{cr}}} - 0.7\right)^2$
Wilson, 1989	$\frac{K_s}{d_{50}} = 5\theta$
Nielsen, 1992	$\frac{K_s}{d_{50}} = 70\sqrt{\theta}$
Madsen et al. 1993	$\frac{K_s}{d_{50}} = 15$
Xu & Wright, 1993	$\frac{K_s}{d_{50}} = 15\,\theta$
Where K_s is the equivalent roughness height for sheet flow condition, $s = \rho_s/\rho_w$, with ρ_s and ρ_w the sediment and water density. θ' is the skin shear stress and θ_{cr} is the critical shear stress. θ is the total shear stress with constitutes both the skin friction and the sheet flow roughness. d_{50} is the 50% quantile of the sediment size. Apart from the Grant & Madsen 1982 formula, all other formulas are thus implicit and require iterative calculations.	

Table 7: Roughness height formulations for sheet flow conditions

THM 3.3 ALTERNATIVE BOUNDARY TREATMENT FOR TURBULENCE MODELLING

Turbulence modelling in 3D computational fluid dynamics with standard linear interpolations and refined grids are incompatible with standard bottom boundary conditions. An alternative boundary treatment procedure has been designed to overcome these limitations.

The generation of turbulence is the major mechanism of loss of wave energy and loss of kinetic energy of currents. The quantification of the impact of currents and waves on coasts has to take that into account. However, the modelling of turbulence is the most problematic issue in computational fluid dynamics, because it concerns motions of water molecules at the smallest scales (the so-called Kolmogorov scales). Exact solutions are not possible and simplified closure models are used to describe turbulence as subgrid scale process. In coastal engineering, two-equation turbulence models are the most popular to account for vertical mixing in 3D simulations, in particular the k-epsilon model. This model solves the balance equations for turbulent kinetic energy (k = TKE) and its dissipation rate (epsilon = TDR). Both parameters vary non-linearly close to solid boundaries, like the sea bottom. However, the numerical model computes values only in discrete nodes and assumes a predefined interpolation function in between. The most common interpolation is done with simple linear interpolations. They do not match well with the exact non-linear behaviour, introducing errors. Some of these errors can be reduced by refining the computational grid towards the bottom.

The implementation in the TELEMAC3D code was found to yield very poor results under certain conditions. This has been investigated systematically, indicating an unacceptable sensitivity to grid structure and “wall distance” (the distance between the grid boundary and the actual bottom, which have to be different to avoid numerical problems in the so-called “wall layer” where the flow

becomes laminar towards the actual bottom). In order to understand this better, this problem has been investigated with other codes as well (OpenFOAM, GOTM and COHERENS). This confirmed that none of the codes is able to generate simultaneously correct results for the three variables velocity, TKE and TDR. It could be demonstrated that the errors are caused by the linear interpolation functions, which generate an underestimation of the velocity gradient at the bottom and an overestimation of the gradient of the turbulent dissipation rate.

New boundary conditions have been formulated that account for the use of the linear interpolation functions and fulfil three conditions: mass flux conservation, generation of the correct bed shear stress and a linear variation of TKE in the bottom layer. The new method has been implemented in TELEMAC3D.

THM 3.4 A PHYSICS-BASED TURBULENCE CLOSURE

Modelling of particle-turbulence interactions remains a key issue in highly concentrated sediment transport modelling. A physics-based turbulence closure is essential for modelling energy dissipation due to sediment motion.

Because sediment particles have a higher density than water, they respond slower to changes in flow conditions, resulting in a difference in velocity between the particle and the surrounding water and shear at the particle scale. The higher density also explains why the highest concentration of suspended particles is found near the bottom, in the layer where turbulence is generated by shear of the current and orbital wave motion. In this layer, additional energy is dissipated by friction and collision between the particles. The net effect of these processes results in a modulation of the global energy budget for currents and waves compared to a system without mobile sediments. Thus far, the effect of sediments on hydrodynamics is indirectly taken into account by manually increasing the friction factor. Since the sediment fluxes vary in time and space, the friction factor should also vary in function of the presence of suspended sediments.

The principle has already been taken into account in the design of a new generalized friction law, used for the first time in a depth-averaged model for the Belgian coast and Scheldt estuary (Bi & Toorman, 2015). The further investigation of these processes requires more detailed data than currently is available from laboratory experiments. Because of the limitations of the present measuring technologies, a 3D modelling tool for sediment transport, based on two-phase flow theory, has been developed and implemented in OpenFOAM to be used as numerical laboratory to generate additional data (Ouda & Toorman, 2019). The application of the model to several laboratory experiments, used for validation, demonstrated that the mixture version for the k-epsilon turbulence model still fails to predict the turbulence damping in the bedload layer correctly. One of these cases is shown in Figure 51. The reasons for this underestimation of the damping could be identified: a significant fraction of the kinetic energy from the fluid is needed to move the sand particles and therefore is not available to produce shear turbulence. A methodology to solve the problem has been developed, consisting of the use of turbulence damping functions, known from low-Reynolds turbulence modelling, taking into account the effective mixture viscosity instead of the fluid viscosity (Toorman et al., 2019).

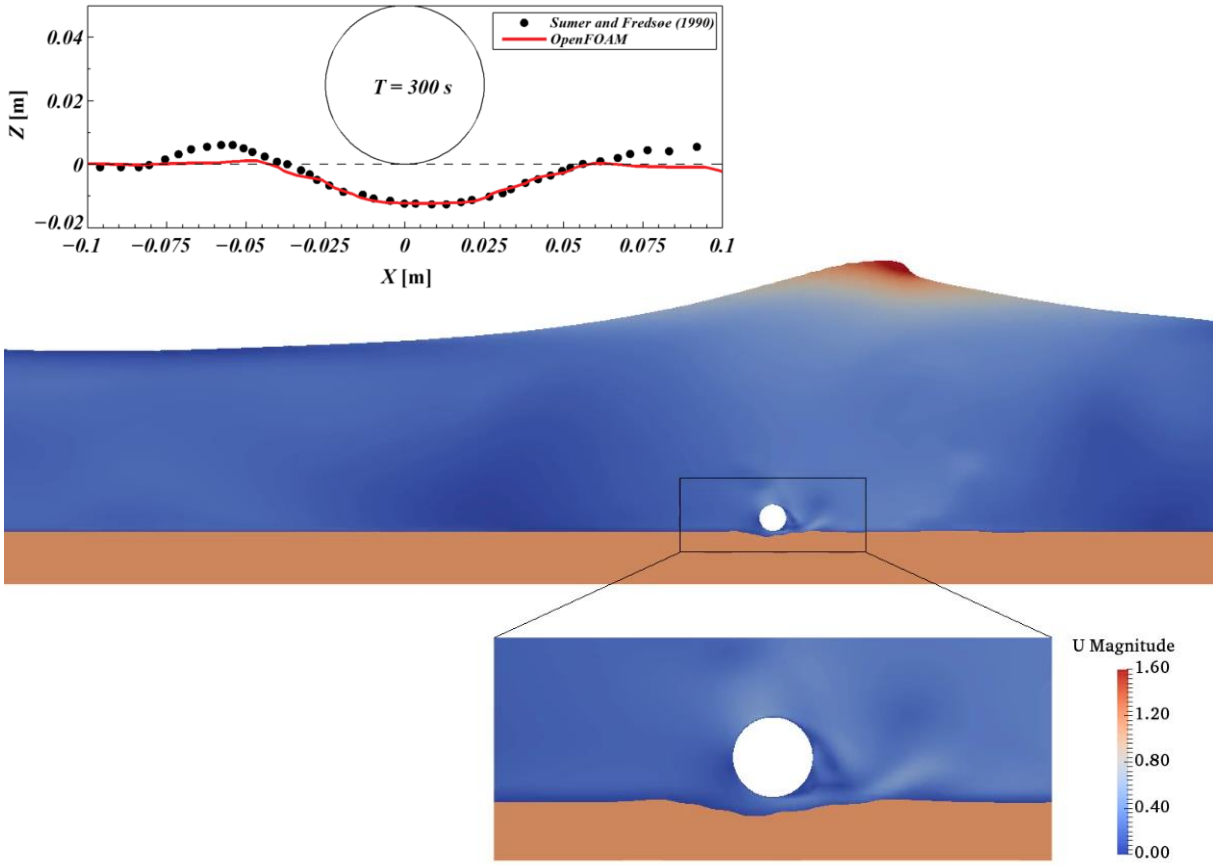

Figure 51: A laboratory experiment of scour under a pipeline by waves simulated with MixtSedFOAM (Ouda & Toorman, 2019). The edges of the equilibrium scour hole are washed out by the excessive turbulence in the model since the turbulence damping by suspended sediment is not yet properly modelled.

THM 3.5 VALIDATION OF A 2D SAND-MUD MODEL FOR THE BELGIAN CONTINENTAL SHELF

A good basis for long term simulation of mixed sediment transport is present in the 2D TELEMAC-TOMAWAC-SISYPHE coastal models. This is good news for management considerations that require large scale and long term simulation of complex scenarios in reasonable time.

The sea bottom in coastal areas in the vicinity of river mouths often contains large fractions of cohesive sediments (mud), which affects the erodability of the bed and may also cause wave damping. Such a large mud patch is also present in front of the Belgian coast around Zeebrugge and is expected to influence the hydrodynamic forcing on the coast and the sand transport, and therefore should be taken into account to understand the resilience of the coast.

A 2D model of the Belgian Coast and the Western Scheldt was developed with the TELEMAC software and its modules TELEMAC 2D (hydrodynamics), TOMAWAC (waves) and SISYPHE (sediments). The model uses the physics-based formulation for bottom friction from (Bi &

Toorman, 2015), and takes into account the presence of mixed sediments: sand which is the basis of the coastal protection system and mud which highly affects the coastal ecosystem.

Comparison with satellite data from the PROBA-V mission showed that both modelled and satellite-retrieved suspended mud concentrations match qualitatively well for a simulation period between March and July 2016. Especially important was the fact that some spatial patterns of the well-known coastal turbidity maximum area between Ostend and the Western Scheldt could be reproduced by the model (see Figure 52).

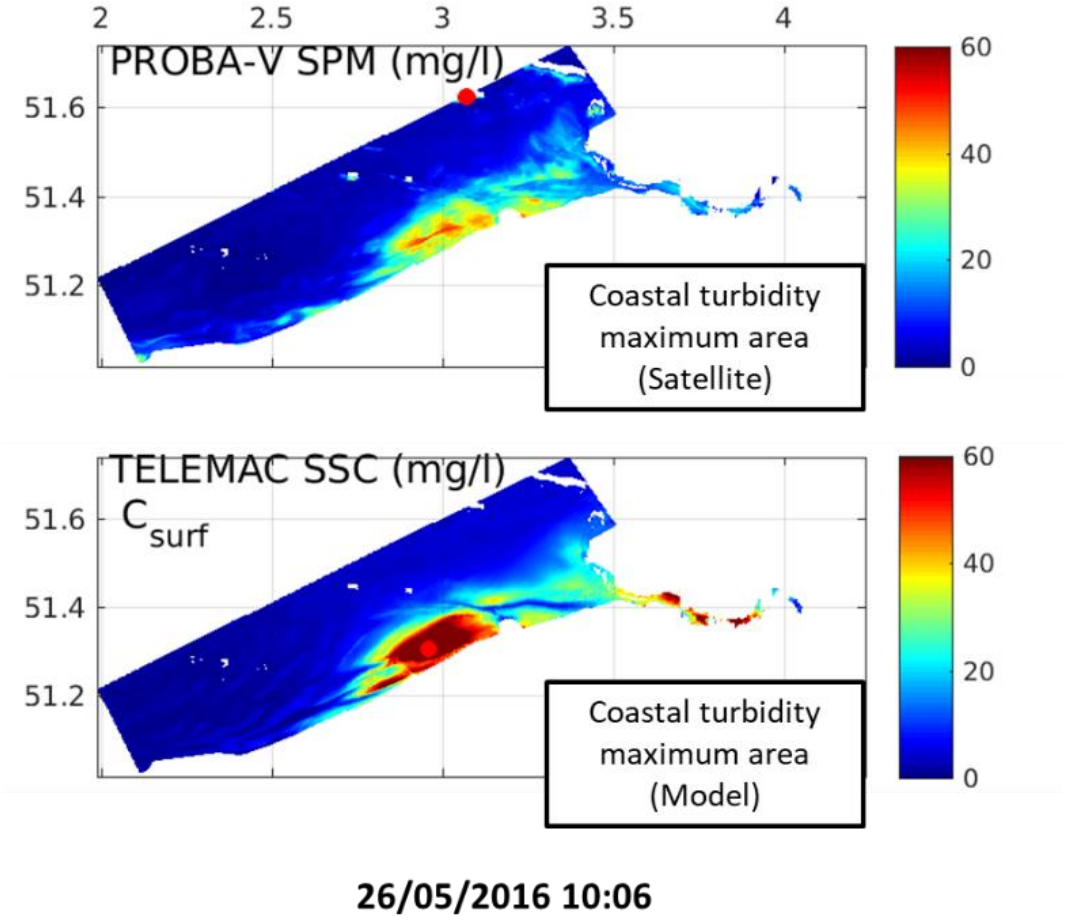

Figure 52: Satellite-retrieved suspended particle mater (PROBA-V) and modelled near-surface mud concentration (C_surf). NaN (Not a Number) values in satellite image (white) have been masked out in the model results too.

This is a useful result considering the complexity of the processes involved (e.g. wave-enhanced shear), the extent of the study area (~3800 km^2) and the fact that an additional algorithm (Van den Eynde, 2018) must be used to convert modelled depth-averaged mud concentrations to near-surface values to match what can be retrieved from the signals in satellite images.

Sand and mud have an impact on the needed dredging activities and on coastal management. With models like this it is possible to simulate in a relatively short time long term and large scale scenarios required by these sectors. Further work is planned to quantify and also compare sand transport patterns.

THM 3.6 COUPLING OF DIFFERENT NUMERICAL MODELS FOR WAVE OVERTOPPING CALCULATIONS

The road to efficient and accurate design of the optimised coastal defence systems of tomorrow – Coupling numerical models enables complex modelling only where necessary: advantages of each model are preserved without suffering their individual downsides.

In order to estimate overtopping processes such as wave overtopping over the safety line and wave force acting on apartment building, which are most relevant to the coastal safety issues along the Belgian coast, one needs to model multi-scaled physics. Many numerical model have been developed and (partly freely) available in the last few decades to study phenomena related to sea waves and their interaction with coastal defences. Some models are good in wave transformation and applicable to a large domain, while others are more suitable for wave-structure interaction detailing hydrodynamics in time steps but in a limited domain. There is no optimum model which can deal with the multi-scaled physics at the same time. In order to provide a solution for real applications, coupling between numerical models can be employed, which enable complex modelling in an efficient and accurate way. The excellence obtained by coupling numerical models is found in the fact that advantages of each model are preserved without suffering their individual downsides. FHR and UGent have been working on the development of the coupling methods in the last years (see Altomare *et al.*, 2015; Altomare *et al.*, 2018 and Verbrugghe *et al.*, 2018).

Figure 53 shows one example of coupling a DualSPHysics model and a SWASH model. DualSPHysics is a meshfree Smoothed Particles Hydrodynamics (SPH) model and SWASH is a non-hydrostatic model. DualSPHysics can simulate wave-structure interaction in an accurate way at the cost of a lot of computational time. SWASH can simulate wave transformation in very efficient way while it cannot deal with complex wave-structure interaction. The coupling of DualSPHysics and SWASH allows modelling both wave transformation and wave-structure interaction and attains a compromise between results accuracy and computational effort. As mentioned above, many coupling methods have been developed for different applications. One can choose one of the methods which is most suitable for one's problem.

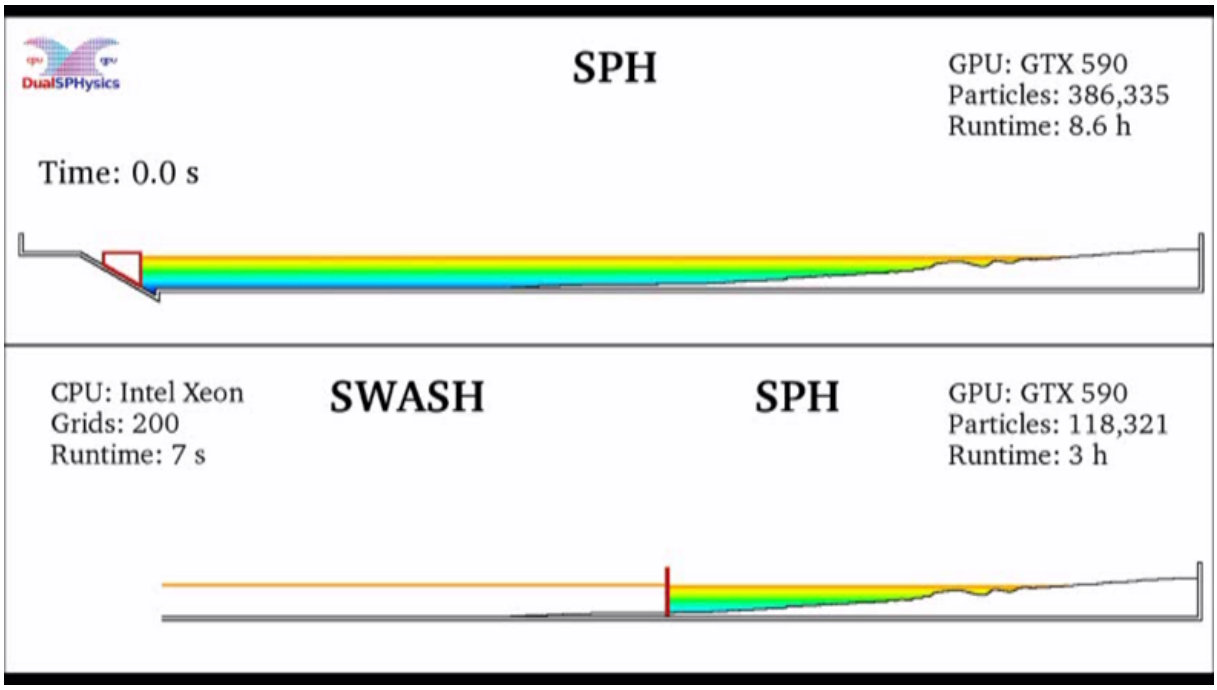

Figure 53: An example of SWASH-DualSPHysics coupling. The calculation is accurate while computational time is reduced in the coupling model. The different colours represent different pressure levels.

THM 3.7 A WEB-BASED TOOL FOR FLOOD VISUALISATION TO INCREASE PUBLIC AWARENESS

Lack of public awareness equals lack of motivation among people to support, or even protest, changes in necessary landscape measures to improve coastal safety. Therefore, there is demand for a good visualisation and communication tool in Flanders that quickly conveys strong messages, condenses complex information, and engages the community in issues of environmental change.

Although scientists widely stress the compelling need to mitigate and adapt to climate change, public awareness lags behind. Mayors of cities, council members, and other policymakers are generally fearful of instilling anxiety in populations who are at risk of coastal flood hazards. Therefore, authorities operate by the principle of "let sleeping dogs lie" and do not inform inhabitants about the risks related to flood hazards. Lack of public awareness equals lack of motivation among citizens to support changes and flood adaptation in the landscape or even to protest necessary measures to improve flood resilience.

Therefore, local governments must engage and educate the local community to adapt to the impacts of flood events. To this end, a comprehensive three-dimensional flood visualisation WebGIS (Web-based Geographic Information System) was developed, as it quickly conveys strong messages, condenses complex information, engages people in issues of environmental change,

and motivates personal actions. This chapter describes a tool that can visualise a flood event so that a community can understand what effect a flood event would have on the area and how these risks might change with a changing climate.

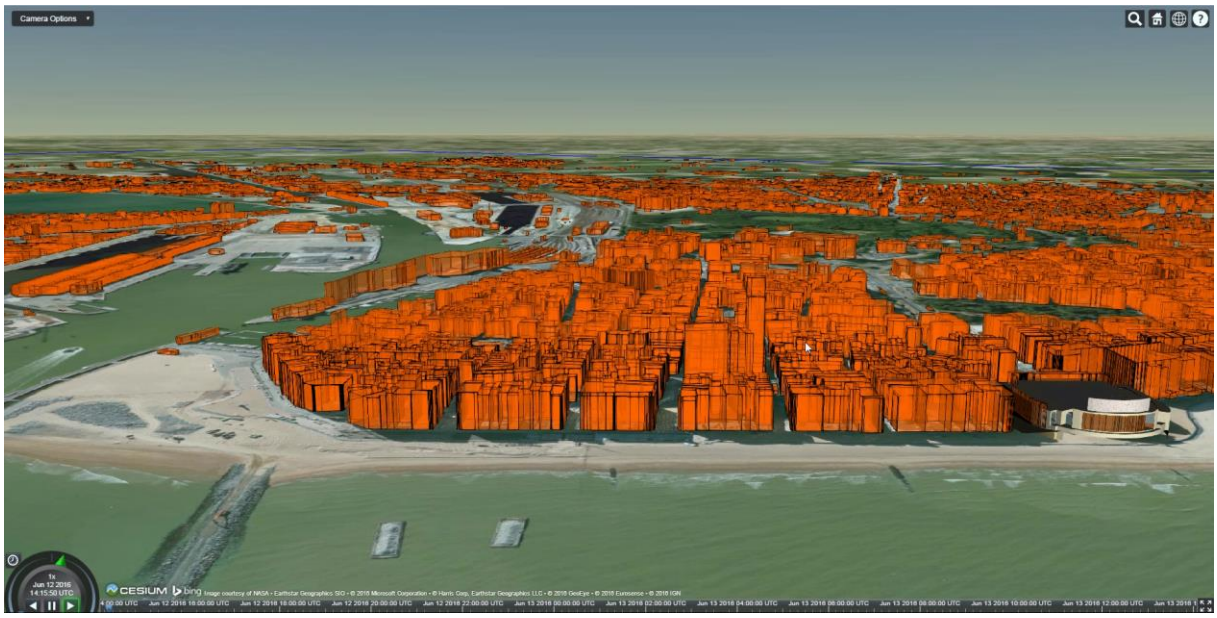

Figure 54: Screenshot of the 3D webGIS prototype (developed with the use of CZML) for the coastal city Ostend, Belgium.

By visualising the consequences of all possible practical adaptations (e.g. inserting gates where needed, adding sluices to prevent ingress of water into drains, raising floor levels in vulnerable town centre properties, installing storm walls, etc.), people are better informed and will support decisions more quickly because they have the feeling they are involved and their opinion is valued.

THM 3.8 INTERNET OF FLOODS AS A DECISION TOOL DURING FLOOD EVENTS

In order to make well-informed decisions, and because time is key during a flood disaster, tools that collect all relevant information to determine the extent of the flood event and its damage as quickly and accurately as possible must be available ahead of time.

Time is key during a flood event. Therefore, it is crucial to respond quickly and to make well-informed decisions in order to evacuate vulnerable people at risk, minimise the socio-economic, ecologic, and cultural impact of the event, and restore a society to working order as quickly as possible. Therefore, detecting a flood in near real-time and assessing the impact of these flood events spontaneously is important. Moreover, tools that filter, collect, process, and analyse data must be available ahead of time, which allows for the gathering of information around flood events from various channels.

At this moment, the Internet of Things (IoT) is the ideal method to accomplish the detection of floods in near real-time. Internet of Things is defined as the networked interconnection of ubiquitous, context-aware devices that are embedded with sensors, software, electronics, and

actuators that enable ambient intelligence. Over the last couple of decades, the IoT has been in a constant state of evolution, thanks to rapid advances in underlying technologies.

IoT is providing remarkable opportunities for more direct integration of the physical world into computer-based systems, resulting in novel applications that promise economic benefits, improvement in quality of life, and reduction of human exertion.

The Internet of Floods[2] (IoF) can be defined as the Internet of Things (IoT) applied to detecting flood events and their impact in near real-time. The introduction of the Internet of Floods (IoF) would serve as an answer to the demand for a holistic tool that connects all possible semi-intelligent devices and people-operated technologies. This allows for the collection of data on a given flood disaster. After collecting said data, the IoF platform filters and searches for relevant data and applies analytics to it, providing comprehensive insight into the extent of the flood event and its impact.

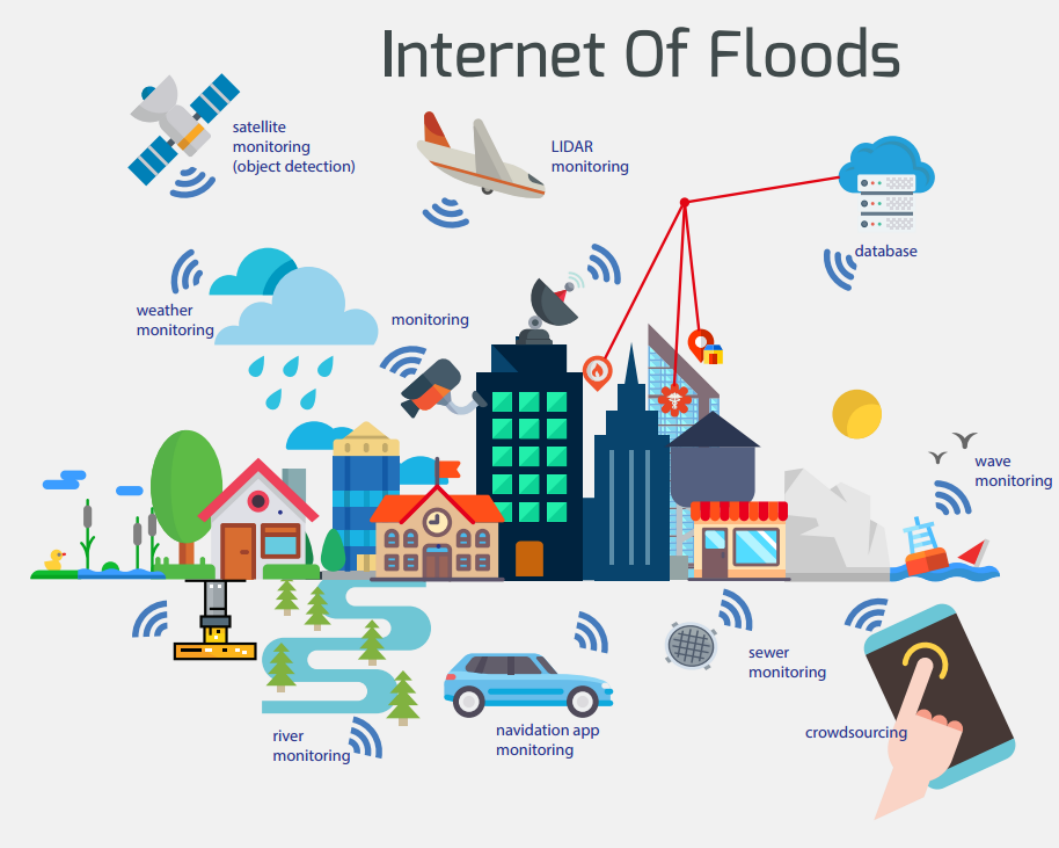

Figure 55: Schematic representation of the Internet of Floods (from Van Ackere et al. 2019a).

The first technology that can be used to detect floods in near real-time is remote sensing techniques, for instance, segmentation on satellite imagery and analysing radar data. Using smart cameras, smart buoys, water level sensors, weather sensors, and smart sewerage systems could significantly enrich the IoF network. Moreover, participatory sensing systems and solicited crowd-sourcing could improve the data source range since, in these types of crowdsourcing, observations

2 "Internet of Floods" is protected during the PhD research of Samuel Van Ackere at the Benelux Office for Intellectual Property (BOIP Merkenregister | Benelux-Bureau voor de Intellectuele Eigendom. Available online: https://www.boip.int/nl/merkenregister (accessed on Jun 6, 2019)

of flood events or socio-economic damage are immediately filled, drawn, or mapped in a structured template by recruited, participating users (De Wille et al., 2019). Adding data of real-time web-based navigation platforms and mobile navigation applications for drivers (Gautama et al., 2017), like Waze, to IoF, where users can report hazards (for example, a small flood event or a massive snow hazard), would be an extra pair of eyes on the road. Finally, social sensing and unsolicited crowdsourcing, smart home technologies, and smart wearables could extract relevant information from the population itself without asking for active participatory involvement.

With IoF, this wide range of possible information sources are recognized, and data collected from these sources could enhance insight into an occurred flood event. As a result, urban search and rescue teams can be deployed quicker and more efficiently and the population can be informed on the location and scale of field hospitals and emergency shelter. Moreover, technologies such as water purification systems, high capacity pumping, CBRN (chemical, biological, radiological, and nuclear) detection, and sampling tools can be deployed at the correct location and scale. In short, the Internet of Floods is the perfect technology for detecting flood events and their impact in near real-time. Moreover, it can be used to communicate to the community through its linked smart devices.

THM 3.9 FLIAT: A NEW RISK ASSESSMENT TOOL

A cloud-based flood risk assessment tool with an object-relational approach, FLIAT, is developed, to improve the accuracy, calculation speed, ease of use, and possibilities for further development of the flood risk and damage assessment methodology in Flanders.

The overall objective of work package 2.5 of the CREST project, was to search for new, innovative tools that can improve the flood risk and damage assessment in Flanders and enhance prevention, protection, and preparedness before a flood event and response and recovery after a flood event. Therefore, a prototype for a new flood damage and risk assessment tool, called FLIAT, was developed.

One of the most notable differences between FLIAT (Van Ackere et al., 2019b) and LATIS (Deckers et al., 2009), is the fact that FLIAT is programmed as a cloud-based impact assessment tool with a vector approach, backed with an object-relational database. As a result, in contrast to LATIS, FLIAT can also handle multiple datasets that are linked to well-defined elements (e.g., multiple activity codes (NACE codes), presence of a basement, number of inhabitants linked to a building, etc.).

Figure 56: FLIAT comes with a relational database that can embed multiple detailed data sets.

Based upon the LATIS expertise, and in combination with enhanced insights and the improvement in server performance and computing power, the FLIAT tool aims to develop unique hybrid technology that outperforms the existing software on the market in terms of accuracy and speed. As a result of a significant improvement in accuracy, it could be used in cost-benefit analysis of infrastructures or measures that can prevent or minimise the impact of coastal floods (e.g., storm surge barriers), river floods (e.g., raising dykes), or pluvial floods (e.g., larger dimensioned sewerage). Moreover, the FLIAT methodology embeds a vulnerability assessment module, which rates the existence of a latent probability of societal collapse. For example, roads used to evacuate inhabitants can now be considered in cost-benefit analysis.

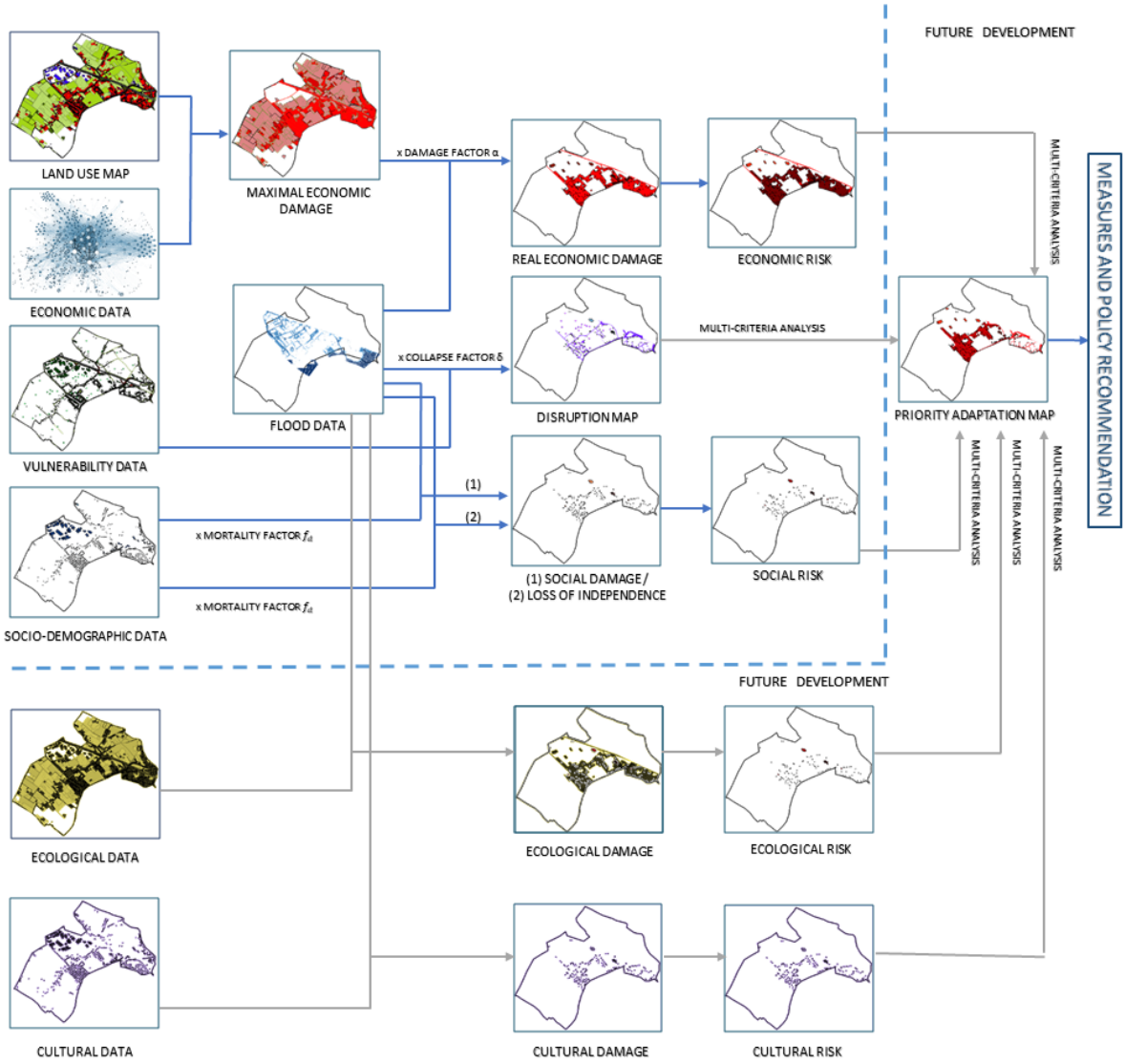

Figure 57: FLIAT methodology, with the indication of future development (ecological and cultural damage and risk calculation and the addition of the development of a priority adaption map methodology).

THM 3.10 VERTICAL EVACUATION TO MINIMISE CASUALTIES DURING STORMS

If a predicted storm is more severe than anticipated, evacuation is necessary. In case available evacuation time is short, a vertical evacuation is preferred above the classical evacuation outside the flood area.

The strength of our dune and dike system is estimated during safety assessments and risk calculations. For different storm water levels (ranging from +6m TAW till +8m TAW) it is known where dikes or dunes might breach, where wave overtopping occurs and which flooding (cf. Figure 58) and damage this can cause.

The OMS (Oceanografisch Meteorologisch Station) gives predictions of expected water levels and wave heights. Once the alarm levels are exceeded, the warning system of Coastal Division is activated. Depending on the water level, involved stakeholders are informed (communities, Civiele Bescherming, sluice operators, Flemish and federal administrations…). Also an action plan can be started up (e.g. closure of gates, construction of mobile storm walls…).

If floodings are expected, the local and provincial BNIP (Bijzonder Nood- en Interventieplan) are activated. The provincial BNIP is updated by the Federal Government/province for the moment and will be completed by end 2019. This plan foresees in evacuation routes (e.g. Figure 58), shelter locations, organisation of preventive measures, guidance of people when returning home…).

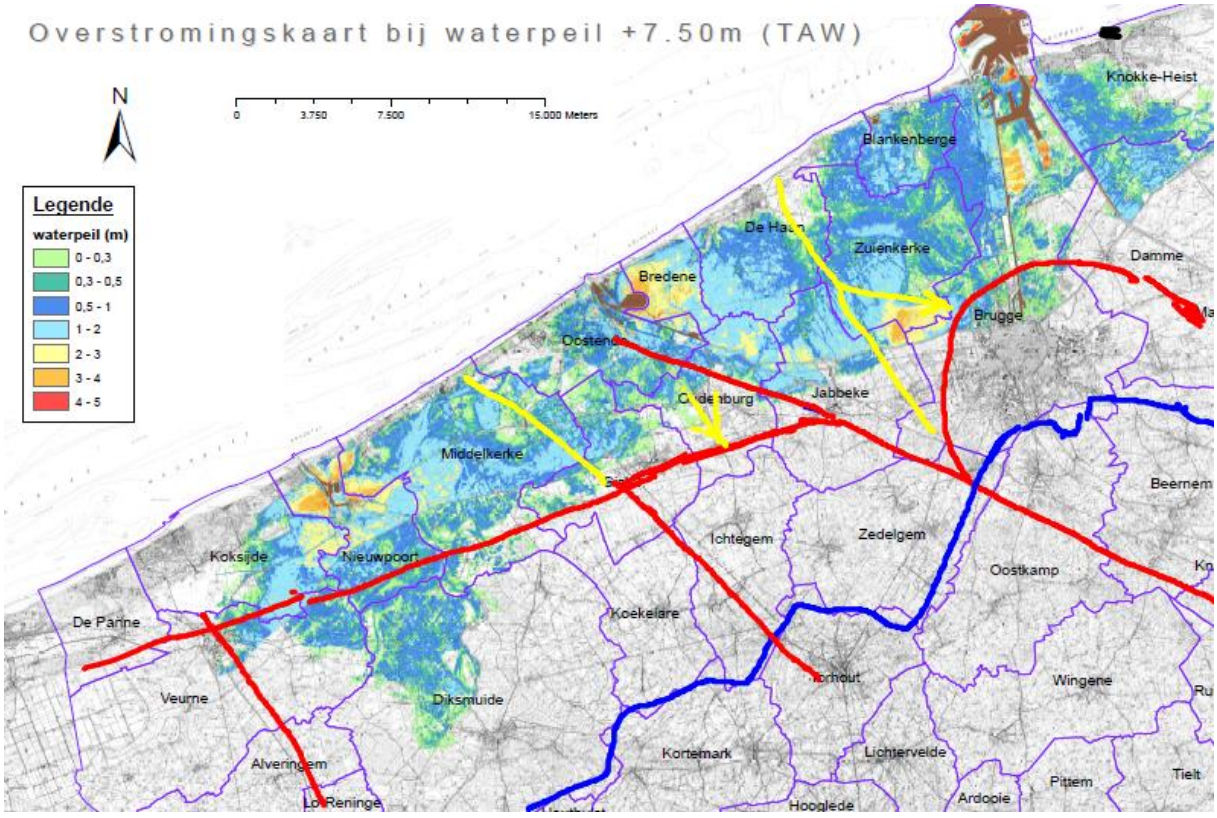

Figure 58: Flood depths and possible evacuation routes.

However, at the peak of the storm wind velocities are very high and a lot of roads will be closed due to obstacles. Also, if a flooding occurs during evacuation, people on the road near the sea are in a very dangerous situation.

An exercise in the Netherlands learned that it is often preferable not to leave the area, but to evacuate to higher levels (presentation Dr. Bas Kolen during the CREST workshop of 24th of April 2019). The number of casualties depends on the location (from low to high):

1. Outside flood area
2. Shelter
3. At home - prepared
4. At home – not prepared
5. On the road

In the exercise for Central-Holland, the number of casualties was estimated depending on the available days for evacuation and for different evacuation strategies. The exercise indicated that if the available time is less than 3 days, a lot less casualties are expected with vertical evacuation compared to horizontal evacuation.

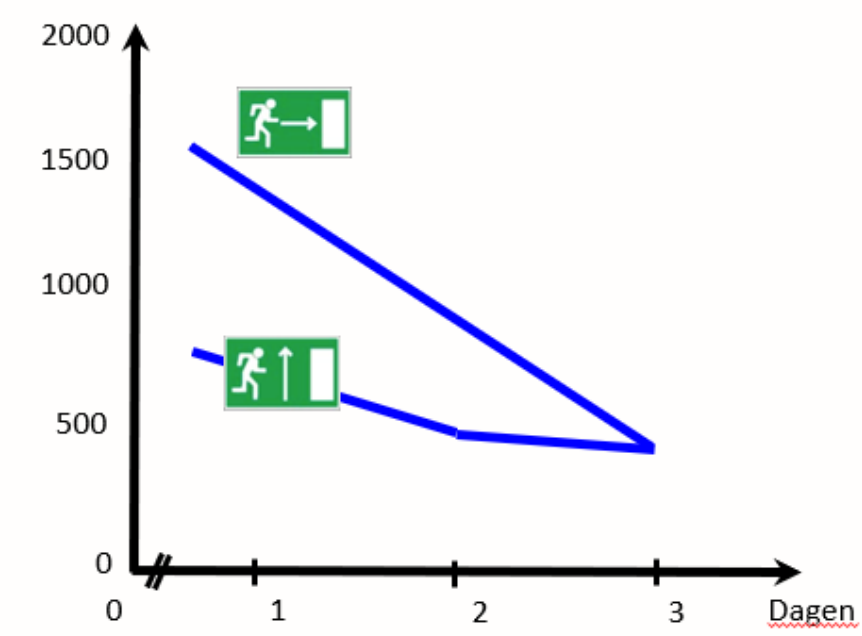

Figure 59: Expected number of casualties depending on the available days for evacuation – comparison vertical and horizontal evacuation.

At our coast, vertical evacuation can consist of the movement of people to higher levels in the building they are living in. Most buildings are stable even if overtopping waves hit the buildings. Although, due to the wind, also in the building potential dangerous situations can occur (e.g. close to windows), this is safer than on the road. In recent severe storms, the major problems occurred in traffic (jams, accidents) not inside buildings.

THEME 4
PREDICTION OF WAVE IMPACT (OVERTOPPING AND LOADS) ON THE DIKE DURING STORMS

The first three Take Home Messages (THM's) are general and are worked out in the detailed THM's.

THM 4.1 INVISIBLE BUT STRONG: LONG WAVES

Hidden in plain sight: imperceptible to the naked eye, very long waves are unexpected adversaries for our coastal defence protection against flooding during violent storms.

THM 4.2 WIDE BEACHES TO PROTECT AGAINST VIOLENT STORMS

Shallow beaches are essential in our hybrid soft-hard coastal defence system – Size matters in the protection against violent storms: wider beaches reduce the wave impact on the dike.

THM 4.3 OUR COMPLEX COASTAL DEFENCE SYSTEM REQUIRES STATE OF THE ART NUMERICAL MODELLING

Complexity begets complexity: the complex shape of our coastal defence system leads to complex hydrodynamics – Accurate prediction of the wave impact on the dike and buildings requires state of the art numerical modelling to avoid over-conservative design.

THM 4.4 IMPROVEMENT OF SAFETY ASSESSMENT METHODOLOGY

Using the more detailed insight in physical processes and the validated numerical tools acquired in the CREST project, the complete calculation methodology for safety assessments and risk calculations can be improved.

It was the aim of CREST to provide the necessary pieces to improve safety assessments and design methodologies for coastal defence systems similar to the Belgian case. In the near future, these pieces will be gradually introduced in the improved design methodologies. The achieved methodology can be used for comparable coastal defence systems elsewhere, or parts of it can be used for other systems with different characteristics.

The safety assessment methodology currently consists of the following steps:

1. Derivation of the hydrodynamic boundary conditions (wave climate and water level) offshore;
2. Transformation of the wave climate to the beach toe (defined at -5m TAW) using SWAN;

3. Morphological modelling of the beach and dune erosion during a storm using XBeach;
4. Transformation of the wave characteristics from -5m TAW towards the toe of the dike (including the effect of directional spreading of waves) using SWASH 2DH (with relative small spatial resolution);
5. Calibration of SWASH 1DH to get the same wave characteristics at the toe of the dike (without directional spreading) using this higher resolution model;
6. Calculation or modelling the wave overtopping on the dike crest using the calibrated SWASH 1DH model and (if possible) using prediction formulae;
7. Comparison with the maximum allowed overtopping discharge (1 l/s/m);
8. Comparing the minimal necessary dune volume with the modelled remaining dune volume;
9. For risk calculations: calculation of flood depths and damage/casualties due to overtopping and flooding.

Based on the CREST project results, the following improvements to the current methodology are suggested and remaining knowledge gaps are identified:

Ad 1)

Boundary conditions (extreme conditions defined using a large return period) for safety assessments depend on the time horizon (climate change). A better estimate on extreme sea level, wave and wind conditions, taking into account climate change scenarios, can be obtained following the results of THM 1.1, THM 1.2 and THM 1.3.

Ad 2)

The offshore boundary conditions consists only of short waves. In TOMAWAC no long wave generation (infragravity waves) was incorporated at the start of CREST. In D.1.1.1 (Zhang et al, 2016) a long wave generation module is incorporated in TOMAWAC for the first time. After validation, this model could be used to get more knowledge of long wave energy on the Belgian Continental Shelf.

Ad 3)

An alternative for XBeach could be TELEMAC suite of models. At the start of CREST this model suite still lacked basic physics such as long wave generation, undertow, avalanching. In D.1.1.1 a selection of these physics has been incorporated. Also other aspects are being developed (influence of sediment concentration on turbulence, mixed sediments). At this moment however, there is no valid alternative for XBeach for beach and dune erosion assessments. Considering the developments still needed, the TELEMAC-suite can only have this potential in the long run.

Ad 4 & 5)

SWASH 2DH is used to take into account the effect of directional spreading on the wave characteristics at the toe of the dike. Directional spreading causes a reduction of the long wave energy, resulting in milder wave characteristics at the toe of the dike, which reduce the overtopping. Since the 2DH SWASH model is calculation time intensive and less stable, a 1DH SWASH model is used for the overtopping discharge calculations. The offshore boundary conditions are tuned in order to obtain equal wave characteristics at the toe of the dike.

In the CREST project wave tank tests (full 3D) with wave generation with varying directional spreading confirmed the reducing effect of directional spreading on the wave characteristics at the toe and on the wave overtopping and forces (CREST report D2.3.1 by Verwaest and Gruwez, 2019). Moreover, it revealed that the directional spreading still has a reducing effect on the overtopping for equal wave characteristics at the toe of the dike. Including this extra effect in the methodology will decrease the overtopping rates and the wave forces. So, we recommend to use a 2DH SWASH model for the overtopping calculations instead of the present two-step method.

Ad 5 & 6)

Physical modelling

At the start of the CREST project, limited validation/calibration data were available. Moreover some strange behaviour was noticed, e. g. the validation with field data of Petten (the Netherlands) showed a good correspondence for the time averaged overtopping discharge, but a serious deviation of the number of overtopping events. If for the same discharge, the number of overtopping events is different, this also means that the maximum volume of water that is overtopped during the storm will be different and thus also the wave force will be significantly different. Secondly, in some cases the modelled wave period ($T_{m-1,0}$) using SWASH was significantly lower than predicted by Hofland *et al.* (2017).

During the CREST project a lot of data became available for further validation:

- Wave flume tests with high spatial resolution monitoring of the short and the long wave characteristics (including reflection) (Gruwez *et al.*, 2018a, 2018b);
- Wave tank tests showing the effect of directional spreading on wave characteristics and overtopping (Altomare *et al.*, 2020);
- The preparation of a field test campaign including an artificial dike for overtopping (Gruwez *et al.*, 2016).

Numerical modelling

SWASH requires relative little CPU-time. On the other hand it assumes hydrostatic behaviour and cannot deal with complex structures such as parapet walls or stilling wave basins. More complex CFD or SPH models can handle these more complex elements but require a lot of computational effort. In CREST, both models are coupled so that the benefits of both are combined. Using these complex coupled numerical models in a time efficient way can reduce the required physical modelling. Moreover, the numerical modelling showed that for vertical walls, SWASH is able to reproduce the hydrostatic horizontal force (but not the dynamic peak). This can be used to study e.g. the effect of the variation of the force with the variation of the wave train (random seed number).

Ad 6 & 7)

In the current safety methodology the time averaged overtopping discharge is used as measure. However, often during the peak of a storm only a few overtopping events occur. If e.g. during two hours five overtopping events occur in which each time during a few seconds a volume of $5m^3/m$ overtops, the averaged overtopping discharge is only $0.0034m^3/s/m$. The same averaged overtopping discharge is obtained if 50 events of $0.5m^3/m$ each occurs. The damage to people or buildings will however be completely different (e.g. the wave forces are 10 times smaller!). In the

CREST project better knowledge is obtained about these individual maximum overtopping volumes and wave forces. This will allow to switch in the future from a norm of averaged overtopping discharge to maximum volumes and forces. But also for the prediction of the averaged overtopping discharge progress is made (effect of directional spreading, better numerical modelling tools, physical model results to calibrate numerical models). (cf. THM's 4.5 to 4.19). Also the impact of beach morphology on overtopping rates is studied (THM 4.20).

Ad 8)

This was not a subject in the CREST-project.

Ad 9)

A new tool is developed for damage estimation (FLIAT, Van Ackere et al., 2019b). One of the most notable differences between FLIAT and the existing damage estimation tool LATIS (Deckers et al., 2009) is the fact that FLIAT can also handle multiple datasets that are linked to well-defined elements (e.g., multiple activity codes (NACE codes), presence of a basement, number of inhabitants linked to a building, etc.). More information is found in THM 3.9. Also in a workshop evacuation plans were discussed, which made clear that if time is short, vertical evacuation is the first choice (THM 3.10).

THM 4.5 IMPACT FORCE ESTIMATE BASED ON A HYDROSTATIC PRESSURE

Large-scale experiments on overtopping wave loads (WALOWA project) suggest that the impact force acting on dike mounted vertical walls with shallow foreshores can be estimated using a hydrostatic pressure assumption.

Experiments were conducted in the Deltares Delta Flume (The Netherlands) within the Hydralab+ project WALOWA (WAve LOads on WAlls) (Streicher et al., 2017, 2019a). A mildly sloping beach made of ~1000m³ sand was built into the Delta Flume (Figure 60). The generated waves broke due to depth limitations and the resulting overtopping bore impacted the dike mounted vertical wall.

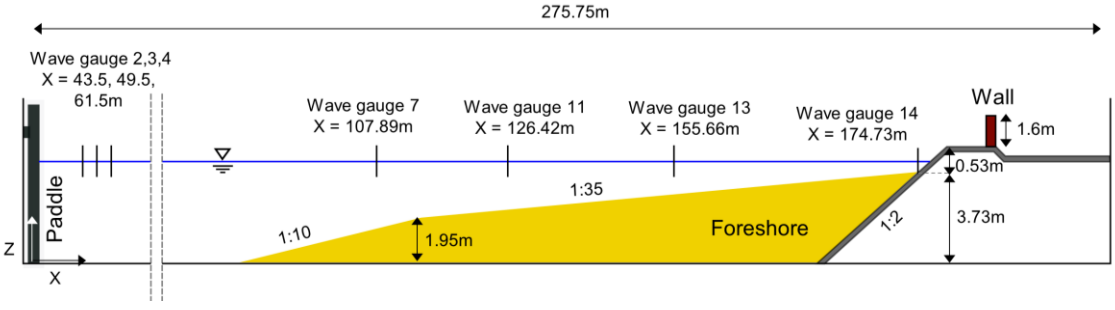

Figure 60: Experimental set-up WALOWA (Wave Loads on Walls) project. The geometry consists of a foreshore (yellow), dike & promenade (grey) and dike mounted vertical wall (red).

It was the objective to study overtopping wave loads on dike mounted vertical walls in shallow water conditions. More specifically, the impact pressures and forces were studied. The dike mounted wall was equipped with two compression load cells (HBM U9, range 20 kN) and 15

pressure sensors (Kulite HKM379, range 1 Bar). Forces and pressures were sampled synchronously in time at 1 kHz.

The analysis was focused on the largest 60 impacts from two tests representative for design storm conditions at the Belgian coast and signals were filtered using the in-house Impact-Analysis-Toolbox (IAT). A double peak horizontal impact force signal shape was observed (Figure 61). The first peak was related to the initial impact of the bore against the wall, called: 'impulsive' or 'dynamic' peak. The second peak was related to the maximum water layer in front of the wall, called: 'quasi-static' peak. The majority (75%) of the largest 60 investigated impacts showed a higher second 'quasi-static' peak.

Hence, a hydrostatic pressure distribution assumption was used to estimate the second force peak F [kN/m] using the maximum run-up ($R_{h,max}$) at the wall (see Figure 61, left). The maximum run-up $R_{h,max}$ at the wall was obtained by motion tracking of the bore leading edge at the wall. Linear regression and fitting of the force peaks to the hydrostatic theory was done by minimizing the MAPE error and a best-fit equation obtained (see Eq. 4.5.1). The prediction results are shown to be within the 95% confidence band (see Figure 61, right).

$$\boldsymbol{F = 0.32 \cdot \rho \cdot g \cdot R_{h,max}{}^{2} \ [\frac{N}{m}]} \tag{4.5.1}$$

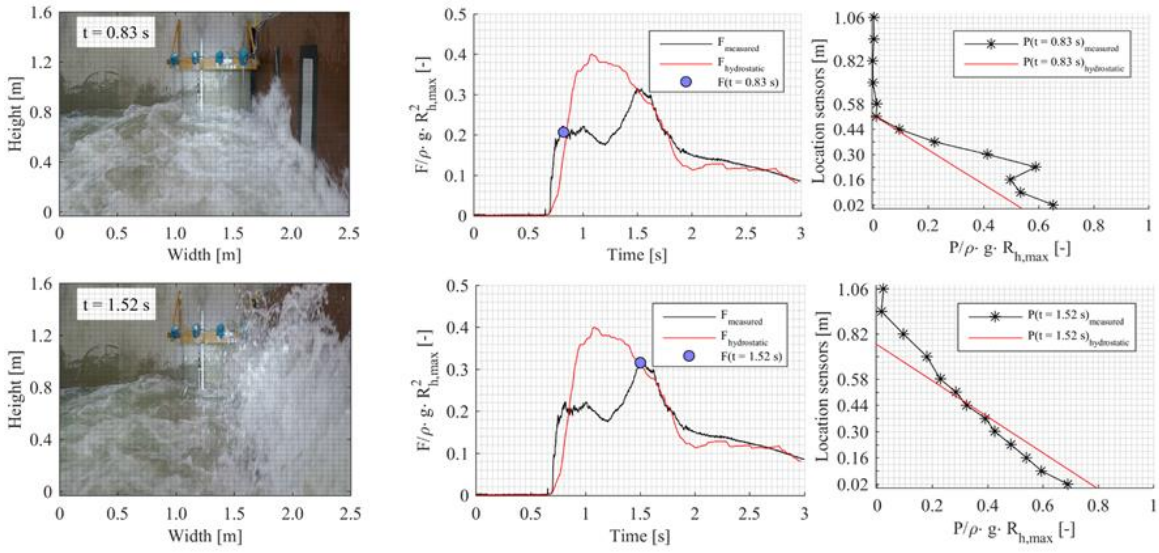

Figure 61: Hydrostatic theory, using the maximum run-up $R_{h,max}$ (left figure) of the bore at the wall, yields a good prediction accuracy (right figure) until F = 20 kN/m.

For practical design guidance and to determine the overturning moment of sea-walls (to design the foundation), Eq. 4.5.1 can also be used inversely to calculate the maximum run-up height $R_{h,max}$ based on any given force.

THM 4.6 WAVE FLUME SCALE MODEL EXPERIMENTS

A new experimental dataset is available of 2D wave flume physical modelling of (individual) wave overtopping and impacts on dikes with very shallow foreshores (very relevant to the Belgian coast). The dataset also includes high spatial resolution measurements of surface elevations along the foreshore slope, allowing a more detailed study of long waves.

The 2D experiments focussed on wave interactions with low-crested sea dikes fronted by a shallow foreshore and mildly to steeply sloping beaches, which is a very typical situation along the Belgian coast.

The 2D small-scale experiments were carried out in the 30.0 m long, 1.0 m wide and 1.2 m high wave flume of the Coastal Engineering Research Group, Department of Civil Engineering at Ghent University. It has a piston-type wave maker controlled by both in-house developed software for first-order wave generation with Active Wave Absorption (AWA), and the AwaSys7 software (Aalborg University, 2018) for second-order wave generation, including AWA.

The geometry of the modelled cross-shore profiles consisted of a dike fronted by a fixed bed very shallow foreshore. The selection of foreshore slopes was based on the range of actual foreshore slopes occurring along the coast of Belgium (i.e. 1/20 – 1/90). The range of tests here covers both steep foreshores (1/20) and mildly sloped foreshores (1/90) to cover the complete range of non-linearity behavior in combination with the shallow foreshore in front of the dike.

The dike had a 1/2 seaward slope, followed by a 1/50 sloped promenade over 20 m (prototype) and a vertical, non-overtopable wall on the crest (representing the façade of the building). For the foreshore slope 1/35 also promenade widths of 10 m and 30 m were tested, including a storm wall at various distances from the dike crest (i.e. 0 m, 10 m and 20 m). Model scales 1:25 and 1:35 were used to be able to accommodate foreshore slopes between 1/20 and 1/80 in the wave flume (**Error! Reference source not found.**), thereby covering the range of slopes actually present along the Belgian coast. The end of the foreshore slope was connected to the flume bottom by a 1/10 transition slope. This transition ended approximately 0.05 m above the bottom to allow a connection with the return flow channel along the bottom of the flume. The foreshore slope 1/50 was modelled in both scales to be able to take into account the differences due to scale effects.

A separation wall was installed over approximately 8.0 m from the dike toe dividing the flume locally over this length into two channels: a main channel 0.75 m wide and a small channel 0.25 m wide. In the main channel, the dike slope was always present. Consequently, it is where the wave overtopping and wave impact force measurements were conducted. In the small channel no dike was constructed, but instead a horizontal levelling-off at the dike toe level was installed. The horizontal part ended in dissipative material, limiting the wave reflection as much as possible. The purpose of the small channel was to be able to measure the incident wave conditions (IWC) at the toe of the dike, simultaneously with each overtopping and wave force test. For foreshore slopes 1/50 (at model scale 1:35) and 1/35 (at model scale 1:25), this small channel set-up was extended over the complete flume width for a couple of tests to be able to investigate its performance. Conversely, the dike geometry, including promenade and vertical wall, was constructed over the complete flume width for the tests with high spatial resolution (HSR) measurement of the surface

elevations. This was done to obtain a correct behavior in the flume of the wave reflection against the dike, and therefore to be able to make unambiguous measurements of the surface elevations along the complete length of the foreshore (before and after the end of the separation wall).

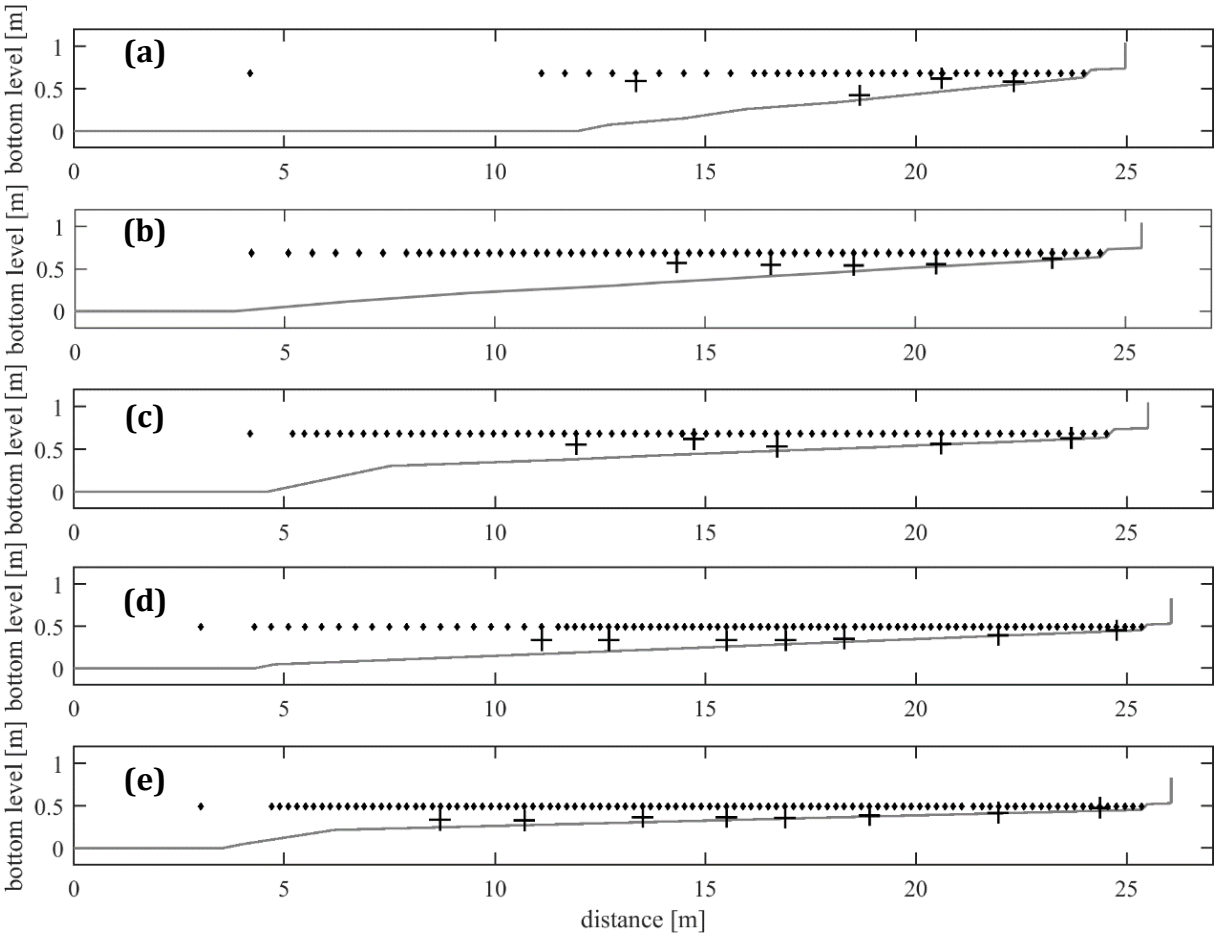

Figure 62: Tested cross-shore bottom profiles, consisting of a dike geometry with foreshore slopes: (a) 1/20 (model scale 1:25), (b) 1/35 (scale 1:25), (c) 1/50 (scale 1:25), (d) 1/50 (scale 1:35), and (e) 1/80 (scale 1:35). Bed level z (flume bottom at z = 0.0 m) is shown by the grey line over the cross-shore distance x from the wave-maker zero position (x = 0.0 m). The wave gauge positions (diamonds) are plotted at the highest water level tested and the plusses are the positions and heights of the electromagnetic current meter for the high spatial resolution tests.

A range of low to high energy irregular and bichromatic wave conditions, a variation in wave steepness and two water levels were tested (Table 8 and Table 9). All generated surface elevation time series were derived by an inverse FFT from a JONSWAP spectrum with peakedness factor γ of 3.3. The wave phases were determined randomly (deterministic method), but with a fixed seed number to obtain the same wave phase combinations for all conditions over all tested foreshore slopes. The dataset includes repeated tests with the same seed number and for one test a variation of the seed number. The duration of the tests was usually ~1000 waves long.

The main goal was to obtain a dataset in which the effects of the infragravity waves on the wave-structure interactions (i.e. wave overtopping and impact forces) can be studied. The wave overtopping was measured at the dike crest and the wave impact loads were measured at the vertical wall (at 1000 Hz), representing the buildings at the end of the promenade. The tests

included high spatial resolution surface elevation measurement tests, which is new for beaches including a dike in the inner surf zone. Inter-wave gauge distances of 0.20 m – 0.40 m were used for the 1:35 model scale tests and 0.28 m – 0.56 m for the 1:25 scale tests (Figure 62) and measured at 40 Hz. The current was measured as well (at 16 Hz) using an electromagnetic current meter (ECM). The HSR tests allow to analyze the reflection of infragravity waves.

Test ID	Order	h_o	$H_{m0,o}$	$T_{p,o}$	$cot(\theta)$	$h_t/H_{m0,o}$	HSR	OVT	WIF
[-]	[-]	[m]	[m]	[s]	[-]	[-]	[-]	[-]	[-]
RS01	2nd	0.65	0.20	2.4	20, 35, 50 (1:25), 50 (1:35), 80	0.06	No	Yes	Yes
RF01	1st	0.65	0.20	2.4	35, 50 (1:25)	0.06	No	Yes	Yes
RS02	2nd	0.65	0.20	2.0	20, 35, 50 (1:25), 50 (1:35), 80	0.06	Yes*	Yes	No
RS03	2nd	0.65	0.20	1.6	20, 35, 50 (1:25), 50 (1:35), 80	0.07	No	Yes	No
RS04	2nd	0.65	0.12	1.6	20, 35, 50 (1:25), 50 (1:35), 80	0.10	Yes*	No	No
RS05	2nd	0.65	0.08	2.4	20, 35, 50 (1:25), 50 (1:35), 80	0.15	Yes	Yes	Yes
RF05	1st	0.65	0.08	2.4	35, 50 (1:25)	0.15	Yes	Yes	Yes
RS06	2nd	0.69	0.20	2.4	20, 35, 50 (1:25), 50 (1:35), 80	0.26	Yes*	Yes	Yes
RS07	2nd	0.69	0.20	2.0	20, 35, 50 (1:25), 50 (1:35), 80	0.26	No	Yes	Yes
RS08	2nd	0.69	0.20	1.6	20, 35, 50 (1:25), 50 (1:35), 80	0.26	No	Yes	Yes
RS09	2nd	0.69	0.12	1.6	20, 35, 50 (1:25), 50 (1:35), 80	0.43	Yes*	Yes	Yes
RS10	2nd	0.69	0.12	2.4	20, 35, 50 (1:25), 50 (1:35), 80	0.43	No	Yes	Yes
RS11	2nd	0.69	0.08	2.4	20, 35, 50 (1:25), 50 (1:35), 80	0.65	Yes	Yes	Yes
RF11	1st	0.69	0.08	2.4	35, 50 (1:25)	0.65	No	Yes	Yes
RS12	2nd	0.69	0.06	2.4	20, 35, 50 (1:25), 50 (1:35), 80	0.87	No	Yes	Yes
RS13	2nd	0.69	0.04	2.4	20, 35, 50 (1:25), 50 (1:35), 80	1.30	No	Yes	Yes

*short test: ~100 waves instead of ~1000 waves

Table 8: Test program for the 2D CREST experiments (values provided for scale 1:25). RS(F): Random Second (First) order wave generation, HSR: high spatial resolution test, OVT: (individual) wave overtopping test, WIF: wave impact force test. h_o: offshore water depth at wave paddle; $H_{m0,o}$ = offshore significant wave height at wave paddle; $T_{p,o}$ = offshore peak wave period at wave paddle; θ = foreshore slope angle.

Test ID	Order	h_o	a_1	a_2	f_1	f_2	f_3	f_m	$cot(\theta)$	HSR	OVT	WIF
[-]	[-]	[m]	[m]	[m]	[Hz]	[Hz]	[Hz]	[Hz]	[-]	[-]	[-]	[-]
BS01	2nd	0.65	0.09	0.01	0.400	0.438	0.038	0.419	35, 50	Yes*	Yes*	No
BS02	2nd	0.65	0.07	0.03	0.400	0.438	0.038	0.419	35, 50	Yes*	Yes*	No
BS03	2nd	0.69	0.09	0.01	0.400	0.438	0.038	0.419	35, 50	Yes*	Yes*	Yes*
BS04	2nd	0.69	0.07	0.03	0.400	0.438	0.038	0.419	35, 50	Yes*	Yes*	Yes*

*very short test: 20 waves instead of ~1000 waves

Table 9: Previous table continued. BS: Bichromatic Second order wave generation. a1,2 = amplitudes of bichromatic wave components; $f_{1,2}$ = primary frequencies of bichromatic wave components; f_3 = frequency of bound infragravity wave; f_m = mean frequency of primary components bichromatic wave.

More details on the test setup and first analysis results are provided by Gruwez et al. (2018a, 2018b) and in CREST report deliverable D2.3.1. The dataset is archived on IMIS (Department of Civil Engineering (UGent), Belgium, 2018).

THM 4.7 WAVE BASIN SCALE MODEL EXPERIMENTS

A new experimental dataset is available of 3D wave basin physical modelling of (individual) wave overtopping and impacts on dikes with very shallow foreshores (very relevant to the Belgian coast). This dataset includes long-crested, obliquely incident long-crested and short-crested wave tests, allowing the study of 3D effects at the dike and directional spreading of the waves.

The physical model tests in the wave basin at Flanders Hydraulics with multidirectional wave generation system consisted of experiments with a fixed bed. A 1:35 foreshore slope was built in concrete, representing an average (eroded) profile along the Belgian coast. The dike height, measured vertically from the toe to its seaward edge is 0.05 m in the model scale. At the end of the promenade a vertical wall is installed, modelling the façade of buildings built along the coastline. The model scale is 1:50 (Figure 63).

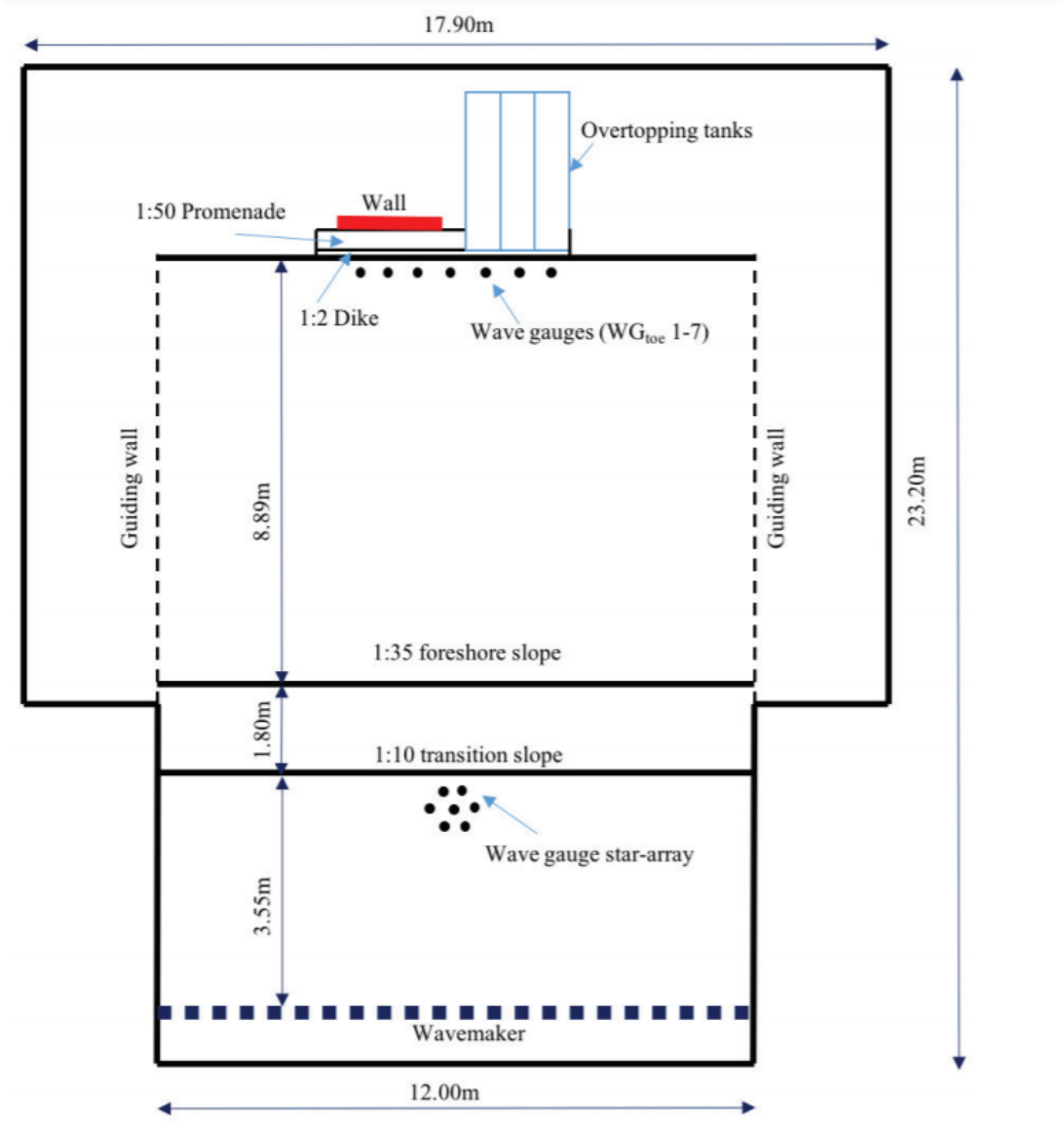

Figure 63: Plan view of the experimental layout (not to scale)

Detailed measurements of wave propagation and transformation on the foreshore and overtopping with impact loading on the buildings on top of the sea dike have been gathered during the experiments. In total 56 instruments have been employed (Figure 64 and Figure 65):

- one star-array consisting in 7 wave gauges to measure the incident offshore wave field and wave directionality;
- two line-arrays of 5 wave gauges each to analyse wave propagation and transformation along the foreshore slope;
- seven wave gauges located at the toe of the dike to measure the wave characteristics at that location (WG_{toe} 1-7);
- twelve wave gauges placed on top of the dike to reconstruct the pattern of layer velocity and thickness of the overtopping flows;
- three stainless steel overtopping tanks to measure average and individual overtopping equipped with load cells (four per overtopping tank) and one water level sensor;
- four pressure sensors to study the distribution of the wave impact along the vertical wall (the distance between each pressure sensor is 12 mm);
- six load cells to measures the total wave forces exerted on the vertical wall;
- one water level sensor to measure the mean water level in the wave basin.

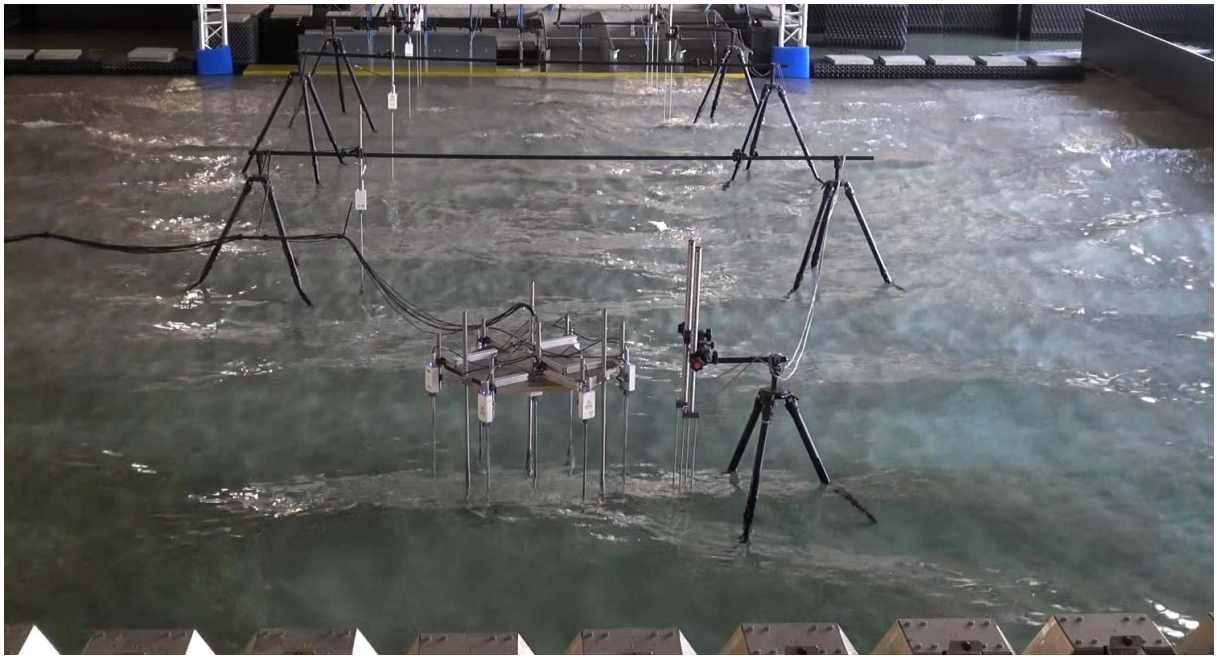

Figure 64: Wave gauges mounted on small tripods are measuring the waves propagating from the paddles (bottom of the picture) to the other end of the wave basin (top of the picture).

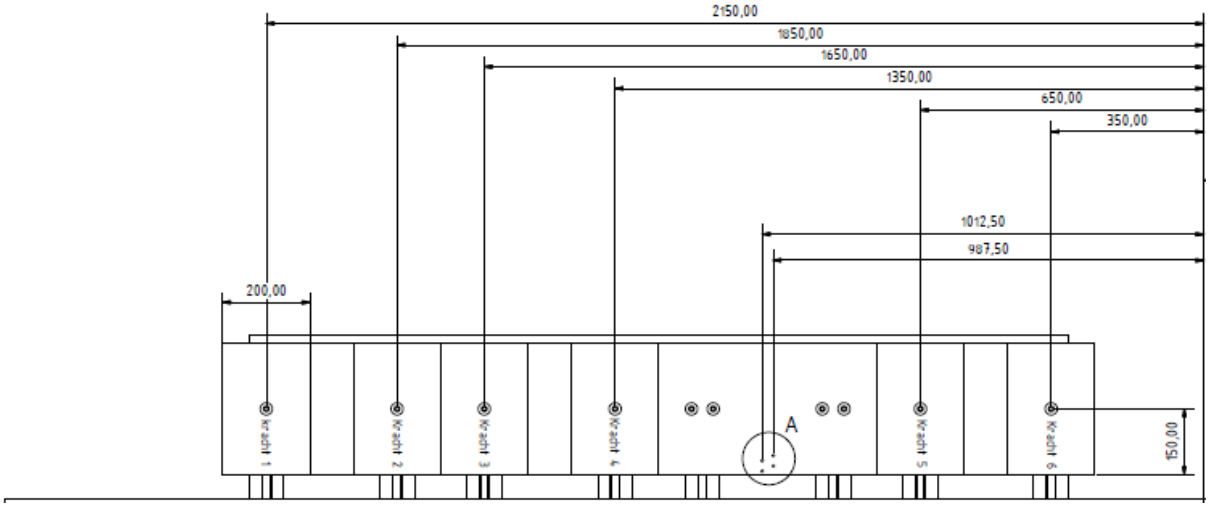

Figure 65: Force and pressure measuring devices on vertical plates representing buildings on the sea dike.

A first series of 138 experiments is carried out in which water level and wave boundary conditions are varied as shown in Table 10. Wave by wave overtopping discharge and hydraulic loading on vertical elements on the dike were measured. The wave generation software did not allow combining directional spreading and obliqueness. Therefore, the main direction of short-crested waves was always perpendicular to the dike & oblique waves were long-crested.

h_t	H_{m0}	T_p	Directional spreading	Obliqueness
0.01 m	0.06 m	1.41 s	0°	0°
0.03 m	0.08 m	1.70 s	12°	5°
	0.10 m		16°	10°
			20°	15°
			31.5°	

Table 10: Hydraulic boundary conditions for the first series of experiments

A second series of 138 experiments is carried out after removal of the sea dike and changing it to a horizontal bottom followed by passive absorption material placed on the rear side of the foreshore slope. Such a configuration guarantees to damp the wave reflection and allows measuring the incident wave conditions at the location corresponding to the dike toe.

Experiments from both series with the same hydraulic boundary conditions are combined to establish a relationship between the incident wave conditions at the toe of the sea dike (from the second series) and overtopping characteristics (from the first series). The range of hydraulic conditions at the toe of the dike is shown in Table 11. One observes long wave periods at the toe of the dike, caused by the heavy breaking and generation of long waves on the shallow foreshore.

H_{m0}	$T_{m-1,0}$	Water depth
0.01 m … 0.03 m	2.8 s … 8.8 s	0.01 m … 0.03 m

Table 11: Range of measured incident wave conditions at the toe of the dike

For more details the reader is referred to CREST report deliverable D2.3.1 (Verwaest and Gruwez, 2019). The dataset is archived on IMIS (Flanders Hydraulics Research, Belgium, 2018).

THM 4.8 SPECTRAL WAVE PERIOD $T_{m-1,0,t}$

The spectral wave period at the toe of the dike, $T_{m-1,0,t}$ is used in all overtopping and wave impact prediction formulas. An existing semi-empirical formula for $T_{m-1,0,t}$ was validated using data from mildly sloping shallow foreshores, but returns an overestimated value for the case of steep shallow foreshore slopes. A modification of the formula has been carried out, making it applicable and more accurate for use in cases with steeper shallow foreshore slopes.

Hofland et al. (2017) proposed for the first time a prediction formula for the spectral wave period $T_{m-1,0,t}$ at the toe of a dike fronted by a shallow ($1.0 < h_t/H_{m0,o} < 4.0$), very shallow ($0.3 < h_t/H_{m0,o} < 1.0$), to extremely shallow foreshore ($h_t/H_{m0,o} < 0.3$) with a mild slope, defined by the following criterion:

$$\theta T_{m-1,0,o}\sqrt{g/H_{m0,o}} < 0.62 \qquad (4.8.1)$$

where θ is the foreshore slope angle (in radians), $T_{m-1,0,o}$ is the offshore spectral wave period, g is the gravitational acceleration and $H_{m0,o}$ is the offshore significant wave height, h_t is the water depth at the toe. Their prediction formula for the spectral wave period at the dike toe $T_{m-1,0,t}$ is:

$$\frac{T_{m-1,0,t}}{T_{m-1,0,o}} - 1 = 6\,exp(-4\tilde{h}) + exp(-\tilde{h}) \qquad (4.8.2)$$

Eq. 4.8.2 estimates the spectral wave period in function of a relative water depth $\tilde{h}$ at the toe of the dike in which the foreshore slope $\cot\theta$ was incorporated:

$$\tilde{h} = \frac{h_t}{H_{m0,o}}\left(\frac{\cot\theta}{100}\right)^{0.2} \qquad (4.8.3)$$

Based on the 2D CREST experimental data (see THM 4.6), the above formulas were checked (Gruwez et al., 2018a, 2018b). In the test series, the criterion for shallow foreshore is met, but the mild slope criterion, however, is not always fulfilled (see Table 12). Especially the steepest slope tested (i.e. 1/20) was not mild enough for Eq. 4.8.2 to be valid, according to Eq. 4.8.1. The data of the mild slopes are compared with the prediction formula in Figure 66. From this figure it can be concluded that Eq. 4.8.2 indeed provides a good estimation, albeit somewhat overestimated: the data are skirting the lower boundary of the confidence interval, especially for relative water depths larger than 0.25. However, the prediction formula tends to overestimate $T_{m-1,0,t}$ for the steeper foreshore slopes 1/20 and 1/35, and significantly so for low water depths at the dike toe. This suggests there is still room for improvement in the prediction formula of Eq. 4.8.2, at least for

foreshore slopes steeper than 1/50, which might not strictly qualify as mild slopes anymore. A modification of the formula in Eq. 4.8.2 is envisaged in the framework of a PhD research, making it applicable and more accurate to steeper foreshore slopes.

Test ID	h_o	$H_{m0,o}$	$T_{m-1,0,o}$	1/20	1/35	1/50	1/80
[-]	[m]	[m]	[s]	[-]	[-]	[-]	[-]
RS01	0.65	0.20	2.2	**0.76**	0.44	0.31	0.19
RS02	0.65	0.20	1.8	**0.64**	0.36	0.25	0.16
RS03	0.65	0.20	1.5	0.51	0.29	0.20	0.13
RS04	0.65	0.12	1.5	**0.66**	0.38	0.26	0.16
RS05	0.65	0.08	2.2	1.21	**0.69**	0.48	0.30
RS06	0.69	0.20	2.2	0.76	0.44	0.31	0.19
RS07	0.69	0.20	1.8	**0.64**	0.36	0.25	0.16
RS08	0.69	0.20	1.5	0.51	0.29	0.20	0.13
RS09	0.69	0.12	1.5	**0.66**	0.38	0.26	0.16
RS10	0.69	0.12	2.2	**0.99**	0.56	0.39	0.25
RS11	0.69	0.08	2.2	**1.21**	**0.69**	0.48	0.30
RS12	0.69	0.06	2.2	**1.39**	**0.80**	0.56	0.35
RS13	0.69	0.04	2.2	**1.71**	**0.98**	**0.68**	0.43

Table 12: Criterion Eq. 4.8.1 check for all test conditions (rows) and each foreshore slope (last three columns). Values not meeting the criterion (≥ 0.62) are indicated in bold.

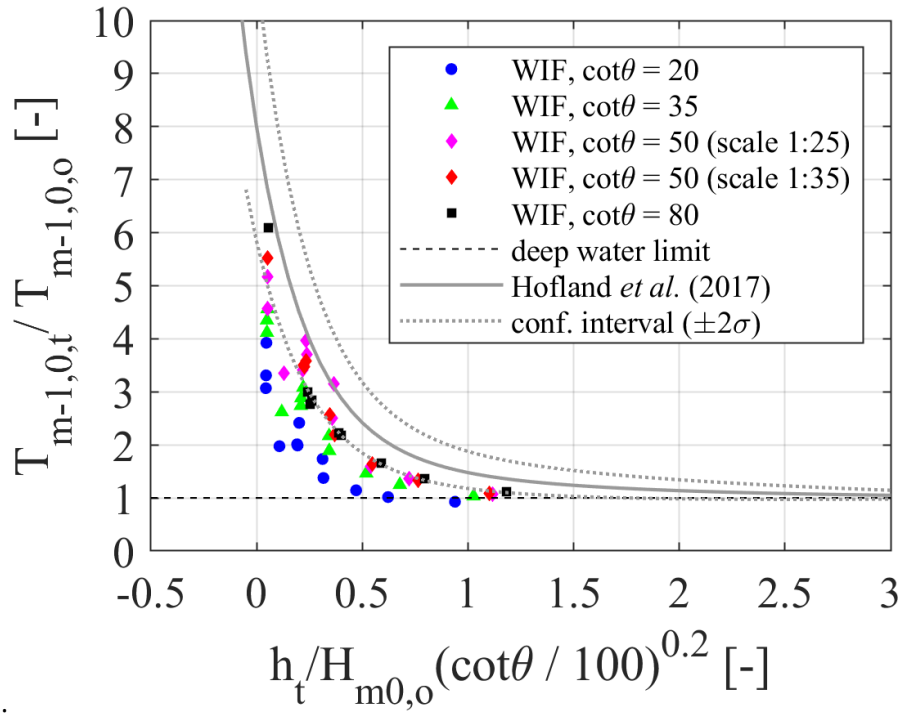

Figure 66: Dimensionless spectral wave period at the toe of the dike versus the relative water depth with slope correction. Experimental data compared to Hofland et al. (2017) for the test results in the small channel during the wave impact force (WIF) experiment.

THM 4.9 EFFECT FORESHORE SLOPE AND DIKE GEOMETRY ON OVERTOPPING AND IMPACT

A significant effect of the foreshore slope angle and the dike geometry (promenade length, inclusion of storm wall,…) on the wave overtopping and wave impact force is discovered. A modification of the existing prediction formulas is ongoing.

Physical model tests (High Spatial Resolution - Incoming Wave – Individual Overtopping Volumes and Wave Impact Forces) for a wide range of foreshore slopes (1/20 to 1/80, see THM 4.6 and (Gruwez et al., 2018a, 2018b)) confirmed the empirical relation of Altomare *et al.* (2016) (Figure 67):

$$\frac{q}{\sqrt{gH_{m0,t}^3}} = 10^{-0.791} exp\left(-\frac{R_c}{H_{m0,t}(0.33 + 0.022\xi_{m-1,0,t})}\right) \quad (4.9.1)$$

in which q is the mean overtopping discharge over the dike crest, R_c the freeboard of the dike crest and the $\xi_{m-1,0,t}$ the breaker parameter, defined as:

$$\xi_{m-1,0,t} = \frac{tan\,\beta}{\sqrt{2\pi H_{m0,t} / gT_{m-1,0,t}^2}} \quad (4.9.2)$$

where tanβ is the equivalent slope, determined according to the procedure described by Altomare *et al.* (2016). It is applicable for foreshore slopes between 1/20 and 1/250, dike slopes between 1/2 and 1/6, and a range of $h_t/H_{m0,t}$ between -0.88 and 2.38. All these criteria are met for all 2D CREST overtopping tests (cf. THM 4.6, Table 8). Most of the 2D CREST data fall within the confidence interval, confirming the applicability of the prediction formula. In terms of differences between the foreshore slopes, it is noticed that an influence of the foreshore slope is still apparent in the dataset but not taken into account in the formula, with the steepest foreshore slope delivering the highest overtopping discharges, especially for the higher dimensionless freeboards tested (i.e. > 3.0 on the horizontal axis of

Figure 67: Semi-logarithmic plot (x-axis: linear scale, y-axis: logarithmic scale) of the dimensionless wave overtopping discharge Q in function of the dimensionless freeboard with shallow foreshore correction and equivalent slope. The experimental wave overtopping results (OVT) of the tests with second order wave generation for foreshore slopes 1/20, 1/50 and 1/80 are compared to the prediction formula of Altomare et al. (2016) with the equivalent slope concept.

).

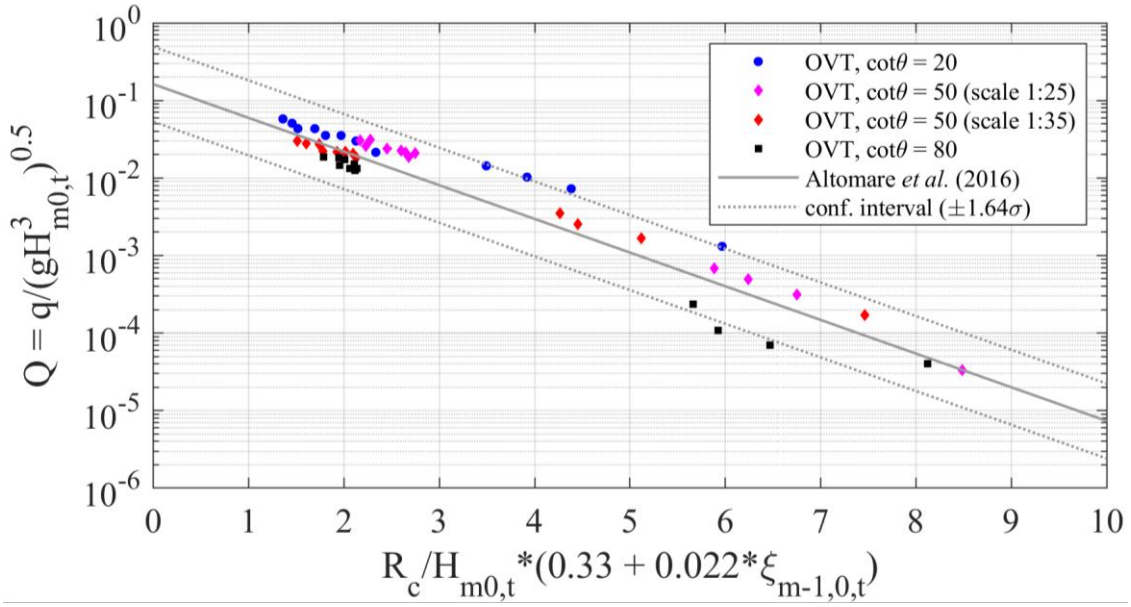

Figure 67: Semi-logarithmic plot (x-axis: linear scale, y-axis: logarithmic scale) of the dimensionless wave overtopping discharge Q in function of the dimensionless freeboard with shallow foreshore correction and equivalent slope. The experimental wave overtopping results (OVT) of the tests with second order wave generation for foreshore slopes 1/20, 1/50 and 1/80 are compared to the prediction formula of Altomare et al. (2016) with the equivalent slope concept.

For wave forces an extensive physical model test campaign was carried out as well in the CREST project both in 2D (wave flume, THM 4.6, De Vos (2019)) as in 3D (wave tank, THM 4.7, Pueyo Estada (2019)). Using these test results, a relation was found between the averaged overtopping discharge and the (quasi-hydrostatic) wave force (Streicher, 2019), depending on the wave characteristics at the toe and the dike geometry (De Vos, 2019). Most of the tests were done with the same wave train (random seed number). Before a general formula can be used in practice, more insight is needed in the variability of the wave force with seed number (see also THM 4.19). This can be done with additional physical model tests or using SWASH since it was found in CREST that SWASH is able to predict the wave force on vertical walls (see also THM 4.17).

However, the preliminary formulae developed within the master thesis of De Vos (2019) already give interesting results. An exercise is done for varying promenade widths between 0 and 30m. The wider the promenade, the smaller the overtopping discharge. Using the empirical formula that predicts the overtopping discharge for varying promenade width (internal report for the design of a new dike in Mariakerke) and wave characteristics at the toe of the dike, the wave height at the toe of the dike that gives the same target overtopping discharge is looked up for several promenade widths. With this wave height and promenade width, the force on the wall is calculated by the wave impact formula (De Vos, 2019). Figure 68 shows these impact forces versus promenade width for the considered conditions. Although the overtopping discharge is equal at the location of the wall for each of these promenade widths, a promenade width of 5 m gives a three times higher force than a promenade width of 20 m. This leads to the idea of a safety norm based on forces and overtopping volumes rather than on averaged overtopping discharges. The developments in CREST make such a transition possible in the future.

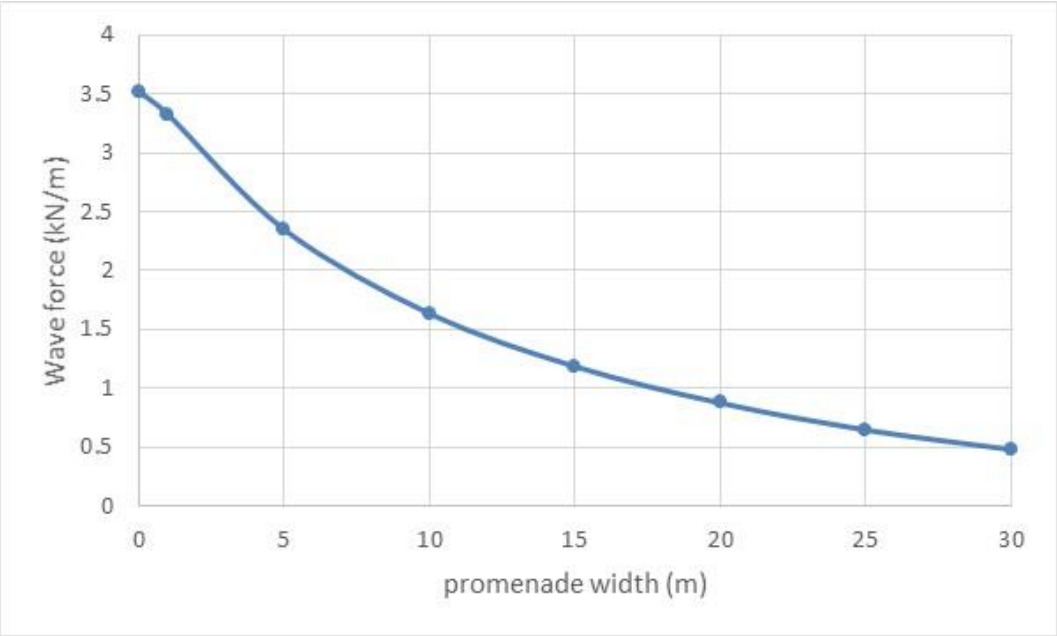

Figure 68: Wave force on a vertical wall for different promenade widths with equal overtopping discharge.

THM 4.10 IMPORTANCE OF LONG WAVES FOR OVERTOPPING/IMPACT

Long waves (or infragravity waves) significantly affect the wave-induced structural response (overtopping, wave impact) of dikes for the case of very shallow foreshores. However, very little is actually known about these long waves in the nearshore region during storm conditions, especially along the Belgian coast. Dedicated field measurements are strongly recommended.

2D experimental wave impact tests have been performed for a dike with a very shallow foreshore (see THM 4.6), for different foreshore slopes (1/20 till 1/80). The same promenade length (i.e. G_c = 20 m) was tested for all foreshore slopes. The effect of long waves on structural response (overtopping, wave impact) is then investigated based on a dimensionless force and wave length. A dimensionless maximum impact force F^* is defined by:

$$F^* = \frac{F_{max}}{\rho g A_c^2} \qquad (4.10.1)$$

where F_{max} is the maximum impact force per test (the post-processing steps to obtain F_{max} are described in De Vos (2019)), ρ the water density, g the gravitational acceleration and A_c the dike crest freeboard. The wave length L is non-dimensionalised as follows:

$$L^* = \frac{L_{m-1,0,t}}{G_c}\frac{h_t}{A_c} \qquad (4.10.2)$$

where G_c is the promenade length, h_t the water depth at the toe of the dike and $L_{m\text{-}1,0,t}$ is the spectral wave length at the toe of the dike (in shallow water) given by:

$$L_{m-1,0,t} = T_{m-1,0,t}\sqrt{gh_t} \qquad (4.10.3)$$

where $T_{m-1,0,t}$ is the spectral wave period at the toe of the dike.

The test results demonstrate that long waves and the slope angle have a large influence on the hydraulic loading on vertical structures on top of the dike.

Figure 69: Dimensionless maximum impact force F* in function of a dimensionless wave length L*. Data points are the CREST 2D experimental data and the lines are fitted exponential curves. Yellow: foreshore slope 1/80, gray: foreshore slope 1/50, orange: foreshore slope 1/35, blue: foreshore slope 1/20.

illustrates that when long waves become more important than short waves at the toe of the dike combined with a higher water depth at the toe of the dike (indicated by increasing L* value), the maximum impact force increases (indicated by increasing F* value). This effect becomes more pronounced in case of steeper or less wide beaches. An exponential relation is found between F* and L* for a fixed foreshore slope.

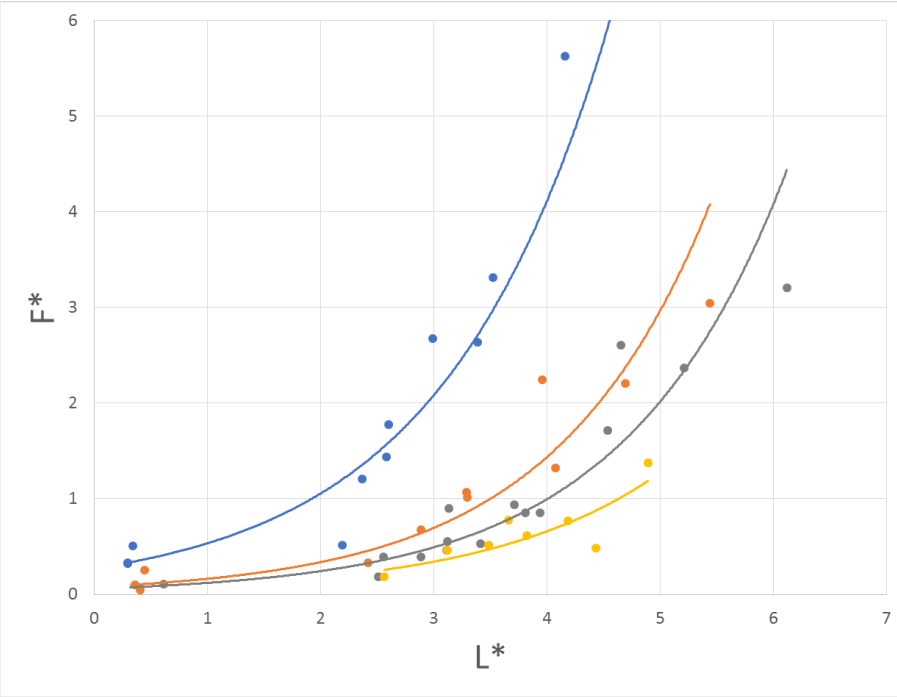

Figure 69: Dimensionless maximum impact force F* in function of a dimensionless wave length L*. Data points are the CREST 2D experimental data and the lines are fitted exponential curves. Yellow: foreshore slope 1/80, gray: foreshore slope 1/50, orange: foreshore slope 1/35, blue: foreshore slope 1/20.

Long waves bound to the incident wave groups are taken into account in physical and numerical modelling. However, free incident long waves originating from e.g. offshore sand banks, edge waves,... are not taken into account. Occurrence of incident free long waves is dependent on the conditions along a specific coast. Therefore, it is important that field measurements of long waves are done to investigate which types of long waves are incident to the coastal structures during storm conditions (Fiedler *et al.*, 2019). Should incident free long waves not be negligible compared

to the bound long waves, then they must be taken into account in the design because of their important impact on wave-structure interactions.

THM 4.11 LONG WAVE REFLECTION

Long waves feature strong reflection from a dike with shallow foreshore, while they might break on mildly sloping beaches in the surf zone and reflect much less from the shoreline in case no dike is present. The presence of the dike therefore affects long wave reflection on mildly sloping beaches. Further research into the role of the dike in this process, might lead to further insight into changes in the hydrodynamics and their influence on the surf zone morphodynamics during storm conditions.

To investigate the short and long wave energy transformation over the foreshore from the 2D CREST experiments (THM 4.6), a separation of the total wave energy spectrum was made into those components (Gruwez *et al.*, 2018a, 2018b). The separation frequency f_{sep} was chosen based on the location of the trough between the bulk of the infragravity wave energy and where the wave energy suddenly increases towards the primary peak of the spectrum at the reference location in front of the toe of the foreshore (e.g. f_{sep} = 0.28 Hz in

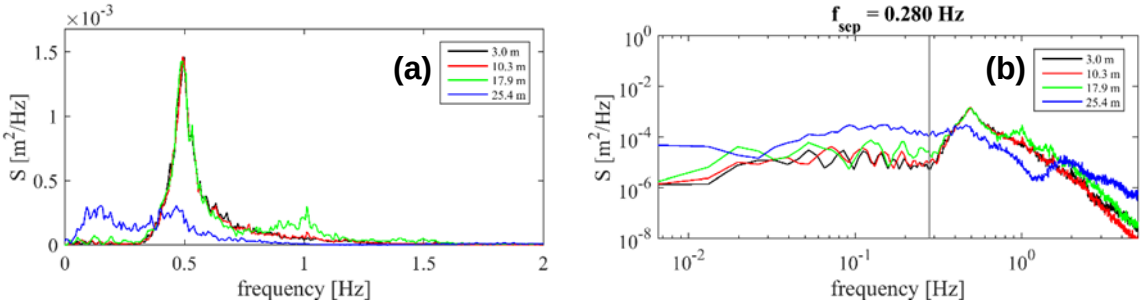

Figure 70: Spectral variance density S over frequency f of condition RS11 at four equidistant locations along the flume (foreshore 1/50 at model scale 1:35), starting at the reference wave gauge and ending at the wave gauge at the toe of the dike, (a) linear scale axes, (b) logarithmic scale axes, with indication of the separation frequency fsep (gray line).

b).

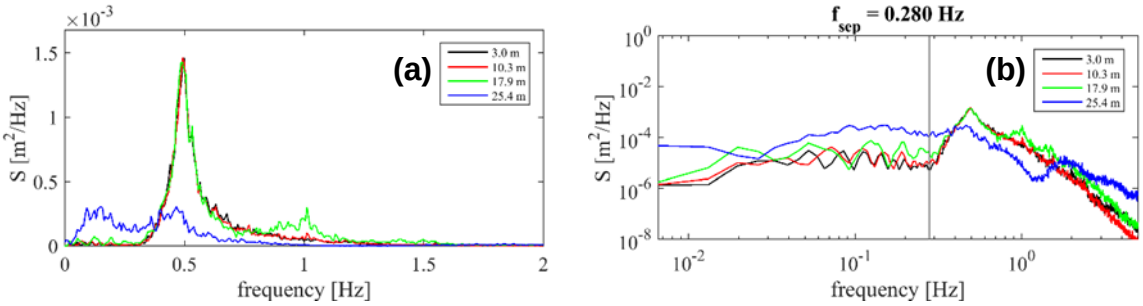

Figure 70: Spectral variance density S over frequency f of condition RS11 at four equidistant locations along the flume (foreshore 1/50 at model scale 1:35), starting at the reference wave gauge and ending at the wave gauge at the toe of the dike, (a) linear scale axes, (b) logarithmic scale axes, with indication of the separation frequency f_{sep} (gray line).

Thanks to the high spatial resolution measurements of the surface elevation along the complete foreshore, a detailed analysis is possible of the wave transformation up to the toe of the dike and of the effects the presence of the dike has on it (Gruwez *et al.*, 2018a, 2018b). The cross-shore evolution of the short wave significant wave height $H_{m0,hf}$ (hf: high frequency), the infragravity or

long wave significant wave height $H_{m0,lf}$ (lf: low frequency), the spectral wave period $T_{m-1,0}$ and the wave setup are presented in Figure 71, for foreshore slope 1/50 (model scale 1:35) and the highest tested water level. The trends of the significant wave height (hf and lf) evolution over the foreshore are similar to those obtained in experiments over a regular beach without dike (Ruessink *et al.*, 2013). However, in the present case a steep-sloped dike was located in the inner surf zone close to the swash zone, and some differences can be observed in this area. One notable example is in the very shallow area in front of the dike, where the infragravity significant wave height strongly increases, instead of remaining constant or slightly decreasing towards the swash zone in the case of a beach without dike (Ruessink *et al.*, 2013). This hints at a different reflection behaviour of the long waves due to the presence of the steep-sloped dike.

The cross-shore evolution of the wave spectrum is shown in Figure 70. Again similar observations can be made compared to a beach without dike, where non-linear energy transfer occurs in the shoaling and surf zones towards the infragravity frequencies (here, f < 0.28 Hz) and twice the peak frequency (f ~ 1.0 Hz). However, at the toe of the dike two distinctive peaks appeared of similar energy content in the infragravity band and primary short wave band. This shows that for the highest tested water level, a non-negligible energy content of the primary short waves was still present at the toe of the dike. These short waves are then also likely reflected strongly by the dike.

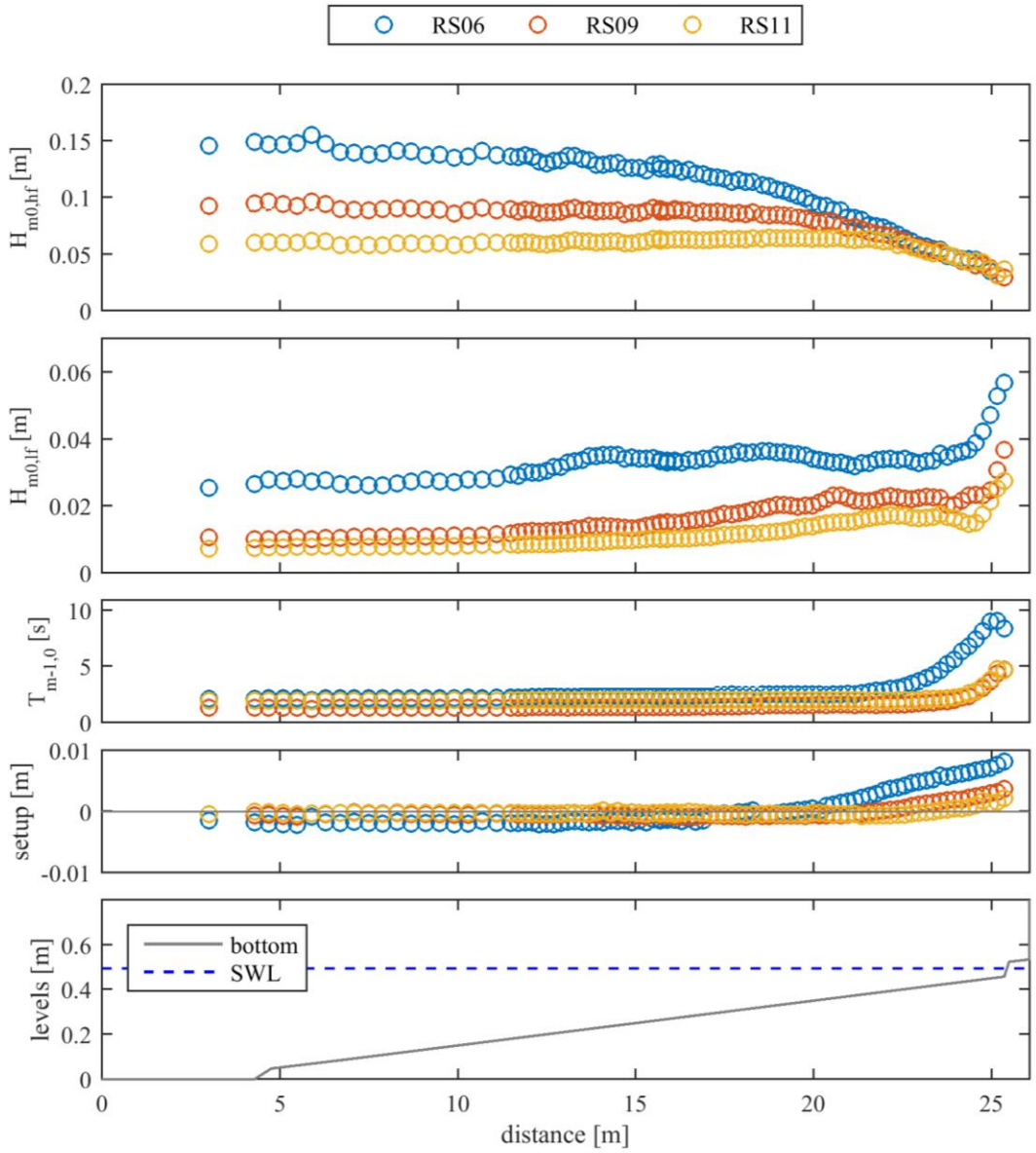

Figure 71: The wave characteristics measured over the complete foreshore (slope 1/50 at model scale 1:35), by way of repeated and combined high spatial resolution surface elevation measurement experiments, (a) the short wave (hf: high frequency) significant wave height $H_{m0,hf}$, (b) the infragravity wave (lf: low frequency) significant wave height $H_{m0,lf}$, (c) the spectral wave period $T_{m-1,0}$, (d) the wave setup, and (e) the bottom profile with indication of the still water level (SWL). For three selected test conditions RS06, RS09 and RS11 (see Table 8, THM4.6).

These initial observations will be further analysed by decomposing the wave field into the incident and reflected long waves and comparing the results more in-depth with a beach profile without a dike. The effect of the dike on the reflection of the long waves has important consequences for the morphology of the beach, since mostly the infragravity or long waves drive morphological changes of a beach during storm conditions (Roelvink *et al.*, 2009).

THM 4.12 IMPORTANCE OF ACTIVE WAVE ABSORPTION OF LONG WAVES

Active wave absorption in physical models should be tuned to include both reflected long waves and seiches (if the wave paddle stroke length allows it) when testing coastal structures with a very shallow foreshore. Otherwise, build-up of long wave energy will significantly affect the measurements of wave-induced structural response.

Especially during long experiments (typically 1000 wave tests) the artificial build-up of long wave energy in the flume experiment due to re-reflection against the paddle can distort a measurement of overtopping or wave impact loads. Short waves travelling on top of the unwanted re-reflected long waves can more easily overtop the dike crest, resulting in higher overtopping discharge and consequent impact load. That is why reflected long waves should be absorbed at the wave paddle to avoid re-reflection into the flume and therefore avoid build-up of long wave energy in the experiments.

Long waves occur in a 2D wave flume typically due to:

- Long waves bound to the incident wave groups and becoming free long waves when the short waves are breaking along the mildly sloping foreshore and non-linear energy transfer occurs towards the infragravity frequencies;
- Spurious free long waves generated by applying 1st order wave generation (can be avoided by applying 2nd order wave generation (see also THM 4.16);
- Seiches resulting from excitation of the eigenfrequency of the combined flume and model set-up.

To showcase the importance of active absorption of long waves in 2D wave flume experiments, a comparative study was conducted between the CREST 2D experiments (see THM 4.6) and other experiments conducted in the Ghent University 2D wave flume facility (Streicher, 2019) prior to the CREST tests. These tests were similar to the CREST 2D experiments in terms of geometry and wave conditions, but had important differences in how the reflected waves were absorbed by the wave paddle. A model geometry was constructed comprised of a mildly sloping foreshore with slope 1:35, a dike with slope 1:2 and attached to the dike a promenade (10 m wide in prototype) with a storm wall on top. Hydraulic boundary conditions similar to a storm with a 1000 year recurrence interval for the Belgian coast were applied. However, contrary to the CREST 2D experiments, waves were generated using in-house developed software for first-order wave generation with Active Wave Absorption (AWA) tuned to absorb reflected short waves. For the CREST 2D experiments, AwaSys7 software (Aalborg University, 2018) was applied instead for first and second order wave generation, including AWA. The AWA in this software was optimised for absorbing reflected long wave energy as much as possible (within the limits of the stroke length of the paddle).

A test with similar hydraulic boundary conditions and with 1st order wave generation was repeated with a) active absorption of long waves disabled and b) active absorption of long waves enabled. The offshore wave spectrum and wave spectrum at the dike toe (extremely shallow foreshore, after (Hofland *et al.*, 2017)) was compared for both tests (Figure 72).

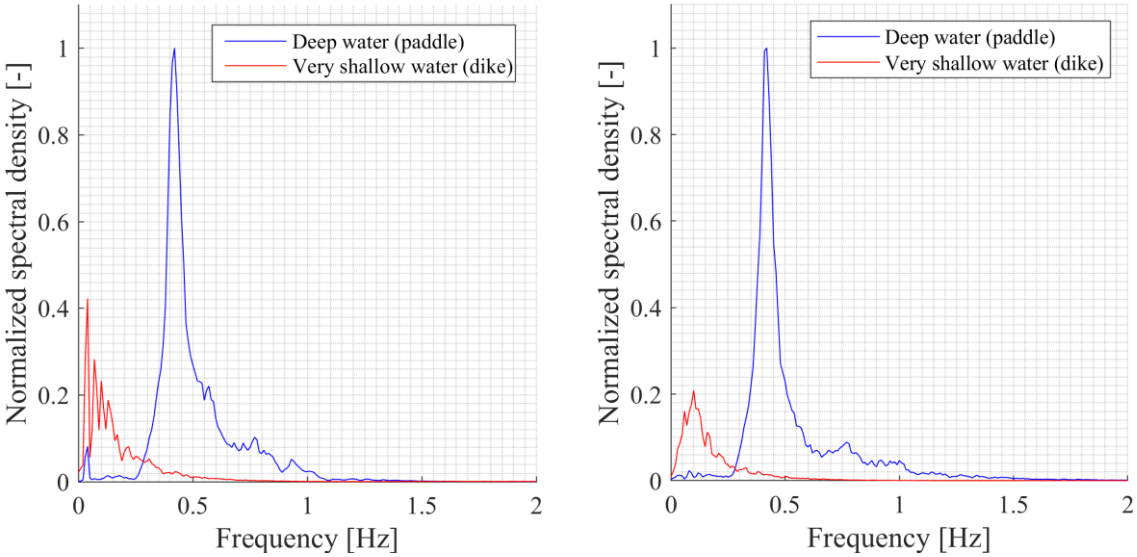

Figure 72: Repeated experiment with active absorption of long waves disabled (left) and enabled (right). The blue line represents the wave energy spectrum at the paddle (offshore) and the red line the wave energy spectrum at the dike toe (very shallow water). Since the offshore incident wave conditions were similar between both tests but not exactly the same, the wave spectra were normalised by the maximum spectral density value of the deep water wave spectrum.

In both cases the primary peak in the wave spectrum disappears due to breaking of the short waves. At the same time a transfer of short towards long wave energy is observed, when moving from the paddle location (deep water) towards the location of the dike toe (extremely shallow water). With the active absorption of long waves disabled (Figure 72**Error! Reference source not found.**, left), long wave energy around 0.04 Hz can be observed even for the measurement in deep water (blue line). 0.04 Hz is approximately the first mode seiche frequency (0.035 Hz) for this model set-up, and – being the first mode – is excited the most (highest energy). Also higher seiche modes are clearly visible (up to mode 5, or even arguably up to mode 8). When the active absorption of long waves is enabled (Figure 72**Error! Reference source not found.**, right), no seiche mode energy peaks are (easily) discernible from the wave spectrum, not even the first mode. This indicates that the seiche waves are absorbed, effectively preventing seiche energy build-up or excessive seiching in the wave flume. In addition, this comparison shows that the wave energy in the infragravity frequency band is also lower when the AWA is able to absorb reflected infragravity waves as well, further reducing the spurious long wave energy at the toe of the dike. This is even less trivial considering the offshore incident significant wave height was lower in case of the test without long wave AWA ($H_{m0,o}$ = 0.16 m) compared to the run with long wave AWA ($H_{m0,o}$ = 0.20 m), meaning that more energy transfer occurred to the infragravity wave band in the case of the test with long wave AWA.

THM 4.13 REPEATABILITY MEASURED IMPACT FORCES

Measured experimental wave impact forces have a low repeatability, because of a high dependence on small changes in environmental conditions. On the other hand, repeatability is important to reduce uncertainty in prediction formulas derived from experiments and for validation of deterministic numerical models. Low-pass filtering of the measured signal of the impact forces in the post-processing step, effectively removing mostly the stochastic part of the dynamic impact types, improves repeatability.

If a real case situation is studied in different physical models to estimate wave forces, different results will be obtained. Even within the same wave flume, different results will be obtained if a test is repeated. Three causes can be distinguished:

(1) Different wave trains (different seed number);
(2) Non-repeatability of exactly the same situation;
(3) Scale effects.

Cause 1 is discussed in THM 4.19.

Cause 2: non-repeatability of exactly the same situation. This is illustrated based on a repeated test from the WALOWA dataset (Streicher *et al.*, 2017), as discussed by Gruwez *et al.* (2020). The horizontal force F_x and pressure p signals were baseline corrected to remove drift and needed to be filtered as well, at least to remove the phenomena related to model effects such as the natural frequency response of the wall to the bore impacts and the electronic current frequency of 50 Hz. As such, Streicher (2019) applied a 4th order Butterworth low-pass filter with a cut-off frequency of 48 Hz. The resultant thereof is hereafter called the base signal. Moreover, the first peak of the double peak force or pressure base signal was caused by the initial bore impact against the wall and was termed a dynamic or impulsive impact, characterised by high frequency oscillations in the base signal (Streicher *et al.*, 2019c), see examples in Figure 73

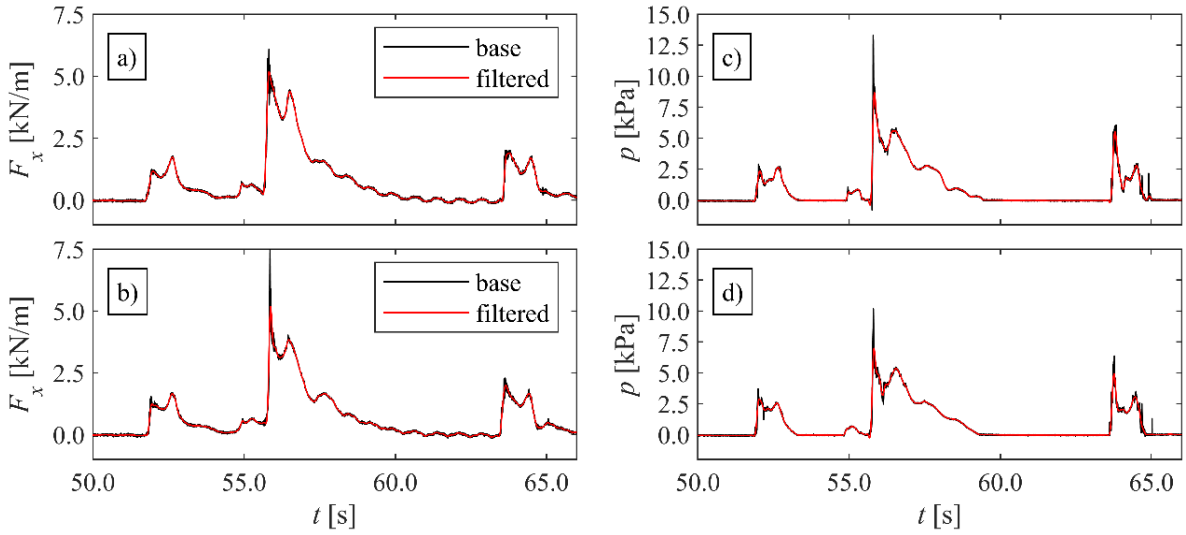

. The processes behind these oscillations are to some extent stochastic, indicated by the strong differences between the repeated tests (e.g. compare Figure 73

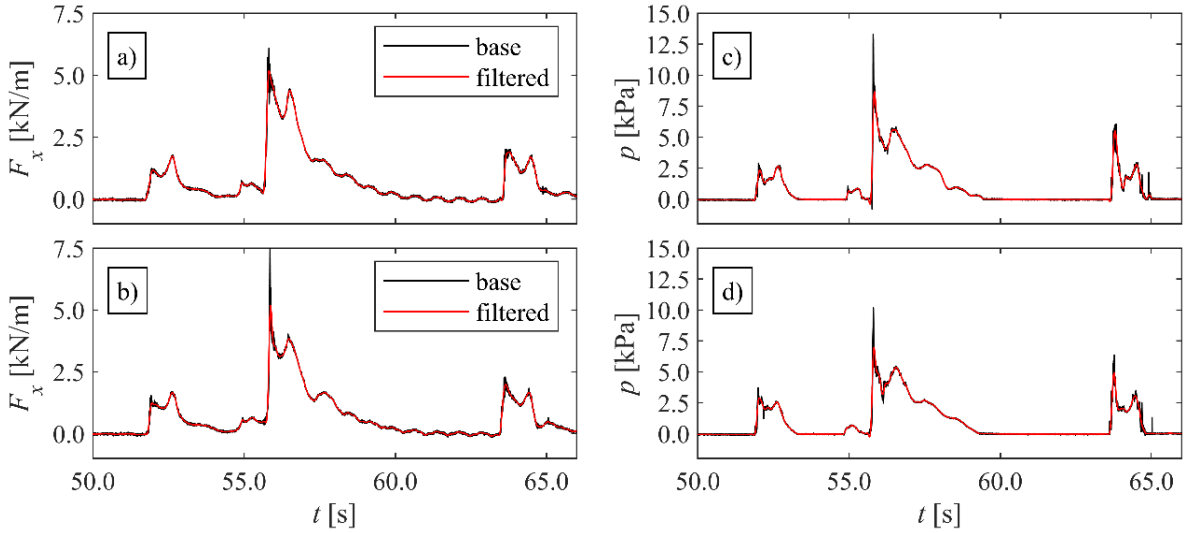

a/c with Figure 73b/d), and can be attributed to 3D effects of the turbulent bore front, air entrapment during wave impact and air entrainment in the turbulent bore front (Streicher *et al.*, 2019b). This stochastic behaviour cannot be reproduced by a deterministic numerical model (Jacobsen et al., 2018). To remove these stochastic dynamic impact oscillations, an additional 3rd order Butterworth low-pass filter with a cut-off frequency of 6.22 Hz was applied to the base signal. This corresponds to a cut-off frequency of 3.0 Hz at prototype scale, which is still well above the natural frequency of about 1.0 Hz for typical buildings found along the Belgian coast (De Rouck and Trouw, 2019). After filtering the base signals, the force and pressure time series of the original experiment (EXP) and the repeated experiment (REXP) converge (Figure 72

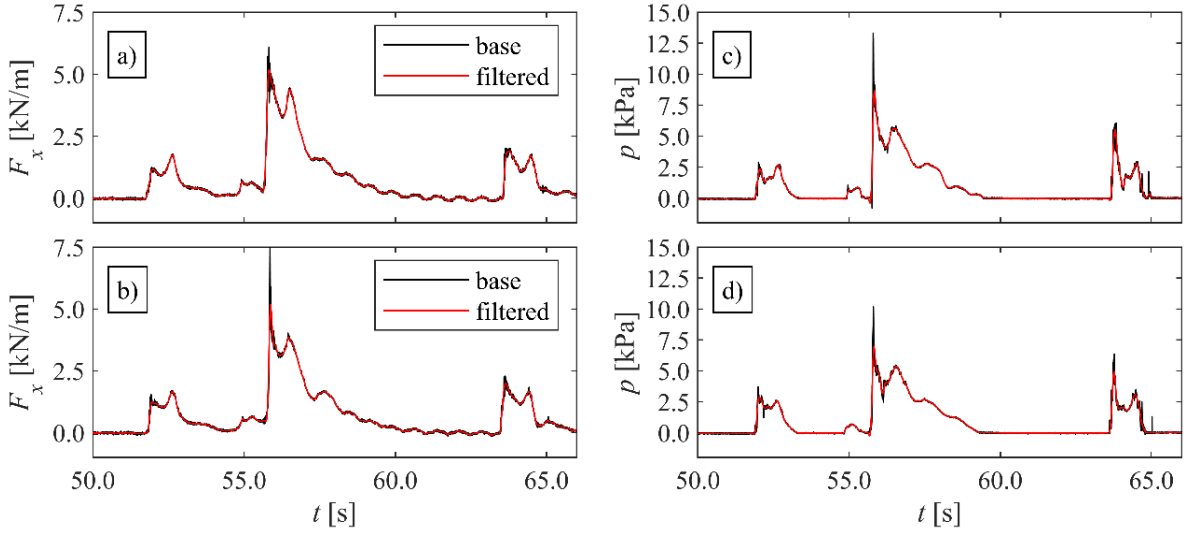

a/c and Figure 73b/d), which means that the measured force becomes more repeatable after applying such a filter that removes the stochastic part of the dynamic impact force.

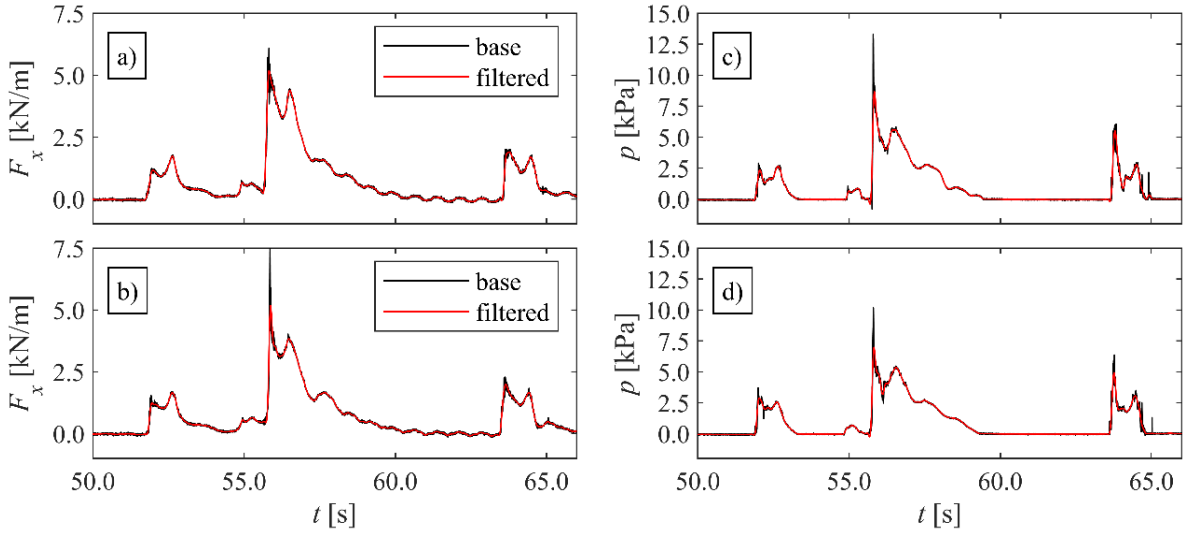

Figure 73: Comparison between the time series of the base and filtered (a/b) horizontal force signal and (c/d) pressure signal measured by pressure sensor PS05, during (a/c) the original (EXP) and (b/d) the repeated experiment (REXP).

The impact of a similar filter applied to the 2D CREST force data is shown by De Vos (2019) (Figure 74**Error! Reference source not found.**). Spatial variability of the measured impact force is clearly present as well, but significantly reduced after applying the filter.

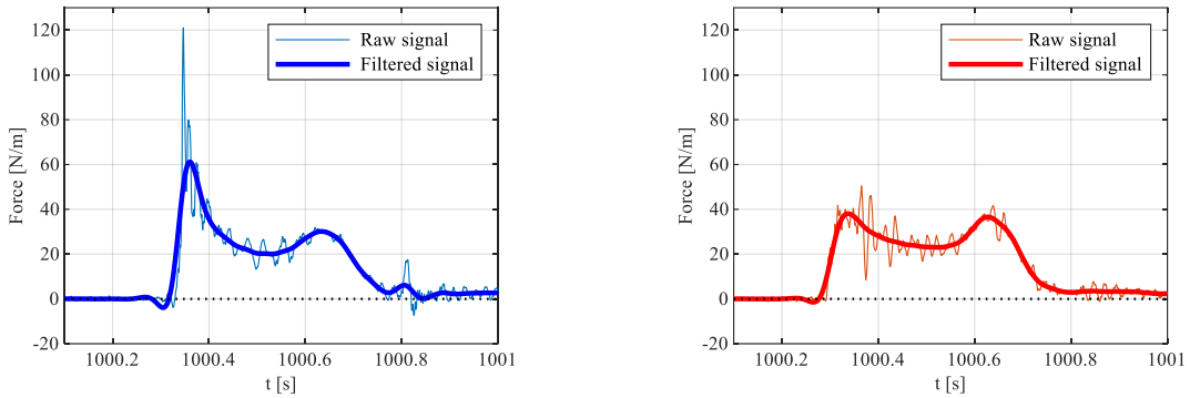

Figure 74: Example of the filtered force data (Gc = 10 m, RS06, FS 1/35). Results for two adjacent load cells measuring during the same test. Left: Load cell A; Right: Load cell B.

Cause 3: Scale effects. Streicher *et al.* (2019b) managed to repeat exactly the same wave train and the same dike configuration in flume experiments with different scales (Deltares at 1:4.3 scale, UGent at 1:25 scale). In the small scale experiment, the number of impacts was 20% lower, while the maximum wave force F_{max} was about 4% smaller. The difference for F_{max} is relatively small compared to the general non-repeatability. However, Streicher *et al.* (2019b) recommends further research e.g. by the use of pressure sensors, a wider range of scale ratios, examining the effect of salinity and improved wave generation/absorption to better represent the long wave characteristics (see also THM 4.12).

THM 4.14 DYNAMIC IMPACT FORCE SAFETY FACTOR

Smaller elements of buildings, such as windows and doors, usually have a higher natural frequency than the recommended low-pass filter for experimentally measured impact forces and are affected by the stochastic part of the dynamic impact types. Therefore, a dynamic impact force safety factor should be applied to a calculated maximum force (determined from low-pass filtered force measurements) for the design of such elements.

The maximum impact force determined from a filtered measured signal (THM 4.13, see De Vos (2019) and Gruwez *et al.* (2020) for the discussion on the need for filtering and filter settings) is applicable to constructions with a relatively low resonance frequency such as buildings on top of the dike (~1Hz, De Rouck and Trouw (2019)). However, smaller elements of buildings, such as windows and doors, usually have a higher natural frequency than the recommended low-pass filter for experimentally measured impact forces and are affected by the stochastic part of the dynamic impact types (that is removed by such filtering). Therefore, a dynamic impact force safety factor should be applied to a calculated maximum force (determined from low-pass filtered force measurements) or the quasi static force peak for the design of such elements:

$$F_{dy} = \alpha_{im} F_{qs} \qquad (4.14.1)$$

Where F_{dy} is the maximum impact force associated with a (high frequency) dynamic impact, F_{qs} with a quasi-static impact (or filtered F_{max}) and with $\alpha_{im} \geq 2.5$, such as recommended by Chen et al. (2017). More research is needed to determine suitable α_{im}-values for specific (type of) structures.

THM 4.15: DIRECTIONAL SPREADING

Directional spreading, expressing the degree of short crestedness of real sea waves, is an essential parameter in the design of beach nourishments and structures for coastal safety. The higher its value, the lower the long wave height is at the dike toe, leading to lower overtopping and impact force. Modification of existing prediction formulas is ongoing. However, there is little known about the amount of directional spreading actually occurring nearshore during storm conditions along the Belgian coast. More analysis of existing field measurements is strongly recommended, in addition to continued and more dedicated field measurements.

Scale model experiments at scale 1:50 were carried out in the wave basin at Flanders Hydraulics Research. The directional spreading was varied and the effect on overtopping and impact forces was measured.

The effect of directional spreading on the average overtopping discharge is shown in Figure 75**Error! Reference source not found.**. Compared to the limiting case for long crested waves (directional spreading 0°) the overtopping decreases with increasing directional spreading. For a

typical storm at the Belgian coast with a directional spreading of 16° a reduction factor of ca. 5 is found for a configuration with an extremely shallow foreshore, and a reduction factor of ca. 1.5 is found for a configuration with a very shallow foreshore. The empirical formula for calculating mean overtopping discharge is adapted by (Altomare et al., 2020) to take the effect of directional spreading into account.

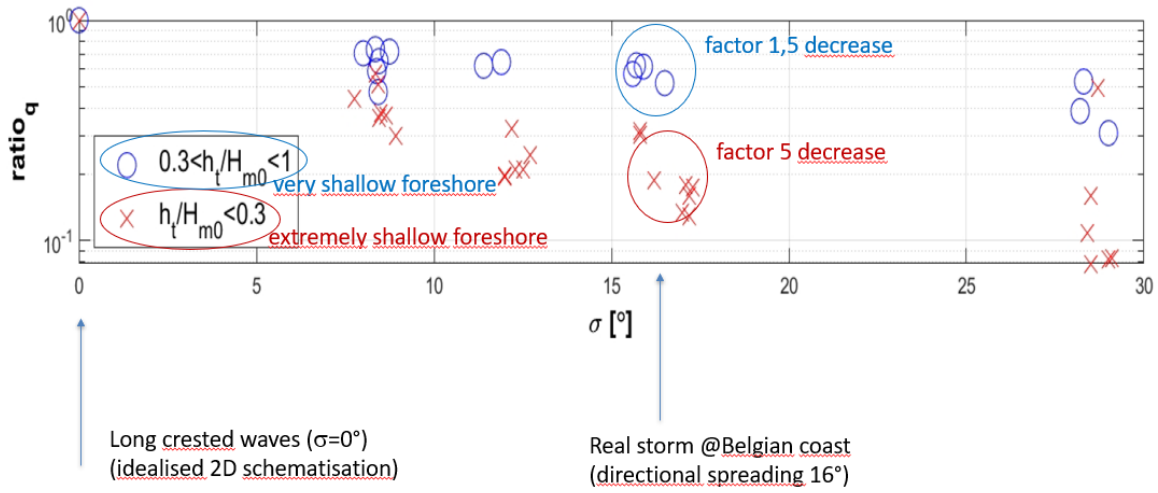

Figure 75: Influence of directional spreading on the average overtopping discharge.

A similar influence is found regarding hydraulic loadings. It was found that the wave characteristics (wave height and wave period) at the toe of the dike are reduced for increasing directional spreading, which can partially explain a reduced overtopping discharge and reduced impact forces (Pueyo Estada, 2019).

However, there is not much known yet about the amount of directional spreading actually occurring nearshore during storm conditions along the Belgian coast. Therefore, more analysis of existing field measurements is strongly recommended, in addition to continued and more dedicated field measurements.

THM 4.16 IMPORTANCE OF 2ND ORDER WAVE GENERATION

First order wave generation at the offshore boundary in nearshore experimental and numerical models introduces spurious, non-physical long waves, which affect the maximum individual overtopping volume and the mean wave overtopping discharge. This is especially true for mean overtopping discharge values in the order of 10 l/m/s and lower. Second order wave generation prevents such spurious long waves and is therefore recommended.

Based on 1st and 2nd order wave generation tests from the CREST 2D dataset (foreshore slope 1/50, model scale 1/25) and extended with validated SWASH model results, an investigation into the effect of 1st or 2nd order wave generation on the wave overtopping on a dike with very shallow foreshores was performed (Lara, 2018).

Both the dominating role of low frequency over high frequency energy (represented by H_{lf}/H_{hf} ratio, **Error! Reference source not found.**a) at the toe of the dike and the differences between incident low frequency energy for 1st and 2nd order cases (given by relative differences, d_{rel} = ($H_{lf,1st}$ - $H_{lf,2nd}$)/$H_{lf,2nd}$, Figure 76b) at the dike toe have been shown dependent on the foreshore shallowness ($h_t/H_{m0,o}$). Low frequency wave energy is more dominating for more shallow cases and more overestimated when using 1st order wave generation. As a result, total H_{m0} values at that location are also more overestimated in case of more shallow foreshores when using 1st order wave generation.

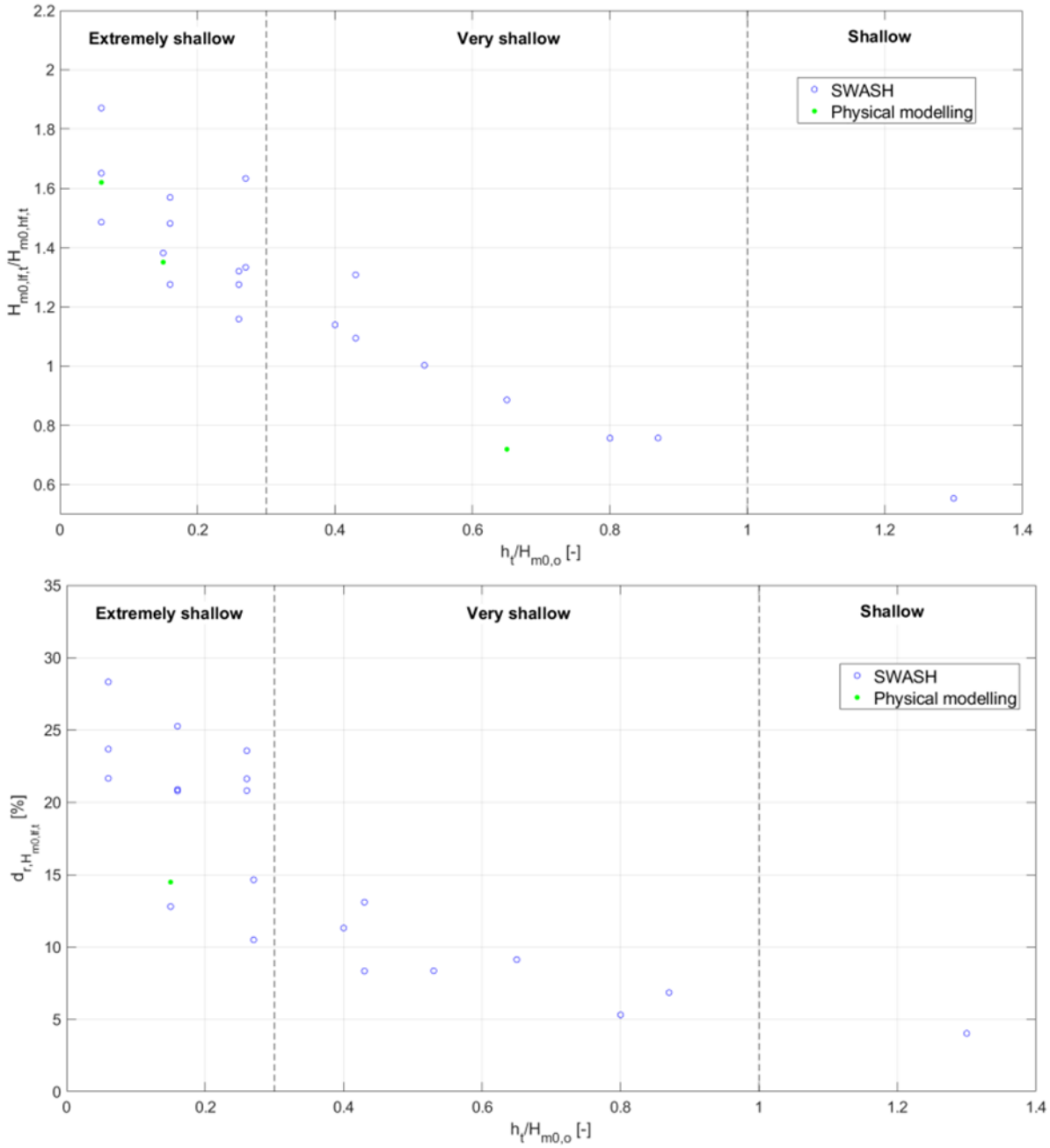

Figure 76: Top: Ratio between $H_{m0,lf,t}$ and $H_{m0,hf,t}$ from 2nd order generated waves against relative water depth ($h_t/H_{m0,o}$) from SWASH (blue) and physical modelling (green). Bottom: relative

differences between incident $H_{m0,lf,t}$ from 1st and 2nd order generated waves against relative water depth ($h_t/H_{m0,o}$) from SWASH (in blue) and physical modelling (green).

Differences in wave setup at the dike toe have been found to be not as much affected. However, in case of extremely shallow foreshores 1st order wave generation has been found to increase the wave setup by up to 20% compared to 2nd order wave generation.

The combined overestimation of H_{m0} and wave setup affects wave-structure interaction phenomena, including wave overtopping. The analysis of wave overtopping shows an overestimation of the maximum individual overtopping value in a given test when comparing 1st order wave generation to 2nd order (Figure 77**Error! Reference source not found.**). Previously it was assumed that this does not affect the mean overtopping discharge q. This is more or less correct for high values of q. However, for lower values of q (especially q < 10 l/m/s, prototype scale value) or high freeboard R_c and low $H_{m0,t}$, also the mean overtopping discharge is affected by an overestimation applying 1st order wave generation (Figure 78).

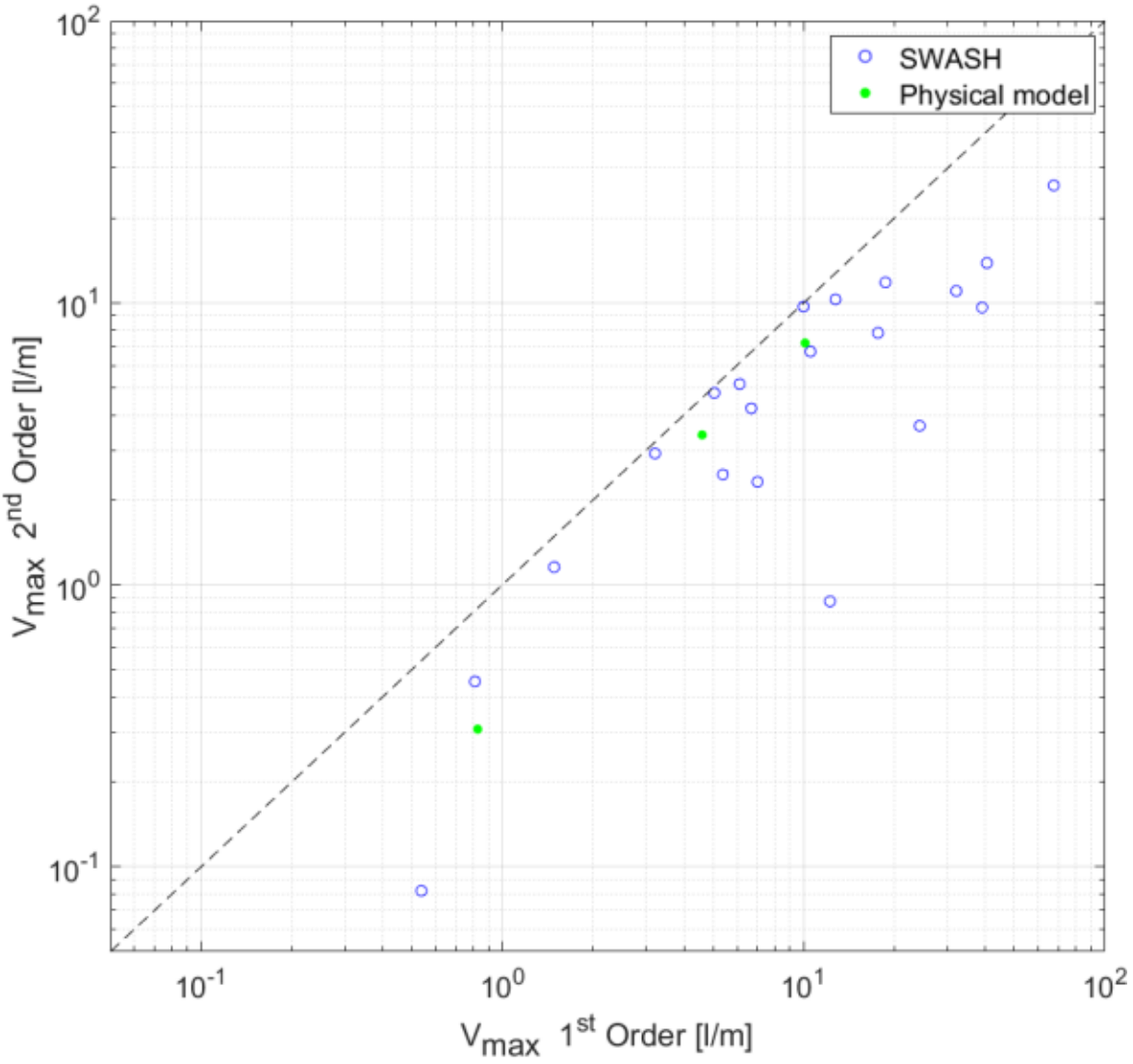

Figure 77: Comparison of the maximum individual overtopping volume Vmax (on the right) from physical modelling (in green) and SWASH (in blue) with 1st and 2nd order wave generation.

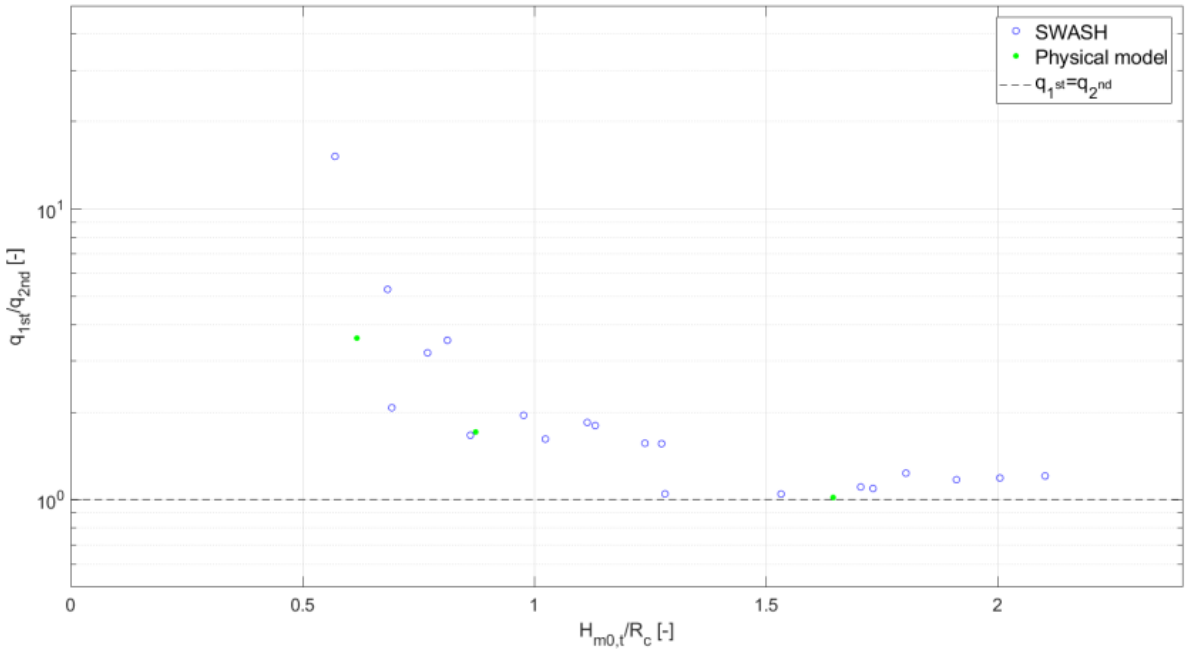

Figure 78: Ratio between q_{1st} and q_{2nd} as function of the total (2nd order) $H_{m0,t}$ normalized with the dike freeboard R_c from physical modelling tests (in green) and SWASH simulations (in blue).

Conclusion is that the use of 1st order wave generation theory is not recommended when studying wave processes on a very/extremely shallow foreshore, as spurious subharmonic waves may lead to erroneous conclusions. Regarding wave overtopping, the overestimation of both individual and average values in case of 1st order wave generation might lead to an overly conservative design.

THM 4.17 ACCURACY OF SWASH FOR WAVE IMPACT

The numerical model SWASH is able to provide an accurate estimation of the maximum force per impact event on dike-mounted vertical walls, by assuming hydrostatic pressure only for the calculation of the force on the vertical wall. Including non-hydrostatic pressure effects might improve results further, particularly for dynamic wave impacts. However, spurious pressure/force oscillations are observed when including the non-hydrostatic pressure. No explanation for this numerical effect has been found yet.

Gruwez *et al.* (2020) present a detailed validation and inter-model comparison of OpenFOAM (OF), DualSPHysics (DSPH) and SWASH (one-layer depth-averaged model: SW1L) for a WALOWA bichromatic wave test.

Unexplained spurious pressure/force oscillations are observed when using the non-hydrostatic pressure from the SW1L model to determine the horizontal impact force F_x on buildings on top of a dike with very shallow foreshore (Figure 79c). However, these spurious oscillations disappear when only considering the hydrostatic pressure (Figure 79**Error! Reference source not found.**d). Even though the hydrodynamic pressure is hereby neglected, SWASH appears to be able to provide an accurate estimation of the maximum force per impact event, even compared to full Navier-Stokes models, such as OF and DSPH(Figure 80).

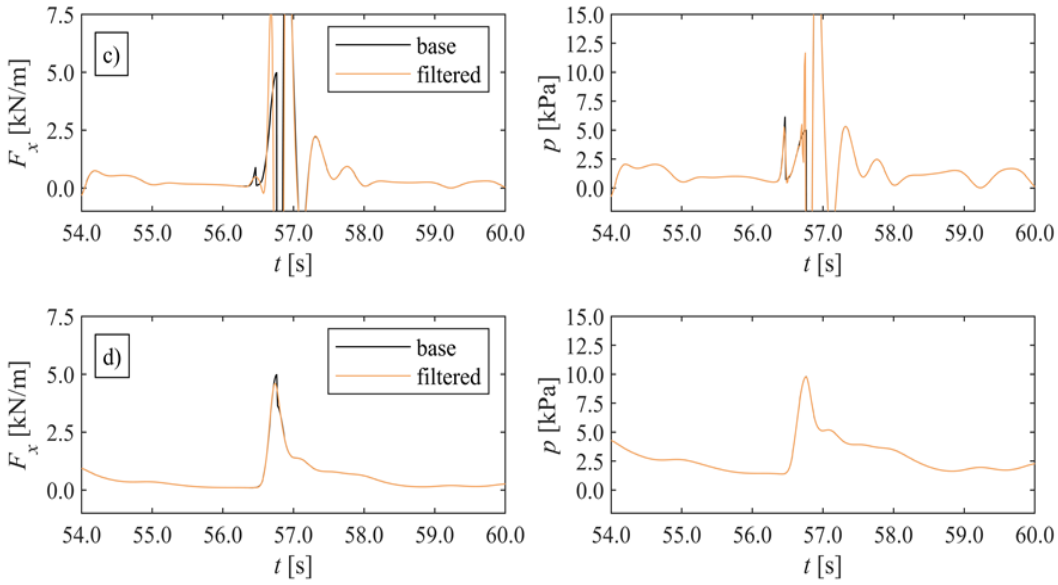

Figure 79: Comparison between the time series of the base and filtered F_x (left) and p (right) signal, for: c) SW1L (total pressure), and d) SW1L (hydrostatic pressure only).

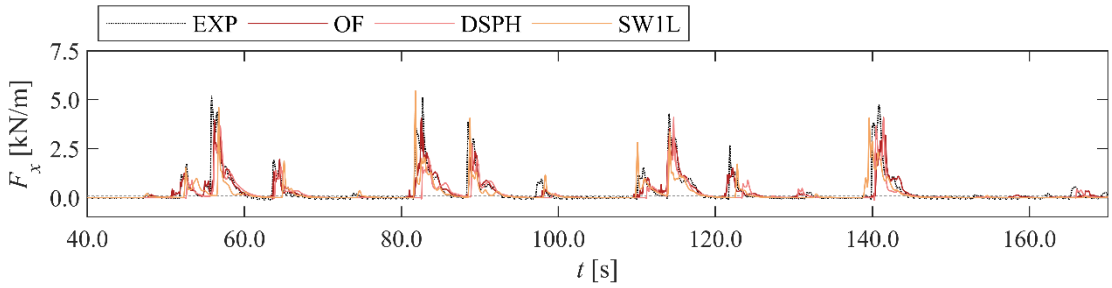

Figure 80: Comparison of the horizontal force time series at the vertical wall. The experiment is the load cell force measurement.

The model performance to reproduce the experimental peak forces of each independent wave impact event during the test is evaluated by Willmott's refined index of agreement d_r (Willmott *et al.*, 2012) between predicted and observed maximum horizontal force per impact event $F_{x,max}$ ($d_{r,Fx,max}$,Table 13). The closer d_r is to 1, the better the agreement between prediction and observation. This statistic confirms that SWASH is at least as able as OF and DSPH to estimate F_x for wave impacts on buildings on top of a dike with a very shallow foreshore (in case no storm wall is present on the promenade).

Parameter	REXP	OF	DSPH	SW1L
$d_{r,Fx,max}$ [-]	0.92	0.85	0.79	0.88

Table 13: Willmott's refined index of agreement d_r for $F_{x,max}$ of each impact event during the bichromatic test. REXP: repeated experiment, OF: OpenFOAM, DSPH: DualSPHysics, SW1L: one-layer SWASH model.

THM 4.18 NECESSITY OF FULL NAVIER-STOKES MODELS

The numerical model SWASH significantly underestimates the impulse of the force per wave impact event on a dike-mounted vertical wall in shallow foreshore conditions, indicating that the wave impact flow is not modelled correctly. More detailed Navier-Stokes models such as OpenFOAM and DualSPHysics are necessary for a more accurate flow modelling along the vertical wall, leading to a better estimation of the duration of wave impact forces.

Gruwez *et al.* (2020) present a detailed validation and inter-model comparison of OpenFOAM (OF), DualSPHysics (DSPH) and SWASH (one-layer and eight-layer depth-averaged model: SW1L and SW8L) for a WALOWA bichromatic wave test.

In THM 4.17 it was established that SWASH is able to predict peak forces well. However, not only peak forces are of interest, but also the duration of the impact is of high significance to structural damage (Bullock *et al.*, 2007). The duration of the wave impact can be evaluated by the impulse of the total horizontal force, I:

$$I = \int_0^{t_N} F_x(t)\, dt \qquad (4.18.1)$$

where t_N is the total duration of the test. To evaluate the model performance a normalised predicted impulse is considered:

$$I^* = \frac{I_p}{I_o} \qquad (4.18.2)$$

where I_p and I_o are the predicted and observed force impulses. The observed total horizontal force impulse is overestimated, equal to or underestimated by the prediction when $I^* > 1$, $I^* = 1$ or $I^* < 0$, respectively. Note that I^* is evaluated for the complete F_x time series, so that phase differences are disregarded. Therefore, I* purely evaluates the correspondence of the total impulse on the vertical wall during the complete test. Even though SWASH is able to provide a very good estimate of the peak force $F_{x,max}$ per impact event, the wave impact impulse is not as well represented, with the worst I* value of the three models (Table 14).

Parameter	REXP	OF	DSPH	SW1L	SW8L
I^* [-]	0.99	0.85	0.64	0.62	0.54

Table 14: Overview of Fx related statistics for each model. REXP: repeated experiment, OF: OpenFOAM, DSPH: DualSPHysics, SW1L: one-layer SWASH model, SW8L: eight-layer SWASH model.

Model snapshots of key time instants are compared during an impact on the vertical wall in Figure 81. The complex flow patterns of bore-interactions and bore impact, run-up and reflection at the vertical wall are captured better by the full Navier-Stokes models (especially OpenFOAM).

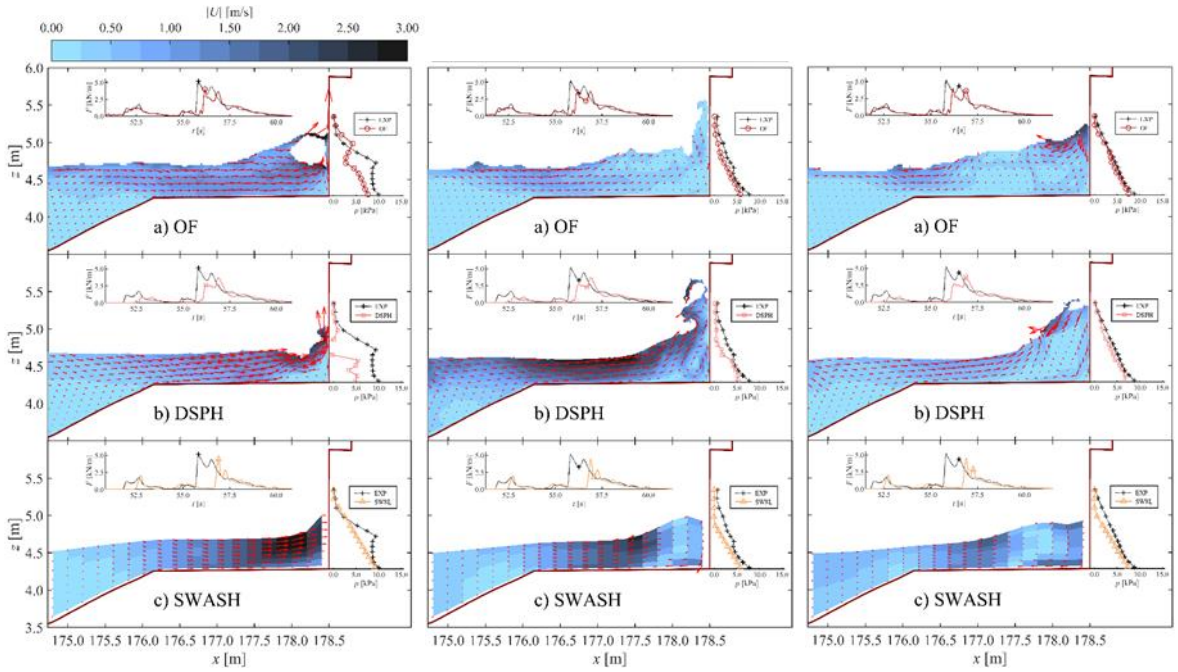

Figure 81: Snapshots of numerical model results on the dike for three key time instants (red arrows are U vectors).

THM 4.19 IMPORTANCE OF SEED NUMBER ON LOW OCCURRENCE OVERTOPPING/IMPACTS

Maximum individual wave overtopping and impact is affected by the wave generation method (seed effect). This effect was tested for a mean overtopping discharge, q, of about 15 l/m/s, and is expected to increase even more for smaller mean overtopping discharges (e.g. q ≈ 1 l/m/s, currently the limit used in the safety assessment). Additional in-depth research into this issue is necessary.

An investigation of the repeatability of the CREST 2D tests was carried out (De Vos, 2019). One specific test (RS01) has been carried out 13 times in total. Of these 13 tests, five were done with exactly the same wave train (fixed seed number). The other eight tests were carried out using the same offshore wave conditions and spectrum (H_{m0}, T_p) while adapting the random seed in the wave train or surface elevation time series generation. Adapting the seed affects the sequences or wave phases of waves approaching the promenade, which yields alternative wave-wave-interactions and affects the maximum measured impact forces. Given the small number of waves that typically overtop a dike with a shallow foreshore, this means that differences in the highest individual wave heights result in different wave overtopping and wave forces. As an illustration of this phenomenon, two repetitions of the same test generated using the same seed are shown in Figure 82 (a) and (b), and a different seed is used in (c). Figure 82 shows that for an identical random seed in (a) and (b), a very similar impact force time-series is observed, exhibiting peaks of comparable magnitude around the same point in time. Figure 82 (c) however, exhibits a completely different impact pattern, yielding a different maximum impact force as well.

The resulting F_{max} and average overtopping discharge q measured throughout this series are shown in Figure 83 and statistics are summarised in Table 15. The coefficient of variation (CV) is defined as the standard deviation divided by the mean (σ/μ) and is often used to express the repeatability in an experiment. The lower the coefficient of variation, the lower the variability around the mean. The results in Table 15 indicate that one should recognize and be mindful of the stochastic variability when dealing with the maximum wave-impact forces. The maximum impact force is greatly dependent on the adopted seed number, even so much that it varies from 6 kN/m to up to almost 19 kN/m for the considered test. On the other hand, the repeated tests (with fixed seed number) show a much lower standard deviation and CV. A similar trend is observed for the mean overtopping discharge q. However, the CV is not as high for the different seed number tests and q is therefore less affected by this. It is expected that the maximum individual overtopping volume V_{max} is similarly affected by this as F_{max}.

The key takeaway from this analysis is that altering the input random seed of the wave train affects the maximum forces to a huge extent, indicated by a coefficient of variation of 21% for the test considered. This needs to be taken into account in the uncertainty of empirical prediction formulae derived from this type of tests. Additional in-depth research into this issue is necessary.

	F_{max} [kN/m]		q [l/s/m]	
	Rep	Randseed	Rep	Randseed
Mean	17.95	11.70	16.12	15.88
Stdev	1.07	2.45	0.42	0.81
CV	6.00%	21.00%	2.60%	5.13%

Table 15: Mean, standard deviation and coefficient of variance for Fmax and q for a 5 times repeated test with same seed number (Rep) and 9 times repeated test with different seed numbers (Randseed).

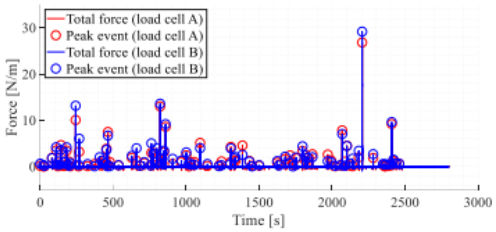

(a) RS01 – rep 1

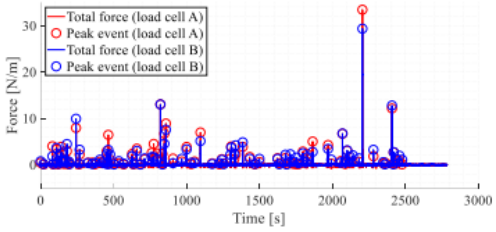

(b) RS01 – rep 2

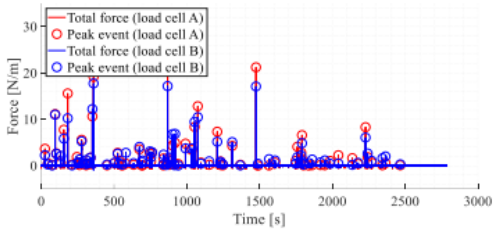

(c) RS01 – Random seed 1

Figure 82: Illustration of the effect of the wave train (seed number) on the wave impact forces. The same seed number or wave train was used for tests (a) and (b), a different seed number or wave train was used for test (c).

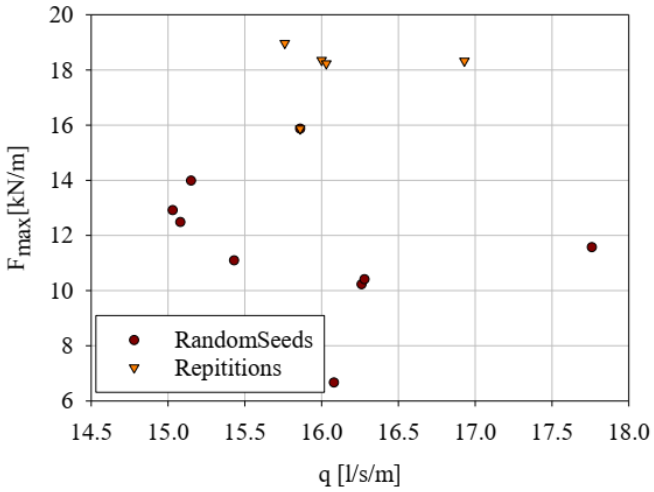

Figure 83: Fmax and q for a 5 times repeated test with same seed number (Rep) and 9 times repeated test with different seed numbers (Randseed).

THM 4.20 EFFECT BEACH MORPHODYNAMICS ON OVERTOPPING

Modelling beach morphodynamics during a storm is a key aspect in understanding and accurately predicting wave overtopping. The sand transport along the beach profile during a storm (beach morphodynamics) triggers profile changes which need to be included in the modelling of wave overtopping over a dike with a very shallow foreshore (very relevant to the Belgian coast).

The effect of sediment transport and the resulting changing beach morphology in front of a sea dike on wave overtopping over the sea dike fronted by a shallow and mildly sloping foreshore was studied. For this purpose, the CFD toolbox OpenFOAM was employed and a sediment transport module was implemented in the source code. This sediment transport module incorporates both suspended load and bedload transport and is implemented according to the traditional approach. This means the suspended load is modelled by the convection-diffusion equation, bedload transport is modelled by an explicit expression and discretized using the Finite Area Method (FAM). The continuity equation for the sediment (Exner equation) is solved to obtain the changes in sand bed elevation. With this information, deformation of the sand bed due to sediment deposition, entrainment and bedload is performed by automatic mesh motion. Unstable slopes are prevented with a sand sliding algorithm.

In the framework of the CREST project, 2D experimental tests were performed to assess wave transformation and wave overtopping over a sea dike fronted by foreshores ranging from 1:20 to 1:80 (see THM 4.6). A numerical simulation of one specific configuration was carried out (foreshore with a slope of 1:20 on a model scale of 1:25). At the inlet, regular waves with a wave height of H = 0.212 m and a wave period of T = 2.4 s in an initial water depth of d = 0.69 m were generated. These chosen parameters represent superstorm conditions (a storm with a return period of about 17000 years). To study the effect of sediment transport and the changing beach morphology, a simulation with and without moving bottom was carried out. The results showed an increase in wave height of 31% if sediment transport and changing beach morphology is included in the simulations, due to beach erosion and the consequent water depth increase (scour hole is formed at the toe of the dike). Additionally, the wave period at the toe of the dike was found to increase with 45%.

As a consequence of the higher wave height and wave period, the average overtopping rate was also found to increase for the case with a dynamic beach profile. The above results confirm that the changes in beach profile during a storm impact the overtopping volumes. When the beach is eroded, the overtopping volumes increase due to higher water depths, and the resulting higher wave heights in front of the dike. Moreover, it should be kept in mind that the current sediment transport module does not take into account the energy loss due to the mobilization of the sediment itself. This effect is currently still being studied by comparing the results of the current model and a more physics-based sediment transport model developed by Ouda and Toorman (2019). It is also still not clear which profile should be taken to do design or safety assessment calculations.

SUMMARY AND CONCLUSIONS

The main objective of the Climate REsilient coaST (CREST) project was to gain a better understanding of the nearshore and onshore physical processes, the flood risks and the resilience of the coastal system, in order to deal in the most appropriate way with the possible impacts of climate change. Five main scientific objectives were identified at the start of the project:

1) better understanding of nearshore and onshore physical processes including improved models and the validation of 'grey' data about coastal dynamics;
2) better understanding of the flood risks along the coast and the impact of wave overtopping on structures, buildings and people;
3) determine the resilience of the natural coastal system (coastal protection) in relation to storms and wind;
4) validate calculations with today's state of the art models on the basis of laboratory and field measurements in selected pilot areas;
5) define improved climate change scenarios for the Belgian coast.

Separate attention was paid to the dissemination of the results of the project which can then be used by other researchers and professionals, such as: biologists, socio-economists, spatial planners.

These objectives were worked out in three research activities and three supporting activities. As can be seen in Figure 1 (redrawn below), each activity focussed on a specific topic, while the supporting activities clearly had links with all of them.

The scientific objectives being ambitious and broad, it is clear that activities had to work on very specific, clearly defined tasks. Gaps in the existing knowledge were identified, and research was aiming to solve one piece at a time, in order to contribute to the global objectives.

Conclusions are formulated in the final activity report to VLAIO on whether objectives have been reached for each specific activity.

Taking one step back, and looking more in general at CREST, it can be concluded that for each of the different objectives formulated above significant progress has been made.

(1) Better understanding of nearshore and onshore physical processes including improved models and the validation of 'grey' data about coastal dynamics;

- A lot of effort has been put in collecting more data: new measurements in the field and the lab, but also the recovery of existing historic data (e.g. bathymetry, beach profiles). These data are crucial since they form the major input for all further analysis.
- A variety of different numerical models has been applied, improved and tested: e.g. TELEMAC, TOWAWAC, SWASH, OpenFOAM, DualSPHysics and one new model two-phase model MixtSedFOAM was developed.
    - CREST being a fundamental research project, this is also the part where a lot of effort is put in improving the modelling of individual physical processes, that later on can be integrated in other models or model approaches (e.g. upscaling, improvements in the Telemac software)
    - Several couplings were developed between the nearshore models SWASH-DualSPHysics and SWASH-OpenFOAM, in order to make them better fit for purpose (less calculation time)
    - The newly developed two-phase (sediment and water) model promises to be a very powerful numerical laboratory to study fundamental processes and is complementary to laboratory experiments.
- Analysis of the newly gathered morphological and hydrodynamical data and the model results brought new insights or confirmed existing hypothesis. The results showed for instance that:
    - There does exist a mechanism of cross-shore feeding of the beaches, which allows for beach recovery after storms. Morphological features of the intertidal bars, the embryonic dunes and the backshore berm play an important role in beach recovery.
    - This cross-shore feeding might explain the natural volume increase of our beaches with about 500.000m^3/year over the last 30 years (net result of an increase at the western and eastern part and erosion in the centre of the Belgian coast). It should be studied further if also other causes can be identified.
    - The intertidal zone in Belgium is not only shaped by waves, but equally by tidal currents and, to a lesser extent, by natural variations in sediment supply.
    - Dune growth at the Flemish coast is primarily caused by aeolian sediment input from the beach by westerly to south-westerly winds. On decadal timescales, the dunes grow linear in time with an average rate of about 6 m^3/m/year, featuring large variations in longshore direction.
    - A significant effect of the foreshore slope angle and the dike geometry (the promenade width, the presence of a storm wall, …) on wave overtopping rates and wave impact

forces is confirmed for the Belgian coast. This will lead to reduced forces in the design and safety assessments and therefore also allows for a more economic design.
    - Long waves (or infragravity waves) significantly affect the wave-induced structural response (e.g. overtopping and wave impact) of dikes for the case of very shallow foreshores.
    - Directional spreading, expressing the degree of short crestedness of real sea waves, is an essential parameter in the design of beach nourishments and coastal protection structures. The higher its value, the lower the long wave height is at the dike toe, and the lower overtopping discharges and impact forces.

(2) better understanding of the flood risks along the coast and the impact of wave overtopping on structures, buildings and people;

- It has been shown in the scale tests that 3D effects have to be taken into account in order to make a good estimate of the flood risks (mainly due to the effects of the directional spreading).
- The numerical model SWASH is able to provide an accurate estimation of the maximum force per impact event on dike-mounted vertical walls, by assuming hydrostatic pressure only for the calculation of the force on the vertical wall.
- A cloud-based flood risk assessment tool with an object-relational approach, FLIAT, has been developed, to improve the accuracy, calculation speed, ease of use, and possibilities for further development of the flood risk and damage assessment methodology in Flanders.
- Vertical evacuation should be considered as first choice in case the available evacuation time is short.
- The knowledge of the effect of different wave generation methods (e.g. reflected wave absorption, second order wave generation) on overtopping and forces has increased.
- Relations between wave overtopping characteristics and wave forces are obtained for specific configurations. Still, further improvements for more general use are necessary.

(3) determine the resilience of the natural coastal system (coastal protection) in relation to storms and wind;

- The resilience of the sandy coast has been studied by investigating the evolution of the coastline (and sand balance) on short (e.g. storms) and long (decades, e.g. climate change) timescales.
    - It has been shown from the in-situ monitoring campaigns that beach recovery occurs after a storm: up to one third of the eroded beach volume recovered at the pilot sites in a few months' time.
    - On longer time scales there is also a clear positive effect of the beach nourishments and the natural feeding from off-shore on the coastal evolution: the additional sand volume effectively mitigates the beach erosion due to sea level rise.
- In order to come to final indicators for coastal resilience, a long list of possible parameters has been identified, but their use and their effectiveness need to be studied further.

(4) validate calculations with today's state of the art models on the basis of laboratory and field measurements in selected pilot areas;

- Extensive field measurements were carried out since 2016 till 2019 in the nearshore, the intertidal zone, and on the dry beach of two study sites, Groenendijk and Mariakerke, along the Belgian coast. Measurements included: topographic data (monthly topographic profiles and (bi-) annual LiDAR surveys, subtidal campaigns, intertidal campaigns, argus system at Mariakerke, meteo-marine and sediment data, and aeolian sand transport. The large dataset collected during this project (measured data in the field and the lab, but also the recovery of existing historic data) has been used for the calibration and validation of the different models.
- A validation and comparison of the nearshore CFD models OpenFOAM, DUALSPHysics and SWASH was performed for the modelling of the wave transformation on the foreshore, the layer thickness and velocity on the dike and the pressure and wave impact on a vertical wall. The outcomes on model accuracy and practical applicability (calculation time, model set-up) resulted in recommendations on the use of each of these models and the application ranges.

(5) define improved climate change scenarios for the Belgian coast.

- Four climate scenarios for the Flemish coast have been defined in cooperation with the project "Coastal Vision" (Dutch: Kustvisie www.kustvisie.be), piloted by the Department of Mobility and Public Works of the Flemish Government. These common climate scenarios are used by the different administrations, research institutes, universities and consultants, so that results all add to the insight in the effects and impacts of these four climate scenarios.
- Although according to projected changes in the climate extreme waves conditions and storm surges are not expected to change much, sea level rise will increase the impact at the Belgian coast unless the level of coastal protection can grow at equal pace..

Although great progress has been made and many of the objectives have been reached, some of the work needs to be further completed or extended.

Also, in order to fully reach some of the scientific objectives, application of the new knowledge in practice is needed. For instance, to value the impact of some of the findings on the flood risk, a new set of complete flood risk calculations needs to be performed with the methodology adapted and improved according to the latest insights. Only then the impact (e.g. the difference with the current predictions) will be known.

Therefore, in the following sections possibilities for further application are discussed, including some recommendations.

VALORISATION AND FURTHER APPLICATION

The impact of CREST does not stop at the end of the project. Already during the project explicit attention was given to valorisation of the new knowledge, methods and tools developed. Specific objectives were formulated at the start of CREST in the project, for the valorisation of CREST in general:

1. provide information and practical advice (including guidelines) about new models for the calculation and simulation of physical coastal processes, wind impact on dunes and beaches and wave impact on structures, buildings and people;
2. provide advice to stakeholders in the context of coastal zone management, particularly coastal safety, contingency planning and land use planning along the coast;
3. provide information to better assess the environmental impact of coastal protection measures, navigation, etc.;
4. provide practical information (e.g. policy indicators, maps and test sites on the beach) to communicate the impact of climate change, storms and wind on our coastline to a broad audience.

(1) Provide information and practical advice (including guidelines) about new models

A nice example of the valorisation of the work done within the CREST project on the Telemac model developments, is the cooperation with Flanders Hydraulics Research (FHR) and IMDC during the development of the Scaldis-Coast model. The Scaldis-Coast model is a new morphologic (TELEMAC) model for Belgian coast, developed by IMDC and FHR within the project "Morfologisch kustonderzoek, Ontwikkeling van een integraal kustmodel" for the Division Maritime Access from the Flemish Government. The model is aiming at predicting long-term morphological changes in the coastal zone on a timescale of years to decades.

- Since the start of the project at Flanders Hydraulics Research, end 2017, there has been frequent interaction with the CREST TELEMAC team (mainly involved in activity 1: integrated multi-scale wave-current-sediment modelling), to exchange information about developments within CREST, but also about other TELEMAC model issues.
- The idea is that new developments from CREST can be included in this new model, especially since the nearshore area and the beach are zones of interest. Results are expected in 2020.
- The same model is also being used by IMDC to study the large-scale morphological evolution of future alternatives for coastal protection within the project "Coastal Vision", commissioned by the Division Maritime Access from the Flemish Government.

Other ongoing or planned initiatives for the valorisation of the numerical models include for instance:

- Many of the numerical model developments will become available to the wider community of numerical modellers and coastal engineers since they have been implemented in open source codes. MixtSedFOAM will be made available on github. The developments in TELEMAC-TOMAWAC-GAIA will be uploaded on the KU Leuven branch of the versioning server of LNH-EDF, from where integration in a new public release of the code will take place.
- Guidelines have been made available on the use of CFD nearshore wave models for the calculation of wave-structure interaction during storm conditions.
- The TELEMAC suite has become one of the major software packages in Flanders for the projects on the Belgian coast and the Scheldt estuary. KU Leuven, Flanders Hydraulics Research and IMDC are now regular invited participants to the yearly TELEMAC-MASCARET scientific committee meetings in Chatou (France), where the future of the code is discussed with the major developers.

(2) Provide advice to stakeholders

Specific attention has been paid to the dissemination of information and results during the project, for different groups of stakeholders:

- A project website was created to inform the interested public on the CREST project: www.crestproject.be. The website describes the project, its deliverables and reports, presentations and any news, activities and events in relation to the project. It also provides a geoviewer, which makes available several GIS layers, including metadata.
- The advisory committee was informed regularly on the progress and results of the project.
- The technical advisory committee, including international experts, advised the CREST researchers from scientific point of view.
- The mid-term and final conference were open to all, and welcomed a large audience with a broad range of backgrounds.
- The coastal mayors have been informed separately about the CREST project.
- CREST being a fundamental research project, a lot of the information on these studies will be published in PhD and MSc theses and scientific papers. This information will complement the CREST deliverables.

Two private partners were involved in CREST for the valorisation of the newly developed tools and methodologies.

- Both partners attended all partner meetings.
- Fides Engineering organized a workshop on emergency planning in the event of flooding, which was attended by scientists, consultants and policy makers (e.g. coastal division, spatial planning, federal administration responsible for evacuation plans).
- Fides Engineering also advised on how the obtained insights and formulas can be used in future designs and assessments of coastal safety and on the optimisation of future monitoring with regards to coastal safety. Also advice is given for further research (using the information obtained within CREST and advice for new numerical and physical modelling) in order to be able to incorporate the different pieces for a new safety methodology.
- IMDC advised on how the results of CREST can be applied for consultancy.

(3) Provide information to better assess the environmental impact of coastal protection measures, navigation

The guidance committee also had the goal of sharing the project with a wide audience. The participants in the supervisory committee represent different sectors and come from universities, governments and administrations, engineering consultants, contractors, other interest groups, or on their own initiative. They were among others representatives from KULeuven, VUB, UGent, KBIN, Flanders Hydraulics Research, VLIZ, MDK - afdeling Kust, MOW - afdeling Maritieme Toegang, Ruimte Vlaanderen, FOD Leefmilieu, ILVO, AGIV, FOD Economie, LRD, IWT, Provincie West-Vlaanderen, Natuurpunt, Jan De Nul Group, Dredging International, IMDC, Fides Engineering, TORGUN BVBA, eCoast, Eurosense, GreenBridge, Maritime Cluster van Vlaanderen, …

The new models and insights from the CREST project in relation to hydrodynamics, sediment transport and morphology will therefore also be used in future studies of the environmental effects of interventions in the coastal zone, for coastal protection and navigation, among others.

(4) Provide practical information to a broad audience

Policy indicators for coastal resilience have been proven difficult to achieve. A long list of possible parameters has been produced, which needs to be studied further. Maps showing the evolution of the coastline and the beach heights (between 1983 and 1996) were included in a Geoviewer (http://www.crestproject.be/geoviewer/?lang=en#!/). Beach profiles (1971-1996) can be explored in an online application at http://crestproject.be/nl/exploring-beach-profiles. All this geographical information was added to the Coastal Portal (Dutch: Kustportaal) of VLIZ and integrated with data of flood risks and maritime spatial planning (http://kustportaal.be/en/flood-protection).

During the monitoring campaigns the CREST flag and informative posters were set up to inform passers-by about the project.

A movie was produced about the CREST project and shown at the kick-off event of the Blue Cluster (Dutch: Blauwe Cluster). This movie is available at http://crestproject.be/nl/media-store.

During different public events a sandbox model from VLIZ was used to inform a wider audience about the effect of sea level rise and beach nourishments at the Belgian coast.

Finally, on World Ocean Day 2017, VLIZ organised a public event at De Grote Post Ostend including an expo related to 13 safety risks at the beach. The CREST information booth included information and practical tests about the dangers of quick sand at the beach and of digging a hole at the beach.

RECOMMENDATIONS

The ultimate goal of the Climate REsilient coaST (CREST) project was to gain more knowledge in order to deal in the most appropriate way with the possible impacts of climate change on the coast. To be able to evolve to such a sustainable coastal management approach, an entire chain of processes – from offshore to nearshore, on the beach, in the dunes and towards the hinterland – has to be correctly understood, in order to predict what will happen in the future and how management choices will impact the system. The CREST project has focussed on the physical aspects of this coastal system.

The previous section already listed some of the ongoing or planned studies, where results and new insights gained during the CREST project will be integrated. While the CREST project covers a wide range of topics, many more initiatives can follow, using or improving the present knowledge. Looking back at the project, some recommendations can be formulated at this stage.

FUTURE FIELD AND LAB MEASUREMENTS

Although Flanders' coast is relatively well monitored, there still exists a need to **continue, improve and extend the field and lab measurements**.

- With regards to the ongoing **bathymetric and topographic surveys**, it has been found within CREST that the uncertainty on the bathymetric surveys has a large impact on the accuracy of the observations. This uncertainty can be reduced by performing independent terrestrial control measurements of the low-tide area immediately following echo sounding. Also, in order to study the morphological relationship between the offshore and the active coastal zone, the surveyed area should be extended seaward, including the shoreface as well as the tidal gullies and sand banks near the coastline.
- Within CREST it has been shown that **long waves** (or infragravity waves) significantly affect the wave-induced structural response (overtopping, wave impact) of dikes for the case of very shallow foreshores. Also, **directional spreading**, expressing the degree of short crestedness of real sea waves, is an essential parameter in the design of beach nourishments and structures for coastal safety. However, very little is actually known about these long waves and the amount of directional spreading actually occurring nearshore during storm conditions along the Flemish coast. Dedicated field measurements and the re-analysis of existing field data (e.g. step gauges) of these long waves and directional spreading are strongly recommended, in addition to the continuation of existing field measurements.
- To better **quantify aeolian sediment transport processes** more innovative monitoring techniques should be applied, especially when **long-term monitoring** is envisaged. A camera-system can monitor the overall weather and wave conditions, bar welding, beach morphology, and the frequency and magnitude of erosion events. The images can then be used to extract moisture maps, beach dimensions, fetch distances and vegetation cover. Also, a self-rotating vertical sand trap can measure the whole transport column from surface to a certain distance above the surface to get information of the entire flux profile.

- Along the entire Flemish coast and in the ports, numerous **human interventions** occur. It is advised to keep all the data related to the dredging executed in navigation channels, the beach and dune nourishments performed and the local interventions on the beach by municipalities such as beach scraping and flattening the beach and dune scarps, in a well-structured database. These data are crucial in relation to the morphological monitoring, since all these activities clearly have a direct impact on the local topography and bathymetry.
- Although within CREST great efforts have been made to finance, design and permit **the Artificial Dike** field measurement campaign, this measurement campaign is no longer possible before the end of the CREST project. The earliest possible will be from the winter 2020-2021 onwards and hopefully for a duration of 7 or more years, provided that the contract for the works can be awarded by the government. A new research project should then be started around this measurement campaign with collaboration between different (CREST) institutions. The main focus being the execution of measurements of wave overtopping and wave impact on large scale, one needs also to think about sharing this test facility to other disciplines, by jointly doing different types of complimentary measurements.
- New insights were obtained about which parameters influence the **wave forces during overtopping**. In the next step this knowledge has to be merged to obtain new formulae. Also the effect of wave randomness (different wave trains) should be studied further. CREST made clear that further 3D physical modelling is necessary.

SHARING RESULTS AND DATA

Not only being valid for this project, but for research in general, is the importance of **making new data and results available** to the research community, policy makers, consultants and contractors. Only then the work done will be correctly valued and valorised.

- Efforts should be made to provide access to newly measured data, accompanied by proper metadata. Within CREST it has been tried to make data as much as possible available through the IMIS database, hosted and maintained by VLIZ. Maintenance of this database is also guaranteed after the project. Adding new data remains possible.
- New models should be well documented, shared and made public, so that others can pick them up, use and further improve them. It is better to share the efforts on one set of models, which then can actually be used, rather than develop in parallel similar but different codes, which will never be used again if not shared and properly documented. Within CREST several of the models which have been developed further are open source (e.g. MixtSedFOAM and TELEMAC-TOMAWAC-GAIA), and improvements have been or will be made available within these model communities. This allows integration in the next model release, and also further testing and validation by other researchers.

This practice of making data and models available to the larger community should even be encouraged more. Although many are absolutely convinced that this is the way to go, it is far from obvious and this for many reasons like the extra effort that is needed versus the short term objectives of contracts and of researchers.

IMPACT ON COASTAL ZONE MANAGEMENT

CREST will have impact on the coastal zone management in Flanders, and possibly also abroad. The outcomes of this research should be used to **improve design and test methodologies for coastal protection and coastal risks**.

Some possible actions have already been identified, such as:

- Based on the obtained insights into the physical processes and the validated numerical tools obtained in the CREST project, the safety assessment and design methodology of the coastal protection can be improved:
    - The methodology of the coastal safety assessment is currently being updated at Flanders Hydraulics Research. The results, new data and models delivered by CREST (e.g. the results of the scale model experiments) will be used. Results are of this are already expected in 2020.
    - No single model or methodology is applicable for all purposes. Also, for the design and testing of coastal protection distinction should be made between the different stages in a project or study. Another phase in a project requires a different approach.
        - The currently applied methods for testing and designing coastal protection measures are all looking into very detailed and time intensive methods. The highest possible accuracy is looked for to provide as much information as possible. This is indeed suitable for a detailed design.
        - However, for projects in feasibility stage, and even for preliminary design, much quicker methods are looked for. A somewhat lower level of accuracy is acceptable, since typically only orders of magnitude, and ranges of costs are looked for. In the CREST project progress is made to estimate overtopping and forces without numerical models.
        - Also other outcomes from CREST are useful. For instance it has been shown that the less computationally demanding SWASH model can, in certain cases, provide estimates for the maximum wave impact force with a comparable accuracy than the computationally more demanding OpenFOAM and DualSPHysics models.
    - It is therefore recommended to provide more insight in the accuracy of models and methodologies. Less accuracy does not always imply a bad methodology. The real value of a result depends also on the knowledge of the uncertainty on the result. A clear insight in the ranges of uncertainty allows for an adequate selection of methods and tools for different types of studies.
- The **FLIAT tool** developed in CREST will allow to perform more accurate cost benefit analyses in the future:
    - The methodology relies on more detailed data to make more detailed predictions. However not all these data are readily available yet. Tools have been developed to extract the relevant data, but in order to get access to more detailed data of buildings (e.g. EPC certificates) there are some privacy issues to be resolved first.
    - Attempts are being made to further develop and maintain this tool in the future by Ghent University and Flanders Hydraulics Research. New projects are yet to be defined.

    - Making the FLIAT model open source might boost the further development and use of this tool. Currently consultants are developing their own similar tools as well (e.g. for use abroad).
- In concertation with the designated authorities (MDK, Coastal Division), a separate project was started during CREST to investigate the **risk of casualties in buildings on the sea dikes** that can be flooded in the event of heavy wave overtopping. The CREST results were a starting point in this project and are being implemented by Flanders Hydraulics Research.
- Flanders Hydraulics Research has studied the **actual morphological trends in all coastal stretches**. A key finding was that the eastern and western part of the Belgian coast is growing, while the central part is eroding. Netto, a volume gain of 500.000m³/year over the last 30 years is obtained. Although CREST provided some insights, the reason for this volume gain should be studied further in order to be more confident in predicting the evolution in the future. This might help understanding how the beaches will develop (without human intervention) due to sea level rise. The knowledge gained during CREST on dealing with uncertainties on the data will be used to provide more insight into the morphological evolution of the coast and the location of the most erosion-prone areas. Results are expected beginning 2020.

FUTURE RESEARCH AND STUDIES

Future research and studies should focus on filling the gaps in knowledge, data and tools needed to complete the chain from offshore towards the hinterland. From a management point of view, it is advised to **focus on those missing links, with the biggest impact.**

Nowadays, some of the missing inputs and knowledge for coastal zone management in Flanders are:

- A complete and **detailed set of coastal hydrodynamic boundary conditions** is required for any coastal study. The current boundary conditions (Hydraulisch Randvoorwaardenboek, 2015) should be updated and further detailed according to the state-of-the-art knowledge and methods.
    - According to the type of process (wave overtopping, breakwater stability, morphology), and the location along the coast or within the harbour, another set of conditions can be more penalising (e.g. depending on directions, water levels, wave characteristics, etc.). For instance, it has been shown before that for beach erosion a shore-perpendicular wave direction is not always the most penalising condition. Also, in the harbours the effect of the wave direction on the penetrating wave is well known. All possible combinations should be identified in these new boundary conditions.
    - More extreme scenarios of sea level rise are considered nowadays (up to 3m in 2100), following the new set of climate scenarios defined by CREST in cooperation with the project “Coastal Vision” (MOW, Division Maritime Access). To be able to perform calculations for future conditions (2050, 2100), also the hydrodynamic boundary conditions for higher sea levels need to be determined. It is clear that even when offshore wave heights do not drastically change, nearshore wave heights will increase due to the higher water depths caused by sea level rise.

    - CREST has shown that there is information lacking on directional spreading of the waves and on the characteristics of the long waves. Once (more) measurements are available for those processes, the set of boundary conditions can be further updated.
    - Flanders Hydraulics Research has recently (November 2019) launched a study for the update of the methodology and the determination of a new set of coastal hydrodynamic boundary conditions.
- A good **knowledge of the behaviour of coastal structures,** such as locks, weirs, gates, outlets, etc. which form an integral part of the coastal protection is needed. A lot of these structures are quite old, and design conditions are not well known, neither the current state of these structures.
    - In order to improve the flood risk calculations, it is not enough to improve the damage predictions, and to perform very detailed dune erosion and wave overtopping calculations (e.g. time intensive CFD type models) to feed the inundation models, if still important assumptions need to be made at all of these structures. Indeed, possible failures or breaches at these structures lead to massive inundation of the hinterland, dominating the calculated flood risks. It is therefore advised to investigate this issue, so that the uncertainty on the failure of these links in the coastal protection can be massively reduced.
    - Flanders Hydraulics Research looks into the stability of these coastal structures, together with the expert unit for Concrete and Steel of the Flemish Government (EBS-Expertise Beton en Staal). First results are expected in 2020.
- The CREST study has shown that **defining resilience indicators** is not straightforward. The morphological response of the beach and dune system to the meteo-marine forcing and the definition of fundamental cause-effect relationships behind observed physical processes is complex. Due to lack of understanding of all the complexities only some parameters are identified. This should be further investigated, and also be linked to the role of and the effect on the whole coastal eco-system including human interference (which was outside the scope of CREST).
- The current safety assessment methodology for the coastal protection in Flanders is quite detailed (except from the coastal structures being missing). This is time consuming but acceptable since it needs to be performed only once every 6 years. However, for the **day-to-day coastal management**, some **more readily available databases and (quickscan) tools** could be developed, which will support management decisions and feed expert advice in a very quick and accessible way.
    - The Morphan system, as being used in the Netherlands by the coastal managers to watch their coastal profiles (kustraaien) and the base coastline (basiskustlijn), is not applicable as such in Flanders. Indeed, the coastal management strategies and available data are different in both countries, and therefore coastal managers in Flanders would benefit from a tailor-made Coastal Zone Management (CZM) system, answering their needs.
        - The relevant authorities (MDK, Coastal Division; MOW, Maritime Access Division) should therefore define the user requirements of a CZM system, and lessons-learned from CREST can be integrated (e.g. in relation to the measurements of bathymetry and topography, and integrating data on human interventions such

as dredging and nourishments, see above). The most appropriate coastal indicators should be integrated, so that a regular follow-up is possible of both the short and long-term morphological evolution of the coast, which impacts coastal safety and accessibility of the harbours.
    - In a second step the system can be further improved, following new insights in the behaviour of the coast, additional coastal indicators or new insights. Models could be linked to this system, not only by using the data available (topography, bathymetry, hydro-meteo, etc.), but also by providing the effects and efficiency of certain planned interventions in the coastal zone (efficiency of a beach nourishment at a certain location, remaining lifetime, etc.)
- Also 'near real-time tools during flooding' could further be developed to assist the coastal managers, the coastal mayors and governor of the province to prepare for and to act during eventual flood events (evacuation planning).

MULTI-DISCIPLINARY APPROACH

A multi-disciplinary approach to **include different expertise including environmental and social sciences into coastal zone management** would be valuable. This can be realised in different ways and on different scales.

- **Understanding dune growth** will for sure need the interaction between morphologists and ecologists. Dunes can grow when enough fine sand is transported from the beach, towards and in the dunes, by aeolian transport. The type and extent of vegetation impacts the amount of sand trapped in the dunes. Better estimates of each of these processes and their interaction are needed to better predict the dune evolution in the short and long term.
- Also, abroad recent research focused on the development of a **linked modelling approach to calculate the sand exchange between water and land.** Such coupled models aim at efficiently and realistically calculating the interactions between the wet and dry beach and dune growth; both in size and variations in space and time. Now at the end of CREST, it should be verified how the combination of the outcomes of these last 4 years of research from CREST can be combined with research from elsewhere, and how these studies can reinforce each other. This linked modelling approach for instance should be tested and further developed, by also including effects of vegetation, human interventions, etc. on both short and longer time scales.
- In CREST it is observed that a **natural feeding from offshore** provides sand to the beaches. However, the processes driving these sand fluxes are not well understood. A new research project should be established to investigate the interaction between the shoreface-connected sand banks and the nearshore gullies with the beaches. A multidisciplinary team consisting of coastal morphologists, numerical modelers, geologists and experimentalists is needed to perform such a challenging research question.
- On an even more global scale, a **multi-sectoral vision on coastal zone management** could be developed.
    - The current initiative of MOW with the project "Coastal Vision" aims at defining the position of the coastline in Flanders on the long term, in 2100. The main focus is guaranteeing enough space for a sustainable and adaptive coastal protection now and

in the future. A lot of the outcomes of CREST provide valuable information for this project (e.g. insight in the coastal evolution, input for design methodologies). Since this project will implicitly define the land use in the long term, it needs, as planned for, the involvement of a wide range of stakeholders and different sectors including environment and socio-economics. However, a shared, common cross-sectoral vision for coastal zone development is another step. Coastal processes and coastal protection will most likely not be the main driver in such a vision, but will remain of course one of the major elements.

EXPERT GROUP COASTAL PROTECTION

One of the major achievements of CREST is that the project brought together most of the expertise on the physical aspects of coastal protection and coastal risks in Flanders.

It is highly recommended that also after the CREST project "**expert workshops coastal protection"** are organised, e.g. on a yearly basis. Such workshops keep contacts between the different organisations and institutes alive and allow the exchange of results of ongoing projects and of launching and clustering new ideas for future projects. Not only partners of the CREST project, but also experts from other disciplines (such as ecology, sociology, etc.) and from industry should be involved. Such an expert group and improved cooperation between universities in Flanders with institutes and consultants will also strengthen their position on the international scene.

REFERENCES

Aalborg University, 2018. AwaSys [WWW Document]. URL https://www.hydrosoft.civil.aau.dk/awasys (accessed 11.12.19).

Altomare, C.; Dominguez, J.M.; Crespo, A.J.C.; Suzuki, T.; Caceres, I.; Gómez-Gesteira, M., 2015. Hybridization of the wave propagation model SWASH and the meshfree particle method SPH for real coastal applications. Coast. Eng. J. 57(4). https://hdl.handle.net/10.1142/S0578563415500242

Altomare, C., Suzuki, T., Chen, X., Verwaest, T., Kortenhaus, A., 2016. Wave overtopping of sea dikes with very shallow foreshores. Coast. Eng. 116, 236–257. https://doi.org/10.1016/j.coastaleng.2016.07.002

Altomare, C., Tagliafierro, B., Dominguez, J.M., Suzuki, T., Viccione, G., 2018. Improved relaxation zone method in SPH-based model for coastal engineering applications. Appl. Ocean Res. 81: 15-33. https://hdl.handle.net/10.1016/j.apor.2018.09.013

Altomare, C., Suzuki, T., Verwaest, T., 2020. Influence of directional spreading on wave overtopping of sea dikes with gentle and shallow foreshores. Coast. Eng. 23., Vol. 157, 103654, https://doi.org/10.1016/j.coastaleng.2020.103654.

American Society for Photogrammetry and Remote Sensing. (2013). LAS Specification v. 1.4 - R13. Retrieved from www.asprs.org.

Anderson, R. S., & Haff, P. K., 1991. Wind modification and bed response during saltation of sand in air. In: Barndorff-Nielsen O.E., Willetts B.B. (Eds) Aeolian Grain Transport 1. Acta Mechanica Supplementum, 1, 21–51.

Arens, S. M., Van Kaam-Peters, H. M. E., & Van Boxel, J. H., 1995. Air flow over foredunes and implications for sand transport. Earth Surface Processes and Landforms, 20, 315–332.

Batnold, R.A., 1937. The size-grading of sand by wind. Proceedings of the Royal Society of Londers, Series A, Mathematical and Physical Sciences, 250-264.

Bagnold, R. A. (1954). The Physics of Blown Sand and Desert Dunes, 2nd Edition. Methuen, London.

Bauer, Bernard O., Sherman, D. J., Nordstrom, K. F., & Gares, P. A., 1990. Aeolian transport measurement and prediction across a beach and dune at Castroville, California. Coastal Dunes, Form and Process, (January), 39–55.

Bauer, Bernard O., Sherman, D. J., & Wolcott, J. F.,1992. Sources of Uncertainty in Shear Stress and Roughness Length Estimates Derived from Velocity Profiles. The Professional Geographer, 44(4), 453–464. https://doi.org/10.1111/j.0033-0124.1992.00453.x

Bauer, B. O., Davidson-Arnott, R. G. D., Hesp, P. A., Namikas, S. L., Ollerhead, J., & Walker, I. J., 2009. Aeolian sediment transport on a beach: Surface moisture, wind fetch, and mean transport. Geomorphology, 105(1–2), 106–116. https://doi.org/10.1016/j.geomorph.2008.02.016

Bauer, Bernard O., Davidson-Arnott, R. G. D., Walker, I. J., Hesp, P. A., & Ollerhead, J., 2012. Wind direction and complex sediment transport response across a beach-dune system. Earth Surface Processes and Landforms, 37(15), 1661–1677. https://doi.org/10.1002/esp.3306

Bauer, Bernard O., & Davidson-Arnott, R. G. D., 2014. Aeolian particle flux profiles and transport unsteadiness. Journal of Geophysical Research: Earth Surface, 119, 2448–2459. https://doi.org/10.1002/2015JF003520

Bi, Q., Toorman, E.A., 2015. Mixed-sediment transport modelling in Scheldt estuary with a physics-based bottom friction law. Ocean Dynamics, 65, 555–587. https://doi.org/10.1007/s10236-015-0816-z

Bitenc, M., Lindenbergh, R., Khoshelham, K., & van Waarden, A. P., 2011. Evaluation of a LIDAR land-based mobile mapping system for monitoring sandy coasts. Remote Sensing, 3(7), 1472–1491. https://doi.org/10.3390/rs3071472

Bullock, G.N., Obhrai, C., Peregrine, D.H., Bredmose, H., 2007. Violent breaking wave impacts. Part 1: Results from large-scale regular wave tests on vertical and sloping walls. Coast. Eng. 54, 602–617. https://doi.org/10.1016/j.coastaleng.2006.12.002

Brand, E., Chen, M., Montreuil, A-L., Dan, S., 2017a. Intertidal beach recovery in relation to nearshore hydrodynamics, Mariakerke, Belgium. Proceedings of HydroSenSoft 2017, 28 February – 3 March 2017, Madrid, Spain¸ 1-7

Brand, E., Chen, M., Montreuil, A-L., Dan, S., 2017b. Spatio-temporal variability in intertidal beach morphology on a seasonal scale, Mariakerke, Belgium. Proceedings of Coastal Dynamics 2017, 12-16 June 2017, Helsingør, Denmark, 1049-1058

Brand, E., Montreuil, A-L., Dan, S., Chen, M., 2018. Macro-tidal beach morphology in relation to nearshore wave conditions and suspended sediment concentrations at Mariakerke, Belgium. Regional Studies in Marine Science, 24, 97-106

Brand, E., Montreuil, A-L., Chen, M., 2019a. The effect of turbulence and particle size on suspended sediment concentration measurements in the intertidal zone. Coastal Sediments 2019, May 2019, 2435-2442

Brand, E., De Sloover, L., De Wulf, A., Montreuil, A-L., Vos, S., Chen, M., 2019b. Cross-shore suspended sediment transport in relation to topographic changes in the intertidal zone of a macro-tidal beach (Mariakerke, Belgium). Journal of Marine Science and Engineering, 7, 1-16

Brand, E., Chen, M., Montreuil, A-L., 2019c. Optimizing measurements of sediment transport in the intertidal zone. Earth-Science Reviews Volume 200, 2020, 103029, https://doi.org/10.1016/j.earscirev.2019.103029.

Brand, E., Montreuil, A-L., Houthuys, R., Chen, M., 2019d. Relating waves, tide, and sediment supply to changes in intertidal beach topography on macro-tidal, sandy beaches. Marine Geology – (under review)

Brand, E., 2019. Intertidal beach morphodynamics of a macro-tidal sandy coast (Belgium). Doctoral dissertation, Free University of Brussels (VUB).

Cahill, T. A., Gill, T. E., Reid, J. S., Gearhart, E. A., & Gillette, D. A., 1996. Saltating particles, playa crusts and dust aerosols at Owens (dry) Lake, California. Earth Surface Processes and Landforms, 21(7), 621–639. https://doi.org/10.1002/(SICI)1096-9837(199607)21:7<621::AID-ESP661>3.0.CO;2-E

Campos, L. D., 2018. Quantification Methods for Aeolian Sand Transport on Beaches. Ph.D. thesis. University of Twente, the Netherlands.

Carstens, M.R., Nielsen, F.M., Altinbilek, H.D., 1969. Bed forms generated in the laboratory under an oscillatory flow: analytical and experimental study. Technical Report TM-28, U.S. Army Corps of Engineers, Coastal Engineering Research Center, Vicksburg, MS.

Chen, X., Jonkman, S.N., Pasterkamp, S., Suzuki, T., Altomare, C., 2017. Vulnerability of Buildings on Coastal Dikes due to Wave Overtopping. Water 9, 394. https://doi.org/10.3390/w9060394

Chepil, W. S., & Milne, R. A., 1941. Wind erosion of soils in relation to size and nature of exposed area. The Journal of Agricultural Science, 21, 479–487.

Clubb G.S., 2001. Experimental study of vortex ripples in full scale sinusoidal and asymmetric flows. PhD thesis, University of Aberdeen.

Complex Project Coastal Vision & CREST, 2019. Output Workshop 'Climate Scenarios Flemish Coast' 12 December 2018 – Flanders Hydraulics Research, Antwerp, 23 pp. http://www.vliz.be/nl/imis?module=ref&refid=311027

Davidson-Arnott, R. G. D., & Law, M. N., 1990. Seasonal patterns and controls on sediment supply to coastal foredunes, Long Point, Lake Erie. In: Nordstrom, K.F., Psuty, N.P., Carter, R.W.G. (Eds.), Coastal Dunes: Forms and Processes., 177–200.

Davies A.G., 2005. Modeling and measurement of sediment transport by waves in the vortex ripple regime. Journal of Geophysical Research, 110(C5).

Deckers P., Kellens W., Reyns J., Vanneuville W., De Maeyer P., 2009. A GIS for Flood Risk Management in Flanders. In: Showalter P., Lu Y. (eds) Geospatial Techniques in Urban Hazard and Disaster Analysis. Geotechnologies and the Environment, vol 2. Springer, Dordrecht https://link.springer.com/chapter/10.1007/978-90-481-2238-7_4

De Hauwere, N.; Claus, S.; Toorman, E.; Monbaliu, J., 2017. CREST - Klimaatbestendige kust. Ondersteunende activiteit – Metadata inventaris. Vlaams Instituut voor de Zee/Katholieke Universiteit Leuven: Oostende, Leuven. 17 pp.

Delgado-Fernandez, I., 2010. A review of the application of the fetch effect to modelling sand supply to coastal foredunes. Aeolian Research, 2(2–3), 61–70. https://doi.org/10.1016/j.aeolia.2010.04.001

Delgado-Fernandez, I., & Davidson-Arnott, R., 2009. Sediment Input to Foredunes Description and Frequency of Transport Events at Greenwich Dunes, PEI, Canada. Journal of Coastal Research, 1(56), 302–306. Retrieved from http://www.jstor.org/stable/25737586

Department of Civil Engineering (UGent), Belgium, 2018. 2D overtopping and wave impact experiments in shallow foreshore conditions (wave flume Ghent University, 2018).

De Rouck, J., Trouw, K., 2019. Masterplan Kustveiligheid - Evaluatie toelaatbaar overtoppingsdebiet. MDK – verslag in opdracht van afdeling Kust & Flanders Hydraulics Research.

De Sloover, L., De Wulf, A., Stal, C., Verbeurgt, J., & Vos, S., 2019. Case Study of a Hypertemporal Terrestrial LiDAR to Monitor a Macrotidal Beach: Assessment of Different Calibration Procedures. 19th SGEM International Multidisciplinary Scientific GeoConference EXPO Proceedings.

De Sloover, L., Brand, E., Strypsteen, G., De Wulf, A., Verbeurgt, J., Van Ackere, S., Chen, M., Rauwoens, P., De Maeyer, P., Montreuil, A.-L., Stal, C., 2020a. Close-Range Multi-Sensor Topographic Monitoring of the Intertidal Belgian Beach: Effects of Morphologic Variability on Elevation Errors. *(in draft, to be submitted to Sensors).*

De Sloover, L., Verbeurgt, J., van Eeden, F., Van Ackere, S., Lonneville, B., Vos, S., Brand, E., Montreuil, A.-L., Chen, M., Strypsteen, G., Rauwoens, P., De Maeyer, P., Stal, C. & De Wulf, A., 2020b. A Hyper-Temporal Terrestrial LiDAR Data Set of Sandy Beach Topography at Mariakerke, Belgium. *(in draft, to be submitted to Geoscience Data Journal).*

De Vos, B., 2019. Wave-induced loading on buildings on top of a Belgian dike with a very shallow foreshore. M.Sc. thesis, Ghent University.

de Vries, S., Southgate, H. N., Kanning, W., & Ranasinghe, R., 2012. Dune behavior and aeolian transport on decadal timescales. Coastal Engineering, 67, 41–53. https://doi.org/10.1016/j.coastaleng.2012.04.002

De Wille, T.; Schäler, R.; Exton, C.; Exton, G., 2019. Crowdsourcing localisation for non-profit projects The client perspective., doi:10.1075/jial.18004.wil.

Dong, Z., Liu, X., Wang, H., & Wang, X., 2003. Aeolian sand transport : a wind tunnel model. Sedimentary Geology, 161, 71–83. https://doi.org/10.1016/S0037-0738(03)00396-2

Donker, J., Maarseveen, M. Van, & Ruessink, G., 2018. Spatio-Temporal Variations in Foredune Dynamics Determined with Mobile Laser Scanning. Journal of Marine Science and Engineering, 6(126). https://doi.org/10.3390/jmse6040126

Ellis, J. T., Li, B., Farrell, E. J., & Sherman, D. J., 2009. Protocols for characterizing aeolian mass-flux profiles. Aeolian Research, 1(1–2), 19–26. https://doi.org/10.1016/j.aeolia.2009.02.001

Elsner, P., Dornbusch, U., Thomas, I., Amos, D., Bovington, J., & Horn, D., 2018. Coincident beach surveys using UAS, vehicle mounted and airborne laser scanner: Point cloud inter-comparison and effects of surface type heterogeneity on elevation accuracies. Remote Sensing of Environment, 208, April 2018, 15–26. https://doi.org/10.1016/j.rse.2018.02.008

European Commission, 2018. Cost-benefit analysis for FAIR research data. Luxembourg: Publications Office of the European Union.

Fang, G.H., J. Yang, Y.N. Chen and C. Zammit, 2015. Comparing bias correction methods in downscaling meteorological variables for a hydrologic impact study in an arid area in China. Hydrology and Earth System Sciences, 19, 2547-2559, doi: 10.5194/hess-19-2547-2015.

Fiedler, J.W., Smit, P.B., Brodie, K.L., McNinch, J., Guza, R.T., 2019. The offshore boundary condition in surf zone modeling. Coast. Eng. 143, 12–20. https://doi.org/10.1016/j.coastaleng.2018.10.014

Gautama S., Atzmueller M., Kostakos V., Gillis D., Hosio S. (2017) Observing Human Activity Through Sensing. 47–68 In: Loreto V. et al. (eds) Participatory Sensing, Opinions and Collective Awareness. Understanding Complex Systems, Springer Cham. https://doi.org/10.1007/978-3-319-25658-0_3

Goossens, D., & Offer, Z. Y. (2000). Wind tunnel and field calibration of five aeolian dust samplers. Atmospheric Environment, 34(7), 1043–1057. https://doi.org/10.1016/S1352-2310(99)00376-3

Grant W.D., Madsen O.S. (1982). Movable bed roughness in unsteady oscillatory flow. Journal of Geophysical Research, 87(C1):469.

Gruwez, V., Gallach-Sanchez, D., Van der Elst, H., Versluys, T., Troch, P., Kortenhaus, A., Mertens, T., Monbaliu, J., 2016. ADVANCED MODELLING OF OVERTOPPING RISKS IN COASTAL URBAN AREAS. Preliminary design artificial dike field measurements. Ghent University, Ghent. Deliverable D.2.3.2 - CREST (Climate Resilient Coast) VLAIO/IWT project 150028.

Gruwez, V., Vandebeek, I., Kisacik, D., Streicher, M., Altomare, C., Suzuki, T., Verwaest, T., Kortenhaus, A., Troch, P., 2018a. 2D experiments of wave dynamics in front of and over a sea dike with a very shallow foreshore. Presented at the Coastlab 2018, pp. 1–10.

Gruwez, V., Vandebeek, I., Kisacik, D., Streicher, M., Verwaest, T., Kortenhaus, A., Troch, P., 2018b. 2D overtopping and impact experiments in shallow foreshore conditions, in: Proceedings of 36th Conference on Coastal Engineering. Presented at the 36th Conference on Coastal Engineering (ICCE 2018), pp. 1–13.

Gruwez, V., Altomare, C., Suzuki, T., Streicher, M., Cappietti, L., Kortenhaus, A., 2020. Numerical modelling of overtopped bore impacts on dike mounted vertical walls in very shallow foreshore conditions – an inter-model comparison (in preparation). J. Mar. Sci. Eng.

Günther, H., S. Hasselmann and P.A.E.M. Janssen, 1992. Wamodel Cycle 4. DKRZ Technical Report No. 4, Hamburg, October 1992, 102 pp.

Hofland, B., Chen, X., Altomare, C., Oosterlo, P., 2017. Prediction formula for the spectral wave period Tm-1,0 on mildly sloping shallow foreshores. Coast. Eng. 123, 21–28. https://doi.org/10.1016/j.coastaleng.2017.02.005

Hoonhout, B. M., & Vries, S. de. (2016). A process-based model for aeolian sediment transport and spatiotemporal varying sediment availability. Journal of Geophysical Research: Earth Surface, 121(8), 1555–1575. https://doi.org/10.1002/2015JF003692

Hoonhout, B., & de Vries, S. (2017). Field measurements on spatial variations in aeolian sediment availability at the Sand Motor mega nourishment. Aeolian Research, 24, 93–104. https://doi.org/10.1016/j.aeolia.2016.12.003

Houthuys, R. and FHR, 2019. Morfologische evolutie van de Vlaamse kust tot 2019. Report commissioned by Coastal Division, Oostende. (in prep.)

Hsu, S.-A., 1971. Wind stress criteria in eolian sand transport. J. of Geoph. Res., Oceans and Atmospheres, 76, 36, pp. 8684-8686. https://doi.org/10.1029/JC076i036p08684

Hulme, M., G.J. Jenkins, X. Lu, J.R. Turnpenny, T.D. Mitchell, R.G. Jones, J.Lowe, J.M. Murphy, D. Hassell, P. Boorman, R. McDonald and S. Hill, 2002. Climate Change Scenarios for the United Kingdom: The UKCIP02 Scientific Report. Tyndall Centre for Climate Change Research, School of Environmental Sciences, University of East Anglia, Norwich, UK, 120 pp.

IPCC, SROCC, 2019: IPCC Special Report on the Ocean and Cryosphere in a Changing Climate [H.-O. Pörtner, D.C. Roberts, V. Masson-Delmotte, P. Zhai, M. Tignor, E. Poloczanska, K. Mintenbeck, A. Alegría, M. Nicolai, A. Okem, J. Petzold, B. Rama, N.M. Weyer (eds.)]. In press.

Jacobsen, N.G., van Gent, M.R.A., Capel, A., Borsboom, M., 2018. Numerical prediction of integrated wave loads on crest walls on top of rubble mound structures. Coast. Eng. 142, 110–124. https://doi.org/10.1016/j.coastaleng.2018.10.004

Jonsson I.G., 1986. Wave boundary layers and friction factors. Coastal Engineering Proceedings, 1(10):9.

Kawamura, R., 1951. Study of sand movement by wind. In *The reports of the Institute of Science and Technology: vol. 5.* University of Tokyo, Tokyo, Japan.

Keijsers, J. G. S., Poortinga, A., Riksen, M. J. P. M., & Maroulis, J., 2014. Spatio-temporal variability in accretion and erosion of coastal foredunes in the Netherlands: Regional climate and local topography. PLoS ONE, 9(3). https://doi.org/10.1371/journal.pone.0091115

Kok, J.F., Parteli, E., J., R., Michaels, T.I., & Karam, D.B., 2012. The physics of wind-blown sand and dust. *Reports on Progress in Physics.* 75 (10), 1-119.

Lara, H.C., 2018. Importance of second-order wave generation for wave overtopping on dikes with a mildly sloping very shallow foreshore. Aalborg University & UGent.

Law, M. N., & Davidson-Arnott, R. G. D. (1990). Seasonal controls on aeolian processes on the beach and foredune. Proceedings of the Symposium on Coastal Sand Dunes, (January 1990), 49–68.

Li, B., Sherman, D.J., Farell, E.J., & Ellis, J.T., 2010. Variability of the apparent von Kármán parameter during Aeolian saltation. *Geophysical Research Letters,* 37 (15).

Longuet-Higgins M.S., Stewart R.W. (1960), Changes in the form of short gravity waves on long waves and tidal currents. Journal of Fluid Mechanics 8: 565.

Luyten, P. (editor), 2016. Coherens – A coupled hydrodynamic-ecological model for regional and shelf seas: user documentation. Version 2.6. RBINS Report, Operational Directorate Natural Environment, Royal Belgian Institute of Natural Sciences, Brussels, Belgium, 1554 pp.

Lynch, K., Jackson, D. W. T., & Cooper, J. A. G., 2016. The fetch effect on aeolian sediment transport on a sandy beach: a case study from Magilligan Strand, Northern Ireland. Earth Surface Processes and Landforms, 41(8), 1129–1135. https://doi.org/10.1002/esp.3930

Madsen O. (1993). Sediment Transport Outside the Surf Zone. Unpublished technical report. Waterways Experiment Station, U.S. Army Corps of Engineer, Vicksburg, Mississippi, USA, 1993.

Madsen, O. S., Wright, L. D., Boon, J. D., and Chisholm, T. A., 1993.:Wind stress, bed roughness, and sediment suspension on the inner shelf during an extreme storm event, Cont. Shelf Res., 13(11), 1303–1324.

Montreuil, A. L., Chen, M., Brand, E., Strypsteen, G., Rauwoens, P., Vandenbulcke, A., Verwaest, T., 2018. Dynamics of Surface Moisture Content on a Macro-tidal Beach. Journal of Coastal Research, 85, 206–210. https://doi.org/10.2112/SI85-042.1

Montreuil, A-L., Brand, E., Strypsteen, G., Roest, B., De Sloover, L., Rauwoens, P., De Wulf, A., Houthuys, R., Chen, M., Verwaest, T., 2019. Scientific Report on Coastal Resilience. Deliverable D 3.4.1 CREST (Climate Resilient Coast) VLAIO/IWT project 150028.

Montreuil, A-L., Chen, M., Brand, E., Verwaest, T., Houthuys, R., 2019. Recovery assessment of macro-tidal sandy beaches with different environmental settings, Belgian coast. (submitted to Geomorphology)

Nielsen P., 1992. Coastal bottom boundary layers and sediment transport. Number v. 4 in Advanced Series on Ocean Engineering. World Scientific, Singapore ; River Edge, N.J.

Noorloos J.C.V, 2003. Energy transfer between short wave groups and bound long waves on a plane slope, Master thesis, Delft University of Technology, the Netherlands.

OGC. (2019). OGC GeoTIFF Standard. Retrieved November 7, 2019, from https://www.opengeospatial.org/standards/geotiff

Ouda M., Toorman, E.A., 2019. Development of a new multiphase sediment transport model for free surface flows. International Journal of Multiphase Flow, 117, 81-102. https://doi.org/10.1016/j.ijmultiphaseflow.2019.04.023

Ozer, J., D. Van den Eynde and S. Ponsar, 2008. Trend analysis of the relative mean sea level at Oostende (Southern North Sea – Belgian coast). Report CLIMAR/X/JO/200807/EN/TR3. Prepared for the Belgian Science Policy, Project CLIMAR, contract SD/NS/01A. Management Unit of the North Sea Mathamatical Models, Brussels, 14 pp.

Ozer, J., S. Ponsar and D. Van den Eynde, 2019. Revisiting the trend analysis of relative mean sea level rise at Oostende (southern North Sea – Belgian coast). Report CREST/X/JO/201906/EN/TR02. Prepared for the CREST Project, Royal Belgian Institute of Natural Sciences, Operational Directorate Natural Environment, Brussels, 28 pp.

Paris agreement (2015), https://unfccc.int/process-and-meetings/the-paris-agreement/the-paris-agreement (last visited 03.12.2019)

Pickering, M.D., N.C. Wells, K.J. Horsburgh and J.A.M. Green, 2012. The impact of future sea-level rise on the European Shelf tides. Continental Shelf Research, 35, 1-15.

Ponsar, S., J. Ozer and D. Van den Eynde, 2007. Impacts of climate change on the physical and chemical parameters of the North Sea (literature study). Management Unit of the North Sea Mathematical Models, Brussels, 70 pp.

Poortinga, Ate, van Minnen, J., Keijsers, J., Riksen, M., Goossens, D., & Seeger, M., 2013. Measuring Fast-Temporal Sediment Fluxes with an Analogue Acoustic Sensor: A Wind Tunnel Study. PLoS ONE, 8(9). https://doi.org/10.1371/journal.pone.0074007

Poortinga, Ate, Keijsers, J. G. S., Maroulis, J., & Visser, S. M., 2014. Measurement uncertainties in quantifying aeolian mass flux: evidence from wind tunnel and field site data. PeerJ, 2, e454. https://doi.org/10.7717/peerj.454

Poortinga, A., Keijsers, J. G. S., Visser, S. M., Riksen, M. J. P. M., & Baas, A. C. W., 2015. Temporal and spatial variability in event scale aeolian transport on Ameland, The Netherlands. GeoResJ, 5, 23–35. https://doi.org/10.1016/j.grj.2014.11.003

Pueyo Estada, I.M., 2019. Statistical characterization of wave overtopping impacts on buildings located on sea dikes in very shallow foreshore condition under short- and long-crested waves action. MSc thesis. Ghent University.

Roelvink, D., Reniers, A., van Dongeren, A., van Thiel de Vries, J., McCall, R., Lescinski, J., 2009. Modelling storm impacts on beaches, dunes and barrier islands. Coast. Eng. 56, 1133–1152. https://doi.org/10.1016/j.coastaleng.2009.08.006

Roest, B. and Houthuys, R., 2019, Belgian coastal volumes 1979-2019. Courtesy of Flanders Coastal Division. http://mda.vliz.be/directlink.php?fid=VLIZ_00000633_5db85ffcb8083

Ruessink, B.G., Michallet, H., Bonneton, P., Mouazé, D., Lara, J., Silva, P.A., Wellens, P., 2013. Globex: wave dynamics on a gently sloping laboraty beach, in: Proceedings Coastal Dynamics 2013. pp. 1351–1362.

Sato S., 1987. Oscillatory boundary ow and sand movement over ripples. PhD thesis, University of Tokyo.

Shao, Y., & Raupauch, M. R., 1992. The overshoot and equilibration of saltation. Journal of Geophysical Research, 97(D18), 20559–20564.

Sherman, D. J., Jackson, D. W. T., Namikas, S. L., & Wang, J., 1998. Wind-blown sand on beaches: An evaluation of models. Geomorphology, 22(2), 113–133. https://doi.org/10.1016/S0169-555X(97)00062-7

Sherman, D. J., & Li, B., 2012. Predicting aeolian sand transport rates: A reevaluation of models. Aeolian Research, 3(4), 371–378. https://doi.org/10.1016/j.aeolia.2011.06.002

Smit, Y., Ruessink, G., Brakenhoff, L. B., & Donker, J. J. A., 2017. Measuring spatial and temporal variation in surface moisture on a coastal beach with a near-infrared terrestrial laser scanner. Aeolian Research. https://doi.org/10.1016/j.aeolia.2017.07.004

Spies, P. J., McEwan, I. K., & Butterfield, G. R., 1995. On wind velocity profile measurements taken in wind tunnels with saltating grains. Sedimentology, 42, 515–521.

Spore, N. J., & Brodie, K. L., 2017. Collection , Processing , and Accuracy of Mobile Terrestrial Lidar Survey Data in the Coastal Environment Coastal and Hydraulics Laboratory.

Stal, C., Incoul, A., De Maeyer, P., Deruyter, G., Nuttens, T., & De Wulf, A., 2014. Mobile mapping and the use of backscatter data for the modelling of intertidal zones of beaches. International Multidisciplinary Scientific GeoConference Surveying Geology and Mining Ecology Management, SGEM, 3(2), 223–230.

Sterk, G., & Raats, P. A. C., 1996. Comparison of Models Describing the Vertical Distribution of Wind-Eroded Sediment. Soil Science Society of America Journal, 60, 1914–1919. Retrieved from https://library.wur.nl/WebQuery/wurpubs/fulltext/210366#page=39

Streicher, M., Kortenhaus, A., Altomare, C., Gruwez, V., Hofland, B., Chen, X., Marinov, K., Scheres, B., Schüttrumpf, H., Hirt, M., Cappietti, L., Esposito, A., Saponieri, A., Valentini, N., Tripepi, G., Pascuali, D., Di Risio, M., Aristodemo, F., Damiani, L., Willems, M., Vanneste, D.F.A., Suzuki, T., Breteler, M.K., Kaste, D., 2017. WALOWA (WAve LOads on WAlls) - large-scale experiments in the delta flume. Presented at the SCACR2017, Santander, Spain.

Streicher, M., 2019. Loads induced by overtopping bores on vertical walls at the end of sea facing promenades : a laboratory study. PhD dissertation, Ghent University.

Streicher, M., Kortenhaus, A., Gruwez, V., Suzuki, T., Altomare, C., Saponieri, A., Pasquali, D., Valentini, N., Tripepi, G., Celli, D., Di Risio, M., Aristodemo, F., Damiani, L., Klein Breteler, M., Kaste, D., 2019a. Overtopped wave loads on walls (WALOWA) - numerical and physical modelling of large-scale experiments in the delta flume. Presented at the Hydralab+ joint user meeting, Bucharest, Romania, pp. 57–67.

Streicher, M., Kortenhaus, A., Hughes, S., Hofland, B., Suzuki, T., Altomare, C., Marinov, K., Chen, X., Cappietti, L., 2019b. Non-repeatability, scale- and model effects in laboratory measurement of impact loads induced by an overtopped bore on a dike mounted wall, in: Proceedings of the ASME 2019 38th International Conference on Ocean, Offshore and Arctic Engineering. Presented at the OMAE2019, Glasgow, Scotland, UK, p. 10.

Streicher, M., Kortenhaus, A., Marinov, K., Hirt, M., Hughes, S., Hofland, B., Scheres, B., Schüttrumpf, H., 2019c. Classification of bore patterns induced by storm waves overtopping a dike crest and their impact types on dike mounted vertical walls – a large-scale model study. Coast. Eng. J. 0, 1–19. https://doi.org/10.1080/21664250.2019.1589635

Strypsteen, G., Montreuil, A.L., & Rauwoens, P., 2017. Aeolian sand transport at the Belgian coast: field campaigns and first results. *Proceeding Coastal Dynamics, 11.* Helsingør.

Strypsteen, G., 2019. Monitoring and Modelling Aeolian Sand Transport at the Belgian Coast. PhD thesis. KU Leuven.

Sünderman, J., G. Becker, P. Damm, D. Van den Eynde, R. Laane, W. Van Leussen, T. Pohlmann, W. van Raaphorst, G. Radach, H. Schultz & M. Visser, 1996. Decadal variability on the North-West European continental shelf. Deutsche Hydrografische Zeitschrift, 48, 3/4, 365-400.

Termonia, P., B. Van Schaeybroeck, L. De Cruz, R. De Troch, S. Caluwaerts, O. Giot, R. Hamdi, S. Vannitsem, F. Duchêne, P. Willems, H. Tabari, E. Van Uytven, P. Hosseinzadehtalaei, N. Van Lipzig, H. Wouters, S. Vanden Broucke, J.-P. van Yperseele, P. Marbaix, C. Villanueva-Birriel, X. Fettweis, C. Wyard, C. Scholzen, S. Doutreloup, K. De Ridder, A. Gobin, D. Lauwaert, T. Stravrakou, M. Bauwens, J.-F. Müller, P. Luyten, S. Ponsar, D. Van den Eynde and E. Pottiaux, 2018. The CORDEX.be initiative as a foundation for climate services in Belgium. Climate Services, 11, 49-61. doi: 10.1016/ j.cliser.2018.05.001.

Toorman E.A., Wongsoredjo S., Bi Q., 2019. A new wall-boundary treatment for the k-ε turbulence model for fine and coarse meshes. (in preparation)

Toorman E.A., Zhang Q., Ouda M., 2019. Bed shear stress, bottom friction and sediment transport under combined wave-current action. Technical Report D1.2. CREST and INDI67 projects, KU Leuven.

Van Ackere, S.; Verbeurgt, J.; De Sloover, L.; Gautama, S.; De Wulf, A.; De Maeyer, P. A, 2019a. Review of the Internet of Floods: Near Real-Time Detection of a Flood Event and Its Impact. Water 2019, 11, 2275. https://www.mdpi.com/2073-4441/11/11/2275

Van Ackere, S.; Beullens, J.; Vanneuville, W.; De Wulf, A.; De Maeyer, P., 2019b. FLIAT, An Object-Relational GIS Tool for Flood Impact Assessment in Flanders, Belgium. Water 2019, 11, 711. https://www.mdpi.com/2073-4441/11/4/711

Van Cauwenberghe, C., 1993. Synopis of the tidal observations along the Belgian Coast – Conclusions with respect to the high water, the mean sea and the low water levels. Report nr. 37 bis of the Hydrografische Dienst der Kust.

Van Cauwenberge, C., 1995. Relative sea level rise: further analyses and conclusions with respect to the high water, the mean sea and the low water levels along the Belgian coast. Report nr 37ter of the Hydrografische Dienst der Kust.

Van Cauwenberghe, C., 1999. Relative sea level rise along the Belgian coast: analyses and conclusions with respect to the high water, the mean sea and the low water levels. Report nr 46 of the Hydrografische Dienst der Kust.

Van den Eynde, D., F. Francken, S. Ponsar and J. Ozer, 2008. Bepaling van de primaire impacten van klimaatsverandering: statistische analyse van metingen van golven, windsnelheid en -richting en van zeewatertemperatuur. Report CLIMAR/X/DVDE/200807/NL/TR4, Voorbereid voor het BELSPO project CLIMAR, contract SD/NS/01A, Beheerseenheid Mathematische Model Noordzee, Brussel, 40 pp.

Van den Eynde, D., R. De Sutter, L. De Smet, F. Francken, J. Haelters, F. Maes, E. Malfait, J. Ozer, H. Pollet, S. Ponsar, J. Reyns, K. Van der Biest, E. Vanderperren, T. Verwaest, A. Volkaert and M. Willekens, 2011. Evaluation of climate change impacts and adaptation responses for marine activities “CLIMAR”, Final Report, Brussels. Belgian Science Policy Office, Research Programme Science for a Sustainable Development, 121 pp.

Van den Eynde, D., S. Ponsar, P. Luyten and J. Ozer, 2019a. Analysis of climate changes in the time series of wind speed, significant wave height and storm surges at the Belgian coast. Report CREST/X/DVDE/201906/EN/TR03. Prepared for the CREST project. Royal Belgian Institute of Natural Sciences, Operational Directorate Natural Environment, Brussels, 69 pp.

Van den Eynde, D., S. Ponsar and J. Ozer, 2019b. Climate change: analysis of time series of sea water temperature at the Belgian coast. Report CREST/X/DVDE/201906/EN/TR01. Prepared for the CREST Project, Royal Belgian Institute of Natural Sciences, Operational Directorate Natural Environment, Brussels, 26 pp.

Van den Eynde, D., 2020. The impact of sea level rise on the wave height near the Belgian coast. Report CREST/1/DVDE/202001/EN/TR04. Prepared for the CREST project. Royal Belgian Institute of Natural Sciences, Operational Directorate Natural Environment, Brussels, in preparation.

Van den Eynde, L., 2018. Modelling of suspended matter for the Belgian coastal zone and the Scheldt estuary by means of PROBA-V remote sensing data. M.Sc. thesis. KU Leuven. Faculty of Engineering Science.

Van Dijk, P. M., Stroosnijder, L., & De Lima, J. L. M. P., 1996. The influence of rainfall on transport of beach sand by wind. Earth Surface Processes and Landforms, 21(4), 341–352. https://doi.org/10.1002/(SICI)1096-9837(199604)21:4<341::AID-ESP542>3.0.CO;2-Z

Van Pelt, R. S., Peters, P., & Visser, S., 2009. Laboratory wind tunnel testing of three commonly used saltation impact sensors. Aeolian Research, 1(1–2), 55–62. https://doi.org/10.1016/j.aeolia.2009.05.001

van Rijn, L.C., 2018. Aeolian transport over a flat sediment surface. https://www.leovanrijn-sediment.com/papers/Aeoliansandtransport2018.pdf

Verbrugghe T., Dominguez J.M., Crespo A.J.C., Altomare C., Stratigaki V., Troch P., Kortenhaus A., 2018. Coupling methodology for smoothed particle hydrodynamics modelling of non-linear wave-structure interactions. COASTAL ENGINEERING, vol. 138, p. 184-198, ISSN: 0378-3839, doi: 10.1016/j.coastaleng.2018.04.021

Verwaest, T., Gruwez, V., 2019. Scale model experiments. Deliverable D2.3.1 CREST (Climate Resilient Coast) VLAIO/IWT project 150028.

Verwaest, T., Spiesschaert, T., Altomare, C., Suzuki, T., Mostaert, F., 2019. CREST golftankproeven: Factual data rapport. WL Rapporten, 17_039. Waterbouwkundig Laboratorium: Antwerpen.

Visser, M., S. Batten, G. Becker, P. Bot, F. Colijn, P. Damm, D. Danielsen, D. Van den Eynde, L. Føyn, A. Frohse, G. Groeneveld, R. Laane, W. van Raaphorst, G. Radach, H. Schutz and J. Sündermann, 1996. Time series analysis of monthly mean data of temperature, salinity, nutrients, suspended matter phyto- and zooplankton at eight different locations on the Northwest European shelf. Deutsche Hydrografische Zeitschrift, 48 (3/4), 299-323 Wiggs, G. F. S., Livingstone, I., & Warren, A. (1996). The role of streamline curvature in sand dune dynamics: Evidence from field and wind tunnel measurements. Geomorphology, 17(1-3 SPEC. ISS.), 29–46.

Vos, S., Lindenbergh, R., & De Vries, S., 2017. CoastScan: Continuous Monitoring of Coastal Change Using Terrestrial Laser Scanning. Coastal Dynamics, (233).

The WAMDI Group, 1988. The WAM Model – A Third Generation Ocean Wave Prediction Model. Journal of Physical Oceanography, 18, 1775-1810.

Wiggs, G. F. S., Livingstone, I., & Warren, A., 1996. The role of streamline curvature in sand dune dynamics: Evidence from field and wind tunnel measurements. Geomorphology, 17(1-3 SPEC. ISS.), 29–46.

Williams, I. A., Wijnberg, K. M., & Hulscher, S. J. M. H., 2018. Detection of aeolian transport in coastal images. Aeolian Research, 35(May), 47–57. https://doi.org/10.1016/j.aeolia.2018.09.003

Wilkinson, M. D. et al., 2016. The FAIR Guiding Principles for scientific datamanagement and stewardship. Sci. Data 3:160018 doi: 10.1038/sdata.2016.18

Willems, P., 2015. Actualisatie van de extreme-waarden-statistiek van stormvloeden aan de Belgische kust. Waterbouwkundig Laboratorium/KU Leuven: Antwerpen. 31 pp.

Willmott, C.J., Robeson, S.M., Matsuura, K., 2012. A refined index of model performance. Int. J. Climatol. 32, 2088–2094. https://doi.org/10.1002/joc.2419

Wilson K.C. (1989). Movable bed friction at high shear stress. Journal of Hydraulic Engineering, 115(6):825-830.

Xu, J., Wright, L. (1993). Tests of bed roughness models using field data from the middle Atlantic Bight. Continental Shelf Research 15 (11–12), 1409–1434.

Youssef, F., Erpul, G., Bogman, P., Cornelis, W. M., & Gabriels, D. (2008). Determination of efficiency of Vaseline slide and Wilson and Cooke sediment traps by wind tunnel experiments. Environmental Geology, 55(4), 741–750. https://doi.org/10.1007/s00254-007-1027-9

Zhang, Q., Toorman, E., Monbaliu, J., 2016. CREST - Climate resilient coast. Integrated multi-scale wave-flow sediment modelling. – Report on updates in the TELEMAC-TOMAWAC suite. KU Leuven. Deliverable D.1.1.1 - CREST (Climate Resilient Coast) VLAIO/IWT project 150028.

Zhang Q., Toorman E., Monbaliu J., 2020. Shoaling of bound infragravity waves on plane slopes for bichromatic wave conditions. Coastal Engineering (accepted for publication).

AGENTSCHAP INNOVEREN & ONDERNEMEN

Vlaanderen is ondernemen